THE
PHYSICAL REVIEW

A journal of experimental and theoretical physics established by E. L. Nichols in 1893

SECOND SERIES, VOL. 72, No. 10 NOVEMBER 15, 1947

Measurement of Transport and Inelastic Scattering Cross Sections for Fast Neutrons. I. Method*

H. H. BARSCHALL,** J. H. MANLEY, AND V. F. WEISSKOPF***
University of California, Los Alamos Scientific Laboratory, Los Alamos, New Mexico

(Received August 4, 1947)

An experimental method for measuring transport and inelastic scattering cross sections for fast neutrons is described. The cross sections are obtained from poor geometry and back scattering measurements by use of detector, the energy response of which rises above an adjustable neutron energy from zero to an almost constant value. A method of evaluation of the data is discussed.

1. INTRODUCTION

THE purpose of the work to be described in the present paper was to measure several of the quantities which would enable one to predict the behavior of fast neutrons in an extended medium, in particular, the reflection of fast neutrons from a thick layer of material. In the first part of the paper an elementary theory of the method used is given, a second part will describe the experimental results, in a third part the evaluation of the experiments will be discussed.

2. DEFINITIONS

The elementary theory to be given in the present first part of the paper will apply only to thin scatterers, while in the third part the finite thickness of the scatterers used will be taken into account. If the scatterer contains N atoms/cm^2 and if the total cross section of an atom for interaction with a fast neutron is σ, the following approximation holds for a thin scatterer: $\exp(-N\sigma)\approx 1-N\sigma$.

Since the scattering process may result in a change of energy as well as direction of the neutron, the notation $\sigma(\theta, E, E_0)$ will be used to denote the probability that a neutron of initial energy E_0 is scattered into a unit solid angle with a deviation θ from its original direction and into a unit energy range at an energy E. In terms of a current $I_0(E_0)$ incident on N scattering centers per square centimeter and a scattered current per unit solid angle and per unit energy range $I(\theta, E, E_0)$

$$\sigma(\theta, E, E_0)=I(\theta, E, E_0)/NI_0(E_0).$$

The total cross section for elastic scattering is defined by

$$\sigma_e(E_0)=\int_0^{\pi}\int_{E_0'}^{E_0}\sigma(\theta, E, E_0)dEd\omega,$$

where

$$d\omega=2\pi\sin\theta d\theta$$

and E_0' is the maximum energy loss permitted

* This paper is based on work performed at Los Alamos Scientific Laboratory of the University of California under Contract No. W-7405-eng-36 for the Manhattan Project and the information contained therein will appear in Division V of the Manhattan Project Technical Series as part of the contribution of the Los Alamos Laboratory.
** Now at the University of Wisconsin.
*** Now at the Massachusetts Institute of Technology.

without excitation of the scattering nucleus. It is to be noted that E and θ are not independent.

The cross section for inelastic scattering is defined for our purpose as

$$\sigma_i(B, E_0) = \int_0^\pi \int_0^B \sigma(\theta, E, E_0) dE d\omega$$

which states that the scattered neutron has an energy less than B. The expression "total inelastic cross section" will refer to all energies of the scattered neutrons as well as all angles:

$$\sigma_i(E_0) = \int_0^\pi \int_0^{E_0'} \sigma(\theta, E, E_0) dE d\omega.$$

The expression "total cross section" will refer to $\sigma(E_0) = \sigma_e(E_0) + \sigma_i(E_0)$.

In order to describe the behavior of neutrons in an extended medium, it is convenient to use the transport cross section. The transport cross section differs from the total cross section in that the contributions of neutrons scattered through various angles θ are weighted according to a factor $(1-\cos\theta)$. The transport cross section σ_t is defined as

$$\sigma_t(E_0) = \int_0^\pi [\sigma_e(\theta, E_0) + \sigma_i(\theta, E_0)](1-\cos\theta) d\omega.$$

In the present work measurements of the transport cross section and of the cross section for inelastic scattering were attempted. An exact determination of these quantities would require a knowledge of the distribution in energy and angle of the scattered neutrons as a function of primary neutron energy. Such detailed measurements were not made, but the use of four primary neutron energies and three angular intervals permits deduction of approximate values of transport and inelastic cross sections.

3. PREVIOUS WORK

Many investigations of the inelastic scattering of fast neutrons and of the angular distribution of scattered neutrons have been carried out in the past.

Measurements of the inelastic scattering of fast neutrons have been performed using radioactive threshold detectors.[1,2] This method has the disadvantage that not enough radioactive detectors with different thresholds particularly in the region up to 3 Mev are available. The observation of gamma-rays produced offers another way of obtaining information on inelastic scattering.[1,3] It is difficult to obtain in this manner the distribution in energy of the inelastically scattered neutrons or reliable absolute values of the scattering cross section. The most complete information on the distribution in energy of inelastically scattered neutrons can be obtained by observing hydrogen recoils in a cloud chamber[4,5] or in a photographic plate. The only drawback of this method is the large amount of work required in evaluating the results.

The most complete study of the angular distribution of scattered fast neutrons was carried out by Kikuchi, Aoki, and Wakatuki[6] who found a strong forward maximum for the scattering of 3-Mev neutrons by heavy elements. Their measurements, however, do not enable one to distinguish between elastically and inelastically scattered neutrons.

Qualitative information on inelastic scattering has been obtained by measuring the distribution in energy of recoiling alpha-particles in an ionization chamber.[7] The method described in the present paper uses a similar technique. Instead of helium, hydrogen or deuterium serves as the detector gas in order to avoid the effects of the resonance in helium around 1 Mev[8] which affects both the scattering cross section and the angular distribution of the recoils.[9] The method used in the present work enables one to obtain more quantitative information about the inelastic scattering than the previous work.

[1] D. C. Grahame and G. T. Seaborg, Phys. Rev. **53**, 795 (1938).
[2] W. D. Allen and C. Hurst, Proc. Phys. Soc. **52**, 501 (1940).
[3] H. Aoki, Proc. Phys. Math. Soc. Japan **19**, 369 (1937); I. Nonaka, Phys. Rev. **59**, 681 (1941).
[4] E. Hudspeth and T. W. Bonner, Phys. Rev. **53**, 928 (1938).
[5] H. F. Dunlap and R. N. Little, Phys. Rev. **60**, 693 (1941).
[6] S. Kikuchi, H. Aoki, and T. Wakatuki, Proc. Phys. Math. Soc. Japan **21**, 232, 410, 656 (1939).
[7] H. H. Barschall and R. Ladenburg, Phys. Rev. **61**, 129 (1942).
[8] H. Staub and W. E. Stephens, Phys. Rev. **55**, 131 (1939).
[9] H. H. Barschall and M. H. Kanner, Phys. Rev. **58**, 590 (1940); T. A. Hall and P. G. Koontz, Phys. Rev. **72**, 196 (1947).

4. DETECTOR

To determine the distribution in energy of the scattered neutrons a threshold detector was used. The ideal threshold detector would count all the neutrons above a given adjustable energy with the same efficiency. No such detector is available, but a gas recoil detector may be used to approximate this condition in the following way: an ionization chamber or proportional counter is filled with a light gas (hydrogen or deuterium) and the stopping power of the gas is chosen so that the range of the recoiling gas nuclei is small compared to the dimensions of the counter. The recoil pulses are amplified by means of a linear pulse amplifier and all the pulses above a given size are counted. The energy corresponding to a minimum pulse height which is counted will be referred to as the bias energy B. If the scattering of the neutrons by the detecting gas is isotropic in the center of mass system the sensitivity of the counter will be proportional to $\sigma(E)[1-(B/E)]$, where $\sigma(E)$ is the total scattering cross section of the detector gas.[10] For the case in which $\sigma(E)$ is proportional to $E^{-\frac{1}{2}}$, as is approximately true for hydrogen over a wide range of energies, the theoretical energy sensitivity of the detector is shown in Fig. 1. As may be seen from Fig. 1, the energy above which neutrons are counted is not well defined, a fact which will lead to considerable uncertainty in the meaning of $\sigma_i(B, E_0)$.

5. GEOMETRY

Two kinds of measurements were carried out, poor geometry and back scattering experiments. The experiments using poor geometry employed the arrangement shown in Fig. 2. A circular disk scatterer of radius a was placed half-way between the source and the detector. As was first pointed out by R. F. Christy, if the neutron source is isotropic, there is a compensation between scattering into the detector from some disk elements and scattering out of the neutron beam by others such that a decrease corresponding to the scattering of all neutrons from θ_m to π is observed, where θ_m represents the maximum angle through which a neutron can be scattered by the disk (edge) and reach the detector.

Let Q be the number of neutrons emitted by the source per unit solid angle and per second and consider single elastic collisions. The current scattered into a detector of unit area is

$$I_1=(QN/4D^2)\int_0^{\theta_m}\sigma(\theta)d\omega$$

with $\theta_m=2\tan^{-1}(a/D)$. The current received by a detector of unit area subtending a solid angle of $1/4D^2$ at the source is reduced by the interposition of the disk. This reduction arises from the scattering out of the beam by the portion of the disk within the solid angle, so that the current at the detector from the reduced direct beam is

$$I_2=(Q/4D^2)\left[1-N\int_0^{\pi}\sigma(\theta)d\omega\right]$$

and the net current

$$I=I_1+I_2=(Q/4D^2)\left[1-N\int_0^{\pi}\sigma(\theta)d\omega\right].$$

$Q/4D^2=I_0$ is the current at the detector without the scatterer. Hence the above relation may be written, for a disk thin compared to the scattering mean-free path, in the exponential form as follows

$$I/I_0=\exp\left(-N\int_{\theta_m}^{\pi}\sigma(\theta)d\omega\right).$$

This result will be called the Christy theorem.

It is possible to vary θ_m by varying D and in this way to measure the angular distribution of the scattered neutrons. Experiments were carried out for values of θ_m of 30°, 60°, and 90°. The accuracy of this method for measuring angular

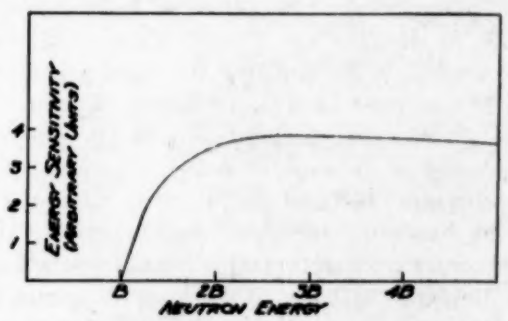

FIG. 1. Theoretical sensitivity of hydrogen detector as a function of neutron energy.

[10] H. H. Barschall and H. A. Bethe, Rev. Sci. Inst. 18, 147 (1947).

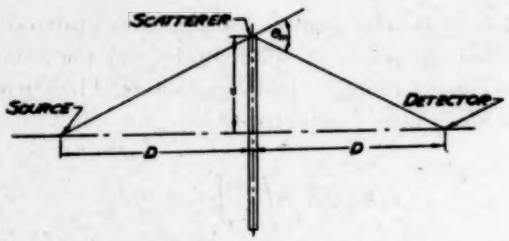

FIG. 2. Scattering geometry for poor geometry experiments.

distributions is affected by the need to take differences. In computing the transport cross section the errors will cancel, however, to a certain extent, since the differences are added again after they have been multiplied by the appropriate weighting factor.

For $\theta_m > 90°$ the method becomes very inaccurate because the transmission is very close to unity. Therefore the scattering into the back hemisphere was investigated by observing the reflected neutrons. As the number of reflected neutrons is small compared to the number of neutrons coming directly from the source, it is necessary either to shield the detector from the direct neutrons by means of a shadow cone or to use a directional detector. The shadow cone defines an annular ring on the disk scatterer from which neutrons may be reflected so that these measurements are equivalent to measurements using ring scatterers. That this is so was checked by ring-disk comparison and by moving the detector off the scattering axis to explore the extent of the shadow.

6. SOURCE

Experiments were carried out for neutrons of 0.2-, 0.6-, and 1.5-Mev energy using the Li(p, n) reaction and at 3 Mev using the d–d reaction. The assumption of an isotropic neutron source made in deriving the Christy theorem is valid neither for the Li(p, n) nor for the d–d reaction. Both sources deviate from spherical symmetry both in intensity and in energy. The effect of this asymmetry can be made to cancel by an appropriate choice of the direction of the scattering axis (line through target, center of disk and center of detector) with respect to the bombarding ions. In Fig. 3 the axis of symmetry S–D makes an angle α_0 with respect to the incident ions. The angle φ is the azimuth of an element of the scatterer with respect to the plane defined by the ion beam and the axis S–D, and α is the angle between the direction of the proton or deuteron beam and that of a neutron emitted from the target. The Christy theorem is valid if the neutron intensity averaged over φ is independent of θ.

For scatterers consisting of heavy nuclei the energy of the elastically scattered neutrons is, within the accuracy of the measurements, the same as that of the primaries. The sensitivity of the detector for elastically scattered neutrons as a function of φ and θ can therefore be measured directly by moving the detector around the source. Let $R(\alpha, B)$ be the response of the detector for a bias energy B at a constant distance from the source. The variation of $R(\alpha, B)$ is due to the dependence of both intensity and energy on α, and, therefore, depends on the bias B. The response of the detector as a function of θ and φ, $R(\theta, \varphi, B)$, may be obtained from $R(\alpha, B)$ by using the geometrical relationship between the angles:

$$\cos\alpha = \cos\alpha_0 \cos\tfrac{1}{2}\theta + \sin\alpha_0 \sin\tfrac{1}{2}\theta \cos\varphi.$$

The Christy theorem holds, provided

$$\bar{R}(\theta, B) \equiv (1/2\pi)\int_0^{2\pi} R(\theta, \varphi, B)d\varphi$$

is independent of θ. If $R(\alpha)$ can be expressed as $R(\alpha) = c_1 + c_2 \cos^2\alpha$, the integral is independent of θ for $\tan\alpha_0 = \sqrt{2}$, and if $R(\alpha)$ is a linear function of $\cos\alpha$, the integral is independent of θ for $\alpha_0 = 90°$.

The anisotropy of the Li(p, n) reaction for 0.2-Mev neutrons is so great that it was not possible to find any angle α_0 for which $\bar{R}(\theta)$ was not a rapidly varying function. Therefore no experiments for which the Christy theorem had to be used were carried out at that energy.

For 0.6-Mev neutrons from the Li(p, n) reaction $\bar{R}(\theta)$ was found from the measured functions $R(\alpha, B)$ to be constant within 5 percent at $\alpha_0 = 60°$, so that $\alpha_0 = 60°$ was chosen for the experiments.

For 1.5-Mev neutrons from the Li(p, n) reaction no angle α_0 was found for which $\bar{R}(\theta)$ was independent of θ. For $\alpha_0 = 40°$ the variation of $R(\theta)$ with θ was smallest, but even for this angle corrections had to be applied.

To denote cross sections measured in various geometries the angle θ_m for the geometry used will be written as a subscript, i.e., σ_{60} denotes the cross section measured in the geometry for which $\theta_m = 60°$, and is computed from the relationship

$$I_{60}/I_0 = \exp(-N\sigma_{60}) = \exp\left[-N\int_{60°}^{180°}\sigma(\theta)d\omega\right],$$

where I_{60} and I_0 denote the neutron intensities measured at the detector with and without the scatterer in the 60° geometry. For σ_{30} the correction for asymmetry of the source is negligible. In order to correct the measured values of σ_{60} and σ_{90}, these cross sections should be replaced by corrected values σ_{60}^* and σ_{90}^* according to

$$\sigma_{60}^* = \sigma_{30} + \beta(\sigma_{60} - \sigma_{30}),$$

$$\sigma_{90}^* = \sigma_{60}^* + \gamma(\sigma_{90} - \sigma_{60}),$$

where

$$\beta = \left[\int_{30°}^{60°}\bar{R}(\theta)\sin\theta d\theta\right] \Big/ \left[\int_{30°}^{60°}R(\alpha_0)\sin\theta d\theta\right],$$

$$\gamma = \left[\int_{60°}^{90°}\bar{R}(\theta)\sin\theta d\theta\right] \Big/ \left[\int_{60°}^{90°}R(\alpha_0)\sin\theta d\theta\right].$$

For the 3-Mev neutrons from the d–d reaction $\alpha_0 = 60°$ was chosen for most of the experiments. This choice was based on the fact that the angular distribution of the $D(d, p)H^3$ reaction may be expressed as $c_1 + c_2\cos^2\alpha$. This would suggest $\alpha_0 = 55°$. Since the dependence of the detector on energy will probably introduce a term in $\cos\alpha$, the somewhat larger value of 60° was used.

The correction for the scattering by light elements is more involved. Even if the source were spherically symmetric, the response of the counter for elastic scattering would vary with the scattering angle because of the recoil energy loss. In order to compute this correction the energy and the intensity distribution of the source must be known. The energy of the emitted neutrons as a function of α, $E(\alpha)$, may be computed using the laws of conservation of energy and momentum. The distribution in angle of the neutrons from the source $Q(\alpha)$, may be determined from the measured function $R(\alpha)$ and the measured energy sensitivity of the detector using $E(\alpha)$.

The coefficients β and γ for light elements are

$$\beta = \left[\int_{30°}^{60°}\bar{Q}(\theta)\bar{S}(\theta)\sin\theta d\theta\right] \Big/ \left[\int_{30°}^{60°}Q(\alpha_0)S(0)\sin\theta d\theta\right],$$

$$\gamma = \left[\int_{60°}^{90°}\bar{Q}(\theta)\bar{S}(\theta)\sin\theta d\theta\right] \Big/ \left[\int_{60°}^{90°}Q(\alpha_0)S(0)\sin\theta d\theta\right],$$

where

$$\bar{Q}(\theta) = (1/2\pi)\int_0^{2\pi}Q(\alpha)d\varphi,$$

and $S(\theta, \varphi)$ is the response of the detector to neutrons emitted in the direction $(\theta/2, \varphi)$ and elastically scattered into the detector with an energy loss depending on θ, $S(0) = R(\alpha_0)$ is the response of the detector to neutrons which are emitted in the direction α_0 and have not lost energy by recoil.

7. EVALUATION

In the evaluation of the measurements the following assumptions or approximations were made:

(a) $\sigma_i(\theta)$ is independent of θ. This assumption appears reasonable from theoretical considerations. There is some experimental evidence that the inelastic scattering is isotropic (cf. reference 7). The assumption did not lead to any contradictions in the evaluation of the data.

(b) Neutrons are considered as scattered elastically if they are detected at the highest bias used in the experiments. Since some neutrons may lose little enough energy in inelastic collisions to be counted at the highest bias some inelastic scattering may be included in the cross section for elastic scattering.

The cross section $\sigma_e(\theta)$ is approximated by three average values in the following three

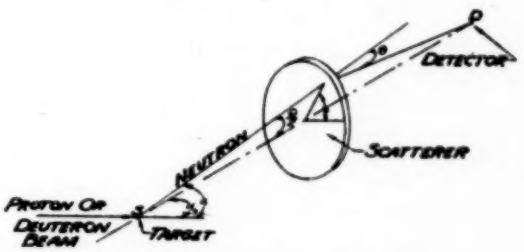

FIG. 3. Geometry used in scattering experiments.

angular intervals: 30° to 60°, 60° to 90°, 90° to 180°. The value for the interval 90° to 180° was taken as that measured in a back scattering geometry corresponding to an average angle of 135°. There is some experimental evidence, however, that the elastic back scattering may not be isotropic. The assumption that the scattering cross section for 135° is characteristic for the whole back hemisphere may, therefore, be in error. The contribution to the transport cross section of $\sigma_e(\theta)$ for $0° \leqslant \theta \leqslant 30°$ was neglected. This does not introduce any appreciable error, even if there is considerable forward scattering, since

$$\tfrac{1}{2}\int_{0°}^{30°}(1-\cos\theta)\,\sin\theta d\theta = 0.0045$$

or less than $\frac{1}{2}$ percent of the integral over all values of θ.

In the evaluation of the data the difference between the cross sections for two values of θ_m is first corrected for the asymmetry of the source and the energy loss in the case of light elements. From the corrected values of the differences, corrected values of σ_{60} and σ_{90} are determined which are used in the subsequent calculations.

The next step in the evaluation is the calculation of the cross section for inelastic scattering. This may be obtained in several ways: from the transmission data alone, from the back scattering, and from a comparison of transmission and back scattering.

From the measured cross sections for back scattering at various biases, σ_{BS}, the cross sections for inelastic scattering are obtained as first differences. Although the measurements of back scattering included only a specific angle in the back hemisphere, σ_{BS} is computed to refer to a 4π solid angle.

A comparison between the cross section for $\theta_m = 90°$ and the cross section for back scattering may be used to obtain values for the cross section for inelastic scattering for the following reasons. The value σ_{90} measured at a bias B is the sum of the cross section for scattering of all neutrons into the back hemisphere and the cross section for neutrons scattered into the front hemisphere with an energy such that they are not detected at the bias B. The cross section for the scattering of neutrons into the back hemisphere with an energy above the bias B is $\frac{1}{2}\sigma_{BS}$. Therefore $\sigma_{90}-\frac{1}{2}\sigma_{BS}$ is the cross section for the scattering of neutrons below the bias B, and allows one to obtain fairly reliable values for the inelastic scattering.

The average of the inelastic scattering obtained from σ_{BS} and from $\sigma_{90}-\frac{1}{2}\sigma_{BS}$ was taken as the most reliable determination of σ_i. The transmission data were then adjusted to give the bias effect corresponding to the previously calculated inelastic scattering. The adjustments necessary were in almost all cases within the experimental error of the measurements.

The value of $\sigma_{90}-\frac{1}{2}\sigma_{BS}$ for the lowest bias used yields the sum of the cross sections for inelastic scattering below the lowest bias and for absorption.

The transport cross section was obtained by adding for a given bias the contributions of the three angular intervals, weighted according to $(1-\cos\theta)$, and the cross section for inelastic scattering below the same bias. The transport cross section, according to its definition, is independent of the bias.

This method of evaluation assumes that a neutron is scattered only once in the scatterer. A method of evaluation taking into account multiple scattering will be given in the third part of this paper.

Measurement of Transport and Inelastic Scattering Cross Sections for Fast Neutrons. II. Experimental Results*

H. H. BARSCHALL,** M. E. BATTAT,*** W. C. BRIGHT, E. R. GRAVES, T. JORGENSEN,**** AND J. H. MANLEY
University of California, Los Alamos Scientific Laboratory, Los Alamos, New Mexico

(Received August 4, 1947)

Measurements of poor geometry scattering and back scattering are described for neutrons of energies of 0.2, 0.6, 1.5, and 3 Mev. The following materials were investigated: C, Be, B^{10}, B^{11}, BeO, Al, Fe, Cu, Co, Ni, Ta, W, Au, and Pb. Values of the cross sections for inelastic scattering and the transport cross sections are given for these materials.

1. INTRODUCTION

IN the first part of the present paper[1] a method was described which allows one to measure the transport and inelastic scattering cross sections for fast neutrons. In Table I the scatterers used in these experiments are described.

2. MEASUREMENTS USING 0.2-MEV NEUTRONS

Source

The 0.2-Mev neutrons were obtained from the Li(p, n) reaction by bombarding a Li target, about 15 kev thick, with protons accelerated by the University of Wisconsin's electrostatic generator at Los Alamos. The proton current integrator served as a monitor for the neutron intensity.

At this energy the source is strongly anisotropic both in energy and intensity. This made it impossible to select an angle α_0 between the proton beam and the scattering axis such that corrections for anisotropic neutron flux were feasible for the 60° and 90° transmission geometries. Only measurements where the scatterer subtended a relatively small angle at the source could be carried out. In order to minimize the effect of the anisotropy of the source, all measurements were carried out with the scattering axis in the direction of the proton beam.

Detector

The most desirable detector for the scattering experiments described in this paper is one the response of which does not depend on the direction of incidence of the neutrons. For most of the experiments at 200 kev a spherical proportional counter[2] was used. The outer electrode was a thin spherical copper shell, 3 inches in diameter. The inner electrode consisted of two circular wire loops with a common center arranged in two planes at right angles to each other. The chamber was filled to a pressure of 25-cm Hg with tank hydrogen, and operated at a voltage of approximately 2200. It was found

TABLE I. Scatterers used in experiments.

No. of sample	Substance	Thickness of sample (cm)	Area (cm^2)	Mass (kg)	Atoms or molecules/cm^2 $\times 10^{-24}$	Inside diameter (cm)	Outside diameter (cm)
			Disks				
1	Be	2.54	506	2.39	0.318		
2	B(normal)	3.18	506	2.28	0.251		
3	B(80.5% B^{10})	3.18	506	2.16	0.251		
4	C	1.27	506	0.981	0.0972		
5	C	3.81	506	3.09	0.306		
6	BeO	1.23	506	1.43	0.0680		
7	BeO	4.37	511	3.91	0.185		
8	BeO	4.44	511	3.12	0.149		
9	Al	2.54	506	3.58	0.153		
10	Fe	2.54	506	10.0	0.214		
11	Ni	2.54	506	11.7	0.237		
12	Co	2.54	506	10.8	0.219		
13	Cu	2.54	506	11.5	0.214		
14	Ta	2.54	506	21.0	0.137		
15	W	4.44	506	7.82	0.0505		
16	W	2.54	506	21.6	0.139		
17	Au	2.54	506	24.9	0.150		
18	Pb	2.54	506	14.6	0.0836		
			Rings				
19	C	1.27	258	0.526	0.103	17.8	25.4
20	C	3.81	258	1.58	0.306	17.8	25.4
21	BeO	2.58	262	1.09	0.100	17.8	25.5
22	BeO	4.37	258	2.01	0.186	17.8	25.4
23	Fe	2.54	258	5.16	0.216	17.8	25.4
24	W	4.37	258	4.37	0.0539	17.8	25.4
25	Pb	2.54	258	7.45	0.0836	17.8	25.4
26	Pb	2.54	324	9.36	0.0836	15.2	25.4

* This paper is based on work performed at Los Alamos Scientific Laboratory of the University of California under Contract No. W-7405-eng-36 for the Manhattan Project and the information contained therein will appear in Division V of the Manhattan Project Technical Series as part of the contribution of the Los Alamos Laboratory.

** Now at the University of Wisconsin.

*** Now at Washington University.

**** Now at the University of Nebraska.

[1] H. H. Barschall, J. H. Manley, V. F. Weisskopf, Phys. Rev. **72**, 881 (1947).

[2] H. M. Agnew, Rev. Sci. Inst. (to be published).

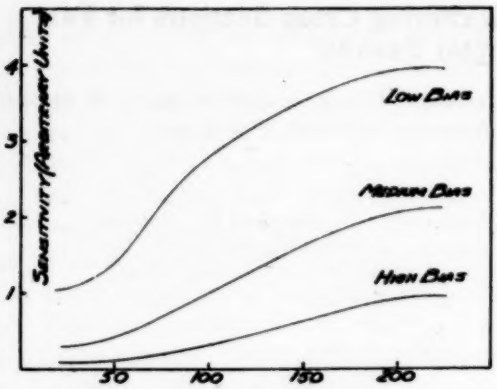

FIG. 1. Response of the spherical proportional counter used for the detection of 200-kev neutrons as a function of neutron energy.

experimentally that the response of the counter was spherically symmetric.

A measurement of the response of the counter as a function of neutron energy (Fig. 1) showed that the energy sensitivity differed greatly from that expected for a gas recoil counter. This behavior is probably due to non-uniform gas amplification in different parts of the counter. Consequently it was not possible to use the counter as a threshold detector and no effort was made to detect inelastic scattering which, at this neutron energy, was not expected to be important.

For the investigation of the scattering of Be, B, and Al a cylindrical proportional counter filled with deuterium to a pressure of one atmosphere was used.

Procedure

Three types of scattering experiments were carried out for 200-kev neutrons: transmission experiments in the geometry[3] for which $\theta_m = 30°$ ($D = 18.7$ in., $\alpha_0 = 0°$), back scattering experiments in the geometry shown in Fig. 2a, and ring scattering experiments in the geometry shown in Fig. 2b with an average scattering angle of 90°.

For the transmission experiments the number of recoils per monitor count in the presence of the scatterer and without the scatterer were counted. A paraffin cylinder, 80 cm long, was interposed between source and detector to measure the background due to room scattering. This background was subtracted from the data. The cross section was computed under the assumption of an exponential decrease of the neutron intensity in the scatterer. For the ring and back scattering experiments the recoil counts per monitor count were recorded for three conditions: with shadow cone and with scatterer, with cone and without scatterer, and without cone and without scatterer. From these data and the geometry the scattering cross section was computed.[4] The method of computation is that used in a previous paper on elastic back scattering of d–d neutrons.[5]

Results

The cross sections obtained in these experiments are tabulated in Table II. In the case of BeO the cross section is given per molecule. All cross sections are given as if they applied over the total solid angle of 4π. For a poor geometry

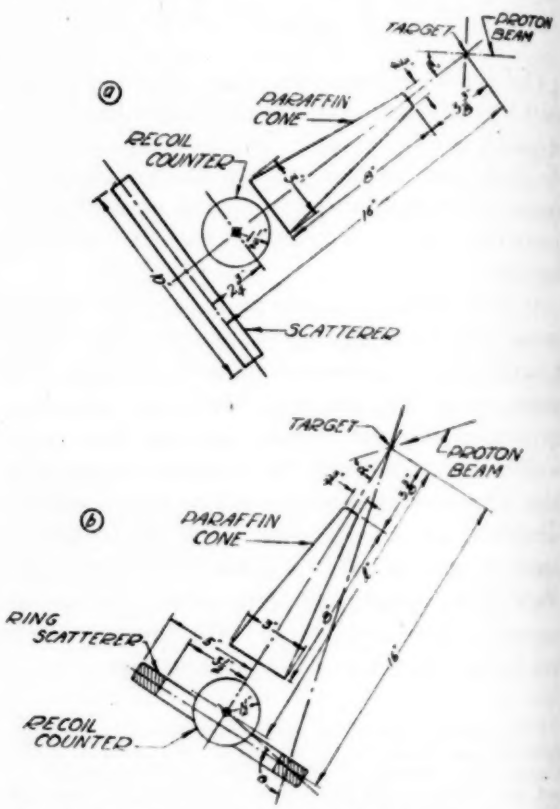

FIG. 2. Geometry used in scattering experiments. (a) Back scattering from a disk. (b) Scattering by a ring.

[3] The notation is defined in Part I (reference 1).

[4] Calculation by P. Olum.

[5] Manley, Agnew, Barschall, Bright, Coon, Graves, Jorgensen and Waldman, Phys. Rev. 70, 602 (1946).

transmission experiment this means that the measured cross section is multiplied by $2/(\cos\theta_m+1)$. All the data are based on at least six separate runs, and were taken simultaneously at three different biases of the discriminator. A measurable bias effect was observed only in C and BeO in the ring and back scattering geometry. This bias effect may be explained entirely by energy loss in elastic collisions. From the consistency of the individual runs the error in the measurements of the cross sections is estimated to be about five percent.

The data in Table II, except the transport cross sections, are not corrected for multiple scattering, nor for energy loss in elastic collisions.

3. MEASUREMENTS USING 0.6-MEV NEUTRONS

Source

The 0.6-Mev neutrons were obtained from the Li(p, n) reaction monitored by the current integrator. By measuring the response of the detector as a function of the angle α it was found by successive approximations that the anisotropy of the source cancelled to within five percent if α_0 was chosen to be 60°, i.e., if the proton energy was such that 0.6-Mev neutrons were emitted from the target at an angle of 60° with respect to the proton beam.

Detector

The detector was a cylindrical proportional counter similar to that described by Coon and Nobles,[6] except that it contained no radiator,

TABLE II. Scattering cross sections for 0.2-Mev neutrons. Cross sections in barns (1 barn = 10^{-24} cm²).

Sample no.	Material	30°-geometry	Bias	90°-ring geometry low	90°-ring geometry medium	90°-ring geometry high	135°-back scattering geometry low	135°-back scattering geometry medium	135°-back scattering geometry high	Transport cross section
1	Be	4.5								
2	B	3.9								
3	B	4.7								
	B^{10}	2.3	(absorption subtracted)							
	B^{11}	3.6								
4	C	4.1					2.7	2.3	1.9	
19	C			2.8	2.5	2.2				
6	BeO	6.9					4.6	3.9	3.4	
21	BeO			4.4	3.6	3.1				
9	Al	5.8								
10	Fe	3.2					2.5	2.4	2.4	3.0
23	Fe			2.5	2.6	2.5				
16	W	6.9					4.6	4.5	4.4	6.0
24	W			4.9	5.1	5.0				
17	Au	7.7					4.9	4.7	4.6	6.4
18	Pb	7.6					5.9	5.8	6.0	7.0
25	Pb			6.1	6.2	6.0				

[6] J. H. Coon and R. A. Nobles, Rev. Sci. Inst. 18, 44 (1947).

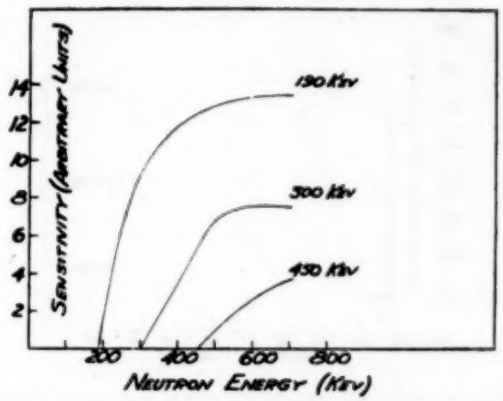

FIG. 3. Response of the cylindrical proportional counter used for the detection of 600-kev neutrons as a function of neutron energy.

and was filled with one atmosphere of deuterium rather than an inert gas. Typical response curves determined experimentally for this counter for three different bias voltages are plotted against neutron energy in Fig. 3. According to the definitions given in reference 1, bias voltages are specified in terms of the neutron energy at which the response of the counter rises above background, but it should be noted that the effective average threshold is considerably higher. The lowest bias was chosen above the maximum pulse height due to gamma-rays. The highest bias was limited by the counting rates.

The response of the counter was not isotropic. The sensitivity to neutrons incident at 30° with respect to the axis of the counter was 10 percent higher than the sensitivity to neutrons incident perpendicularly to the axis for the lowest bias. The corresponding figure for the highest bias was 20 percent. A correction for the anisotropic response of the counter was made in the evaluation.

Results

Poor geometry measurements were made for $\theta_m=30°$, 60°, and 90°. Back scattering experiments were carried out for an average scattering angle of 135° (see Fig. 2a). The results are tabulated in Table III. The errors of the measurements, apart from systematic errors, are again estimated to be about five percent. The data are not corrected for anisotropic response of the detector, multiple scattering, or energy loss in elastic collisions. The last column of Table III

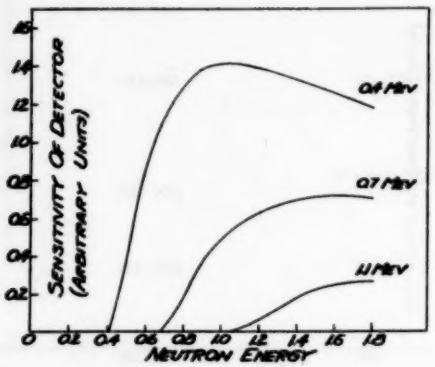

FIG. 4. Response of the spherical ionization chamber used for the detection of 1.5-Mev neutrons as a function of neutron energy.

lists results computed for transport cross sections. These are corrected for anisotropic response of the detector and energy loss in elastic collisions. The values given in parentheses are not corrected for multiple scattering and are calculated according to the method described in reference 1, while those given without parentheses are based on the accurate method to be described in Part III of this paper. The evaluation showed that the observed bias effect in the light elements can be explained entirely by elastic scattering. In none of the heavier elements was the bias effect sufficiently large to yield a measurement of inelastic scattering. Considering the error of the measurements, this corresponds to an upper limit of approximately 3×10^{-25} cm^2 for the cross section of 0.6-Mev neutrons for inelastic scattering by the elements listed in Table III. The biases at which measurements are reported are different for different substances, partly because the measurements were

TABLE III. Scattering cross section in barns for 0.6-Mev neutrons. Bias voltages in italics are in kev.

Sample No.	Material	30°-geometry	60°-geometry			90°-geometry			Back scattering			Transport cross section
			190	*300*	*450*	*190*	*300*	*450*	*190*	*300*		
1	Be	3.3	2.7	3.2	3.9	2.8	4.0	5.0	2.1	1.2		3.4
			190	*300*	*450*	*190*	*300*	*450*	*190*	*300*		
2	B	2.7	1.9	2.1	2.9	1.8	2.2	2.9	1.4	0.8		
			190	*300*	*450*	*190*	*300*	*450*	*190*	*300*		
3	B (80.5% B^{10})	3.6	3.0	3.3	3.8	3.1	3.8	4.4	1.4	0.7		
			190	*300*	*450*	*190*	*300*	*450*	*190*	*300*		
	B^{10} (absorption subtracted)	3.0	2.1	2.4	2.9	1.7	2.3	3.0	1.4	0.7		3.9 (includes absorption)
			190	*300*	*450*	*190*	*300*	*450*	*190*	*300*		
	B^{11}	2.4	1.6	1.8	2.6	1.1	1.8	2.4	1.4	0.8		2.1
			80	*175*	*360*	*80*	*175*	*360*	*80*	*175*	*360*	
5	C	3.0	2.4	2.4	2.8	1.6	2.0	2.8	2.0	1.9	0.9	2.8 (2.5)
			80	*175*	*360*	*80*	*175*	*360*	*80*	*175*	*360*	
6	BeO	6.2	4.4	4.5	5.1	2.8	3.0	4.6	4.4	3.9	1.9	5.0 (5.2)
			100	*200*	*375*	*100*	*200*	*375*	*100*	*200*	*375*	
9	Al	3.6	2.7	2.7	2.9	1.8	1.8	2.2	2.5	2.4	2.1	3.0 (3.1)
			80	*175*	*360*	*80*	*175*	*360*	*80*	*175*	*360*	
10	Fe	2.1	1.6	1.5	1.5	0.8	1.0	1.0	1.7	1.6	1.4	2.0 (1.8)
			100	*200*	*375*	*100*	*200*	*375*	*100*	*200*	*375*	
13	Cu	3.5	2.7	2.7	2.8	1.8	1.8	2.2	3.0	3.0	2.9	(3.5)
			100	*200*	*375*	*100*	*200*	*375*	*100*	*200*	*375*	
12	Co	3.4	2.5	2.5	2.5	1.6	1.8	2.2	3.0	2.9	2.7	(3.4)
			80	*175*	*360*	*80*	*175*	*360*	*80*	*175*	*360*	
18	Pb	5.1	4.4	4.3	4.0	3.8	3.8	4.0	4.5	4.4	4.4	4.4 (4.4)
			80	*175*	*360*	*80*	*175*	*360*	*80*	*175*	*360*	
16	W	5.4	4.1	4.1	4.4	2.8	3.0	4.0	4.2	3.9	3.1	4.7 (4.6)

TABLE IV. Scattering cross section in barns for 1.5-Mev neutrons. Bias voltages in italics are in kev.

Sample no.	Material	30°-geometry	60°-geometry			90°-geometry			Back scattering			Transport cross section
			370	*790*	*950*	*370*	*790*	*950*	*370*	*790*		
1	Be	1.9	1.5	1.6	1.7	1.2	2.0	2.2	0.9	0.2		1.4
			370	*790*	*950*	*370*	*790*	*950*	*370*	*790*	*950*	
2	B	2.0	1.9	2.1	2.4	1.8	2.6	2.9	1.5	0.8	0.5	
			370	*790*	*950*	*370*	*790*	*950*	*370*	*790*	*950*	
3	B (80.5% B^{10})	2.0	1.8	2.0	2.2	2.0	2.5	2.6	1.0	0.5	0.2	
			370	*790*	*950*	*370*	*790*	*950*	*370*	*790*	*950*	
	B^{10} (absorption subtracted)	1.4	1.0	1.2	1.3	0.8	1.2	1.3	0.9	0.4	0.1 (includes absorption)	2.1
			370	*790*	*950*	*370*	*790*	*950*	*370*	*790*	*950*	
	B^{11}	2.0	2.0	2.2	2.4	1.8	2.6	3.0	1.7	0.9	0.6	2.2
			400	*950*	*1300*	*400*	*950*	*1300*	*400*	*950*	*1100*	
5	C	1.8	1.6	1.9	2.1	1.2	2.2	2.8	1.6	0.6	0.2	1.8 (1.8)
			400	*950*	*1300*	*400*	*950*	*1300*	*400*	*950*	*1100*	
7	BeO	3.6	2.7	3.5	3.9	2.4	4.0	5.6	2.8	0.9	0.4	3.6 (3.1)
			370	*790*	*950*	*370*	*790*	*950*	*370*	*790*	*950*	
9	Al	2.7	2.1	2.3	2.7	1.8	2.2	2.4	1.3	1.0	0.8	1.7
			400	*950*	*1300*	*400*	*950*	*1300*	*400*	*950*	*1100*	
10	Fe	2.6	2.1	2.5	2.7	2.0	3.0	3.4	1.9	1.3	1.1	2.2 (2.2)
			470	*750*	*1150*	*470*	*750*	*1150*	*470*	*750*	*1150*	
11	Ni	2.7	2.3	2.4	2.5	2.0	2.2	2.6	2.0	1.9	1.4	(2.3)
			470	*750*	*1150*	*470*	*750*	*1150*	*470*	*750*	*1150*	
12	Co	2.7	2.3	2.4	2.7	2.2	2.4	3.2	2.0	1.7	1.2	(2.2)
			470	*750*	*1150*	*470*	*750*	*1150*	*470*	*750*	*1150*	
13	Cu	2.6	2.4	2.4	2.7	2.4	2.8	3.4	1.6	1.3	1.0	(2.2)
			470	*750*	*1150*	*470*	*750*	*1150*	*470*	*750*	*1150*	
14	Ta	5.5	4.1	4.5	4.8	5.0	6.2	7.4	1.9	1.3	0.9	(3.9)
			400	*950*	*1300*	*400*	*950*	*1300*	*400*	*700*	*1100*	
16	W	5.1	4.0	4.8	5.6	4.2	6.0	6.8	2.7	1.9	1.2	4.7 (4.0)
			400	*950*	*1300*	*400*	*950*	*1300*	*400*	*700*	*1100*	
18	Pb	3.8	3.2	3.5	4.0	3.4	4.0	4.0	3.1	2.6	2.4	3.4 (3.1)

carried out at different times over a period of over a year and the detecting equipment was altered during that period.

4. MEASUREMENTS USING 1.5-MEV NEUTRONS

Source

The 1.5-Mev neutrons were likewise obtained from the Li(p, n) reaction. The angle α_0 was chosen to be 40°. The proton current integrator served as a monitor. The Li target was about 70 kev thick which produces an energy spread of 80 kev in 1.5 Mev.

Detector

The detector was a spherical ionization chamber,[2] 3 inches in diameter. The collecting electrode, a ball $\frac{1}{4}$ inch in diameter, was mounted on a $\frac{1}{8}$-inch brass rod in the center of the sphere. The chamber was filled with a mixture of 24

TABLE V. Scattering cross section in barns for 1.5-Mev neutrons. Bias voltages in italics are in kev.

Sample no.	Material	90° ring geometry			115° ring geometry			135° ring geometry		
		400	*950*	*1100*	*400*	*950*	*1100*			
20	C	1.6	0.9	0.6	1.5	0.6	0.3			
		400	*950*	*1100*	*400*	*950*	*1100*			
22	BeO	2.8	1.4	0.8	2.7	0.9	0.4			
		400	*950*	*1100*	*400*	*950*	*1100*			
24	W	2.6	1.8	1.4	2.8	1.9	1.8			
		400	*950*	*1100*	*400*	*950*	*1100*			
25	Pb	3.1	2.5	2.4	4.0	3.5	3.2			
								400	*700*	*1100*
26	Pb							3.1	2.6	2.5

TABLE VI. Inelastic scattering cross section for 1.5-Mev neutrons in barns.

Element	Below low bias	Below medium bias	Below high bias
Fe	0	0.6	
	(0)	(0.7)	
Ni	(0)	(0.1)	(0.6)
Co	(0)	(0.2)	(0.8)
Cu	(0.3)	(0.6)	(0.9)
Ta	(1.4)	(2.0)	(2.7)
W	0.9	2.1	
	(0.6)	(1.6)	
Pb	0	0.4	
	(0)	(0.4)	

lb./in.^{2} of argon and 12 lb./in.^{2} of hydrogen. Under these conditions the range of a 1.5-Mev proton is about one inch. A negative collecting voltage of 2100 was applied to the outer shell. The sensitivity of the detector as a function of neutron energy at three biases is shown in Fig. 4. The response of the detector as a function of the angle of incidence of the neutrons was found to be uniform.

Results

In Table IV the results for poor geometry and back scattering experiments are listed. The last column of Table IV shows values of transport cross section, the results corrected for multiple scattering being given without parentheses while the results which do not take into account multiple scattering are given in parentheses.

Table V shows the results obtained in several ring scattering geometries (see Fig. 2b). The 135° ring scattering geometry should yield results identical with the disk back scattering geometry. The results for Pb in these two geometries (Tables IV and V) are in good agreement, indicating that the geometric shadow of the paraffin cone defines the active ring on the disk scatterer.

The cross sections for the inelastic scattering of 1.5-Mev neutrons are given in Table VI. For the light elements the energy degradation due to elastic collisions masks any inelastic scattering which might be present. Calculations[4] showed that the bias effect observed in elements lighter than iron may be attributed entirely to elastic scattering, except in the case of aluminum where there is an indication of an inelastic cross section of 1 or 2×10^{-25} cm^2 which, however, is within the accuracy of the measurements. The cross sections computed taking into account multiple scattering are given without parentheses in Table VI, while cross sections which are not corrected for multiple scattering are shown in parentheses. For Fe, Pb, and W the cross sections for inelastic scattering below the high bias could not be determined because different biases were used in the transmission and back scattering experiments. For the same reason the high bias data were not used in the calculation of transport cross sections.

5. MEASUREMENTS USING 3-MEV NEUTRONS

Source

The 3-Mev neutrons were obtained from the $d-d$ reaction. A thick D_2O ice target was bombarded with unanalyzed 200-kev deuterium ions which were accelerated by means of a Cockcroft-Walton set. The accompanying $d(d, p)H^3$ reaction was used for monitoring the neutron intensity.

The measurements were at first carried out at an angle $\alpha_0=60°$ in order to minimize the effect of the anisotropy of the neutron source. At this angle the neutron energy is approximately 2.8 Mev. It was found, however, that it was extremely difficult to carry out back scattering experiments in the geometry for which $\alpha_0=60°$. The count due to the small number of back scattered neutrons was less than the background due to neutrons formed in parts of the accelerator other than the target. However, by carrying out the experiments in the forward direction ($\alpha_0=0°$, neutron energy 3.1 Mev) the detector was shielded by the shadow cone from the neutrons from spurious sources in the accelerator. All the back scattering experiments and some of the transmission experiments were carried out in this geometry. In this case the background was

TABLE VII. Scattering cross section in barns for 2.8-Mev neutrons.

Sample no.	Material	30°	60°			90°		
		Bias (Mev)→0.7	1.4	2.1	0.7	1.4	2.1	
5	C	1.6	1.2	1.5	1.5	1.0	1.4	2.0
8	BeO	3.3	1.6	1.8	2.1	1.0	1.3	1.9
9	Al		1.7	1.9	2.4	0.8	1.4	2.2
10	Fe	2.8	1.7	2.1	2.5	1.4	2.2	3.2
16	W	4.8	4.0	4.5	4.8	3.8	5.4	6.2
17	Au		4.1	4.7	4.9	5.0	6.0	6.6
18	Pb	4.8	4.0	4.4	5.2	3.4	4.0	5.0

TABLE VIII. Scattering cross section in barns for 3-Mev neutrons.

Sample no.	Material	30° Bias (Mev)→	60° 0.75	60° 1.5	60° 2.25	90° 0.75	90° 1.5	90° 2.25	Back scattering 0.75	Back scattering 1.5	Back scattering 2.25	Transport cross section
1	Be	2.5										
2	B	1.7										
3	B	2.0										
	B^{10}	1.5 (absorption subtracted)										
	B^{11}	1.6										
5	C					1.4	1.8	2.6	1.6	1.1		(1.7)
8	BeO					2.4	3.2	4.2	1.9	1.0		(2.7)
9	Al	2.4	1.6	1.7	1.9	1.4	1.6	2.0	1.0	0.7	0.4	1.4 (1.5)
10	Fe					2.2	2.8	3.6	1.2	0.8	0.5	2.0 (2.2)
12	Co	2.7							1.0	0.6	0.4	(2.1)
13	Cu	2.6	2.1	2.5	2.7	2.6	3.6	3.6	1.0	0.5	0.3	(2.1)
16	W					4.8	5.8	6.4	1.2	0.6	0.4	3.8 (3.6)
17	Au	4.8	4.3	4.7	4.8	5.6	6.6	7.0	0.9	0.4	0.3	(3.7)
18	Pb	4.6	3.9	4.5	4.7	4.2	4.8	5.2	2.3	1.9	1.5	4.1 (3.6)

always smaller than the count due to the scatterer.

Detector

The detector was the same as the one used for the experiments at 1.5 Mev except that it was filled with a mixture of 2 atmospheres of hydrogen and 4 atmospheres of argon. Since no neutron source was available, the energy of which could be varied continuously up to 3 Mev, no direct determination of bias energies was possible. Instead, the counting rate as a function of bias was measured for 3-Mev neutrons. It was assumed that the extrapolation of the bias curve to zero counting rate would give the pulse height corresponding to the primary energy and that other bias energies could be obtained by taking a linear dependence of pulse height on neutron energy.

Results

In Table VII the results obtained at $\alpha_0 = 60°$, neutron energy 2.8 Mev, are listed. Table VIII gives measurements carried out in the forward direction. The latter require an appreciable correction for the anisotropy of the source. The correction was calculated from the measured response of the detector when it was moved on a circle around the source. The last column of Table VIII shows calculated transport cross sections. The calculation of the transport cross sections assumes that there is no significant difference in the cross sections between 2.8 and 3.1 Mev. The correction for the anisotropy of the source was applied. In view of the fact that energy sensitivity curves for the detector were not available, the calculation of the transport cross section for light elements is subject to considerable uncertainty. Only the data taken at the low bias were used for obtaining the transport cross section for C and BeO, since the effect of energy loss in elastic encounters will be least noticeable at the low bias. Only the values of σ_t given without parentheses are corrected for multiple scattering.

Table IX gives a summary of inelastic cross sections. The lack of knowledge of the energy sensitivity of the detector made it impossible to determine inelastic cross sections for light elements.

TABLE IX. Inelastic scattering cross section for 3-Mev neutrons in barns.

Element	Below low bias	Below medium bias	Below high bias
Fe	0.3	0.7	1.1
	(0.5)	(1.0)	(1.4)
Cu	(0.6)	(1.3)	(1.5)
Au	(2.1)	(2.8)	(3.0)
W	1.4	2.4	2.8
	(1.8)	(2.5)	(2.8)
Pb	0.7	1.2	1.6
	(0.7)	(1.2)	(1.6)

ACKNOWLEDGMENTS

We are indebted to Professor J. H. Williams for allowing us to use the electrostatic generator and are grateful for the cooperation of the operating crews of the generator, in particular, Messrs. J. M. Blair, K. Greisen, A. O. Hanson, J. M. Hush, E. D. Klema, L. W. Seagondollar, R. F. Taschek, and C. M. Turner. Messrs. H. M. Agnew, G. Foster, K. Kupferberg helped in the operation of the Cockcroft-Walton set. The electronic equipment used in the experiments was designed and constructed by the Los Alamos electronics group under the direction of Dr. D. K. Froman and Mr. W. A. Higinbotham. Professor V. F. Weisskopf and Mr. P. Olum gave advice and help on theoretical problems throughout the experiments.

PHYSICAL REVIEW VOLUME 72, NUMBER 10 NOVEMBER 15, 1947

Thermal Neutron Activation Cross Sections†

LEO SEREN,* HERBERT N. FRIEDLANDER,** AND SOLOMON H. TURKEL***
Argonne National Laboratory, University of Chicago, Chicago, Illinois

(Received February 20, 1947)

The activation method of measuring slow neutron cross sections is discussed, in connection with the survey made at Argonne Laboratory. A table is given listing 131 activation cross sections of 65 elements and properties of the radio isotopes produced.

1. INTRODUCTION

MOST radioactive isotopes produced from natural isotopes by thermal neutron capture have half-lives and activities which have been observed in the laboratory. The charge-to-mass ratio of these artificially produced radioactive isotopes is usually too low for stability, so they emit β^--rays.[1] When the decay is complete, one β^--ray will have been emitted for every neutron which was captured by the original stable nucleus. Thus the counting of β^--rays enables the determination of the number of neutrons captured by certain isotopes. If, in addition, the thermal neutron flux is known, and the number of atoms doing the capturing is measured, the thermal neutron capture cross section can be calculated. This is the essence of the activation method of measuring neutron cross sections.[2] At the Argonne Laboratory in June, 1943 a program was started to measure as many thermal neutron activation cross sections as possible. This paper describes the experimental method and lists the cross sections measured. The work was all done on the graphite pile except that starting in July, 1944, irradiations were begun in the heavy-water pile.

Several of the 137 different half-lives produced by slow neutron capture gave rise to daughter activities, since the isotopes produced by β^--decay were not stable in these cases. An example is 26-min. $_{46}Pd^{111}$ produced by slow neutrons from $_{46}Pd^{110}$. A 7.5-day $_{47}Ag^{111}$ daughter activity was

† The work reported herein was part of a program of the Argonne Laboratory which was initiated by Dr. H. L. Anderson and for which he provided much of the technique and special apparatus. His guidance and invaluable counsel during the course of the work are hereby acknowledged. W. Sturm, W. Moyer, G. Miller, and H. Kubitscheck at various times rendered valuable assistance. H. H. Goldsmith contributed useful advice on isotopes and cross-section measurements in general.

The work was completed in October, 1944. It was done under contract between the Manhattan District, Corps of Engineers, War Department, and the University of Chicago, at the Argonne Laboratory.

* Present address: General Electric Research Laboratory, Schenectady, New York.

** Present address: Department of Chemistry, University of Chicago.

*** Present address: Nuclear Engineering Powered Aircraft Dept., Fairchild Engine and Airplane Corporation, P. O. Box 415, Oak Ridge, Tennessee.

[1] There are also several cases of positron emission, K-capture, and isomeric transition.

[2] The first surveys of slow neutron cross sections by the activation method were made independently by Franco Rasetti, Phys. Rev. **58**, 869 (1940) and R. D. O'Neal and M. Goldhaber *ibid.* **59**, 102 and 109 (1941).

formed, but $_{48}Cd^{111}$ is stable, ending the chain. The number of neutrons captured by the $_{46}Pd^{110}$ was computed from the β^--ray count of both $_{46}Pd^{111}$ and $_{47}Ag^{111}$.

2. DESCRIPTION OF MEASUREMENTS

A. Thermal Activation Formula $\nu = nv\sigma N$

When a thin detector is placed in the interior of a diffusing medium the number of thermal neutron captures per unit time is given by[3]

$$\nu = nv\sigma N$$

where nv = thermal neutron flux, σ = thermal neutron cross section (follows $1/v$ law), N = number of atoms of detector. Thus to calculate σ, the problem is to measure ν, nv, and N. Note that since σ is proportional to $1/v$, ν is really proportional to neutron density n.

B. Measurement of ν

To measure the number of neutron captures per unit time, the number of β-disintegrations per unit time was measured after the irradiation had been completed, and the detector foil observed to decay with the proper half-life. With the aid of the radioactive-decay laws, the number of β-disintegrations observed at a given decay time was reduced to the number of β-disintegrations at saturation, which equals the number of neutron captures per unit time. The β-disintegrations were recorded on either a Duraluminum (51 mg/cm²) or a mica-window (4 mg/cm²) Geiger counter. Beta-rays of maximum energy less than 0.85 Mev were always counted on the latter counter. The counting rate of the Geiger counter was converted into β-disintegrations per unit time by correcting for the geometrical and absorption loss of β-rays. The geometrical factor was computed by using UX_{II} and RaE β-ray standards. Since β-rays in the early part of their range are absorbed exponentially, the external and self-absorption loss of β-rays were computed with this exponential relationship. Thus the total efficiency of the counter was taken as

$$E = G \exp\left(-\frac{\mu}{\rho}x\right)$$

where G = geometry factor, μ/ρ = mass-absorption coefficient for the β-rays, and x = thickness of counter wall, foil cover, and half of foil thickness. For the UX_{II} and RaE β-ray standards, the mass-absorption coefficients were found to be 6.1 and 16.9 cm²/g Al, respectively, and using these values in the above formula the Duraluminum counter-wall thickness was found to be 51 mg/cm². This is equivalent to aluminum of 7-mil

TABLE I. Comparison of activation with transmission cross sections.

Element	Half-life	$\sigma_{capture}$ (from activation) (barns)	$\sigma_{total} - \sigma_{scattering}$* (from transmission) (barns)	Ratio: $\frac{\sigma_{capture\ from\ total\ activation}}{\sigma_{capture\ from\ transmission}}$
Rh	44 s	150		
	4.2 m	12.8		
	Total	162.8	150	1.09
Ag	22 s	51.3		
	2.3 m	25.3		
	225 d	1.1		
	Total	77.7	59.2	1.31
In	13 s	54		
	54 m	150		
	48 d	2.7		
	Total	206.7	189	1.09
Au	2.7 d	105	96	1.09

* $\sigma_{scattering}$ assumed to be 5×10^{-24} cm² and σ_{total} is for a neutron speed of 2200 meters/sec.

[3] H. A. Bethe, Rev. Mod. Phys. 9, 132 (1937).

thickness. For every different activity observed, the mass-absorption coefficient μ/ρ of the β-rays was measured.

C. Measurement of *nv*

Every substance irradiated in the thermal column was accompanied by a standard monitor (described below) for measuring *nv*. After calibration, *nv* was obtained by simply multiplying the saturated activity of the *nv* monitor by the calibration factor.

The calibration of the *nv* monitors was done by three methods. One calibration was made by using Mr. Kubitschek's apparatus.[4] This measures *nv* directly with BF_3 counter, and includes measurements of the cross section of the boron-trifluoride gas used, the velocity of the neutrons and the number of $B^{10}(n, \alpha)$ disintegrations per mole of gas and per unit area of neutron beam. This calibration made the cross sections come out 1.06 ± 0.03 lower than from the first standardization and was considerably more accurate.

Another check on the *nv* monitors was made by comparing the activation cross sections for the elements $_{45}Rh$, $_{47}Ag$, $_{49}In$, $_{79}Au$ with accurate transmission measurements made by Fermi (see Table I). These results made the cross sections come out by a factor 1.09 lower than the first standardization. These last two calibrations were for 2200-meters per second neutrons so that the cross sections measured were then automatically for 2200-meters per second neutrons.

The use of standard indium, manganese and copper monitors enabled all ranges of *nv* to be measured. The ranges for which *nv* could be conveniently measured were:

Indium	1×10^{2} to 1×10^{8} neutrons/cm²-sec.,
Manganese	2×10^{3} to 5×10^{6},
Copper	2×10^{5} to 1×10^{9},
Silver	1×10^{7} to 2×10^{11}.

The practical limit of irradiation which could be given to substances in the graphite pile thermal column was 10^{11} neutrons/cm². When greater irradiations were required, the substances were irradiated in the center of the pile.

The number of neutrons/cm²-kwh had been determined by standard indium foils measured at the same time that the watts being dissipated were determined from heating of a central uranium lump. A rough check on this value was made by computing the number of fissions necessary to give 1-watt power dissipation. Finally, this value was checked with the standard copper monitors which have no appreciable resonance activation.

Some substances were left in the center of the graphite pile for as long as two months. The number of kwh for any irradiation was determined from the gold-foil pile monitors, described by Mr. Sturm.

D. Measurement of *N*

The number of atoms of detector, N, was measured simply by weighing the foil on an analytical balance and dividing by the molecular weight of the compound. Substances which were not reagent grade were assayed by Mr. Bane's group of the Chemistry Division. For β-ray counting the powders were brushed on Scotch Tape over an area of 5 to 7.5 cm². The Scotch Tape was weighed before and after deposition of the powder and the accuracy of weighing was found to be 0.2 mg. The β-ray foils ranged in weight from 2 mg to $\approx$200 mg.

E. Types of Foils Used

For β-ray counting, foils were made by brushing a thin layer of the desired compound (ground up finely) onto Scotch Tape. The powder was spread over a measured area by means of a mask, and then covered with another layer of Scotch Tape. For long half-life activities, the powder was irradiated while spread out in a Lusteroid test tube. For short half-life activities it was necessary to make up the foil before irradiation, and irradiate together with the Scotch Tape covering. In a few cases of short half-life combined with small cross section it was necessary to irradiate a blank Scotch Tape foil and subtract from the measured foil the activity induced in the blank foil.[5] When very soft β-rays were being detected (example: $_{16}S^{35}$ with $\mu/\rho = 290$ cm²/g) the active deposit had no Scotch Tape cover.

[4] A description of standardization of neutron flux will be published in the Plutonium Project Report.

[5] The short half-life activity in Scotch Tape could be ascribed to 2.4-min. $_{13}Al^{28}$ and 14.8-hr. $_{11}Na^{24}$.

Metallic elements which could be obtained in a malleable state were prepared by rolling the pure element to the desired thickness (examples: $_{46}$Pd, $_{47}$Ag, $_{48}$Cd, $_{49}$In, and $_{50}$Sn).

Elements like gadolinium and samarium which have a very high total neutron capture cross section were irradiated by diluting the rare-earth oxide powder one-hundred fold with BeO powder. This dilution prevented self-absorption of neutrons, but reduced the accuracy somewhat because it was hard to mix the two powders homogeneously.

For counting x-rays and γ-rays, where a greater foil thickness was desired, the active substance was pressed in the form of a pellet in a 1-inch circular die with the aid of a hydraulic press. These pellets were from $\approx\frac{1}{2}$ mm to 4 mm thick. Substances which did not press easily could be rendered so by adding 1 part of inactive sulfur to 2 parts of the active substance.

F. Measurement of ν for x-rays and γ-rays

For the few isotopes which decayed by K-capture, the disintegration rate was determined by detecting either the K_α X-rays of the next lower element or by detecting the γ-rays when the disintegration energy levels were well known. The x-rays were always detected using the technique of Alvarez, i.e., by taking absorption coefficients in the proper adjacent elements, so as to display K-critical absorption edge, thus identifying the element emitting the x-ray.

The efficiency of the counter for different energy x-rays and gamma-rays was computed to enable a determination of the disintegration rate. The γ-ray efficiency of the counter was found experimentally to be $\frac{1}{2}$ percent for the 0.5-Mev annihilation γ-rays from $_{29}$Cu^{64} and was assumed to be proportional to the γ-ray energy.[6]

G. Discussion of Errors

The measurement of cross sections by the activation method is not an accurate measurement. The following discussion of the errors involved in the measurement of ν, $n\nu$, N and τ shows that the accuracy is limited 10 to 20 percent. With this in mind, the program at the Argonne Laboratory was aimed at a rapid survey of all the cross sections, rather than a precise measurement of a few of them.

Errors connected with the measurement of ν by detecting β-disintegrations are as follows: Gamma-rays which accompany the β-disintegration give rise to conversion electrons which the Geiger-counter counts as β-particles. This effect is more pronounced for soft γ-rays and high atomic number. The difficulty is that the fractional number of conversion electrons compared to the total β-ray spectrum is unknown for almost all radioactive isotopes. In one of the worst possible cases, that of $_{79}$Au^{198}, it was known that the conversion electrons comprised 14 percent of the β-ray spectrum. This correction was used in computing the cross section of $_{79}$Au^{197}, but was unknown for other isotopes and may make some of the calculated cross sections too high by as much as $\sim$15 percent. Note that isotopes which had β-rays of $\approx$1-Mev maximum energy or greater, and also had soft γ-rays of $\approx$0.4 Mev or less, were counted on the Duraluminum counter, which absorbed the conversion electrons completely.

The inaccuracy of the measurement of the mass-absorption coefficient of the β-rays and the extrapolation of the absorption of the β-rays in the counter wall to zero wall thickness give rise to errors as high as 15 percent.

Gamma-rays, when they accompany the β-disintegration, are also counted by the Geiger counter. But the sensitivity of the Geiger counter of 1-Mev gamma-rays is only 1 percent, so that gamma-rays may make the calculated cross section high by not more than $\sim$3 percent.

The calibration of the Geiger counters (geometrical factor and wall thickness) was done with four UX_{II} standards and three RaE β^--ray standards. The standards were prepared by weight and α-counting, respectively, and the average deviation in β^--counting rates was $\sim$4 percent, so that the calculated cross section could be rendered either high or low by this amount.

Geiger counters themselves change their sensitivity and plateau region with time. Even though β^--ray standards were always used to check the operation of the Geiger counters, it has been found by experience that individual foil counting rates check to only 2 percent.

Errors connected with the measurement of $n\nu$,

[6] F. Norling, Phys. Rev. **58**, 277 (1940).

TABLE II. Thermal neutron activation cross sections.

Item No.	Natural isotope (1)	Natural abundance (percent) (2)	Half-life of the $A+1$ isotope (3)	Isotopic cross section (barns) (4)	Natural atom cross section (barns) (5)	Probable error (percent) (6)	Mass-absorption coefficient of β-rays in cm^2/g of aluminum (7)	Substance used (8)	Place of irradiation (9)	(10)	Remarks (11)
1	$_8O^{18}$	0.20	31 sec.	0.00022	0.000,000,4	±20	2.56	Distilled H_2O	Pile	*	Cf. Phys. Rev. 70, 561 (1946).
2	$_9F^{19}$	100	12 sec.	0.0094	0.0094	±20	0.93	CaF_2	Pile		
3	$_{11}Na^{23}$	100	14.8 hr.	0.63	0.63	±20	8.1	NaCl Na_2CO_3	Pile		σ may be high due to conversion electrons.
4	$_{12}Mg^{26}$	11.1	10.2 min.	0.048	0.0054	±20	6.1	Mg-metal powder	Pile		
5	$_{13}Al^{27}$	100	2.4 min.	0.21	0.21	±20	2.5	Al foil	Thermal column		
6	$_{14}Si^{30}$	4.2	170 min.	0.116	0.00485	±20	8	Si metal powder	Pile		
7	$_{15}P^{31}$	100	14.3 d	0.23	0.23	±20	5.3	Red P powder	Pile		
8	$_{16}S^{34}$	4.2	87.1 d	0.26	0.011	±20	290	S flowers	Pile	*	
9	$_{17}Cl^{35}$	75.4	87.1 d for $_{16}S^{35}$	0.169	0.13	±20	290	NH_4Cl NaCl	Thermal column	*	This reaction $_{17}Cl^{35}(n, p)_{16}S^{35}$ goes with thermal neutrons.
10	$_{17}Cl^{37}$	24.6	37 min.	0.56	0.137	±20	8.7 3.2	NaCl	Thermal column		Two groups of beta-rays.
11	$_{19}K^{41}$	6.61	12.4 hr.	1.0	0.067	±20	2.56	K_2CO_3 $K_2C_2O_4H_2O$	Pile		
12	$_{20}Ca^{40}$	96.96	8.5 d	<0.000125	<0.00012	±40	K-capture X-rays	CaF_2 $CaCO_3$ $Ca(NO_3)_2$	Pile		See Table III.
13	$_{29}Cu^{64}$	2.06	180 d	0.63	0.013	±20	128 7.5	CaF_2	Pile		Two groups of β-rays. Ratio of soft to hard ~450
14	$_{20}Ca^{43}$	0.19	30 min.	0.55	0.00105	±20	~5.8	CaF_2 $CaCO_3$	Pile		See Table III. Nuclear isomer.
15	$_{20}Ca^{43}$	0.19	150 min.	0.205	0.00039	±20	5.8	CaF_2 $CaCO_3$	Pile		See Table III. Nuclear isomer.
16	$_{21}Sc^{45}$	100	85 d	22	22	±20	71	Sc_2O_3 $K_3Sc(SO_4)_3$	Pile		See Table III.
17	$_{22}Ti^{50}$	5.34	6 min.	0.141	0.0075	±20	5.4	Ti-metal powder	Pile		Half-life previously reported 2.8 min. We find 6 min. over 3 half lifes.
18	$_{22}Ti^{50}$	5.34	72 d	0.039	0.0021	±20	65	TiO_2	Pile		Nuclear isomer.
19	$_{23}V^{51}$	100	3.9 min.	4.50	4.50	±20	3.9	V_2O_5	Thermal column		
20	$_{24}Cr^{50}$	4.49	26.5 d	11	0.50	±40	K-capture conversion electrons	Cr_2O_3	Pile		See Table IV.
21	$_{24}Cr^{54}$	2.30	1.3 hr.	~0.0061	~0.00014	±40	~8.3	Cr_2O_3	Pile		Reported half-lifes of 1.6 to 2.3 hr. We find weak activity of 1.3 hours.
22	$_{25}Mn^{55}$	100	2.59 hr.	10.7	10.7	±20	4.85	Mn-metal powder	Thermal column		
23	$_{26}Fe^{58}$	0.28	47 d	0.36	0.0010	±20	43	Fe_2O_3	Pile	*	
24	$_{27}Co^{59}$	100	10.7 min.	0.66	0.66	±20	147 12.9	Co_2O_3	Thermal column		See Table III.
25	$_{27}Co^{59}$	100	5.3 yr.	21.7	21.7	±20	79	Co_2O_3	Pile		
26	$_{28}Ni^{64}$	0.88	2.6 hr.	1.96	0.0173	±20	7.3	Ni-metal NiO	Thermal column		
27	$_{29}Cu^{63}$	70.13	12.8 hr.	2.82	2.0	±20	33	Cu-metal powder	Thermal column		

TABLE II.—*Continued.*

Item No.	Natural isotope (1)	Natural abundance (percent) (2)	Half-life of the $A+1$ isotope (3)	Isotopic cross section (barns) (4)	Natural atom cross section (barns) (5)	Probable error (percent) (6)	Mass-absorption coefficient of β-rays in cm^2/g of aluminum (7)	Substance used (8)	Place of irradiation (9)	(10)	Remarks (11)
28	$_{29}Cu^{65}$	29.87	5 min.	1.82	0.56	±20	3.2	Cu-metal powder	Thermal column		
29	$_{30}Zn^{64}$	50.9	250 d	0.51	0.26	±20	107	Zn foil	Pile		See Table III.
30	$_{30}Zn^{68}$	17.4	57 min.	1.09	0.19	±20	17.1	Zn foil	Thermal column		Nuclear isomer.
31	$_{30}Zn^{69}$	17.4	13.8 hr.	0.31	0.054	±20	10.3	Zn foil	Pile		Nuclear isomer.
32	$_{31}Ga^{69}$	61.2	20 min.	1.40	0.855	±20	6.5	Ga_2O_3	Thermal column		
33	$_{31}Ga^{71}$	38.8	14.1 hr.	3.36	1.30	±20	9.6	Ga_2O_3	Pile		
34	$_{32}Ge^{70}$	21.2	40 hr.	0.073	0.0155	±20	25.7	GeO_2	Pile		Positron activity.
35	$_{32}Ge^{70}$	21.2	11 d	~0.45	~0.095	±40	*K*-capture X-rays	GeO_2	Pile	*	See Table III.
36	$_{32}Ge^{74}$	37.1	89 min.	0.38	0.14	±20	13.3	GeO_2	Pile		
37	$_{32}Ge^{76}$	6.5	12 hr.	0.085	0.0055	±20	7.8	GeO_2	Pile		
38	$_{33}As^{75}$	100	26.8 hr.	4.2	4.2	±20	4.3	As_2O_3	Thermal column		
39	$_{34}Se^{74}$	0.9	115 d	22	0.2	±40	*K*-capture X-rays	Se-metal powder	Pile	*	See Table III.
40	$_{34}Se^{78,80}$		19 min.		0.23	±20	7.9	Se-metal powder	Thermal column		Nuclear isomer.
41	$_{34}Se^{78,80}$		57 min.		0.017	±20	7.9 for daughter	Se-metal powder	Pile		Nuclear isomer.
42	$_{34}Se^{82}$	9.3	30 min.	0.060	0.0056	±20	15.6 for $_{35}Br^{82}$	Se-metal powder	Pile		σ calculated by observing 140 min. $_{35}Br^{82}$.
43	$_{35}Br^{79}$	50.6	18 min.	8.1	4.1	±20	6.4	KBr	Thermal column		Nuclear isomer.
44	$_{35}Br^{79}$	50.6	4.4 hr.	2.76	1.39	±20	5.3	KBr	Thermal column		Nuclear isomer.
45	$_{35}Br^{81}$	49.4	34 hr.	2.25	1.11	±20	35	KBr	Pile		
46	$_{37}Rb^{85}$	72.8	19.5 d	0.72	0.52	±20	6.7	$RbNO_3$	Pile		
47	$_{37}Rb^{87}$	27.2	17.5 min.	0.122	0.033	±20	2.6	$RbNO_3$	Thermal column		
48	$_{38}Sr^{88}$	9.86	2.7 hr.	1.29	0.128	±20	9.6 conversion electrons	$Sr(NO_3)_2$	Thermal column	*	See Table III.
49	$_{38}Sr^{88}$	82.56	55 d	0.0050	0.00415	±20	8.8	$SrCO_3$	Pile		
50	$_{39}Y^{89}$	100	60 hr.	1.24	1.24	±20	4.7	$Y_2(SO_4)_3$	Pile		
51	$_{40}Zr^{92}$	22	63 d	0.33	0.073	±40	60	Zr metal $ZrO(NO_3)_2$	Pile		Isotopic assignment not certain.
52	$_{40}Zr^{94}$	17	17.0 hr.	0.053	0.009	±20	9.4	Zr-metal powder	Pile		Gives rise to 75-min. $_{41}Cb^{95}$.
53	$_{40}Zr^{96}$	1.5	6 min.	~1.07	~0.016	±40	~5	Zr-metal powder	Thermal column		
54	$_{41}Cb^{93}$	100	6.6 min.	~1.0	~1.0	±40	9.5	Cb metal Cb_2O_5	Thermal column		Decay of $_{41}Cb^{94}$ is mainly by *K*-capture or isomeric transition. See Table III.
55	$_{42}Mo^{100}$	9.25	19 min.	0.475	0.044	±20	10	MoO_3	Pile		
56	$_{42}Mo^{98}$	24.1	67 hr.	0.415	0.10	±20	11.7	MoO_3	Pile		
57	$_{42}Mo^{92}$?		7 hr.		<0.001	±40	*K*-capture?	MoO_3	Pile		No 7-hr. activity was found.
58	$_{44}Ru^{102,104}$		4 hr.		0.122	±20	11	Ru-metal powder	Pile		

TABLE II.—*Continued.*

Item No.	Natural isotope (1)	Natural abundance (percent) (2)	Half-life of the $A+1$ isotope (3)	Isotopic cross section (barns) (4)	Natural atom cross section (barns) (5)	Probable error (percent) (6)	Mass-absorption coefficient of β-rays in cm^2/g of aluminum (7)	Substance used (8)	Place of irradiation (9)	(10)	Remarks (11)
59	$_{44}Ru^{?}$		37 hr.		0.15	±20	40	Ru-metal powder	Pile	*	Other investigators have reported a 20 hr. half life.
60	$_{44}Ru^{?}$		40 d		0.37	±20	161	Ru-metal powder	Pile	*	Other investigators reported 45±5 days.
61	$_{45}Rh^{103}$	100	44 sec.	137	137	±10	3.9	Rh-metal powder	Thermal column		Nuclear isomer.
62	$_{45}Rh^{103}$	100	4.2 min.	11.6	11.6	±10	4.4	Rh-metal powder	Thermal column		Nuclear isomer.
63	$_{46}Pd^{108}$	26.8	13 hr.	11.2	3.0	±20	16.1	Pd-metal foil	Thermal column		
64	$_{46}Pd^{110}$	13.5	26 min.	0.39	0.0525	±20	6.9	Pd-metal foil	Thermal column		Gives rise to 7.5 day $_{47}Ag^{111}$.
65	$_{47}Ag^{107}$	51.9	2.3 min.	44.3	23	±20	6.7	Ag-metal foil	Thermal column		
66	$_{47}Ag^{109}$	48.1	22 sec.	97.0	46.6	±20	2.9	Ag-metal foil	Thermal column		
67	$_{47}Ag^{109}$	48.1	225 d	2.3	1.1	±20	36.5	Ag-metal foil	Pile		σ computed assuming one particle per disintegration. Resonance contribution to the cross section is suggested by the work of M. Goldhaber, Phys. Rev. 70, 89 (1946).
68	$_{48}Cd^{114}$	28.0	2.5 d	1.1	0.30	±20	10.7	Cd-metal foil	Pile		Gives rise to 4.1 hr. $_{49}In^{115*}$
69	$_{48}Cd^{114}$	28.0	43 d	0.14	0.040	±20	7.0	Cd-metal foil	Pile	*	Cf. Seren *et al.*, Phys. Rev. 71, 409 (1947).
70	$_{48}Cd^{116}$	7.3	3.75 hr.	1.4	0.10	±20	8.5	Cd-metal foil	Pile		Gives rise to 2 hr. $_{49}In^{117}$.
71	$_{48}Cd^{?}$		2 min.		0.05	±20	5.7	Cd-metal CdO	Pile		
72	$_{49}In^{113}$	4.5	48 d	56.0	2.52	±10	6.35 for 72 sec. daughter	In-metal foil	Thermal column		Gives rise to 72-sec. $_{49}In^{114}$.
73	$_{49}In^{115}$	95.5	13 sec.	51.8	49.5	±10	5.4	In-metal foil	Thermal column		Nuclear isomer.
74	$_{49}In^{115}$	95.5	54 min.	144.6	138	±10	17.2	In-metal foil	Thermal column		Nuclear isomer.
75	$_{50}Sn^{119}$	1.1	105 d	~1.1	~0.012	±40	K-capture X-rays	Sn-metal foil	Pile	*	See Table III.
76	$_{50}Sn^{124}$	6.8	9 min.	0.574	0.039	±20	5.2	Sn-metal foil	Pile		
77	$_{50}Sn^{123}$		40 min.		0.0142	±20	13.6	Sn-metal foil	Pile		
78	$_{50}Sn^{123}$		26 hr.		0.072	±20	75	Sn-metal foil	Pile		
79	$_{50}Sn^{123}$		10 d		0.009	±20	66	Sn-metal foil	Pile		
80	$_{50}Sn^{123}$		400 d		0.018	±20	29	Sn-metal foil	Pile		
81	$_{51}Sb^{121}$	56	2.8 d	6.8	3.8	±20	~10	Sb-metal powder	Pile		
82	$_{51}Sb^{123}$	44	60 d	2.5	1.1	±20	14	Sb-metal powder	Pile		
83	$_{52}Te^{128}$	19.0	9.3 hr.	0.78	0.15	±20	27 2	Te-metal powder	Pile	*	Nuclear isomer.
84	$_{52}Te^{128}$	19.0	90 d	0.073	0.014	±20	~24	Te-metal powder	Pile	*	Nuclear isomer gives rise to 9.3-hr. Te^{127}.

TABLE II.—*Continued.*

Item No.	Natural isotope (1)	Natural abundance (percent) (2)	Half-life of the $A+1$ isotope (3)	Isotopic cross section (barns) (4)	Natural atom cross section (barns) (5)	Probable error (percent) (6)	Mass-absorption coefficient of β-rays in cm^2/g of aluminum (7)	Substance used (8)	Place of irradiation (9)	(10)	Remarks (11)
85	$_{52}Te^{128}$	32.8	72 min.	0.133	0.0436	±20	12.6	Te-metal powder	Pile	*	Nuclear isomer.
86	$_{52}Te^{128}$	32.8	32 d	0.0154	0.00504	±20	~12.6	Te-metal powder	Pile	*	Nuclear isomer. Gives rise to 72-min. Te^{129}.
87	$_{52}Te^{130}$	33.1	25 min.	0.222	0.0735	±20	7.1	Te-metal powder	Thermal column		Nuclear isomer. See Table III.
88	$_{52}Te^{130}$	33.1	30 hr.	<0.008	<0.003	±40	~7.1	Te-metal powder	Pile		Nuclear isomer. Gives rise to 25-min. Te^{131}.
89	$_{53}I^{127}$	100	25 min.	6.25	6.25	±20	5.33	PbI_2	Thermal column		
90	$_{55}Cs^{133}$	100	3 hr.	0.016	0.016	±20	~8	$CsNO_3$	Pile		Nuclear isomer.
91	$_{55}Cs^{133}$	100	1.7 yr.	25.6	25.6	±20	23	$CsNO_3$	Pile		Nuclear isomer.
92	$_{56}Ba^{138}$	71.66	86 min.	0.511	0.367	±20	7.9	BaO_2	Thermal column		
93	$_{57}La^{139}$	100	40 hr.	8.4	8.4	±20	9.6	La metal $La(NH_4)_2(NO_3)_5$	Pile		
94	$_{59}Pr^{141}$	100	19.3 hr.	10.1	10.1	±20	5.4	Pr_6O_7	Thermal column		
95	$_{62}Sm$?		21 min.		1.10	±20	8.25	Sm_2O_3	Thermal column		
96	$_{62}Sm^{152}$	26	46 hr.	138	35.8	±20	27.5	Sm_2O_3	Thermal column		
97	$_{62}Sm$?		60 d		<0.008	±40		Sm_2O_3	Pile		See Table III.
98	$_{63}Eu^{151}$	49.1	9.2 hr.	1380	681	±20	6.7	Eu oxalate	Thermal column		See Table III.
99	$_{63}Eu^{151,153}$		5–8 yr. (6.5 yr.)		390	±20	26	Eu oxalate	Pile		See Table III. This long period activity is due to both Eu^{152} and Eu^{154}. See M. G. Ingram and R. J. Hayden, Phys. Rev. 71, 130 (1947).
100	$_{64}Gd$?		9.5 hr.		2.3	±20	8.7	Gd_2O_3	Pile		Reported half-life is 8 hr.
101	$_{64}Gd$?		20 hr.		~0.9	±40	~20	Gd_2O_3	Pile	*	May be due to impurities in Gd_2O_3.
102	$_{64}Gd$?		8.6 d		~0.6	±40	~30	Gd_2O_3	Pile		May be due to impurities in Gd_2O_3.
103	$_{64}Gd$?		160 d		<0.25	±40		Gd_2O_3	Pile		No 160-day activity was found during 210 days decay.
104	$_{65}Tb^{159}$	100	3.9 hr.	10.7	10.7	±20	~10	Tb_4O_7	Thermal column		
105	$_{66}Dy^{164}$	27.6	140 min.	2620	725	±10	12.4	Dy_2O_3	Thermal column		Cadmium ratio is 97±7.
106	$_{66}Dy^{164}$	27.6	1.25 min.	120	33	±40	~50	Dy_2O_3	Thermal column		Our cross section assumes beta-ray decay and is probably erroneous because the later work of Ingraham, Shaw, Hess, and Hayden, Phys. Rev. 72, 515 (1947) indicates a soft gamma-ray decay (isomeric transition to the 140-min. activity).
107	$_{67}Ho^{165}$	100	30 hr.	59.6	59.6	±20	7.1	Ho_2O_3	Thermal column		Half-life sometimes given as 35 hr., but we find 30 hr.
108	$_{69}Tm^{169}$	100	105 d	106	106	±20	17.3	Tm_2O_3	Thermal column		

TABLE II.—*Continued.*

Item No.	Natural isotope (1)	Natural abundance (percent) (2)	Half-life of the $A+1$ isotope (3)	Isotopic cross section (barns) (4)	Natural atom cross section (barns) (5)	Probable error (percent) (6)	Mass-absorption coefficient of β-rays in cm^2/g of aluminum (7)	Substance used (8)	Place of irradiation (9)	(10)	Remarks (11)
109	$_{71}Lu^{175,176}$		3.4 hr.		15.9	±20	12.0	Lu_2O_3	Thermal column		
110	$_{71}Lu^{176}$	2.5	6.6 d	3640	91.0	±20	50.0	Lu_2O_3	Thermal column		Refer to Ingram *et al.*, Phys. Rev. 71, 270 (1947).
111	$_{72}Hf^{180}$	35.14	46 d	10.0	3.5	±20	47.0	$HfOCl \cdot 7H_2O$	Pile		Listed half-life is 55 days. We find 46±3 days over 2½ half lifes.
112	$_{73}Ta?$		16.2 min.		0.034	±20	85	Ta-metal foil	Thermal column	*	See Table III. Cf. Seren, Friedlander, and Turkel, Phys. Rev. 72, 163 (1947).
113	$_{73}Ta^{181}$	100	117 d	20.6	20.6	±20	46	Ta-metal foil	Thermal column		$\int \sigma \frac{dE}{E} = 800$ See Table III.
114	$_{74}W^{184}$	30.1	77 d	2.12	0.64	±20	70	W-metal powder	Pile		
115	$_{74}W^{186}$	29.8	24.1 hr.	34.2	10.2	±20	20.7	W-metal powder	Thermal column		
116	$_{75}Re^{185}$	38.2	90 hr.	101	38.5	±20	16.9	Re-metal powder	Thermal column		
117	$_{75}Re^{187}$	61.8	18 hr.	75.3	46.5	±20	5.5	Re-metal powder	Thermal column		
118	$_{76}Os^{190}$	26.4	30 hr.	2.50	0.66	±20	14.5	Os-metal powder	Pile		Literature half-lives are 29 hr. and 32±2 hr. We find 30 hr.
119	$_{76}Os^{192}$	41.0	17 d	5.34	2.19	±20	187	Os-metal powder	Pile		
120	$_{77}Ir^{191}$	38.5	1.5 min.	260	100	±40	~28 Isomeric transition	Ir-metal powder	Thermal column		This isomer decays into the 70 days activity listed below. See Table III.
121	$_{77}Ir^{191}$	38.5	70 d	1000	388	±20	33.5	Ir-metal powder	Thermal column		Half-life in literature is 60 days. We find 70±2.5 days. The cross section listed here *includes* the contribution from 1.5-minute activity. See Table III.
122	$_{77}Ir^{193}$	61.5	20.7 hr.	128	79.0	±20	6.1	Ir-metal powder	Thermal column		Half-life in literature is 19 hr. We find 20.7±5 hr.
123	$_{78}Pt^{196}$	26.6	18 hr.	1.1	0.30	±20	26	Pt-metal foil	Pile		
124	$_{78}Pt^{196}$	26.6	3.3 d	4.5	1.20	±20	114	Pt-metal foil	Pile		See Table IV.
125	$_{78}Pt^{198}$	7.2	31 min.	3.92	0.292	±20	9.4	Pt-metal foil	Thermal column		
126	$_{79}Au^{197}$	100	2.7 d	96.4	96.4	±10	19.3	Au-metal foil	Thermal column		A 14 percent correction for conversion electrons has been made.
127	$_{80}Hg^{204}$	6.7	5.5 min.	0.34	0.0228	±20	9.4	HgO powder	Thermal column		
128	$_{80}Hg^{202,204}$		51.5 d		0.725	±20	77	HgO powder	Pile		
129	$_{81}Tl^{203}$	29.1	4.23 min.	0.273	0.079	±20	10	$TlNO_3$	Thermal column		
130	$_{81}Tl^{205}$	70.9	3.5 yr.	3.1	2.2	±20	25.6	$TlNO_3$	Pile		
131	$_{84}Bi^{209}$	100	5.0 d	0.015	0.015	±20	16.0	Bi-metal powder	Pile		

the thermal neutron flux, are as follows: After intercalibrating the standard indium monitors with the standard manganese and copper monitors, the effect on the calculated value of the cross sections was about ±15 percent. The nv determinations from gold-foil pile monitors was only accurate to ±15 percent. This largest source of error was reduced considerably by two other independent nv calibrations (Kubitschek's BF_3 counter and cell and comparison with Fermi's transmission measurements) each of which were accurate to about 3 percent. As a result of these calibrations, all the cross sections measured in the thermal column were reduced by the factor 1.09.

Errors connected with the measurement of N, the number of atoms on the foil, were: The accuracy of weighing on the analytical balance was 0.2 mg, so for the lightest foils of 2.0 mg this leaves an error of ±10 percent, and considerably less on the heavier foils. The error of assay was quite small, less than 0.3 percent.

Errors connected with the measurement of τ, the mean life, arose as follows: In general, no attempt was made to accurately measure the half-life, and the value listed in Seaborg's table of radioactive species was taken. In a few cases the value listed was found to be quite different from the observed half-life. The latter was then used. These are noted under "Remarks" in the tables. An example is 60-day iridium which we followed for 2 half-lives and found 70±2.5 days. The error in half-life is thus probably less than 5 percent unless stated otherwise.

In general the error for any calculated cross section was less than the sum of all the errors listed above. For each cross section listed in Table III the probable error was computed on the basis of the number of trial runs made, the type of radiation detected, the strength of the β-rays, and the presence or absence of gamma-rays. The probable errors are listed as ±10, ±20, or ±40 percent.

3. RESONANCE NEUTRON ACTIVATIONS

The survey of all the slow neutron activities was conducted by irradiating in the thermal column of the graphite pile. But when this did not give sufficient intensity, the substances were irradiated in the center of the pile[7] where the thermal flux was 470 times greater, and, in addition, resonance neutrons from fission energy and below were present. Thus substances which received pile neutron irradiations were activated by resonance neutrons in addition to thermal neutrons. *The exact contribution from resonance activation was unknown, hence, was not subtracted off in the calculation of the thermal cross section.* However, the following will show that the resonance contribution was small for most cases.

Column 9 of Table II indicates that pile irradiations were used mostly[8] for substances with low thermal cross sections. Low thermal cross sections usually indicate a very small value of $\int\sigma(E)dE$, and hence would give very little resonance activation.

Substances prepared for pile irradiation were spread out in a Lusteroid test tube lying flat in the center of the pile. This allowed 95 percent or more transmission in the thermal region, but resonance neutrons would be strongly self-absorbed. The strong resonance absorption is caused by the sharp peaks in the resonance cross-section *vs.* energy curve.[9] Hence, the self-absorption reduces the resonance activation.

The intended program at Argonne included the measurement of $\int\sigma(E)dE/E$ for all activities possible, but because of more urgent experiments, only a few of these values have been obtained so far. Mr. W. Sturm has developed the technique and will report on it independently. The value of $\int\sigma(E)dE/E$ for a few activities was obtained by measuring cadmium ratios, as follows:

$$\frac{\nu_{\text{res}}}{\nu_{\text{thermal}}}=\frac{(q\lambda/\xi)N\int\sigma(E)dE/E}{nv\sigma(v)N}.$$

Now $nv/q=390$ cm from the observed cadmium ratio in the graphite pile with standard indium

[7] Except that after July, 1944, the thermal column of the Argonne heavy-water pile was used whenever possible.

[8] More explicitly, pile irradiations were used for substances for which σ_{atom}/half-life was quite small, so that a few substances with a very long half-life received pile irradiations in spite of rather large cross section; for example ${}_{27}Co^{59}$ giving rise to a 5.5-year activity with $\sigma=22.5\times10^{-24}$ cm².

[9] The 1.4-ev resonance of 54-min. ${}_{49}In^{116}$ has been investigated with a velocity selector by W. W. Havens, Jr. and J. Rainwater, Phys. Rev. 70, 154 (1946) and has a peak value of $26{,}000\times10^{-24}$ cm².

foils. Also for graphite, $\lambda=2.7$ cm and $\xi=0.158$. Using A for activity instead of ν for capture processes.

$$\int \sigma(E)dE/E = 22.8(A_{\text{res}}/A_{\text{thermal}})\sigma(v).$$

Since

$$A_{\text{no Cd}}/A_{\text{with Cd}} = (A_{\text{res}}+A_{\text{thermal}})/A_{\text{res}} = \text{C. R.},$$

the desired ratio is then

$$A_{\text{res}}/A_{\text{thermal}} = 1/[\text{C. R.}-1].$$

The cadmium ratio (C. R.) is determined by irradiating identical foils, one covered with cadmium, in the center of the pile. The foils were made thin enough to allow a resonance peak of $30{,}000\times10^{-24}$ cm^2. The values of $\int\sigma(E)dE/E$ found are listed in column 11 of Table II.

4. COMPARISON OF ACTIVATION METHOD WITH OTHER METHODS OF MEASURING SLOW NEUTRON CROSS SECTIONS

The other methods of measuring slow neutron cross sections utilize the absorption properties of the total atom, rather than specific isotopes. In a beam geometry the intensity of the beam both with and without the absorbing element is measured by a suitable thermal neutron detector. The general scheme of measuring the reduction of intensity of thermal neutrons by a known weight of the desired absorber can also be applied in a diffusing medium of thermal neutrons, such as paraffin or graphite, and also at the surface of such a medium.[10] Volz[11] utilized a Helmholtz tube filled with radon gas and beryllium to obtain a uniform density of neutrons in water. With the advent of the chain-reacting pile, it has been found possible to measure absorption effects quite accurately by poisoning a few cells with the desired element.[12] Calibration is then made by a similar poisoning with a "black" substance (such as cadmium) of known area. All of the methods which utilize a diffusing medium measure the absorption cross section of the atom, while the beam geometry measures the absorption plus the scattering cross section.

The main differences between measuring the absorption cross section by the absorption and activation methods are:

(1). The absorption method measures the cross section for the whole atom, whereas the activation method measures the cross section for the isotope producing the observed activity. For elements with only one stable isotope, the results should be essentially the same.

(2). The absorption method requires the order of grams to kilograms of material, while the activation method requires the order of milligrams. Volz[11] used from 1 to 4200 grams of the different elements in his survey, while β-ray foils in this survey were from 2 to 200 milligrams.

(3). The absorption method requires the element to be either in pure form or in a compound with other elements whose cross sections are very much smaller. The activation method requires only that the desired induced activity can be separated from the induced activity of all other isotopes present. This property of the activation method allows a wide choice of compounds. For example, it was found possible to measure the cross section of $_{11}Na^{23}$ by using NaCl. However, $_{17}Cl$ has a cross section which is about 50 times greater than $_{11}Na^{23}$, so that this compound could not be used for the absorption method.

(4). When the scattering cross section is of the same order or larger than the absorption cross section, it is not possible to use the beam-absorption method, but the activation method is not even affected by scattering.

5. ACTIVATION CROSS SECTIONS MEASURED

In Table II, the first column lists the isotope, the second column gives the percent natural abundance of this isotope, the third column gives the half-life of the $(A+1)$ isotope (i.e., the isotope produced by neutron capture). Note that the half-life enters into the value of the cross section, and any small change in the accepted value of the half-life would mean a linear change in the cross section value. The cross sections for the isotope and natural atom are given in columns 4 and 5, respectively, and refer to a neutron velocity of 2200 meters per second (one barn equals 10^{-24} cm^2). Note that column 4 is obtained by dividing the value of column 5 by that of column 2. In column 6 is given an estimate of the probable error (see Section 2G). The external absorption coefficient of the β-ray activity, as measured with aluminum absorbers, is given in column 7. Two values are given in column 7 when two distinct groups of β-rays

[10] J. W. Coltman and M. Goldhaber, Phys. Rev. 69, 411 (1946), measured the capture cross sections of 19 elements in this manner.

[11] Helmut Volz, Zeits. f. Physik 121, 201 (1943) measured the absorption cross section of 49 elements in this manner.

[12] A. Wattenberg has investigated about 50 elements in this manner. See Anderson, Fermi, Wattenberg, Weil, and Zinn, Phys. Rev. 72, 16 (1947).

could be separated. Column 8 gives the type of foils used and column 9 the place of irradiation, and column 11 gives pertinent remarks. Pile irradiations may result in high cross sections because resonance effects have not been subtracted (see Section 3). An asterisk (*) in column 10 indicates that the production of the radioisotope by thermal neutrons had not been reported in the literature previous to this work.

Table III gives information about certain isotopes decaying by K-capture and new properties of isotopes discovered in our survey.

TABLE III. Additional remarks concerning certain isotopes.

Remarks

$_{20}Ca^{40}(n, \gamma)_{20}Ca^{41}$ 8.5 day

The reported $_{20}Ca^{41}$ isotope decays by K-capture. An attempt was made to observe the 1.1 Mev γ-ray accompanying each disintegration. The observed activity did not show a fixed half-life but tailed off from 6.1 days to $\gg$8.5 days. Hence, the upper limit of cross section was computed. The last run was made with especially pure $Ca(NO_3)_2$ from which $CaCO_3$ was precipitated out after irradiation. *Note added in proof:* Overstreet and Jacobson, Phys. Rev. **72**, 349 (1947), also fail to find this reported 8.5-day Ca activity.

$_{20}Ca^{48}(n, \gamma)_{20}Ca^{49}$ 30 min., 150 min.

The decay of $_{20}Ca^{49}$ required a somewhat unusual treatment to obtain the cross sections because its isomeric activities of 150-minutes and 30-minutes half-life, both give rise to the same 57-minute half-life daughter, $_{21}Sc^{49}$. This in turn decays to the stable $_{22}Ti^{49}$. Graphs were first drawn from values obtained from the theoretical equations of such relationship in order to study the decay. These were approximate because the equations assumed the initial number of daughter atoms to be zero, whereas they actually were growing and decaying exponentially with the decay of the parent while being irradiated. A general equation was then derived in which the entire activity, without approximations, was extrapolated to include all the growth and decay, during irradiation and afterwards. The cross sections submitted are a result of the application of this equation.

$_{21}Sc^{45}(n, \gamma)_{21}Sc^{46}$ 85 day

The cross section was computed by assuming 95 percent decay by β-rays and 5 percent by K-capture, from Walke, *et. al.*, Proc. Roy. Soc. London **A171**, 372 (1939).

$_{24}Cr^{50}(n, \gamma)_{24}Cr^{51}$ 26.5 day

Cross section computed by observing the γ-rays and assuming 0.03γ per disintegration, from Walke, *et. al.*, Phys. Rev. **57**, 171 (1940).

$_{27}Co^{59}(n, \gamma)_{27}Co^{60}$ 10.7 min.

Concerning the 10.7-minute Co^{60}, Livingood and Seaborg[1] suggested that the radiation consisted largely of conversion electrons resulting from an isomeric transition to the longer lived (5.3 year) Co^{60}. Later Nelson, Pool, and Kurbatov[2] claimed that the radiation was that of continuous beta-rays of end point 1.35$\pm$0.1 Mev and a γ-ray of 1.5$\pm$0.02 Mev but no conversion electrons. Finally, Deutsch and Elliott[3] found that the direct transitions constitute only 10 percent or less of the disintegrations. The β-ray has a maximum energy of 1.50$\pm$0.15 Mev and is followed by a γ-ray. At least 90 percent of the disintegrations proceed by an isomeric transition; a 0.056$\pm$0.003-Mev γ-ray with corresponding conversion electrons. Our findings are, as a whole, in accord with that of Deutsch and Elliott. We find that 10.8 percent or less of the disintegrations produce a β-ray whose μ/ρ in Al is 12.9 cm^2/g while the rest of the disintegrations (89.2 percent) show up in the form of low energy electrons whose μ/ρ in Al is 147.5 cm^2/g. These low energy electrons must have been produced by a γ-ray of greater than 0.07 Mev in order for our counter to observe them. The cross section has been calculated on the basis of this β-, γ-branching, assuming that each particle (hard or soft) represented a disintegration.

$_{30}Zn^{64}(n, \gamma)_{30}Zn^{65}$ 250 day

Cross section computed assuming 0.6γ per disintegration and 5 percent of disintegration by positron emission. Deutsch, Roberts, and Elliot, Phys. Rev. **61**, 389A (1942).

$_{32}Ge^{70}(n, \gamma)_{32}Ge^{71}$ 11 day

By means of critical absorption in different elements, it was verified that the x-rays observed from 11-d. germanium are actually gallium x-rays, hence come from K-capture of 11-d. germanium. From Compton and Allison's book on x-rays, p. 784 and p. 792.

$_{31}Ga$ K_α x-ray line is 1.34A.
$_{32}Ge$ K_α x-ray line is 1.255A.
$_{29}Cu$ K-absorption limit is 1.37A.
$_{30}Zn$ K-absorption limit is 1.28A.

We observed very marked absorption in copper, but very little absorption in zinc, showing that the x-ray was a Ga K_α-x-ray. Mass-absorption coefficients observed are:

for Scotch Tape (hydrogen, carbon, oxygen)	6.13 cm^2/g
for 13 aluminum	40.8
for 29 copper	165.0
for 30 zinc	57.8

The energy of the Ga K_α-x-ray is only 9.23 kilovolts. No β-rays or electrons were observed. The efficiency of the mica-window Geiger counter for these x-rays was computed by using a value of the mass-absorption coefficient in argon from Compton and Allison, p. 802. The counter was filled with a 10 to 1 mixture of argon-alcohol, but the contribution from the alcohol was negligible.

$_{34}Se^{74}(n, \gamma)_{34}Se^{75}$ 115 day

$_{34}Se^{75}$ has been reported as a K-capture isotope with a half-life of 48 days and also of 160 days. We found a K-capture activity produced by an (n, γ) reaction on selenium with a half-life of 115$\pm$5 days. One sample has been followed for over 180 days. This is the first report of this activity produced by an (n, γ) reaction. To prove that this was a selenium activity, 99.9964 percent pure Hilger Spectroscopic selenium was irradiated in the Argonne pile. From the active material $_{32}Ge$, $_{33}As$, and $_{35}Br$ were separated. No activity was found in any of these fractions. The $_{34}Se$ fraction was then found to contain all the original activity. The K-capture decay to stable As^{75} was demonstrated both in the cloud chamber and by x-ray critical absorption edges which show that arsenic K x-rays are produced. The arsenic K x-rays are more strongly absorbed in gallium than in germanium; while the selenium K x-rays would be weakly absorbed in both. Gallium and germanium absorbers were

TABLE III.—*Continued.*

Remarks
prepared and the following mass-absorption coefficients were obtained: μ/ρ for $_{13}$Al = 42 cm²/g, μ/ρ for $_{31}$Ga = 102 cm²/g, μ/ρ for $_{32}$Ge = 56 cm²/g. Several γ-rays were found by absorption in lead including an intense one of about 0.4 Mev. The cross section was calculated both on the basis of the cloud-chamber work, an estimation of the counters efficiency for arsenic K x-rays, and on the basis of an estimated efficiency for the γ-rays. The three calculations checked fairly well. A weighted average of these calculations is reported for the cross section. To prove that this activity was that of Se^{75}, arsenic (which consists of only one isotope, As^{75}) was bombarded at the St. Louis cyclotron with 12-Mev deuterons thereby producing Se^{75} by a $(d, 2n)$ reaction. This is the only possible selenium isotope that could be produced which is not stable. The selenium was then separated from the arsenic and the decay of this sample has been followed for a month. It too gives a half-life of 115±10 days. Cf. Friedlander, Seren, and Turkel, Phys. Rev. **72**, 23 (1947).
$_{38}Sr^{86}(n, \gamma)_{38}Sr^{87*}$ 2.7 hr.
The 2.7-hr. activity of Sr is due to $_{38}Sr^{87*}$, an isomer of the stable isotope. In the past this isotope has easily been produced by fast neutrons on Sr with some indication that the reaction $_{38}Sr^{86}(n,$ gamma$)Sr^{87*}$ also took place. Stewart, *et al.* (Phys. Rev. **52**, 901 (1937)) produced 2.7-hr. $_{38}Sr^{87*}$ by irradiating Sr inside of a few cm of paraffin with Li+D neutrons. Although thermal neutrons were present, the few cm of paraffin could not remove all the fast neutrons, so the experiment was not conclusive. H. Reddeman (Naturwiss. **28**, 110 (1940)) showed that the fast neutron activity on Sr was due to the $_{38}Sr^{87}(n, n)_{38}Sr^{87*}$ reaction. By irradiating in the same geometry with fast *and slow* neutrons, the 2.7-hr. activity was doubled, thus indicating that the reaction $_{38}Sr^{86}(n, \gamma)_{38}Sr^{87*}$ also took place. In the thermal column of the Argonne pile (where the cadmium ratio is >20,000) we irradiated $Sr(NO_3)_2$ and observed the 2.7-hr. $_{38}Sr^{87*}$ activity. Since no fast neutrons are found in the thermal column, this seems to indicate conclusively that the reaction $_{38}Sr^{86}(n, \gamma)_{38}Sr^{87*}$ does take place. The identification of our slow neutron produced activity as Sr^{87*} was made from (a) the 2.7-hr. half-life, (b) the shape of the absorption curve which clearly indicated conversion electrons instead of a continuous β-ray spectrum, (c) the end point of the particles of 0.36 Mev, all of which agree with the properties of Sr^{87*} listed in Seaborg's tables. Cf. Seren, Engelkemeir, Sturm, Friedlander, and Turkel, Phys. Rev. **71**, 409 (1947).
$_{41}Cb^{93}(n, \gamma)$ 6.6 min.
The radio-isotope produced decays either by K-capture or isomeric transition. We are indebted to M. Goldhaber and W. J. Sturm **70**, 111 (1946), who discovered this, and corrected our old erroneous value of the cross section based on Cb^{94} β^- decay.
$_{50}Sn^{112}(n, \gamma)_{50}Sn^{113}$ 105 day
The indium x-rays produced by the K-capture of $_{50}Sn^{113}$ were detected by taking absorption curves with $_{45}$rhodium, $_{46}$palladium, and $_{47}$silver absorbers. From Compton and

Remarks
Allison's book on x-rays: For 49 Indium: $\lambda K_{\alpha 2} = 0.5155$A, $\lambda K_{\alpha 1} = 0.5111$A, $\lambda K_{\beta 2} = 0.4542$A, $\lambda K_{\beta 1} = 0.4536$A, $\lambda K_{\beta 2} = 0.4441$A K-critical absorp λ's: for $_{45}$Rh, λ = 0.5330A; $_{46}$Pd, λ = 0.5080A; $_{47}$Ag, λ = 0.4845A Note that both the $K_{\alpha 1}$ and $K_{\alpha 2}$ x-ray lines of $_{49}$In would be strongly absorbed in $_{45}$Rh but not in $_{46}$Pd or $_{47}$Ag. The $K_{\alpha 1}$ and $K_{\alpha 2}$ comprise 84.3 percent of the x-ray transitions of $_{49}$In and the K_β lines the remainder. On the absorption curve, the absorption points taken with $_{45}$Rh absorbers fall lower than the $_{46}$Pd or $_{47}$Ag absorber points due to the presence of In K_α x-rays. The Sn foil was covered first with lucite to remove all the electrons. S. W. Barnes has produced the Sn^{113} isotope by proton bombardment of $_{49}$In and finds 2 γ-rays, 0.85 Mev and 0.39 Mev in equilibrium with the 105 day x-rays.
$_{52}Te^{130}(n, \gamma)_{52}Te^{131}$ 25 min., 30 hr.
Both the 25-min. and 30-hr. periods induced in $_{52}Te^{130}$ by neutron-capture decay into 8.0 day $_{53}I^{131}$. The cross section computed on the basis of the latter activity is almost exactly equal to the cross section computed on the basis of the former two activities, but this is more of a coincidence rather than a demonstration on the accuracy of our measurements. Note that the cross section of all three isotopes $_{52}Te^{126, 128,}$ and ^{130} is only 0.287×10^{-24} cm² per natural atom.
$_{62}Sm(n, \gamma)_{62}Sm$ 60 day
No 60-day activity was found. The decay showed a half life of 46 hours for 33 days, and then leveled off into some activity of half-life >3 years.
$_{63}Eu(n, \gamma)_{63}Eu$ 9.2 hr, 5–8 yr.
The 9.4-hr. $_{63}Eu^{152}$ and 6.5-year $_{63}Eu^{152, 154}$ have been found to emit negative particles (Fajans and Steward, Phys. Rev. **56**, 625 (1939)). Hence the mode of disintegration seems to be β-rays, although the possibility of K-capture exists because $_{62}Sm^{152}$ and $_{62}Sm^{154}$ are stable as well as $_{64}Gd^{152}$ and $_{64}Gd^{154}$. The cross sections reported here assume β-ray disintegrations, and K-capture would make the cross sections even larger because the Geiger counter is less sensitive to x-rays than to β-rays. The cross section of long-period Eu was computed assuming that the half-life was 6.5 years, since it is reported from 5 to 8 years.
$_{73}Ta(n, \gamma)_{73}Ta$ 16.2 min., 117 day
$_{73}$Ta has only one known stable isotope. A new period of 16.2±0.5 minutes was discovered by irradiating tantalum in the heavy-water pile thermal column. The well known ~100-day $_{73}Ta^{182}$ is also produced by slow neutrons. The new 16.2-minute activity was shown to be tantalum because (1) Very pure (99.9 percent) tantalum foil gave this activity when irradiated with only slow neutrons. (2) No other element gives a known 16.2-minute activity with slow neutrons, hence it is unlikely that the observed activity was due to an impurity. (3) Finally, the element, was confirmed as Ta by chemical separations. A soluble salt, $(NH_4)_2TaF_7$, was irradiated in the thermal column and then put into Hf solution. Addition of NH_4OH precipitates the tantalum, which was then washed, redissolved, reprecipitated, and counted. The ratio of short period to long period β-rays was found to be

TABLE III.—*Continued.*

Remarks
the same for (a) the chemically separated, Ta, (b) the unseparated $(NH_4)_2TaF_7$ salt, (c) the Ta metal foil. This shows that both activities are produced by slow neutron capture of $_{73}$Ta. The new 16.2-min. Ta activity may be an isomer of the ~100-day $_{73}Ta^{182}$ activity or it may be produced by an undiscovered stable isotope. The former possibility would require two independent β-ray transitions because the 16.2-min. activity does not show any growth after short irradiation, and the shape of its absorption curve indicates a continuous β-ray spectrum rather than a line of conversion electrons. The β-rays of 16.2-min. Ta have a short range of ~50 mg/cm^2 Al or ~0.2 Mev., and a γ-ray or x-ray is also present. It is difficult to explain the low energy β-ray for such a short half-life. Tantalum and caesium seem to be strikingly similar in that both have only one stable isotope, give rise to two periods upon slow neutron capture, and the long period has a cross section of the order 1000 times greater than that for the short period. Concerning the long-period $_{73}Ta^{182}$, we have followed the decay for 2 half-lives and find 117 days ±3 days instead of 97 days which is listed in the tables. Our value of 117±3 days is confirmed by Zumstein, *et al*, Phys. Rev. **63**, 59 (1943). Using this value half-life, a new value of the cross section for *thermal* neutrons was obtained by irradiating in the heavy-water pile thermal column. This value is 40 percent lower than the previously reported value obtained by irradiating in the center of the graphite pile. That the difference was due to *resonance* capture was checked by obtaining the cadmium ratio of 1.6 for the 11 mg/cm^2 Ta foil.
$_{77}Ir^{191}(n, \gamma)_{77}Ir^{192}$ 1.5 min., and 70 day We are indebted to M. Goldhaber, C. O. Muehlhause and S. J. Turkel, Phys. Rev. **71**, 372 (1947), who called to our attention the fact that the 1.5-min. Ir^{192} decays into its 70-day isomeric state.
$_{78}Pt^{196}(n, \gamma)_{78}Pt^{197}$ 3.3 day As much as 0.5 barns of the reported natural atom cross section of 1.2 barns may be due to 3.3-day activity of $_{79}Au^{199}$ formed by the decay of $_{78}Pt^{199}$.

[1] Livingood and Seaborg, Phys. Rev. **60**, 913 (1941).
[2] Nelson, Pool, and Kurbatov, Phys. Rev. **62**, 1 (1942).
[3] Deutsch and Elliott, Phys. Rev. **62**, 559 (1942).

Cloud-Chamber Energy Measurement of Photo-Neutron Sources*

D. J. HUGHES AND C. EGGLER
Argonne National Laboratory, Chicago, Illinois

(Received August 4, 1947)

The energy distributions of the neutrons from several photo-neutron sources have been measured by means of the range distribution of recoil protons produced in a hydrogen-filled cloud chamber. It is shown that slowing-down in the source itself produces a broad spread in energy instead of the almost monoenergetic spectrum to be expected from a single γ-energy. The values of the mean neutron energy, E, and the maximum energy, E_M, for the sources measured are as follows:

Source	E (kev)	E_M (kev)
Na−Be	800	1020
Na−D_2O	220	320
Mn−Be	300	375
	<150	<150
In−Be	300	400
	<150	<150
Sb−Be	35	68

As the E_M values should be directly related to the energies of each of the γ-sources, they are compared to the γ-energies as reported by different observers for each source.

I. INTRODUCTION

THE advent of chain-reacting piles has made available intense γ-sources which can be used to produce photo-neutrons by the photo-disintegration of the deuteron or of beryllium. Such photo-neutron sources have proved to be extremely useful and convenient neutron sources in the region 30 kev to 1 Mev. If only a single γ-ray above the photo-disintegration threshold is present and the amount of deuterium or beryllium is very small, then the emitted neutrons show practically no spread in energy. Such a monoenergetic neutron source is, of course, much superior to the usual Ra (α) Be source with its great spread in neutron energy. Actually, in order to obtain sufficient intensity the amount of deuterium or beryllium which must be used is large enough so that significant moderation of the neutrons occurs by elastic scattering, and a broad band of energies results.

During the year 1944 Wattenberg[1] investigated the production and calibration of photo-neutron sources, using various γ-emitters produced in the Argonne pile. The γ-sources were surrounded by amounts of deuterium or beryllium about one centimeter in thickness in order to obtain sufficient intensity, and, as a result, the nearly monoenergetic neutrons emitted in the photo-disintegration were slowed down appreciably in the surrounding material. Wattenberg estimated the average energy of his sources by measuring the average scattering cross section of hydrogen for the neutrons of each source. The energy corresponding to the observed hydrogen cross section was then obtained from the curve of Bohm and Richman.[2] The energies as determined from the hydrogen scattering were always less than that expected from the γ-energy, thus showing that the moderator did have a definite effect in lowering the average neutron energy.

In order to aid in the understanding of the actual energy distribution of the neutrons emitted by the sources it was decided to measure the neutron energies by means of recoil protons in a hydrogen-filled cloud chamber. In addition, it was hoped that investigation of the actual energy distribution would show whether some of the sources consisted of several neutron groups instead of a single one. Some of the γ-sources had been reported as having more than one

* This document is based on work performed in 1945 under Contract No. W-31-109-eng-38 for the Atomic Energy Project at the Argonne National Laboratory. It was submitted for declassification June 6, 1947.

[1] A. Wattenberg, Phys. Rev. 71, 497 (1947).

[2] D. Bohm and C. Richman, Phys. Rev. 71, 567 (1947).

γ-energy above the photo-disintegration threshold, but it was impossible to ascertain from the average energy, as measured by the hydrogen scattering, whether multiple groups were present or not.

II. METHOD

The main difficulty in the measurement of the neutron energies with the cloud chamber is caused by the fact that while the sources are only moderate in neutron strength, they are intense in γ-activity. Thus a source strong enough to give one recoil proton per expansion when placed about two feet from the chamber must be several curies in γ-strength. Such an intense γ-activity near the chamber makes it rather difficult to obtain clear proton tracks. It was found, however, that if the photo-neutron source was surrounded by several inches of lead to reduce the γ-activity to some extent, and if the expansion ratio of the chamber was kept quite low (which emphasizes proton over beta-tracks), it was possible to obtain quite sharp contrast between the protons and the intense background of beta-tracks. The presence of the lead does not change the neutron energy spectrum appreciably because energy losses for elastic scattering with lead are small, and inelastic scattering does not take place at photo-neutron energies.

The apparatus is shown diagrammatically in Fig. 1. It was placed on supports about 6 ft. above the floor in a large room to reduce the scattering of neutrons from walls and floor. The γ-source could be lowered by remote control into a large lead pot on the floor while the chamber was being adjusted, film changed, etc. Then it could be replaced in operating position and several hundred pictures taken without the necessity of approaching the apparatus. The photo-neutron source itself is of the same construction as those described by Wattenberg, that is, a tube 2 cm in diameter and 5 cm long, containing the γ-source, located in a cylinder of beryllium or a deuterium-filled cylindrical can 3.8 cm in diameter and 5.1 cm long with a 2.2-cm diameter axial hole.

The cloud chamber, 30 cm in diameter, is very similar to that described by Jones and Hughes.[3] For most of the sources measured it was filled with hydrogen gas and water vapor to a pressure of 82 cm of mercury. The stereoscopic pictures were taken with a standard mirror arrangement, using 35-mm Eastman *XX* film and an *f*:3.5 lens. The light source was a xenon-filled capillary, flashed by discharging a 50 μf condenser bank at 2000 volts. The xenon lamp is a General Electric "Flashtube FT 26" and has proved to be an extremely convenient cloud-chamber light source.

The lengths of the recoil protons, and their direction of motion relative to the incident neutrons, were determined by a stereoscopic reprojection of the negatives. The proton ranges in standard air were obtained by comparison with the observed range in the chamber of the alphas from a plutonium source mounted in the chamber. In the comparison, a correction was made for the fact that the stopping power of the chamber for alphas relative to protons is a function of the proton range. The proton range in air was converted to energy units, using the range-energy curves given by Livingston and Bethe,[4] and the neutron energy calculated from the proton energy and the angle, θ, between the neutron and proton directions. The energy spectrum of the neutrons from the source could then be plotted from the observed numbers of recoil protons as a function of energy. A correction must be made, of course, for the effect of the change in the scattering cross section of hydrogen with neutron energy, but because of the nearly monochromatic nature of the sources such a correction is small.

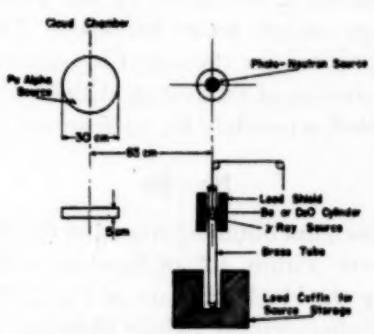

FIG. 1. Experimental arrangement of source and cloud chamber for the measurement of photo-neutron energies.

[3] H. Jones and D. Hughes, Rev. Sci. Inst. 11, 79 (1940).

[4] M. S. Livingston and H. A. Bethe, Rev. Mod. Phys. 9, 245 (1937).

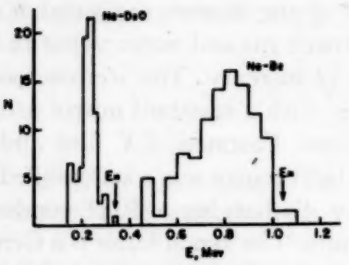

FIG. 2. Measured spectra of the photo-neutrons from Na−Be and Na−D_2O. E_M denotes the maximum neutron energy calculated from a γ-energy of 2.76 Mev.

III. RESULTS

If no slowing down takes place in the deuterium or beryllium of the source itself, then the energy spread in the emitted neutrons should be very small. The energy spread in this ideal case is caused by the difference in direction, θ, of the neutron and the γ-ray and is given by

$$\delta = E_\gamma \cos\theta \left(\frac{2(A-1)(E_\gamma - Q)}{931 A^3} \right)^{\frac{1}{2}},$$

where δ is the deviation from the average energy, E_γ the γ-energy, A the mass of the target nucleus, and Q the threshold energy (all energies in Mev). The value of this energy spread is usually of the order of one percent, which is much less than the energy spread caused by slowing down in an actual source. Because of the low atomic weight of deuterium and beryllium they are excellent moderators and distort the neutron energy spectrum even when present in small amounts. The resulting energy spectrum is expected to have a maximum neutron energy corresponding to that given by the γ-energy but an average energy somewhat lower. The actual energy spectra were measured for several photo-neutron sources of interest, and the findings will be discussed separately for each source.

Na−Be

The spectrum obtained from 106 recoil protons which were within 30° of head-on collisions is shown by the block diagram of Fig. 2. It is seen that the distribution, while showing no great spread in energy similar to a Ra−Be source, is by no means monoenergetic. The spectrum is, of course, distorted to some extent by errors of measurement. However, if only those recoils are chosen which are within 20° of head-on, the spectrum does not narrow appreciably, the full width at half-maximum, which is 33 percent of the maximum energy in Fig. 2, changing only to 31 percent in the 20° case. The true width is probably slightly less than the latter value, say about 25 percent.

The most probable neutron energy from Fig. 2 is about 825 kev, while the arithmetic mean energy is 800 kev. Wattenberg finds a mean energy for this source from the mean hydrogen scattering cross section of 830 kev. It seems then that the spectrum of Fig. 2 is a good representation of the actual neutron distribution of a source made according to Wattenberg's method.

The maximum energy in the spectrum can, of course, be identified with those neutrons which are unmoderated and which should therefore correspond to the energy calculated from the Na γ-energy. The Na γ-energy has been measured as 2.76 Mev recently by Siegbahn,[5] in agreement with an earlier measurement of Elliot, Deutsch, and Roberts.[6] Other measurements have given values for the energy ranging as high as 2.94 Mev. The maximum neutron energy (including the energy spread δ) to be expected, assuming E_γ to be 2.76 Mev, is marked as E_M in Fig. 2. Considering the inevitable straggling of the experimental points, it is seen that the agreement between E_M and the observed upper limit is quite satisfactory. A γ-ray has been reported of energy higher than that of the γ-ray of energy 2.76 Mev, but no tracks were found in the present spectrum (or in the Na−D_2O spectrum), to indicate the presence of such a γ-ray. If it exists, it does not contribute an appreciable number of neutrons in the photo-neutron source.

Na−D_2O

The spectrum based on 75 recoils is shown in Fig. 2. The theoretical maximum, based on a γ-energy of 2.76 Mev and a D_2O threshold of 2.18 Mev is indicated (E_M), and it is seen that the maximum neutron energy corresponds quite well with the theoretical value. The most prob-

[5] K. Siegbahn, Phys. Rev. **70**, 127 (1946).
[6] Elliot, Deutsch, and Roberts, Phys. Rev. **67**, 273 (1945).

able value of the distribution and the average are at about 220 kev (70 percent of E_M) which is the same as the mean energy which Wattenberg finds for this source by the hydrogen cross section method. The width of the energy distribution at half-maximum for the Na$-D_2O$ source is 20 percent of E_M.

Mn–Be

Gamma-ray measurements[7,8] for Mn^{56} had shown two γ-rays of energy 1.81 and 2.13 Mev. As both these energies are higher than the threshold in Be, one would expect two groups of photo-neutrons. Wattenberg actually found from the scattering cross section of hydrogen that the photo-neutrons he observed were due to a γ-ray of energy 1.83 Mev. (He also found an extremely weak group of photo-neutrons in deuterium which would indicate a γ-ray of energy 2.7 Mev.) As his method of estimating energies from the hydrogen scattering cross section gives only the mean energy of the neutron group, it was impossible for him to say whether there were any neutrons from the 2.1-Mev γ-ray.

The energy spectrum of the Mn–Be neutrons was measured in the cloud chamber to determine whether only one group of neutrons was present, as seemed likely from Wattenberg's result, or if two groups were present, as would be indicated by the γ-ray energies. The results are shown in the lower curve of Fig. 3. It was found that two groups of neutrons were definitely present (no effort was made to study the small number of neutrons which would be caused by the 2.7-Mev γ-ray). The energy of the most abundant group was too low to be measured accurately as the recoil protons were of such short range. The energy is roughly 100 kev, which would give an approximate γ-ray energy of 1.8 Mev. The higher energy group has an average energy of 300 kev, and it is possible to estimate the energy of the γ-ray causing the group. The maximum energy, E_M, is chosen as 375 kev, by taking E_M slightly less than the apparent maximum energy in analogy with the spectra of Fig. 2. A value of 375 kev for E_M then gives 2.05 ± 0.03 Mev for the γ-ray energy. This energy is somewhat less than the earlier value 2.13 Mev, but agrees extremely well with a recent determination of this γ-ray by Siegbahn[9] of 2.06 Mev. It is definite then that the 2.06-Mev γ-ray produces photo-neutrons in addition to the 1.81-Mev γ-ray.

The relative numbers of photo-neutrons in the low and high energy groups are about 90 percent and 10 percent, respectively, as determined by counting recoil protons and correcting for the change of hydrogen cross section with energy. Because of the low intensity of the high energy group, it was not indicated as a discrete group by Wattenberg but probably increased his average energy slightly. Thus the 1.83-Mev γ-ray energy that he inferred is probably high for this reason. Siegbahn's[9] recent determination of the low energy γ-ray is 1.77 Mev.

In–Be

Indium is of doubtful value as a γ-emitter for photo-neutron sources because of its short half-life (54 min.). However, if only one group of neutrons were present then the difficulty caused by the short half-life would not be insurmountable. Gamma-ray measurements had indicated energies of 1.8 (spectrometer) and 2.3 Mev (cloud chamber) for those γ's higher than the Be threshold, so it was decided to measure the photo-neutron spectrum to see if several groups were actually present. The spectrum obtained, shown in the upper part of Fig. 3, contains two

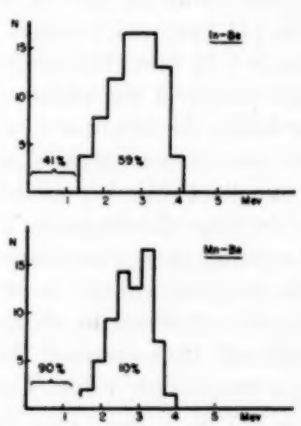

FIG. 3. Photo-neutron spectra of In–Be and Mn–Be.

[7] M. Deutsch and A. Roberts, Phys. Rev. **60**, 362 (1941).
[8] L. G. Elliot and M. Deutsch, Phys. Rev. **63**, 321 (1943).
[9] K. Siegbahn, Ark. Mat. Astr. Fys. **33A** (2), Paper 10 (1946).

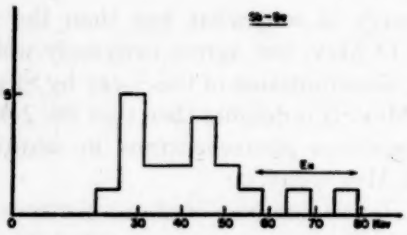

FIG. 4. Photo-neutron spectrum of Sb—Be. The energy range shown for E_M gives a value for the γ-energy of 1.70±0.02 Mev.

groups of neutrons, one of mean energy about 300 kev, and a group of energy too low (about 100 kev) to be measured accurately. The higher energy neutron group comprises 59 percent of the total, and its E_M gives a value of 2.08±0.04 Mev for the indium γ-ray. The low energy group cannot be measured accurately, but it indicates a γ-ray of roughly 1.8 Mev. It seems therefore that both energies are present in indium and in such intensities that they give roughly comparable groups of photo-neutrons. Because of the presence of the two neutron groups the value of In—Be as a photo-neutron source is much reduced.

Sb—Be

The highest energy γ-ray from Sb has been reported[10,11] as having energies ranging from 1.70 to 1.82 Mev. This discrepancy in the γ-ray energy is large enough so that the calculated photo-neutron energy is quite indefinite. Scharff-Goldhaber and Klaiber[12] measured the energy of the photo-neutrons from an Sb—Be source and found E_M to be 115 kev, which would indicate a γ-energy of about 1.75 Mev. Wattenberg's value for the average energy of the photo-neutrons is 24 kev, from which he obtains a γ-energy of 1.67 Mev. The spectrum of photo-neutrons was studied with the cloud chamber mainly in order to investigate the large discrepancies in both the γ-energy and neutron energy measurements.

Because the neutron energy is so low, the cloud chamber was modified to allow operation at low pressure and thus increase the range of the protons to a measurable value. The chamber could be operated with hydrogen at a minimum pressure of about 8 cm, using water as the vapor. Under such conditions the range is about 25 times the range in air and a 20-kev proton, which would have a range of about 0.3 mm in air, will have a range of almost a centimeter in the chamber. The observed ranges in the chamber could not be converted to energies by using the method described for the higher energy sources because the Pu α's would have ranges much greater than the chamber diameter. The stopping power of the chamber gas was therefore determined by measuring the range of the protons produced in the $N^{14}(n,p)C^{14}$ reaction which have an energy of 558 kev. The low energy proton ranges could then be obtained by taking into account the change of the stopping power of hydrogen and oxygen with proton energy.[13]

The source strength of Sb—Be is very low, so it was possible to obtain only 20 recoil protons caused by nearly head-on collisions. The distribution obtained is plotted in Fig. 4. In spite of the extremely small number of tracks it appears that a single group of neutrons of average energy of about 35 kev is present. This value is in rather good agreement with the mean energy of the photo-neutrons of 25±15 kev measured by Wattenberg. Because the neutrons are of such low energy, it should be possible to use the photo-neutron energy to determine the γ-energy rather accurately. Unfortunately, the straggling at the upper end of the measured spectrum of Fig. 4 is quite large, and E_M cannot be determined very accurately. In fact, the possibility that two closely spaced groups might be present cannot be ruled out because of the small number of tracks. However, E_M seems to be within the range shown, that is, 68±11 kev. The value of the γ-energy resulting from this E_M is 1.704 ±0.012 Mev. The error in this determination of the γ-ray is actually somewhat greater than 12 kev because the error in the photo-neutron threshold should be included, as well as errors in the determination of the stopping power of the chamber gas. Inclusion of these two errors would probably increase the error in the γ-energy to about 20 kev. The γ-energy determined

[10] P. G. Kruger and W. E. Ogle, Phys. Rev. **67**, 273 (1945).
[11] Mitchell, Langer, and McDaniel, Phys. Rev. **57**, 1107 (1940).
[12] G. Scharff-Goldhaber and G. S. Klaiber, Phys. Rev. **61**, 733A (1942).
[13] J. Ashkin, Los Alamos Report 12-R (September 23, 1943). Also published as Manhattan District Declassified Document No. 276 (September 10, 1946).

from the present experiment agrees very well with the latest direct γ-energy determination of Kruger and Ogle[10] which gave 1.70 ± 0.02 Mev. It is somewhat higher than the value 1.67 Mev which Wattenberg obtains from the mean energy of the photo-neutron source.

We wish to extend thanks to Dr. A. Wattenberg for his help in preparation of the sources used and for valuable discussion, to T. Brill for the design of cloud-chamber control circuits, and to N. Goldstein and S. Jashemski for aid in taking data.

PHYSICAL REVIEW VOLUME 72, NUMBER 10 NOVEMBER 15, 1947

Scattering of Neutrons in Polycrystals*

R. J. FINKELSTEIN**
Argonne National Laboratory, Chicago, Illinois

(Received May 23, 1947)

Although elastic and first-order inelastic cross sections for a neutron against a Debye crystal have already been determined, expressions for higher order inelastic collisions have not been calculated, and would be very complex for the Debye model. The calculation of the total inelastic cross section involving the emission of an arbitrarily large number of phonons is here presented for a neutron against an Einstein polycrystal. The result, as one would expect, is essentially the same as that given by Fermi for amorphous scatterers, except at high neutron energies where we have calculated the cross section for the ejection of the struck nucleus from its lattice. The coherent elastic cross section is also determined; it is important for energies as high as 1 volt, and does not differ appreciably from that previously calculated for a Debye crystal. The total cross section, the sum of the coherent and incoherent parts, is compared with the experimental data on beryllium.

1. INTRODUCTION

THE scattering of a neutron by a crystal may be described qualitatively in the following manner. As long as its energy is large compared to the chemical binding energy of the lattice, the neutron is scattered as if the nuclei forming the lattice were free. A fast neutron therefore slows down by dislocating effectively free nuclei until its energy becomes of the order of the crystal bond. It then makes inelastic collisions with the lattice as a whole, until it loses so much more energy that its wave-length exceeds the amplitude of the temperature vibrations of the scattering nuclei. At this point elastic collisions with the lattice become the most probable process and further cooling of the neutron takes place very slowly. Finally, if the neutron energy is somehow made still lower, inelastic scattering becomes important again, since the neutron begins to absorb energy from the crystal.

In this paper the cross sections for these different kinds of scattering are calculated for the Einstein crystal. The elastic and first-order inelastic cross sections have already been determined for the Debye crystal.[1] The difference between our formula for elastic scattering and that deduced from the Debye model is insignificant. For first order inelastic collisions the Debye type of formula is to be preferred, but for higher order collisions, in which many phonons are exchanged, the equations of the Debye model become too complex. In these higher order collisions the cross section computed from the Einstein model is essentially identical with the cross section calculated by Fermi[2] to describe

* This work has been carried out under the auspices of the Atomic Energy Commission. It was submitted for declassification on March 10, 1947.

** Now at the Institute for Advanced Study, Princeton, New Jersey.

[1] I. Pomerantschuk, Physik. Zeits. d. Sowjetunion **13**, 65 (1938); R. Weinstock, Phys. Rev. **65**, 1 (1944). See also Halpern, Hamermesh, and Johnson, *ibid.* **59**, 981 (1941); Wick, Physik. Zeits. **38**, 403 (1937); Seeger and Teller, Phys. Rev. **62**, 37 (1942).

[2] E. Fermi, Ricerca Sci. **7**, 13 (1936); H. A. Bethe, Rev. Mo d. Phys. **9**, 124 (1937).

the thermalization of neutrons in hydrogenous substances. The cross section is incoherent and the formula for it is hence applicable to amorphous matter. In the same energy interval in which higher order inelastic collisions become dominant, the elastic cross section, which is a discontinuous function of energy in the thermal region, becomes effectively continuous. Finally, at still higher neutron energies the Einstein model of the crystal must be modified because the nucleus struck by the neutron may be ejected from the lattice.

Before describing the calculations, we distinguish between two ways of regarding a crystal as a set of equivalent oscillators. (a) The nuclei comprising the crystal may be considered as independent oscillators whose frequencies are all equal. In this picture an inelastic collision in which many phonons are absorbed or emitted by the lattice occurs when a single oscillator makes a *many-quantum* transition. (b) The motions of the individual nuclei may be analyzed into $3N$ lattice vibrations whose frequencies are all equal. In this picture a collision involving many phonons is described as a combination of simultaneous *one-quantum* transitions of many lattice vibrations. Description (b) is easier to connect with the Debye model, whereas description (a), which we use here, can be reduced to the problem of scattering by a single isotropic oscillator.

2. THE MATRIX ELEMENTS

The wave function for a composite system consisting of a crystal and a free neutron is

$$\psi(\mathbf{k}, \mathbf{n}_1 \cdots \mathbf{n}_N) = \exp(i\mathbf{k}\cdot\mathbf{r}) \prod_1^N \varphi(\mathbf{u}_j, \mathbf{n}_j). \quad (1)$$

In Eq. (1), $\mathbf{k}$ and $\mathbf{r}$ are wave number and position vectors of the neutron; $\mathbf{u}_j$ is the displacement of the jth oscillator from its equilibrium position, and $\mathbf{n}_j$ is the set of three quantum numbers needed to describe this oscillator. The functions, φ, are products of Hermite functions. We calculate the matrix element for a transition in which the neutron changes from state $\mathbf{k}$ to $\mathbf{k}'$ while the crystal simultaneously makes a transition from $(\mathbf{n}_1 \cdots \mathbf{n}_N)$ to $(\mathbf{n}_1' \cdots \mathbf{n}_N')$ as a result of the following interaction potential[2] between the neutron and the crystal:

$$V = \sum_1^N A_j \delta(\mathbf{r} - \mathbf{r}_j) \quad (2)$$

where $\mathbf{r}_j$ is the instantaneous position of the jth nucleus. The evaluation of this matrix element depends on whether the collision is elastic or inelastic. The results are

$$(\mathbf{k}, \mathbf{n}_1 \cdots \mathbf{n}_N | V | \mathbf{k}'\mathbf{n}_1 \cdots \mathbf{n}_N) = \sum_1^N A_j (\mathbf{n}_j | I | \mathbf{n}_j) \exp[i(\mathbf{k}-\mathbf{k}')\cdot\mathbf{R}_j] \quad (3a)$$

for elastic collisions, and

$$(\mathbf{k}, \mathbf{n}_1 \cdots \mathbf{n}_p \cdots \mathbf{n}_N | V | \mathbf{k}'\mathbf{n}_1 \cdots \mathbf{n}_p' \cdots \mathbf{n}_N) = A_p (\mathbf{n}_p | I | \mathbf{n}_p') \exp[i(\mathbf{k}-\mathbf{k}')\cdot\mathbf{R}_p] \quad (3b)$$

for inelastic collisions. Here

$$(\mathbf{n}_j | I | \mathbf{n}_j') = \int_{-\infty}^{+\infty} \exp[i(\mathbf{k}-\mathbf{k}')\cdot\mathbf{u}_j] \varphi(\mathbf{u}_j, \mathbf{n}_j) \times \varphi(\mathbf{u}_j, \mathbf{n}_j')^* d\mathbf{u}_j \quad (4)$$

and $\mathbf{R}_j (= \mathbf{r}_j - \mathbf{u}_j)$ is the equilibrium position of the jth nucleus. The probability of an elastic collision, being proportional to the square of the sum in (3a), contains cross terms which represent interference between neutron waves scattered from different oscillators; elastic scattering is therefore coherent. On the other hand, matrix elements describing inelastic collisions consist of single terms only, so that there is no interference; inelastic scattering by an Einstein crystal is hence incoherent and the scattering is isotropic. This feature of the present model is in error for *nearly* elastic scattering, which is not isotropic either according to the Debye model or to the experimental evidence on x-rays; but for larger energy transfers our simple model should be correct.

3. THE SCATTERING CROSS SECTION

In terms of the matrix element M_{AB} the cross section for a transition from state A to state B is, per unit solid angle,

$$\sigma_{AB} = a |M_{AB}|^2$$
$$a = (4\pi^2 m_N^2 / N h^4)(V'/V)$$

where A and B refer to states of the composite

system consisting of the crystal and the neutron. The initial and final velocities of the neutron are V and V', and its mass is m_N. The cross section is here normalized by dividing by the number, N, of nuclei in the crystal. If P_A is the probability that the crystal is in state A, then the total cross section is

$$\sigma = a \sum_{A,B} P_A |M_{AB}|^2. \quad (5)$$

The total elastic cross section σ^0 is obtained by carrying the sum (5) over only those final states for which $E_A = E_B$, where E is the energy of the indicated state of the crystal. Likewise the sum giving the total-absorption (emission) cross section, $\sigma^+(\sigma^-)$, is limited by the conditions $E_B > E_A$ and $E_B < E_A$, respectively; here emission (absorption) means emission (absorption) of phonons by the *neutron*.

If the matrix elements (3) are put in (5), one gets the scattering cross section of a monocrystal in terms of single oscillator functions. The results are, of course, quite different for the elastic and inelastic cases.

A. Inelastic Cross Section

The result for the inelastic case is

$$\sigma^{\pm} = (m_N/\mu)^2 \sigma_i J^{\pm} \quad (6)$$

where

$$J^{\pm} = \int I^{\pm} d\Omega \quad (6a)$$

is the integral of $I^{\pm}$ over all solid angle, and

$$I^{\pm} = (1/4\pi) \sum (V'/V) P(\mathbf{n}) |(\mathbf{n}|I|\mathbf{n}')|^2. \quad (6b)$$

$P(\mathbf{n})$ is the probability that a single oscillator is in the state $\mathbf{n}$; $(\mathbf{n}|I|\mathbf{n}')$ is given by (4). In Eq. (6) σ_i is the incoherent cross section of a unit cell, namely,

$$\sigma_i = (1/p) \sum{}' \sigma_p \quad (6c)$$

where the sum is to be carried over all p nuclei in a unit cell; σ_p is the cross section of a free nucleus.

$$\sigma_p = (16\pi^2\mu^2/h^4) A_p^2 \quad (6d)$$

where μ is the reduced mass of the neutron and free nucleus.

Since the inelastic scattering is incoherent, it is the same for the polycrystal as for the monocrystal.

B. Elastic Cross Section

The elastic cross section[3] of a single crystal, also found by putting (3) in (5), is per unit solid angle

$$\sigma^0 = (m_N/\mu)^2 [(2\pi^2 I^0 \sigma_e/B) \delta(\mathbf{k} - \mathbf{k}' - 2\pi\boldsymbol{\tau}) + Q\sigma_i/4\pi] \quad (7)$$

where B is the volume of a unit cell, and

$$2\pi\boldsymbol{\tau} = l_1\mathbf{b}_1 + l_2\mathbf{b}_2 + l_3\mathbf{b}_3. \quad (7a)$$

Here l_1, l_2, and l_3 are integers; the $\mathbf{b}_i$ are reciprocal lattice vectors.

$$I^0 = |\sum_n P(\mathbf{n})(\mathbf{n}|I|\mathbf{n})|^2, \quad (7b)$$

$$Q = \sum_n [P(\mathbf{n}) - P(\mathbf{n})^2] |(\mathbf{n}|I|\mathbf{n})|^2, \quad (7c)$$

$$\sigma_e = (1/p) |\sum{}' \sigma_j^{\frac{1}{2}} \exp(i2\pi\boldsymbol{\tau} \cdot \mathbf{R}_j)|^2. \quad (7d)$$

In Eq. (7d) $\mathbf{R}_j$ is the position of the jth nucleus in a unit cell; the sum runs over the unit cell; the sign of $\sigma_j^{\frac{1}{2}}$ in general depends on j.

The δ-function, arising from the sum in (3a), is characteristic of crystal-diffraction problems and restricts scattering to the direction of the Laue spots. These directions are determined by the equation

$$\mathbf{k} - \mathbf{k}' = 2\pi\boldsymbol{\tau}. \quad (8)$$

Since $k = k'$, one has $2k \sin\theta/2 = 2\pi\tau$, and hence

$$\pi\tau \geqslant k. \quad (8a)$$

The second term in (7) gives rise to an isotropic, incoherent scattering, which disappears if the crystal is cooled to 0°K; it is introduced by the randomness of the initial state of an oscillator.

The polycrystalline elastic cross section is calculated by averaging the monocrystalline cross section over all orientations of the single crystal. This may be done by averaging over $\boldsymbol{\tau}$, since $\boldsymbol{\tau}$ is fixed relative to the axes of the single crystal. Finally the cross section is integrated over all scattering angles in the neighborhood of $\mathbf{k}' = \mathbf{k} + 2\pi\boldsymbol{\tau}$. The result is that the total cross section associated with a given value of τ is

$$\sigma^0 = (m_N/\mu)^2 [\pi\sigma_e I_0/2Bk^2\tau + Q\sigma_i]. \quad (9)$$

The total-elastic polycrystalline cross section is obtained by summing (9) over all allowed

[3] Reference 1, R. Weinstock.

directions. The result is

$$\sigma^0=(\pi m_N{}^2/2\mu^2Bk^2)\sum_{\iota}{}^{\tau\leqslant k/\pi} I^0\sigma_c/\tau. \quad (10)$$

The isotropic term is omitted from (10) because it vanishes if all oscillators are in their ground state, and in any case it is small.

4. THE SINGLE OSCILLATOR FUNCTIONS

The elastic and inelastic cross sections are given by Eqs. (10) and (6) respectively, but the one-oscillator functions appearing in them must now be calculated. These functions are based on the matrix element $(\mathbf{n}|I|\mathbf{n}')$ which is defined in Eq. (4) where

$$\varphi(\mathbf{u},\mathbf{n})=\varphi(u_x,n_x)\varphi(u_y,n_y)\varphi(u_z,n_z).$$

Hence $(\mathbf{n}|I|\mathbf{n}')$ can be broken into three factors, one of which is

$$(n_x|I|n_x')=\int_{-\infty}^{+\infty}\exp[i(k_x-k_x')u_x \times\varphi(u_x,n_x)\varphi(u_x,n_x')^*du_x. \quad (11)$$

The φ are the oscillator wave functions

$$\varphi(u,n)=(\pi^{\frac{1}{2}}a2^nn!)^{-\frac{1}{2}}\exp(-\tfrac{1}{2}\xi^2)H_n(\xi) \quad (11a)$$

where

$$\xi=u/a \quad \text{and} \quad a=(\hbar/m\omega)^{\frac{1}{2}}. \quad (11b)$$

Here m and ω are the mass and frequency of an average nucleus in the lattice. Let

$$\chi(\xi,n)=a^{\frac{1}{2}}\varphi(u,n). \quad (12)$$

Then use can be made of the result that the Fourier transform of the product $\chi(\xi,n)\chi(\xi,n')$ of two orthonormalized Hermite functions is an associated Laguerre function. That is,

$$\int_{-\infty}^{+\infty}e^{iq\xi}\chi(\xi,n)\chi(\xi,m)^*d\xi =(-)^{\frac{1}{2}(m-n)}\Phi_m{}^{(m-n)}(q^2/2) \text{ with } m>n \quad (13)$$

where

$$\Phi_{n+\lambda}{}^{\lambda}(x)=\frac{(n!)^{\frac{1}{2}}}{[(n+\lambda)!]^{\frac{1}{2}}}e^{-x/2}x^{\lambda/2}\frac{d^{\lambda}L_{n+\lambda}(x)}{dx^{\lambda}} \quad (13a)$$

and where $\lambda=m-n$. Here $L_n(x)$ is the nth Laguerre polynomial. The functions $\Phi_{n+\lambda}{}^{\lambda}$ are the orthonormalized-associated Laguerre functions.[4] Equation (13) can be proved as follows.

By use of the generating function

$$\exp(-t^2+2tx)=\Sigma H_n(x)t^n/n!$$

it is easily shown that

$$y=\sum_{n=0}^{\infty}\sum_{m=0}^{\infty}\frac{t^n}{n!}\frac{s^m}{m!}I_{nm} \quad (14)$$

where

$$I_{nm}=\int_{-\infty}^{\infty}\exp(-x^2)H_n(x)H_m(x)e^{iqx}dx$$

and

$$y=e^{2ts}\int_{-\infty}^{\infty}\exp[-(t+s-x)^2]e^{iqx}dx =\pi^{\frac{1}{2}}\exp(-q^2/4)e^{2ts+iq(t+s)}.$$

Hence

$$I_{nm}=\left(\frac{\partial^{n+m}y}{\partial t^n\partial s^m}\right)_{s=t=0} =\left[\frac{\partial^n}{\partial t^n}(2t+iq)^my\right]_0.$$

By performing the indicated differentiations one now shows that y generates the Laguerre functions. In fact the required integral is

$$(\pi 2^{n+m}n!m!)^{-\frac{1}{2}}I_{nm}=[n!(n+\lambda)!]^{-\frac{1}{2}} \times\exp(-q^2/4)\Sigma_{\nu}\binom{n+\lambda}{\nu+\lambda}\frac{n!}{\nu!}\left(-\frac{q^2}{2}\right)^{\nu+\lambda/2}. \quad (15)$$

This last expression is readily identified with the Laguerre functions as stated in Eq. (13).

The required matrix elements are

$$(\mathbf{n}|I|\mathbf{n}')=(-)^{\frac{1}{2}(\lambda_x+\lambda_y+\lambda_z)}\Phi_{n_x,\lambda_x}(q_x{}^2) \times\Phi_{n_y,\lambda_y}(q_y{}^2)\Phi_{n_z,\lambda_z}(q_z{}^2) \quad (16)$$

where

$$\mathbf{q}=(a/\sqrt{2})(\mathbf{k}-\mathbf{k}'). \quad (16a)$$

Now the probability that the x-oscillator will be in the state n_x is

$$P(n_x)=z^{n_x}/\sum z^n=(1-z)z^{n_x} \quad (17)$$

where

$$z=\exp(-\hbar\omega/kT). \quad (17a)$$

But by (7b) and (16)

$$I^0=(1-z)^2|[\sum z^n\Phi_n{}^0(q_x{}^2)]|^2. \quad (18)$$

The square bracket in (18) is just the generating function of the Laguerre functions, i.e.,

$$\sum_0^{\infty}z^n\Phi_n{}^0(x)=(1/1-z)\exp[-x(1+z)/2(1-z)]$$

[4] The integral (13) is calculated by Weinstock but the result is not identified as a Laguerre function.

so that

$$I^0=\exp[-q^2(1+z)/(1-z)].$$

Since we are considering the case of elastic scattering we also have $\mathbf{q}=(a/\sqrt{2})2\pi\boldsymbol{\tau}$. Hence I^0 may be written

$$I^0=\exp(-A\tau^2) \tag{19}$$

where

$$A=(\hbar^2/2mk\Theta)\coth(\Theta/2T). \tag{19a}$$

In (19a) k is Boltzmann's constant and Θ is the Einstein temperature of the lattice ($\hbar\omega=k\Theta$).

An exact calculation of the function $I^{\pm}$ given in (6b) appears difficult, but may be avoided by use of the following approximations. To calculate the emission cross section assume that the initial state of the oscillator is always the ground state: $P(n)=\delta(n,0)$. On the other hand, to calculate the absorption cross section assume that the final state of the oscillator is always the ground state. Under these assumptions the matrix elements for emission and absorption are equal: $(0|I|\mathbf{n})=(\mathbf{n}|I|0)^*$.

The absorption cross section becomes important only for very slow neutrons. For these neutrons it varies with the energy, E, as $E^{-\frac{1}{2}}$ for the Einstein model and as E^{-1} for the Debye model. In this case the latter model is, of course, to be preferred; the Einstein picture fails here, as it does for specific heats, because it does not take account of low frequency vibrations. For this reason further discussion of absorption cross sections will not be given.

The calculation of J^- has been given elsewhere,[2] under the above assumption $P(n)=\delta(n,0)$. The result, which is to be inserted in Eq. (6), is

$$J^-=\sum_{1}^{n\leqslant\epsilon} J_n^- \tag{20}$$

where

$$J_n^-=(m/4m_N\epsilon)[f_n(q_1^2)-f_n(q_2^2)], \tag{20a}$$

$$f_n(x)=e^{-x}(1+x+\cdots+x^n/n!), \tag{20b}$$

$$q_1=(m_N/m)^{\frac{1}{2}}[\epsilon^{\frac{1}{2}}-(\epsilon-n)^{\frac{1}{2}}], \tag{20c}$$

$$q_2=(m_N/m)^{\frac{1}{2}}[\epsilon^{\frac{1}{2}}+(\epsilon-n)^{\frac{1}{2}}], \tag{20d}$$

$$\epsilon=E/\hbar\omega. \tag{20e}$$

Before discussing these results we consider the case in which the harmonic-oscillator model of the crystal is not appropriate.

5. NEUTRON ENERGY LARGE COMPARED TO CHEMICAL BINDING ENERGY

If the energy absorbed by the scattering nucleus exceeds the energy by which it is bound to the crystal, then the collision ejects the nucleus from its original lattice site. To calculate the cross section for this event, assume for simplicity that the wave function of the final state of the nucleus is the unbound plane wave $\exp(i\mathbf{K}\cdot\mathbf{r})$ where $\hbar\mathbf{K}$ is the momentum of the free nucleus.

The relevant matrix element is now

$$(0|I|K)=(a^{3/2}/\pi^{3/4})\int\exp(-\tfrac{1}{2}\xi^2+ia\mathbf{S}\cdot\boldsymbol{\xi})d\xi$$
$$=(2a)^{3/2}\pi^{3/4}\exp(-\tfrac{1}{2}S^2a^2). \tag{21}$$

where

$$\mathbf{S}=\mathbf{k}-\mathbf{k}'-\mathbf{K}. \tag{21a}$$

$\mathbf{S}$ is the momentum given to the lattice. The total probability for the ejection of the scattering nucleus into the continuous spectrum is determined by the following integral, which replaces the sum in (6b),

$$I^-=(1/32\pi^4)\int_{K_b}^{K_m}\int_0^{2\pi}\int_0^{\pi}(k'/k)|(0|I|\mathbf{K})|^2K^2\sin\omega d\omega d\alpha dK$$

where $\hbar\mathbf{K}_b$ is the momentum which a nucleus needs in order to escape from its position in the lattice and $\hbar\mathbf{K}_m$ is the maximum momentum which a nucleus can acquire in a collision with the neutron. Here (ω,α) is the recoil direction of the nucleus. The total cross section is by (6)

$$\sigma=(m_N/\mu)^2\sigma_i(a^3/4\pi^{5/2})\int_{K_b}^{K_m}\int_0^{2\pi}\int_0^{\pi}\int_0^{2\pi}\int_0^{\pi}(k'/k)$$
$$\times\exp(-S^2a^2)\sin\omega d\omega d\alpha\sin\theta d\theta d\varphi K^2dK \tag{22}$$

where (θ,φ) is the recoil direction of the neutron. Integration over all recoil directions of the nucleus gives

$$\int_0^{2\pi}\int_0^{\pi}\exp(-S^2a^2)\sin\omega d\omega d\alpha$$
$$\cong(\pi/lKa^2)\exp[-(l-K)^2a^2] \tag{23}$$

where $\mathbf{l}=\mathbf{k}-\mathbf{k}'$. (This last equation is approximate since it is based on the assumption $lKa^2\gg1$ or $\hbar^2lK/2m\gg\hbar\omega/2$. This condition is well satisfied, however, since $l=|\mathbf{l}|=|\mathbf{S}+\mathbf{K}|\geq K$. Hence $\hbar^2lK/2m\geq\hbar^2K^2/2m\geq\hbar^2K_b^2/2m$. But $\hbar^2K_b^2/2m\gg\hbar\omega/2$. $\therefore$ $\hbar^2lK/2m\gg\hbar\omega/2$.) Put Eq. (23) in (22), and integrate over (θ,φ). As the variable of integration it is convenient instead of θ to use

$$x=a(l-K).$$

The result is

$$\sigma=\sigma_i(m_N/2\mu k)^2\int_{K_b}^{K_m}[\Phi(x_2)+\Phi(x_1)]KdK \tag{24}$$

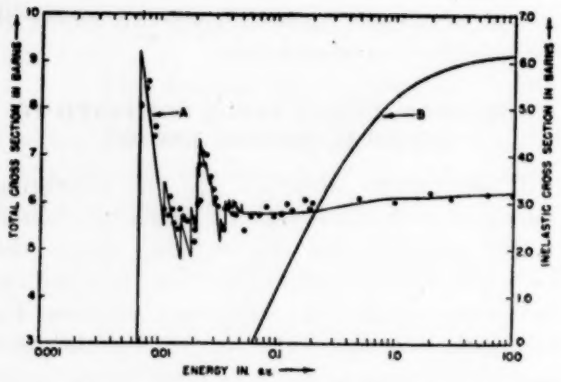

FIG. 1. Total cross section (Curve A) and inelastic cross section (Curve B) for the scattering of neutrons by microcrystalline Be. (Note the different scales for curves A and B.) Curve B actually intersects the energy axis with a vertical tangent and in addition has a discontinuous structure. These features are not shown in the figure because the discontinuities of slope contributed by both the elastic and inelastic cross sections have been smoothed out at higher energies.

where

$$x_2=[k+k[1-(m_N/m)(K/k)^2]^{\frac{1}{2}}-K]a, \quad (24a)$$

$$x_1=[-k+k[1-(m_N/m)(K/k)^2]^{\frac{1}{2}}+K]a, \quad (24b)$$

and Φ is the error function

$$\Phi(x)=(2/\pi^{\frac{1}{2}})\int_0^x \exp(-x^2)dx. \quad (24c)$$

The maximum momentum which the recoiling nucleus can take from the incident neutron is

$$K_m=(m/m_N)^{\frac{1}{2}}k. \quad (24d)$$

This large value of K is allowed, but improbable, since the integrand of (24) is small unless momentum is conserved between neutron and nucleus alone. Equation (24) gives the cross section for collisions in which a nucleus is dislocated. The total cross section consists of (24) plus the contribution from (6) where the sum in (20) is, of course, only to be carried as high as the binding energy.

6. DISCUSSION OF RESULTS

By Eqs. (10) and (17) the total elastic cross section of an Einstein polycrystal is

$$\sigma^0=(\pi m_N^2/2\mu^2Bk^2) \times \sum_{\mathbf{l}}{}^{\tau\leq k/\pi} \sigma_e(\tau)\tau^{-1}\exp(-A\tau^2). \quad (25)$$

The sum is extended over all triplets of integers $\mathbf{l}=(l_1, l_2, l_3)$ not excluded by either the vanishing of σ_e or the maximum value of τ. Each term in the sum may be interpreted as expressing the scattering by a set of parallel planes (with Miller indices: l_1, l_2, l_3). Equation (25) agrees closely with the one deduced for a Debye crystal;[5] the only difference is the expression for A (Eq. 17a), but even here the difference between the two formulas is insignificant. The factor $\exp(-A\tau^2)$ is in any case nearly unity; although even at $T=0$, it is not exactly unity because of the zero-point energy.

When the kinetic energy of the neutron is of the order of 1 volt, the sum in (25) is conveniently replaced by an integral, namely,

$$\sigma_i\int_0^{k/\pi}\tau^{-1}\exp(-A\tau^2)\rho(\tau)d\tau \quad (26)$$

where $\rho(\tau)d\tau$ is the number of points in $\mathbf{l}$-space inside of the ellipsoidal shell $(\tau, \tau+d\tau)$. The equation of the ellipsoid, τ, is

$$\tau^2=\sum(l_i\mathbf{b}_i)^2=\sum l_il_j\mathbf{b}_i\mathbf{b}_j.$$

Let the diagonal values of $||\beta_{ij}||$, where $\beta_{ij}=\mathbf{b}_i\cdot\mathbf{b}_j$, be β_1, β_2, and β_3. The volume of the ellipsoid associated with τ is $4\pi\tau^3/3(\beta_1\beta_2\beta_3)^{\frac{1}{2}}$. Hence $\rho(\tau)=4\pi\tau^2/(\beta_1\beta_2\beta_3)^{\frac{1}{2}}$. But the invariant $\beta_1\beta_2\beta_3=|\beta_{ij}|=B^{-2}$ where B is the volume of a unit cell. Hence $\rho=4\pi B\tau^2$. Using this density in (26) one finds

$$\sigma^0=(\sigma_i\pi^2m_N^2/\mu^2Ak^2)[1-\exp(-Ak^2/\pi^2)]. \quad (27)$$

The elastic cross section given by (25) is a discontinuous function of neutron energy in the thermal region, but Eq. (27) obviously represents a continuous function in the region in which it is valid.

The inelastic cross section is given by Eqs. (6) and (20), for the case in which the scattering nucleus is not knocked out of its lattice site. For large ϵ and low n, Eq. (20) shows that

$$J_n=m/4m_n\epsilon. \quad (28)$$

Finally, if the scattering nucleus is dislocated, one uses (24) in conjunction with (6), (20), and (28). These equations may be combined to give

[5] See the papers of Weinstock and Halpern, Hamermesh, and Johnson, reference 1.

the approximate formula, valid for large k,

$$\sigma=\sigma_i[(m_N/2\mu k)^2\int_{K_b}^{K_m}[\Phi(x_2)+\Phi(x_1)]KdK+(M/4\mu)(E_b/E)] \quad (29)$$

where $M=m+m_N$ and E_b is the binding energy.

Formula (29), of course, simplifies for large k. In fact, if $k\gg K\gg 1/a$, then x_2, $x_1\gg 1$, so that $\Phi\cong 1$. Hence (29) becomes

$$\sigma\cong\sigma_i(m_N/2k\mu)^2K_m^2. \quad (30)$$

It has been remarked in the previous section that momentum is usually conserved between neutron and nucleus alone, although there is a small probability that some momentum will be lost to the lattice. The improbability of transferring momentum to the lattice is clearly displayed in Eq. (21) which shows that the probability that the lattice acquires the momentum S is proportional to $\exp(-\frac{1}{2}S^2a^2)$, where a measures the tightness of the chemical binding. The same effect is brought out by the fact that the integrand of (29) is very small for values of K larger than

$$K_m=2k\mu/m_N. \quad (31)$$

which is the limit correct for a two-body collision. The effective upper limit in (29) is therefore given by (31) and not (24d). Substitution of Eq. (31) into (30) then leads to the correct limiting condition

$$\sigma=\sigma_i.$$

In Fig. 1 the theoretical cross section for Be computed from Eqs. (6), (20), (24), (27), and (28) (and the constant $\Theta=740°$K) is compared with the experimental data.[6] The data are compatible with a binding energy, E_b, of 3.3 volts, the cohesive energy of Be. Although the theoretical curve is not changed much if E_b is taken greater than this value, it is changed if E_b is taken much smaller; but the curve is not very sensitive to E_b. It should perhaps also be noted that the effect of binding is underestimated by our simplifying assumption that the final state of the struck nucleus is free; whereas it is overestimated by the other extreme assumption, $E_b=\infty$, according to which the final state is also bound.

The formulas obtained here for the inelastic cross section may be useful in an investigation of the slowing down of neutrons in crystalline materials. For example, the average energy loss in a collision is

$$\langle\epsilon\rangle_{Av}=\sum\epsilon(\sigma_\epsilon/\sigma)$$

where σ_ϵ is the cross section for losing the energy ϵ in a collision and where σ is the total cross section.

I wish to thank R. G. Sachs and R. Sternheimer for comments, and S. Moszkowski for the numerical computations and for the figure.

[6] E. Fermi, W. J. Sturm, and R. G. Sachs, Phys. Rev. 71, 589 (1947). There the theoretical *elastic* cross section is compared with the data.

Calculations in the Liquid-Drop Model of Fission

S. FRANKEL* AND N. METROPOLIS
Institute for Nuclear Studies, University of Chicago, Chicago, Illinois

(Received May 6, 1947)

The liquid-drop model of fission as developed by Bohr and Wheeler and others has been studied with the use of an electronic calculator, the Eniac. Classical deformation energies have been calculated for many shapes not all near-spherical. The shapes considered were axially and primarily, but not exclusively, bilaterally symmetric, and single-valued in polar representation. Previous calculations are confirmed and extended. Agreement with observed fission thresholds and spontaneous fission rates is obtained. No explanation of asymmetric fission is found.

1. INTRODUCTION

IT has been recognized since the discovery of fission that this phenomenon permits a classical interpretation in terms of the liquid-drop model of the nucleus. It was pointed out by Meitner and Frisch[1] that the stability of the spherical shape of the liquid-drop model nucleus, owing to the surface tension characteristics of the short range nuclear forces, is, to a large extent, counteracted for very heavy nuclei by the Coulomb repulsion. Shortly thereafter a more detailed study of the effects of these opposing influences was made by Bohr and Wheeler[2] and independently by Frenkel.[3] They showed that a uniformly charged droplet is unstable with respect to deformation at constant volume into a prolate spheroid if the ratio of the Coulomb energy to surface tension energy exceeds 2. Following Bohr and Wheeler, this ratio is here denoted by $2x$.

For lesser values of this ratio the spherical shape is stable with respect to any small deformation. However, for any value of this ratio greater than 0.70, i.e., for $x>0.35$, the potential energy (surface plus Coulomb) is diminished by separating the drop into two equal spheres far removed from each other. Thus for x between 0.35 and 1.0 (true for all heavy nuclei) the initial spherical configuration is a relative (local) minimum of the potential energy but not an absolute minimum. If the nucleus is continuously deformed from its initial spherical configuration to this two-droplet final configuration the potential energy first rises, say by an amount ΔE, then falls to less than its initial value. The least of these values, ΔE, considering all possible deformation trajectories, is the reaction threshold and the deformation at which it occurs must be a saddle-point of the potential energy.

The reaction threshold can be calculated for nuclei close to the stability limit, i.e., x close to unity, by the following method.[2-5] The deformation is assumed axially symmetric and expressed as a series in Legendre polynomials. The potential energy is then expanded as a power series in the coefficients of this expression. By evaluating a few terms in this power series the potential energy can be found for small deformations. If x is sufficiently close to unity the saddle-point occurs within this range of deformations and its position and potential energy can be determined.

Bohr and Wheeler[2] used this method to determine the first two terms in the expansion of ΔE as a function of $(1-x)$. This required calculating terms up to the fourth power of the P_2 component of the deformation and the square of the P_4 component.

Present and Knipp[4] extended this series somewhat and introduced also odd terms, P_3 and P_5. F. Reines, working with Present and Knipp, included additional terms to an extent sufficient to permit the determination of the saddle-point shape and the reaction threshold in the range $1.0 \geqslant x \geqslant 0.8$.[5] The value and derivative

* Now with Frankel and Nelson, Los Angeles.
[1] L. Meitner and O. R. Frisch, Nature **143**, 239 (1939).
[2] N. Bohr and J. Wheeler, Phys. Rev. **56**, 426 (1939).
[3] J. Frenkel, Phys. Rev. **55**, 987 (1939) and J. Phys. U.S.S.R. **1**, 125 (1939).
[4] R. D. Present and J. K. Knipp, Phys. Rev. **57**, 751, 1188 (1940).
[5] R. D. Present, F. Reines, and J. K. Knipp, Phys. Rev. **70**, 557 (1946).

of the threshold at $x=0$ have been given by Bohr and Wheeler.[2] Using these values and his results Reines determined by interpolation the value of the threshold for $x=0.74$ (corresponding to U^{239}). His estimated limit of error is ± 15 percent.

During the last stages of the development of the Eniac (the "electronic numerical integrater and computer") Professor Fermi suggested to the authors that the use of the Eniac might permit a straightforward numerical calculation of the potential energy values beyond the range of validity of the power series.

2. THEORY

The potential energy of a deformed nucleus in the liquid-drop model is the sum of two terms

$$E=E_s+E_c, \tag{1}$$

where E_s is a surface-tension-like energy arising from the lack of saturation of the binding forces of particles near the surface, and is proportional to the surface, while E_c is the Coulomb energy of the charge of the nucleus which is assumed uniformly distributed throughout its volume. The energy of the undeformed (spherical) nucleus is denoted by

$$E^0=E_s^0+E_c^0=E_s^0(1+2x). \tag{2}$$

Only axially symmetric distortions are considered. These are specified by giving the radius, R^1, as a function of the cosine of the co-latitude, μ. The unit of length is the undistorted radius. It is convenient to introduce a scale factor, R_0, and write

$$\begin{aligned} R^1(\mu)&=R_0R(\mu),\\ R(\mu)&=1+\alpha_1P_1(\mu)+\alpha_2P_2(\mu)+\cdots, \end{aligned} \tag{3}$$

where P_i is the ith Legendre polynomial. A particular distortion is specified by the coefficients α_i of this expansion. Only terms up to P_{10} have been considered.

It may be observed that (3) does not represent all axially symmetric deformations but only those described by single-valued functions, $R^1(\mu)$. Thus a deformation into two almost spherical parts connected by a thin filament cannot be so represented.

The scale factor R_0 is determined by the constant volume condition,

$$\tfrac{1}{2}\int_{-1}^{1}(R^1)^3d\mu=R_0^3V=1,$$

$$V=\tfrac{1}{2}\int_{-1}^{1}R^3(\mu)d\mu.$$

The energies, E_s and E_c, are represented in terms of their original values,

$$E_s=B_sE_s^0,\quad E_c=B_cE_c^0=2xB_cE_s^0. \tag{5}$$

The relative surface energy, B_s, is the ratio of the distorted to the undistorted surface.

$$B_s=\tfrac{1}{2}V^{-2/3}\int_{-1}^{1}R[R^2+\nu^2(dR/d\mu)^2]^{\frac{1}{2}}d\mu, \tag{6}$$

where

$$\nu^2=1-\mu^2.$$

B_c is similarly calculated for the volume bounded by $R(\mu)$, then normalized by multiplication by $V^{-5/3}$.

$$B_c=(15/16\pi^2)\left[V^{-5/3}\int\phi d\tau\right], \tag{7}$$

$$\phi=\int\frac{d\tau'}{|r-r'|}=\int_{-1}^{1}d\mu'\times\int_0^{R'(\mu')}r'^2dr'\int_0^{2\pi}\frac{d\psi'}{|r-r'|}. \tag{8}$$

The calculation of B_c thus involves calculating a sixfold integral, threefold in $d\tau'$ and threefold in $d\tau$. Since the shape is axially symmetric the azimuthal integration of $d\tau$ is trivial. B_c can be reduced further, to a fourfold integral, by the following device:[6] Consider another distorted drop having the same shape and charge density but scaled up in all linear dimensions by a factor $(1+\epsilon)$ where $\epsilon\ll 1$. Then the volume of the

TABLE I. Threshold values and saddle-point shapes.

x	ξ	B_s	B_c	α_2	α_4	α_6	α_8	α_{10}
0.9	0.0007	0.0195	0.0107	0.23	0.019	−0.0016	—	—
0.81	0.0050	0.0731	0.0420	0.47	0.083	−0.006	−0.006	—
0.77	0.009_2	0.094_2	0.055_1	0.5_5	0.1_1	−0.01	−0.01	—
0.74	0.0136	0.1371	0.0834	0.70	0.193	−0.008	−0.020	−0.0025
0.65	0.0400	0.3044	0.2034	2.4	1.15	−0.11	−0.22	0.03

[6] This method was suggested to us by Dr. H. Hurwitz.

second drop, hence also its charge, is greater than that of the first by a factor $(1+3\epsilon)$ and its electrostatic energy is greater by a factor $(1+5\epsilon)$. This second drop may be produced from the first by adding a thin layer of the (charged) material to its surface. The increase of electrostatic energy in this process is the work required to bring the added surface charge from infinity and thus depends only on the potentials on the surface.

$$5\epsilon E_c = 5\epsilon \int \phi d\tau = \int \phi(R, \omega)(\epsilon R) R^2 d\omega. \quad (9)$$

Hence

$$B_c = (3/8\pi V^{5/3}) \int \phi_s R^2 d\mu, \quad (10)$$

where ϕ_s is the potential at the surface as given by (8).

The azimuthal integration in the evaluation of ϕ can be carried out analytically and results in an elliptic integral of the first kind.

$$\int_0^{2\pi} [R^2+r'^2-2Rr'(\mu\mu'+\nu\nu'\cos\psi')]^{-\frac{1}{2}} d\psi'$$

$$= \int_0^{2\pi} [A_0^2 \cos^2(\psi'/2)+G_0^2 \sin^2(\psi'/2)]^{-\frac{1}{2}} d\psi'$$

$$\equiv I(A_0, G_0), \quad (11)$$

where

$$A_0^2 = R^2+r'^2-2Rr'(\mu\mu'+\nu\nu'),$$

$$G_0^2 = R^2+r'^2-2Rr'(\mu\mu'-\nu\nu').$$

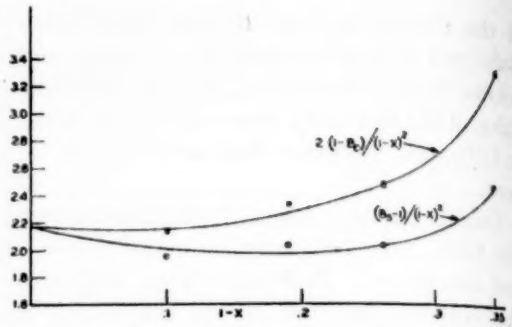

FIG. 2a. Dependence of the relative Coulomb energy, B_c, and the surface energy, B_s, of saddle-point shapes on x. (Cf. Eqs. (5)–(7)).

Landen's transformation,[7]

$$I(A_n, G_n) = I(A_{n+1}, G_{n+1}) \quad (12)$$

$$A_{n+1} = (A_n+G_n)/2, \quad G_{n+1} = (A_nG_n)^{\frac{1}{2}}$$

provides the basis of a convenient[8] iterative scheme for evaluating $I(A_0, G_0)$. On successive applications of this transformation the difference, $|A_n-G_n|$, rapidly approaches zero. Then denoting the common limit of A_n and G_n by M (the "arithmetic-geometric mean" of A_0 and G_0),

$$I(A_0G_0) = 2\pi/M. \quad (13)$$

The number of steps in the iteration procedure was left free in the planning of the problem. Calculating experience showed that sufficient accuracy was obtained by carrying the calculation to A_4 (cf. Appendix II).

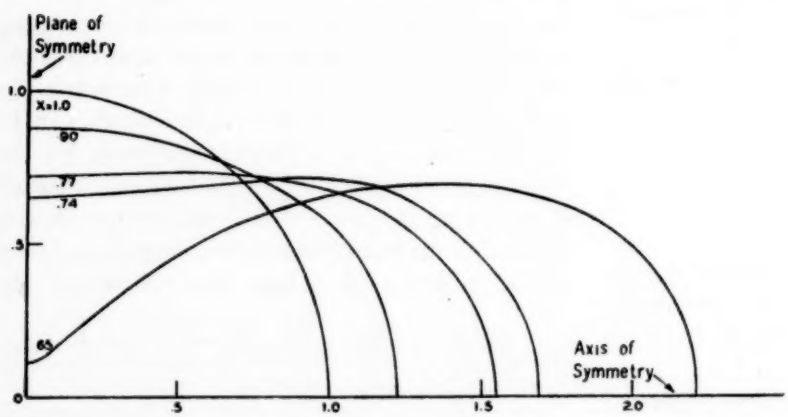

FIG. 1. Saddle-point shapes for various values of the nuclear parameter x. The unit of length is the undistorted radius.

[7] E. T. Whittaker and G. N. Watson, *Modern Analysis* (Cambridge University Press, Teddington, England, 1915), p. 533.

[8] In treating this problem with a desk calculator the use of a table of the first elliptic integral in this step would be far easier. However, in setting up the problem for the Eniac the economy in program controls and programming labor of this procedure seemed to us adequate compensation for the increase in computing time. It seems likely that the use of high speed calculating machines will often effect changes of this kind in the economy of calculating procedures.

The radial integration in the evaluation of ϕ and both co-latitude integrations were carried out numerically. In the radial integration the relative radius

$$y=r'/R'(\mu') \tag{14}$$

with the range (0, 1) was used as argument. A five-point integration rule was used,[9]

$$3\int_0^1 f(y)y^2dy\cong\sum_{i=1}^{5} e_i f(y_i), \tag{15}$$

$y_i=0.2,\ 0.4,\ 0.6,\ 0.8,\ 1.0,$

$e_i=0.014881,\ 0.148809,\ 0.089286,\ 0.565476,\ 0.181548.$

The coefficients are so chosen that the equality sign holds for any fourth-degree polynomial, $f_4(x)$.[10]

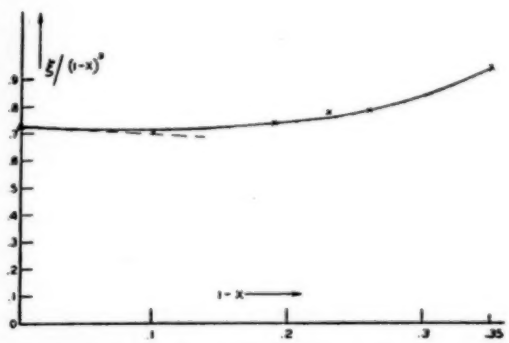

FIG. 2b. Relative threshold values. It is convenient to use $\xi/(1-x)^3$ as ordinate rather than ξ itself; cf. Eq. (23). The initial slope and intercept are taken from Bohr and Wheeler.

The co-latitude integrations in ϕ, B_c, B_s, and V are performed with a 10-entry gauss integration rule.[11] Denoting the ten roots of $P_{10}(\mu)$ by μ_i and the integration coefficients normalized to unity by c_i the equation

$$\tfrac{1}{2}\int_{-1}^{1} f(\mu)d\mu=\sum_{i=1}^{10} c_i f(\mu_i) \tag{16}$$

holds with the equality sign if $f(\mu)$ is a polynomial of 19th degree. Thus the various integrals are approximated by summations as follows:

$$V\cong\sum_{i=1}^{10} c_i R_i^3, \tag{17}$$

$$R_i=1+\sum_{j=1}^{10}\alpha_j P_j(\mu_i), \tag{18}$$

$$(dR/d\mu)_i=\sum_{j=1}^{10}\alpha_j P_j'(\mu_i),$$

$$B_s\cong V^{-2/3}\sum_{i=1}^{10} c_i R_i[R_i^2+\nu^2(dR/d\mu)_i^2]^{\frac{1}{2}}, \tag{19}$$

$$B_c\cong V^{-8/3}\sum_{i=1}^{10}\sum_{j=1}^{10}\sum_{k=1}^{5} c_i c_j e_k R_i^3 R_j^3/M_{ijk}, \tag{20}$$

$$2\pi/M_{ijk}=I(A_0, G_0), \tag{21}$$

$$A_0^2=R_i^2+R_j^2y_k^2-2R_iR_jy_k(\mu_i\mu_j+\nu_i\nu_j),$$

$$G_0^2=R_i^2+R_j^2y_k^2-2R_iR_jy_k(\mu_i\mu_j-\nu_i\nu_j).$$

The contributions to B_s for $k=5$ ($x_5=1.0$) require special treatment. The surface potential (say at R_j, μ_j) produced by a shell of material at the surface is represented by the integral

$$\int_{-1}^{1} d\mu'/M(\mu_j, \mu') \tag{22}$$

where $M(\mu_j, \mu')$ is the arithmetic-geometric average of the maximum and minimum distances from the point $(R_j, \mu_j, 0)$ to the circle (R, μ', ψ'). For $\mu'=\mu_i$, $i\neq j$, M has the value $M_{j,i,5}$ as defined in (21). However as μ' approaches μ_j the integrand, $1/M$, approaches infinity logarithmically. Thus the numerical approximation (16) is inapplicable to the integral (22). This difficulty is circumvented by separating the integrand, $1/M$, into a non-singular part which is integrated numerically in the usual way and a simple singular part which is integrated analytically. In the summation (20) each term, $1/M_{i,j,k}$, for which $i=j$, $k=5$ is replaced by the sum of two terms, one of which is the

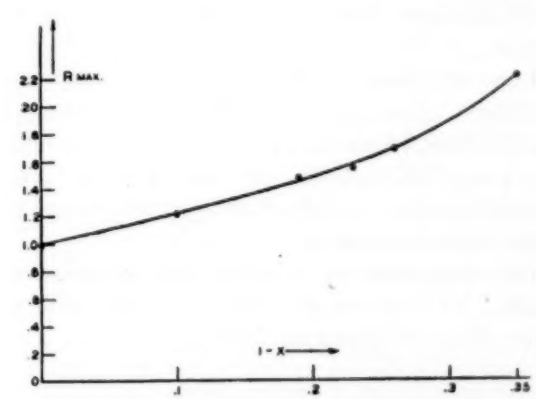

FIG. 2c. Maximum radii of saddle-point shapes.

[9] It proves convenient in the following to choose a unit normalization for the coefficients, e_i.

[10] Cf. Appendix I.

[11] Lowan, Davids, Levenson, Bull. Am. Math. Soc. **48**, 739 (1942).

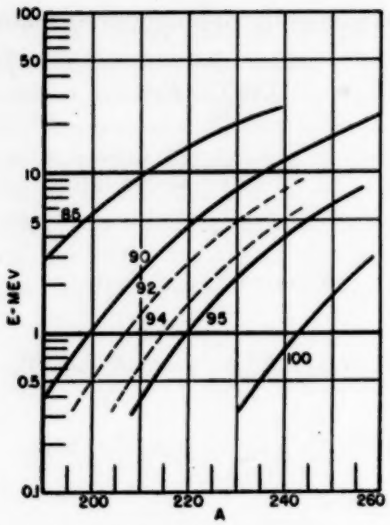

FIG. 3. Fission thresholds for nuclei near uranium. Curves for various Z values are given. Quantum-mechanical effects are not included.

integral of the singular part of $1/M$, the other the ith contribution to the numerical integral of the singular part. The details of this separation are given in Appendix II.

The change in the total energy of the nucleus produced by the deformation is expressed by the quantity

$$\xi \equiv \frac{\Delta E}{E_s^0} = B_s - 1 + 2x(B_c - 1). \qquad (23)$$

3. RESULTS

The most accurate and extensive study was made for $x=0.74$, the value calculated by Present, Knipp, and Reines[5] for U^{239}. The ξ-value found for its symmetric saddle-point is 0.013_6. (Cf. Table I.) This value coincides with the upper limit estimated by them;[12] the interpolated value given by Bohr and Wheeler[2] is 0.01_1.

The threshold value found for $x=0.90$, $\xi=0.0007$, agrees with the value found by Reines and Present. However at $x=0.81$, which bounds the range of validity of their series, their threshold value is some 8 percent less than the Eniac value, $\xi=0.0050$.

The threshold for $x=0.77$ was investigated briefly. An approximate threshold and saddle-point shape are given in Table I.

[12] We are indebted to Present, Reines, and Knipp for access to a more complete description of their work than their publication, reference 5.

The neighborhood of the saddle-point as determined by this procedure for $x=0.65$ was investigated with some care. The results obtained are listed in Table I.

The deformation shape near this indicated saddle-point ($x=0.65$) borders on the region in which multiple-valued R *vs.* μ description is required. The saddle-point shapes which have been obtained are shown in Fig. 1. It appears likely that for values of x somewhat less than 0.65 the true saddle-point shape requires a multiple-valued description and can therefore not be treated by the present method.

In Fig. 2a the values obtained for $(B_s-1)/(1-x)^2$ and $2(1-B_c)/(1-x)^2$ for the saddle-point shapes are plotted. Smooth curves have been drawn; the values at $x=1$ were taken from the series development of Bohr and Wheeler. In Fig. 2b the values obtained for $\xi/(1-x)^3$ are plotted. A smooth curve, consistent with the curves of Fig. 2a, is drawn: the initial value and slope are taken from Bohr and Wheeler. In Fig. 2c the maximum radii of the normalized saddle-point shapes are drawn.

In Fig. 3 the fission threshold (e.g., for photo-fission) is shown for nuclei near uranium. The constants used to evaluate these energies are those used by Present, Reines, and Knipp. They correspond to a value of 0.74 for x and to 538 Mev as the unit of energy in which ξ is measured for U^{239}. These energies may be regarded as the classical fission thresholds, i.e., the energy differences as computed with the liquid-drop model between the initial spherical equilibrium shape and the saddle-point unstable equilibrium shape.

Two quantum-mechanical effects must be taken into account in comparing observed photo-fission thresholds with the energies of Fig. 3. Photo-fission will be observed for energies below the saddle-point energy by reason of the tunnel effect. Moreover the zero-point energy of the mode of vibration which leads to fission effectively increases the energy of the equilibrium state. To calculate these effects requires the determination of a suitable trajectory of deformations leading to fission and of the momentum conjugate to the deformation coordinate so introduced.

To determine a suitable trajectory of deformations for a particular x value, say x_0, consider

first the quantum-mechanical problem of spontaneous fission which requires the traversal by tunnel effect of most of the region of positive ξ. The rate of spontaneous fission will be determined primarily by the minimum of the Gamow factor exponents for all such trajectories. It is clearly reasonable to suppose that a trajectory possessing this minimum value passes through or very close to the classical saddle-point of x_0. It furthermore seems reasonable to assume that this minimizing trajectory also lies close to the saddle-point deformations determined by other x-values than x_0. For this reason, and by reason of its convenience, the sequence of shapes of Fig. 1 is taken for the "fission trajectory." The maximum radius will be used as the coordinate specifying the deformation and will be denoted by $1+a$.

The evaluation of the Gamow factor requires the use of an effective mass, M_a, such that the kinetic energy associated with a motion along the fission trajectory is $\frac{1}{2}M_a(da/dt)^2$. Of all possible motions of an incompressible fluid consistent with the prescribed motion of the surface the minimum kinetic energy, hence, the minimum M_a is that of an irrotational motion. This minimum value of M_a is the value required for the Gamow factor calculation. The zero-rotation condition, together with the prescribed motion of the surface, uniquely determines the motion and permits the calculation of M_a.

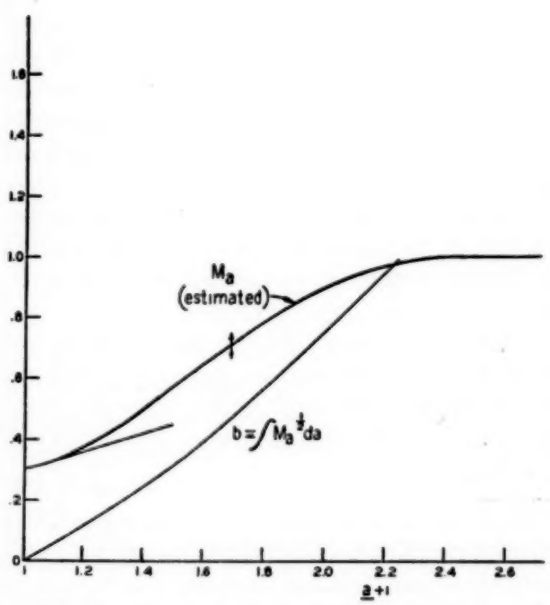

FIG. 4. The upper curve represents the effective mass for barrier penetration in units of the total mass. The lower curve is the transformed deformation coordinate b for which the effective mass is the total mass.

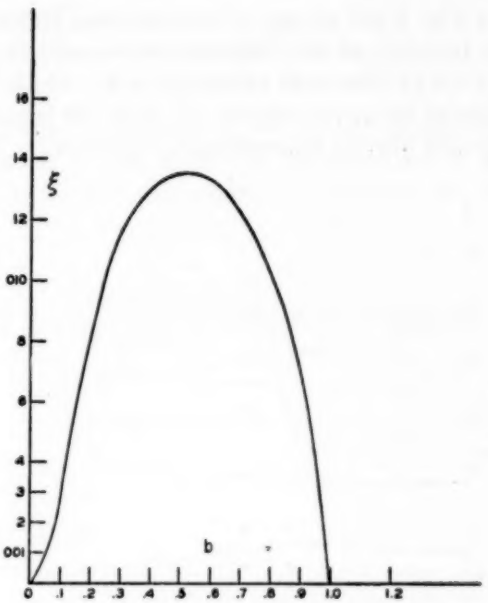

FIG. 5. The energy of deformation for $x=0.74$. The coordinate b is plotted in Fig. 4. The unit of energy is taken as 538 Mev and the unit of length is the initial nuclear radius.

For small a the surface is described by

$$R(\mu)=1+aP_2(\mu)+0(a^2).$$

The pattern of motion can be shown to be

$$\bar{v}=(da/dt)\ \mathrm{grad}(r^2P_2(\mu))$$

and

$$M_a=0.3M(1+a)+0(a^2),$$

where M is the total mass of the nucleus. After fission (i.e., for large a) M_a approaches M. A numerical calculation has been carried out for one intermediate value of a, $a=0.69$ corresponding to the saddle-point for $x=0.74$. The value obtained is $M_a=0.71M$ with an estimated probable error of 5 percent. These values were used to draw the approximate M_a *vs.* a curve of Fig. 4. This determination of M_a permits the transformation to another coordinate specifying the deformation,

$$b=\int(M_a/M)^{\frac{1}{2}}da,$$

for which the effective mass is the total mass, M.

In Fig. 5 the energy of deformation is drawn as a function of this deformation coordinate, b, for $x=0.74$. The unit of energy is E_s^0 which for values of the mass number, A, near 238 is taken to be 538 Mev as determined by Feenberg.[13] The unit of length in which b is measured is the initial nuclear radius which is taken as $A^{\frac{1}{3}}1.47\times10^{-13}$ cm as determined by Bohr and Wheeler.[2]

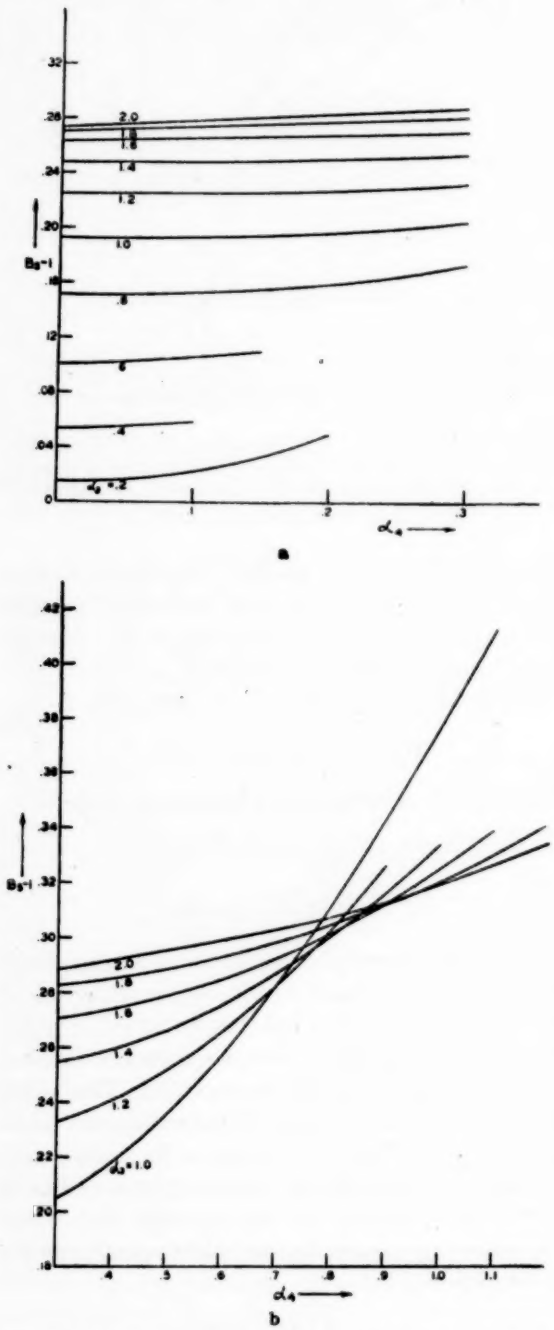

FIG. 6. Relative surface energies as functions of the deformation parameters α_2, α_4; cf. Eq. (3).

[13] E. Feenberg, Phys. Rev. **55**, 504 (1939).

The energy *vs.* deformation relationship of Fig. 5 has been used to calculate the Gamow penetration probability for various excitation energies. This penetration probability is found to be well represented by

$$G=10^{-7.85\Delta E}, \tag{24}$$

where ΔE is the energy deficit at the saddle-point in Mev.

The zero-point energy of vibration as calculated with the initial curvature of Fig. 5 is 0.4 Mev corresponding to a vibration frequency of 2×10^{20} sec.$^{-1}$ in agreement with the value calculated by Bohr and Wheeler.[2]

Using this value for the zero-point energy and Eq. (24), the mean life for spontaneous fission may be calculated.[14]

$$T_s=10^{-21}\ \text{sec}/G=10^{26}\ \text{yr}. \tag{25}$$

(Cf. Table II.)

The excitation energy required for fission will be approximately E_{cl} less the zero-point energy, 0.4 Mev., where

$$E_{cl}=E_s^0\xi_{\max}.$$

A corresponding set of values has been calculated for $x=0.75$. The results are listed in Table II. It will be seen there that if x is assumed to have the value 0.74 for U^{238}, reasonable agreement with experimental results on photo-fission[15] and spontaneous fission[16] is obtained. This choice represents a slight revision of the conclusions reached by Bohr and Wheeler who chose $x=0.74$ by similar considerations based on their interpolated ξ-curve.

It should be noted that the fission trajectories for which these calculations have been made are not precise minimal trajectories, thus the mean-life values for spontaneous fission given in Table II are upper limits.

[14] T_s is reduced by a factor of 5 for the degeneracy of this mode of vibration. Cf. reference 2.

[15] R. O. Haxby, W. E. Shoupp, W. E. Stephens, and W. H. Wells, Phys. Rev. **59**, 57 (1941).

[16] G. Scharff-Goldhaber and G. S. Klaiber, Phys. Rev. **70**, 229 (1946); W. Maurer and H. Pose, Zeits. f. Physik **121**, 285 (1943); H. Pose, Zeits. f. Physik **121**, 293 (1943); G. N. Flerov and K. A. Petrzhak, J. Phys. U.S.S.R. **3**, 275 (1940).

In order to represent deformation energies for shapes other than those on the assumed fission trajectories, a number of Eniac calculations were performed for deformations specified by various values of α_2 and α_4, with all other α's vanishing. The values obtained for B_s and B_c are presented separately in Figs. 6a, 6b and 7a, 7b. The corresponding ξ-values for $x=0.74$ are shown in Fig. 8. It may be noted (cf. Fig. 1) that the saddle-points for $x \gtrsim 0.74$ are closely approximated in this α_2, α_4 representation.

4. ASYMMETRIC DEFORMATIONS

Deformation energies, B_s, B_c, and ξ have been calculated for a few asymmetric shapes. Unfortunately this investigation was by no means complete or systematic.

It is to be expected that the interesting effects due to asymmetric terms in the $R(\alpha)$ expansion, Eq. (3), will arise primarily from the P_1 and P_3 terms. The higher odd harmonics will serve primarily as refinements as do the higher even harmonics in symmetric fission. The use of odd harmonics introduces one "spurious" degree of freedom since a symmetric deformation shape can be represented by an asymmetric series if the origin of the polar-coordinate systen is displaced along the axis of (rotational) symmetry. This degeneracy of the description may be removed by the imposition of one condition on the expansion coefficients. A convenient form for this condition is the requirement that the center of gravity shall remain at the origin. In the present work no such condition was systematically applied. The effect of the addition of various combinations of P_1 and P_3 to a few symmetric expansions was determined.

It was hoped that this brief investigation of asymmetric shapes might lead to an explanation of the observed asymmetry of fission.[17] However no evidence was found that the influences producing the asymmetry of fission are represented in this model.

Small amounts of P_1 and P_3 were added to the initial spherical shape. The B_s and B_c values obtained were consistent with the power series expansion of Bohr and Wheeler (reference 2, Eq. (9)).

$$B_s = 1+5\alpha_3^2/7+0(\alpha^4),$$
$$B_c = 1-10\alpha_3^2/49+0(\alpha^4). \qquad (26)$$

In these expansions there are no terms in α_1^2 because to this order the introduction of a P_1 component serves merely to displace the drop

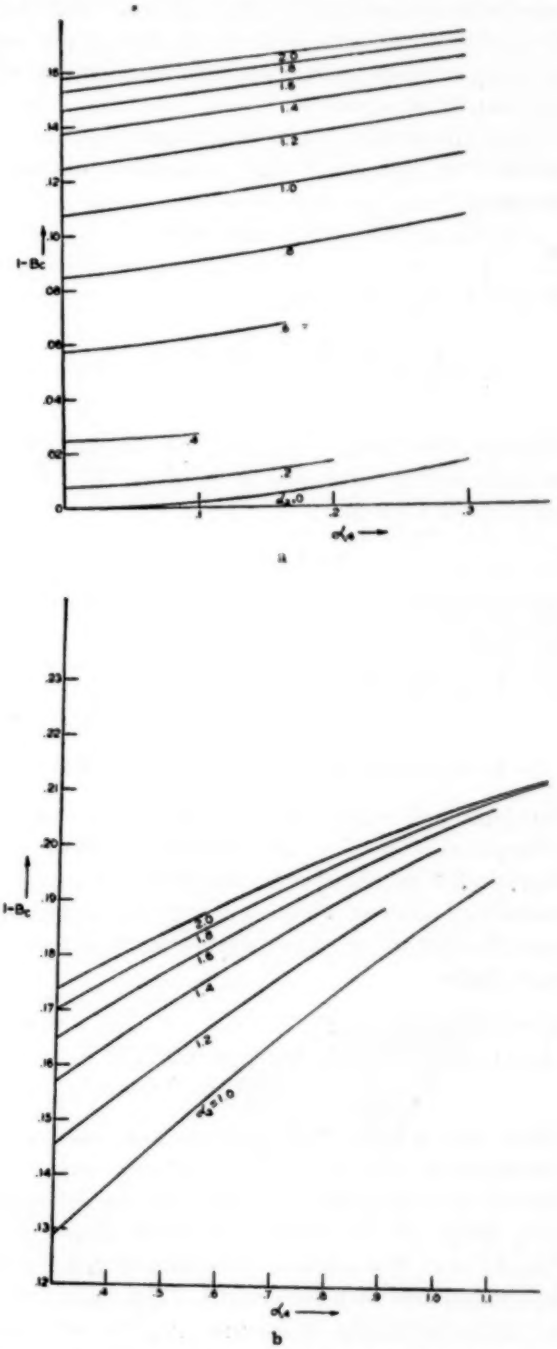

FIG. 7. Relative Coulomb energies as functions of α_3, α_4.

[17] The Plutonium Project, Rev. Mod. Phys. 18, 513 (1946).

TABLE II. Energies and mean lives for $E_s^0=538$ Mev., $A=238$, $r_0=1.47\times10^{-13}$.

x	ξ	$E_{sl}-0.4$ (Mev.)	T_s (yrs.)
0.74	0.0137	6.9_7	10^{26}
0.75	0.0120	6.0_7	10^{17}

parallel to the polar axis. Thus for small deformations from the spherical shape the center of gravity condition is approximately equivalent to the restriction $\alpha_1=0$.

More generally, a small displacement, δ, parallel to the polar axis, transforms the expansion

$$R(\mu)=1+\sum\alpha_iP_i(\mu)$$

to

$$R'(\mu)=1+\sum\alpha_iP_i+P_1\delta+(\delta/R)\sum\alpha_i\frac{i(i+1)}{2i+1}(P_{i+1}-P_{i-1})+0(\delta^2). \quad (27)$$

Thus for the sphere, $R(\mu)=1$, the displacement is described by a change in α_1 alone. However, for a shape such as

$$R=1+0.7P_2$$

(an approximate saddle-point for $x=0.74$) which becomes

$$R'=1+0.7P_2+P_1\delta+[0.84\delta/(1+0.7P_2)]\times(P_3-P_1)+0(\delta^2)$$
$$=1+0.7P_2+0.20\delta P_1+1.05\delta P_3-0.28\delta P_5+\cdots,$$

the principal effect of the displacement is to change α_3. Thus in the neighborhood of the heavy-nucleus thresholds the effect of α_3 is of secondary interest while α_1 makes the important contribution to the asymmetry. For the deformation shape

$$R=(1+0.7P_2)+\alpha_1P_1,$$
$$\xi=(1.12783-0.247\alpha_1^2)+2x(-0.07132+0.238\alpha_1^2)+0(\alpha_1^4). \quad (28)$$

Thus for $x>0.52$ the deformation energy is *increased* by this introduction of asymmetry. It should be noted that the effect on the deformation shape of the term α_1P_1 is to narrow the "neck," i.e., the relative minimum of $R(1-\mu^2)^{\frac{1}{2}}$, in comparison with the length. Thus in addition to the introduction of asymmetry, this term has a geometric effect similar to that of an increase of α_2. On the other hand the introduction of asymmetry, by shiting material from one side to the other, has in part the effect of restoring the original spherical shape. Thus the P_1 term has two effects, that of producing asymmetry and that of changing the symmetric distortion in an ambiguous way. As α_2 is increased from 0.7, ξ increases if $x<0.88$, decreases if $x>0.88$ (cf. Figs. 6–7). Since the P_1 term increases ξ throughout the range $0.52<x<1.00$ it seems likely that that part of its effect due only to asymmetry is uniformly unfavorable.

For a more quantitative study of the effect of asymmetry on the deformation energy, small amounts of P_1 and P_3 were added to the symmetric saddle-point expansion for $x=0.77$. It may be seen from Eq. (27) that the displacement by a distance δ of a symmetric-deformation shape introduces changes in the even-harmonic coefficients, α_2, α_4, etc., of order δ^2. At the saddle-point these changes affect the deformation energy only to order δ^4. Thus if small odd-harmonic terms are added to the saddle-point expansion the change in ξ of order α_{odd}^2 is due entirely to the true asymmetry which they produce and not the change in the symmetric distortion produced by their "equivalent displacement." The change in ξ for small α_{odd} was found to be

$$\Delta\xi_{x=0.77}\cong0.246(0.659\alpha_1-0.752\alpha_3)^2+0.010(0.752\alpha_1+0.659\alpha_3)^2. \quad (29)$$

The coefficient of the second term would be zero if all the odd terms produced by a displacement were taken into account. The corresponding expression for the (spherical) saddle-point of $x=1.0$ is (cf. Eq. (26))

$$\Delta\xi_{x=1.0}=0.306\alpha_3^2+0.000\alpha_1^2. \quad (30)$$

The slight decrease in the first coefficient as x decreases from 1.0 to 0.77 suggests that with increasing symmetric deformation a small amount of asymmetry becomes energetically less unfavorable and may even become favorable for very great distortion. To check this possibility the deformation energy has been calculated analytically for the extreme deformation represented by two spheres in contact.[18] The

[18] We are indebted to Dr. John Mauchly and to Dr. Leonard Schiff for this suggestion.

result is

$$\xi=(V^{\frac{1}{3}}+W^{\frac{1}{3}})-1+2x[V^{5/3}+W^{5/3}+5VW/3(V^{\frac{1}{3}}+W^{\frac{1}{3}})-1], \quad (31)$$

where V and W are the fractions of the original volume in the two spheres. The derivative,

$$d\xi/dV=2(V^{\frac{1}{3}}-W^{\frac{1}{3}})/3V^{\frac{1}{3}}W^{\frac{1}{3}}\times[20xV^{\frac{1}{3}}W^{\frac{1}{3}}/3(V^{\frac{1}{3}}+W^{\frac{1}{3}})-1]$$

consists of two factors, the first increasing from 0 to $+\infty$ as V increases from 0.5 to 1.0, the second decreasing monotonically from $5x/3-1$ to -1. Thus for $x>0.6$, ξ has a relative minimum at $V=W=0.5$ and no other. For $x<0.6$ no minimum exists. Figure 9 shows the dependence of ξ on V for various x-values.

In order to compare this result with the previously evaluated effects of asymmetry, Eqs. (29) and (30), the two-sphere shape may be expressed in a form analogous to the Legendre polynomial expansion.

$$R=2|\mu|+\alpha_1\mu=(1+\alpha_2P_2+\alpha_4P_4+\cdots)+\alpha_1P_1$$

where

$$\alpha_{2n}=\tfrac{1}{2}(4n+1)\int_{-1}^{1}P_{2n}(\mu)2|\mu|\,d\mu.$$

Reexpressing the energy, Eq. (31), by the use of the relationship

$$V=(1+\alpha_1/2)^3/2(1+3\alpha_1^2/4)$$

gives

$$\Delta\xi=2^{1/3}(1+17x/12)+2^{-5/3}(5x/3-1)\alpha_1^2+\cdots.$$

For $x=0.75$ (for example) the coefficient of α_1^2 is 0.0788, which is considerably smaller than the leading coefficients in Eqs. (29) and (30) but is still appreciably greater than zero. Figure 9 shows, moreover, that the increase of energy with increasing asymmetry extends to quite great asymmetries.

The above evidence seems to us to suggest strongly, although not to prove conclusively, that asymmetric fission is not favored in the liquid-drop model.

ACKNOWLEDGMENTS

We wish to thank the Army Ordnance Department and the University of Pennsylvania, particularly General G. M. Barnes, Colonel L. E. Simon, and Dr. L. S. Dederick for the use of the Eniac and to Professor J. von Neumann and Dr. and Mrs. H. H. Goldstine for instruction in its operation. We particularly wish to acknowledge our indebtedness to the capable operating staff of the Eniac, who proved quite indispensable in

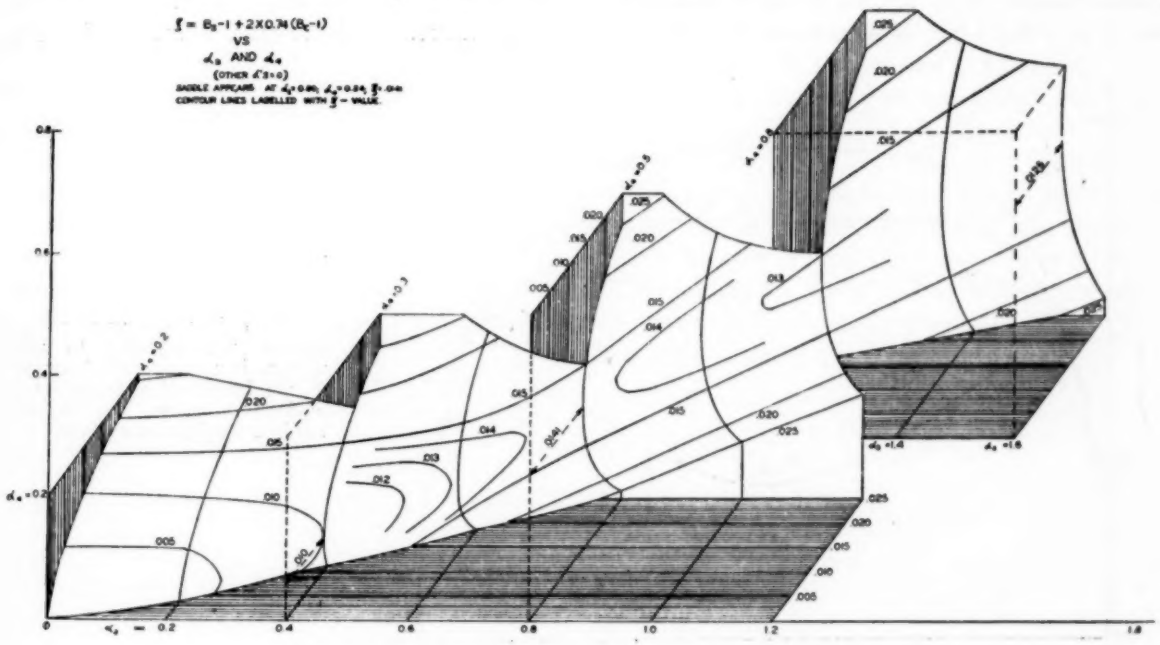

FIG. 8. Relative total energies as functions of α_2, α_4 for $x=0.74$.

the execution of this and a preceding problem. We are also indebted to Professors E. Fermi and E. Teller, Mr. J. P. Eckert, Jr., and Dr. J. Mauchly for their help in many valuable discussions.

APPENDIX I

An Alternative Radial Integration Rule

An alternative integration rule (analogous to the Gauss rules) was developed for use in the event that the rule of Eq. (15) proved insufficiently accurate. The gauss rules for the approximate evaluation of integrals in the range $(-1, 1)$ with unit weight factor are based on the orthogonality property of the legendre polynomials in this range and with this weight. For the present problem we make use of the polynomial, $F_4(x)$, which is orthogonal to polynomials of lower degree with the weight factor x^2.

This polynomial can be constructed from the legendre polynomials, P_i, scaled to the interval (0,1),

$$p_i(x) \equiv P_i(2x-1),$$

$$x^2F_4(x) = \begin{vmatrix} p_4(x) & p_5(x) & p_6(x) \\ p_4(0) & p_5(0) & p_6(0) \\ p_4'(0) & p_5'(0) & p_6'(0) \end{vmatrix}.$$

The determinant and its first derivative evidently vanish at $x=0$, thus it does contain the factor x^2. $x^2F_4(x)$ is a linear combination of $p_4(x)$, $p_5(x)$, and $p_6(x)$ and is therefore orthogonal to any cubic polynomial in (0,1). Any seventh degree polynomial, $f_7(x)$ may be divided by $F_4(x)$ leaving a cubic remainder.

$$f_7(x) = Q_3(x)F_4(x) + R_3(x)$$

thus

$$\int_0^1 f_7(x)x^2dx = \int_0^1 R_3(x)x^2dx.$$

If x_j is one of the four (real) roots of $F_4(x)$

$$f_7(x_j) = R_3(x_j).$$

The cubic polynomial, $R_3(x)$, may be expressed in terms of these four of its values

$$R_3(x) = \sum_{j=1}^{4} R_3(x_j)F_4(x)/(x-x_j)F_4'(x_j),$$

thus

$$3\int_0^1 f_7(x)x^2dx = \sum_{j=1}^{4} e_jf_7(x_j)$$

where

$$e_j = 3\int_0^1 [x^2F_4(x)/(x-x_j)F_4'(x_j)]dx.$$

The roots and coefficients have the values

$$x_j = 0.204149,\ 0.482953,\ 0.761399,\ 0.951499,$$
$$e_j = 0.031057,\ 0.205902,\ 0.430376,\ 0.332665.$$

This method can obviously be extended to other weight functions and to other numbers of entries.

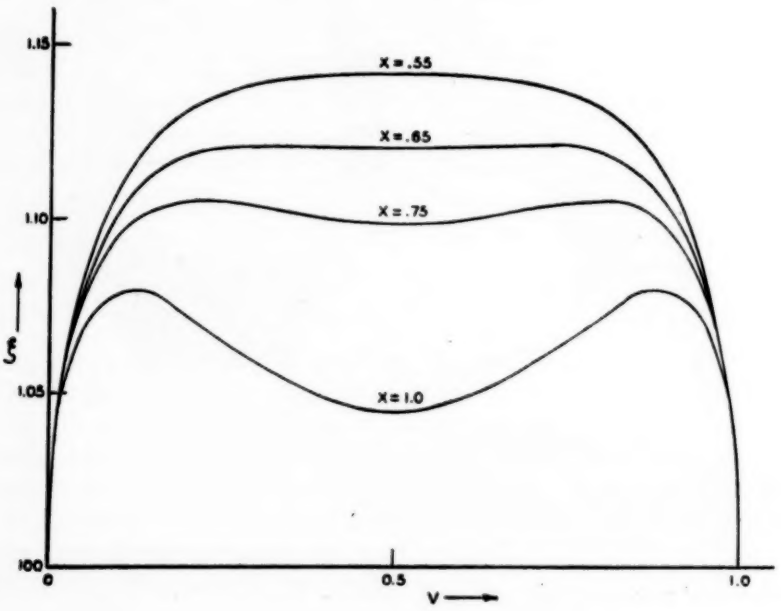

FIG. 9. The energy of deformation corresponding to two spheres in contact as a function of the fractional volume V for various x values. No central minimum exists for $x < 0.60$.

APPENDIX II

The separation of the singular part of the surface integral.

The integral

$$B_e = V^{-5/3}\int_{-1}^{1}\tfrac{1}{2}d\mu\int_{-1}^{1}\tfrac{1}{2}d\mu'\int_{0}^{1}3x^2dx \times R^3(\mu)R^3(\mu')/M(\mu,\mu',x)$$

is to be approximated by the finite sum of Eq. (20). Special treatment is required for $x=1.0$ ($k=5$ in Eq. (20)) since there the μ' integral is singular. For small values of $|\mu-\mu'|$, $1/M(\mu,\mu',1)$ becomes infinite as $-\ln|\mu-\mu'|/R$. Thus the integral over μ' may be separated as

$$\int[R'^3/M(\mu,\mu',1)]\tfrac{1}{2}d\mu' = \int[R'^3/M+R^2(\mu)\ln|\mu-\mu'|/\pi]\tfrac{1}{2}d\mu' + R^2(\mu)\psi(\mu)/\pi, \quad (32)$$

where

$$\psi(\mu) = -\int_{-1}^{1}\tfrac{1}{2}d\mu'\ln|\mu-\mu'| = 1-\tfrac{1}{2}\ln(1-\mu^2)-\tfrac{1}{2}\mu\ln\frac{1+\mu}{1-\mu}.$$

The remaining integrand is now sufficiently smooth to permit numerical integration. Its value for $\mu=\mu'$ is, apart from the factor R'^3,

$$\frac{1}{2\pi R}\ln\left[\frac{64R^2(1-\mu^2)}{R^2+(1-\mu^2)(dR/d\mu)^2}\right]. \quad (33)$$

To evaluate this quantity the minimum distance, A_0 of Eqs. (11) and (12), is given (instead of zero) the value

$$\epsilon=\delta[(dR/d\mu)^2+R^2/(1-\mu^2)]^{\frac{1}{2}}, \quad 0<\delta\ll 1, \quad \mu=\mu_i, \quad R=R(\mu_i)$$

and the iterative process carried out to determine $1/M_i$. The expression (33) then has the value

$$1/M_i+Q/R$$

where

$$Q=\ln\delta/\pi+0(\delta^2\ln\delta).$$

Now approximating the integral of the right side of Eq. (32) by the gaussian integration formula gives

$$\int[R'^3/M(\mu_i,\mu',1)]\tfrac{1}{2}d\mu' \cong R_i^3\psi(\mu_i)/\pi + \sum_{j\neq i}c_j[R_j^3/M_{ij5}+R_i^3\ln|\mu_i-\mu_3|/\pi] + c_iR_i^3[1/M_i+Q/R_i]=\sum_{j=1}^{10}c_jR_j^3\lambda_{ij}, \quad (34)$$

where

$$\lambda_{ij}=1/M_{ij5} \quad \text{for } j\neq i$$
$$=1/M_i+P_i/R_i \quad \text{for } j=i$$
$$P_i=\psi(\mu_i)/\pi c_i+\sum_{j\neq 1}c_j\ln|\mu_i-\mu_j|/\pi c_i+Q.$$

In calculating ϵ, δ was taken as 10^{-4}. The remaining factor in ϵ is the ratio of two numbers available at this stage of the calculation. The ten constants, P_i, were stored in a function table. In the Eniac routine it was possible to make the above indicated changes in procedure at the "singular points" with relative ease: the numbers entering into the calculation of $1/M$ were there chosen in a special way. Because of the smallness of δ the number of iterations (Eq. 12) was doubled. $1/M$ is added to P_i/R_i and is then entered into the series in the normal fashion.

Energy Distribution of the Fragments Resulting from the Fission of U^{235} and Th^{232} by Slow and by Fast Neutrons*

J. L. Fowler and Louis Rosen
University of California, Los Alamos Scientific Laboratory, Los Alamos, New Mexico

(Received August 11, 1947)

The distribution of energies of the fragments from U^{235} fission produced by slow and by fast neutrons were compared. The energy was determined by using a 10-channel amplitude discriminator to analyze pulses from a Frisch-grid ionization chamber. No difference was found outside the experimental error. The energy distribution of the fragments from thorium fission was also determined. The high energy tails of the distributions were especially investigated for the purpose of detecting the occurrence of triple fission. This indicated a negative result. A possible correlation between the most probable mode of disintegration of the nucleus and its atomic number suggests itself.

1. INTRODUCTION

A CONSIDERABLE number of experiments have been performed in which the primary objectives were to measure the kinetic energy liberated in the fission of uranium and to determine how this energy is distributed between the fission fragments.[1–11] Of all these studies, the only ones which are in good agreement on the details of the energy distribution of the fission fragments are those of Jentschke and Deutsch.

In virtually all of the investigations made to date, where the energies of the individual fission fragments were determined, the experimental procedure involved the photographing and subsequent measuring of the ionization pulses produced by the fission fragments, a procedure which necessarily limits the statistical accuracy of the results.

The present investigation was undertaken for three reasons:

Table I. Comparison of data on fission products from U^{235} and Th^{232}.

	Position of high energy peak (Mev)	Position of low energy peak (Mev)	Width at half-maximum for high energy peak (Mev)	Width at half-maximum for low energy peak (Mev)	Ratio of minimum to high energy peak (%)	Ratio of peak energies	Ratio of peak heights	Foil thickness (mg/cm²)
$_{92}U^{235}$—Slow neutrons								
Jentschke	95.5	65	13	20	5	1.47	1.49	0.04
Deutsch	94	60	11	18	12.5	1.56	1.57	0.001
Fowler and Rosen	92.5	61.2	15	24.5	14.4	1.50	1.46	0.029
Fowler and Rosen	93	61.8	17.8	25.5	21	1.50	1.43	0.105
$_{92}U^{235}$—Fast neutrons								
Fowler and Rosen	92.5	62	14.7	25	16.1	1.49	1.44	0.029
$_{90}Th^{232}$								
Jentschke	91	60	14.6	23.3	20	1.51	1.5	0.04
Fowler and Rosen	92.6	58.3	19.1	23	24	1.59	1.12	0.146

* This document is based on work performed at Los Alamos Scientific Laboratory of the University of California under Contract No. W-7405-eng-36 for the Manhattan Project and the information contained therein will appear in Division V of the Manhattan Project Technical Series as part of the contribution of the Los Alamos Laboratory.

[1] M. Deutsch, Los Alamos Declassified Document No. 257.
[2] J. E. Brolley, Chicago Document on Chemistry No. 1840.
[3] M. H. Kanner and H. H. Barschall, Phys. Rev. **57**, 372 (1940).
[4] W. Jentschke, Zeits. f. Physik **120**, 165 (1943).
[5] A. Flammersfeld, Zeits. f. Physik 120, 450 (1943).
[6] W. Jentschke and F. Prankl, Physik. Zeits. **40**, 706 (1939).
[7] G. V. Droste, Naturwiss. **27**, 198 (1939).
[8] M. C. Henderson, Phys. Rev. **56**, 703 (1939).
[9] O. Haxel, Zeits. f. Physik **112**, 681 (1939).
[10] E. T. Booth, J. R. Dunning, and F. O. Slack, Phys. Rev. **55**, 981 (1939).
[11] E. T. Booth, J. R. Dunning, and G. N. Glasoe, Phys. Rev. **55**, 982 (1939).

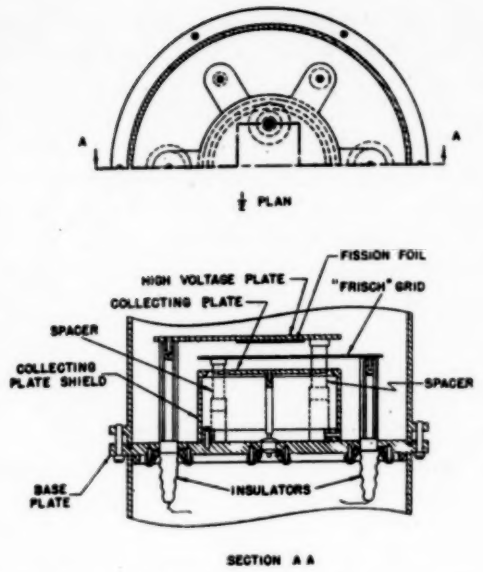

FIG. 1. Schematic diagram of the ionization chamber.

(1) To obtain the energy-distribution curve for the fission fragments from U^{235} by the use of an electronic method for measuring and counting the ionization pulses produced by these fragments in an ionization chamber;

(2) To determine whether the energy-distribution curve is a function of the incident-neutron energy;

(3) To investigate the high energy portion of the curve for any indication of additional peaks which one might expect if some nuclei divided into more than two fragments.

Item (2) has been investigated to a certain extent by D. Frisch[12] for isotope 92^{237}. He found that the distribution of the fragments in the high energy peak was the same to the accuracy of his measurements when the fission was produced by neutrons of three different energies: 500, 720, and 900 kev.

2. EXPERIMENTAL METHOD

The method used in the present experiments was fundamentally the same as that used in preceding experiments; namely, the comparison of the ionization produced by the individual fission fragments with the ionization produced by α-particles of known energy.

The ionization chamber, Fig. 1, was of the electron-collection type. The screen, which shields the collecting electrode from the positive ions, was made of No. 36 parallel copper wires spaced 1.5 mm apart. The high voltage electrode, on which was mounted the fissionable foil, was kept at 2150 volts while the screen was kept at 1050 volts. This made the field between the screen and collecting electrode slightly higher than the field outside the screen. However, this was desirable in order to insure that the screen should capture a minimum number of electrons.

In order to obtain the energy spectrum of the fission fragments, the chamber was filled with argon to a pressure of 232-cm Hg. This pressure was more than sufficient to stop the highest energy fission fragments before they reached the grid. The gas was continuously purified by circulating it over calcium metal at 300°C. Also, for the sake of purity, the only organic material inside the counter consisted of several rubber washers which exposed very little surface to the gas in the chamber.

The saturation voltage for the ionization chamber was established by determining the position of the energy peaks of the fission-fragment energy spectrum as a function of voltage. When a voltage was reached above which the position of the peak no longer shifted, it was assumed that the chamber was saturated. The counter was operated at approximately 500 volts above the saturation voltage.

The recording equipment consisted of a 10-channel discriminator,[13] each channel having such a width as to accept pulses over a range of about 0.8 Mev for the amplification used. It was possible to shift the bias of all the channels by the same amount so that the entire energy spectrum could be obtained, 9 points at a time. The channel widths had a tendency to drift by ± 5 percent over periods of 10 to 12 hours, but

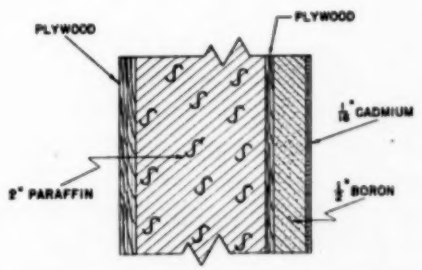

FIG. 2. Wall cross section of paraffin-boron-cadmium "ice box."

[12] D. H. Frisch, Phys. Rev. 71, 478 (1947).

[13] This instrument, developed by the Los Alamos Scientific Laboratory Electronics Group, will be reported in a future paper by M. Sands and E. Dexter.

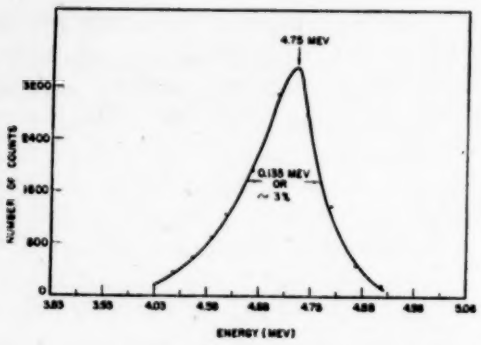

FIG. 3. Energy distribution of uranium^{234} alpha-particles.

much of this error was eliminated by calibrating the channel widths every 30 minutes. A check could always be had on the effectiveness of this procedure as a result of the fact that when the bias on the chamber was shifted, channels 1, 2, and 3 in the new position overlapped channels 7, 8, and 9 of the preceding setting. When everything operated properly the overlapping channels gave values within ± 3 percent of each other. The 10-channel discrimator was fed by a "model 100"[14] amplifier, which in turn was fed by a "model 100" preamplifier adjoining the ionization chamber. The so-called "model 100"[14] amplifier was stabilized by inverse feedback and had a rise time of 0.5μ sec. Instead of using an RC clipping circuit at the input of the amplifier, the incoming pulse was reduced to $\frac{1}{3}$ its size after 9μ sec., step fashion, by superimposing on this signal its inverse reflection. This was accomplished by using a shorted delay line. The 9μ-sec. clipping time appeared to be about three times as great as the electron collection time. The amplifier and 10-channel discriminator was shown to be linear, by use of a precision pulser, to within ± 1 percent.

The neutron source used for these experiments was the Los Alamos cyclotron, using the $Be^9(d,n)B^{10}$ reaction. For the "slow"-neutron experiments, the counter was shielded by 9 inches of paraffin on two sides and by 23 inches of paraffin on the side facing the target (the fourth side faced the cyclotron water tanks). There was also 4 inches of paraffin above the counter and 4 inches below it. For irradiation by "fast" neutrons, the counter was surrounded by a layer of Cd, then by 4 inches of boron and the whole assembly placed inside a parafin, boron, Cd box, a cross section of one of the walls of which is shown in Fig. 2. In order to arrive at some estimate of the energy distribution of the so-called "fast" neutron flux, a U^{238} foil was substituted for the U^{235} foil and the number of fissions for an equivalent beam intensity was determined. From the known cross sections of U^{235} and U^{238} and from the known amounts of active material on the foils, one can arrive at a rough approximation of the energy distribution of the incident neutrons. It turns out that approximately 10 percent of the "fast" flux is comprised of neutrons having energies in excess of 1 Mev while very few of the remainder have energies of less than 1000 ev.

The determination of the energy of the fission fragments in terms of the ionization produced was made on the assumption that α-particles expend the same energy in producing an ion pair as do the fission fragments. In order to determine the ionization produced by U^{234} alpha-particles, it was necessary to increase the pressure in the chamber, by the addition of argon, to 290-cm Hg so as to stop all the alphas before they reached the grid (the fission-fragment energy spectrum was checked at this pressure with no resulting change in the position of the peaks). The ratio of the pulse sizes due to the fission fragments, at various points of the energy-spectrum curve, to the pulse size due to the U^{234} alphas was established by calibrating the amplifier and 10-channel discriminator with a precision pulser.

The width at half-maximum of the α-particle distribution, Fig. 3, serves as a measure of the resolution of the ionization chamber. The noise level, due to the ionization noise and amplifier noise, was equivalent to a particle energy of

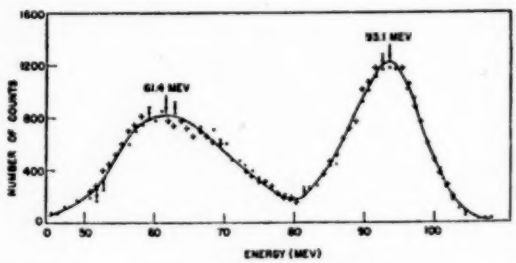

FIG. 4. Energy spectrum of uranium^{235} fission fragments for "slow" neutrons.

[14] Los Alamos Scientific Laboratory designation.

0.4 Mev (the best previous work was done by Deutsch who had a noise level corresponding to a particle energy of 1.5 Mev).

Two foils of 94 percent U^{235} were investigated. These were mounted on 10-mil platinum and contained 0.332 mg and 0.19 mg of metal uniformly distributed over 3.14 cm^2 and 7.07 cm^2, respectively. The foils were made by Robert M. Potter and James S. Gilmore of the Los Alamos Scientific Laboratory.

The reason for investigating two foils of different thicknesses was to attempt to obtain data which would aid in correcting for the finite thickness of the foil. Jentschke calculated that for a foil thickness of 0.04 mg/cm^2, one Mev should be added to the energies of the light and heavy fragments. Since this thickness of foil is slightly greater than the thickness of our thin foil, it would seem that such a correction would be in order for our data, except for the fact that

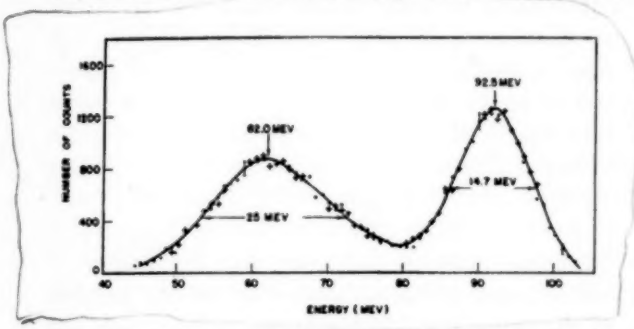

FIG. 5. Energy spectrum of uranium^{235} fission fragments for "fast" neutrons.

in our case almost half of this error is compensated by the energy loss of the alpha-particles used for calibration. This would leave a correction of slightly more than 0.5 Mev to be added to the energy of the light and heavy fragments and this is well within the experimental error. It is therefore not surprising that no difference can be detected between the curves for the foils of thicknesses 0.026 mg/cm^2 and 0.106 mg/cm^2 as far as the position of the peaks is concerned.

3. RESULTS

Characteristic sets of determinations of the fission-fragment distribution as a function of energy for "slow" and for "fast" neutrons are plotted in Figs. 4 and 5. As a check on these curves, it was determined that the area under

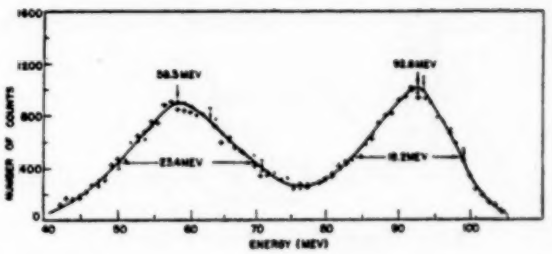

FIG. 6. Energy spectrum of thorium^{232} fission fragments.

each of the two peaks in each curve was the same to within 4 percent. Table I compares the results given here with the best values previously obtained.

There seem to be no significant differences between the curves for "fast" and for "slow" neutrons, although the minimum in the case of the "fast" neutrons appears to be about 1.5 percent higher than the minimum in the case of the "slow" neutrons.

No extra peaks are discernable in the high energy region for fast or for slow neutrons. In order to check this conclusion for high energy neutrons (up to 26 Mev), a Li target, made by Stanley Hall, was substituted for the Be target at one stage of the experiment but the curve still showed no signs of extra peaks. The data permit one to conclude that if certain atoms break up into more than two fragments of comparable masses, this phenomenon occurs less frequently than once in 1000 fissions.

The energy distribution of the fission fragments for Th^{232} was also determined. The thorium foil was also prepared by Potter and Gilmore. This curve is given in Fig. 6. This experiment had previously been performed by Jentschke

TABLE II. Data on high and low energy fission products.

Isotope	Investigator	Ratio of energy of high energy peak to low energy peak	Most probable ratio of energy of fragments
$_{90}Th^{232}$	Jentschke[4]	1.51	
	Fowler and Rosen	1.59	
$_{92}U^{235}$	Jentschke[4]	1.47	
	Deutsch[1]	1.57	1.49
	Fowler and Rosen	1.51	
$_{92}U^{238}$	Kanner and Barschall[3]	1.52	
$_{94}Pu^{239}$	Deutsch[1]	1.43	1.32

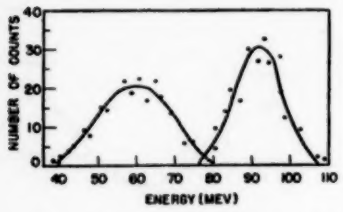

FIG. 7. Jentschke's curve for thorium[233].

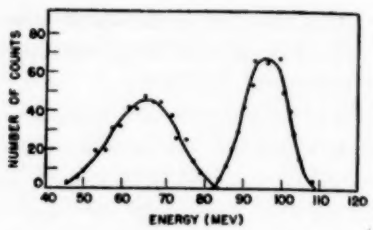

FIG. 8. Jentschke's curve for uranium[235].

and his results are given in Fig. 7. Jentschke arrived at a curve very similar to his curve for U^{235} shown in Fig. 8. Table I also shows a comparison between our results and Jentschke's for thorium. It should be pointed out that our foil was relatively thick (0.14 mg/cm^2) while Jentschke's foil contained only 0.04 mg/cm^2. This probably accounts for the discrepancy as regards the minimum between the two peaks, in view of the difference in minima obtained for the two foils of U^{235} (Table I), which foils differed in thickness by a factor of about 3. Considerable difference exists between the spectra for thorium, aside from the difference in the minima. It should be pointed out, however, that Jentschke's curves were determined with very poor statistics; the statistical error of his high energy peak being approximately 18 percent. Further experiments will be resorted to in order that this discrepancy may be resolved.

It is of considerable interest to compare the energy distribution of fragments for all the different isotopes measured. This involves comparing the results of several different experimenters. Perhaps the most reliable quantity determined is the ratio of energy of the high energy peaks to that of the low energy peaks, since this quantity depends on the linearity of the detecting apparatus and not on an absolute-energy scale. Because of conservation of momentum, this ratio gives also the ratio of the masses of the fragments for the most probable mode of fission. This is not quite true because of the momentum of the prompt neutrons emitted during the fission process, however, only a slight error is introduced on this account particularly if the neutrons are emitted with about equal probability by both fragments. Table II gives the ratio of the peak energies for four isotopes. There seems to be a considerable discrepancy between the value of the ratio as determined by different investigations. In the case of Deutsch's experiment in which both fragments of a pair are measured, by use of a double counter, the most probable ratio of the energies of a pair seems to be somewhat lower than the most probable ratio of peak energies. The former value of the ratio seems to be in better agreement with the results of Jentschke and of this report in the case of U^{235}. All the separate experiments, however, show a tendency for the fission to become more symmetrical as the atomic number of the original nucleus is increased. Holding the atomic number constant and increasing the atomic weight does not seem to affect the asymmetry as markedly. A consistent set of data with good statistics on all the isotopes, however, is needed in order to establish this apparent variation of asymmetry of fission with charge of the nucleus.

We wish to acknowledge the contribution of Stanley H. Hall who ran the cyclotron during this experiment.

Natural Radiocarbon from Cosmic Radiation

E. C. ANDERSON AND W. F. LIBBY
Institute for Nuclear Studies and Department of Chemistry, University of Chicago, Chicago, Illinois

AND

S. WEINHOUSE, A. F. REID, A. D. KIRSHENBAUM, AND A. V. GROSSE
Houdry Process Corporation, Marcus Hook, Pennsylvania

(Received August 4, 1947)

C^{14} produced by the $N^{14}(n, p)$ reaction of cosmic-ray neutrons has been detected and identified. The C^{14} concentration of biological methane was enriched by factors of up to 260-fold by thermal diffusion to raise the activity to convenient levels for counting. The pure methane was used as the filling gas in large Geiger-Müller counters.

The activity in biological methane was found to be 10.5 disintegrations per minute per gram C, or 0.95×10^{-12} gram C^{14} per gram C. This is in reasonable agreement with the value predicted from the estimated values of the cosmic-ray neutron flux and the amount of carbon in exchange equilibrium with the atmosphere. No significant activity was detected in petroleum methane.

A discussion of the thermal diffusion enrichment factor is given.

1. INTRODUCTION

IT is well established[1–7] that neutron secondaries are produced in the atmosphere by the cosmic radiation. Less well established is the total number, Q, of neutrons produced per cm^2 of the earth's surface per second. The recent paper of Korff and Hammermesh[7] allows a rough estimate of Q to be made. Integration of their curve for neutron production rate per gram *vs.* depth from the top of the atmosphere gives Q as 0.8 neutrons/cm^2/sec.

The neutrons probably are produced with several Mev energy[3] and collide with air molecules until they are captured. From the known large, slow neutron-capture cross section for $N^{14}(n, p)C^{14}$ it is quite clear that the main part of Q must result in the formation of C^{14} atoms in the atmosphere. Korff[8] has given this conclusion previously.

As suggested earlier[9a] this radiocarbon should be detectable in living matter, and the present article reports evidence for its existence in about the expected amount. The existence of such "cosmic radioelements" has been anticipated by one of us[9b] shortly after the discovery of artificial radioactivity.

The amount to be expected can be estimated by realizing that a state of radioactive equilibrium must have been established if the flux of incoming neutrons, Q, has remained essentially unchanged over the last ten to fifteen thousand years (two to three C^{14} half-lives); i.e., the number of C^{14} atoms disappearing per second by emission of beta-particles must just equal the number being formed per second. The latter number will be $5.1\cdot10^{18}\ Q$, where $5.1\cdot10^{18}$ is the earth's surface area in cm^2. This means that there must be just enough C^{14} on earth to emit $5.1\cdot10^{18}\ Q$ beta-particles per second, and taking the half-life to be about 5000 years[10a, b] we find this to be equivalent to some 22 metric tons, or 110-million curies of radiocarbon. Thus the total amount will be known to the same accuracy that Q is known.

Since it is known that most of the neutrons are formed and captured again in the upper half or two-thirds of the atmosphere, we must assume

[1] C. G. and D. D. Montgomery, Phys. Rev. **56**, 10 (1939).
[2] S. A. Korff, Rev. Mod. Phys. **11**, 211 (1939).
[3] H. A. Bethe, S. A. Korff, and G. Placzek, Phys. Rev. **57**, 573 (1940).
[4] E. T. Clarke and S. A. Korff, J. Frank. Inst. **232**, 217 (1941).
[5] S. A. Korff and E. T. Clarke, Phys. Rev. **61**, 422 (1942).
[6] S. A. Korff and M. Kupferberg, Phys. Rev. **65**, 253 (A) (1944).
[7] S. A. Korff and B. Hammermesh, Phys. Rev. **69**, 155 (1946).
[8] S. A. Korff, Terr. Mag. **45**, 133 (1940).
[9a] W. F. Libby, Phys. Rev. **69**, 671 (1946).
[9b] A. V. Grosse, J. Am. Chem. Soc. **56**, 1922 (1934).
[10a] A. F. Reid, J. R. Dunning, S. Weinhouse, and A. V. Grosse, Phys. Rev. **70**, 431 (1946).
[10b] W. D. Norris and M. G. Inghram, Phys. Rev. **70**, 772 (1946).

TABLE I.

Source	Sample number	Calculated C^{14} enrichment	C^{13} concentration from mass spectrometer, %	% CH_4 in gas before final purification	Date taken	Total count rate including background (counts per minute)
Petro methane	I	1	1.04	99.6	10/16/46	340.6±1.0
	II	1	1.04	99.6	10/16/46	342.6±1.0
	III	25	6.55	97.2	1/ 6/47	345.8±1.3
	III	1	1.04	99.4	12/ 5/46	342.9±2.0
Bio-methane	I	10	7.36	93.6	10/17/46	348.7±1.3
	VII	32	11.02	99.9	12/ 2/46	364.0±1.5
	VIII	260	63.5	97.2	2/10/47	562.0±2.9

that the radiocarbon will enter the life cycle by conversion to CO_2 by reaction with atmospheric oxygen, and thus will be distributed throughout all living matter and all inorganic substances containing carbon which are in exchange with atmospheric CO_2 on a 5000-year scale (principally dissolved carbonates in sea water). By estimating from geochemical data the amount of carbon existant on earth in living matter, atmospheric CO_2, and ocean carbonate, we then can predict the specific radioactivity to be expected. We shall take in this estimate the biosphere[11] to contain $5 \cdot 10^{13}$ metric tons, the ocean carbonate[12] $3 \cdot 10^{13}$ tons, and the atmospheric[11] CO_2 $6 \cdot 10^{11}$ tons, for a total of $8.1 \cdot 10^{13}$ tons, or 1.3 moles of carbon per cm^2, on earth. Assuming further that due to the 5000-year half-life ample time has been available for the establishment of a nearly uniform world-wide distribution throughout all living matter, we calculate that $0.3 \cdot 10^{-12}$ grams of radiocarbon should be found per gram of living carbon or that the specific activity of living carbon should be 3 beta-particles per minute per gram. The accuracy of the estimate depends on the accuracies with which the neutron production rate, Q, and the amount of living and exchangeable matter are known. The error in Q may be as much as a factor of two or three, and the amount of living and exchangeable carbon may not be known to better than a factor of two, principally due to uncertainty about the biosphere value, so we expected the specific activity to lie between outside limits of 1 and 10 disintegrations per minute per gram. The value reported here is 10.5, in reasonably good agreement.

[11] W. J. Vernadsky, *Geochemie in Ausgewählten Kapiteln* (Akademische Verlagsgesellschaft, Leipzig, 1930).

[12] V. M. Goldschmidt, *Geochemische Verteilungsgesetze der Elemente* (Norwegian Academy, Oslo, 1938), Vol. 9.

2. METHOD

The difficulty of detecting the expected specific activity of about 10^{-12} curies per gram of living carbon made isotopic concentration before measurement extremely desirable. Since the thermal diffusion columns at the Houdry Process Corporation operate normally on methane for the production of C^{13} enriched material, it was hoped that methane derived immediately from living material could be obtained. This proved to be possible through the kindness of the city of Baltimore. The Patapsco Sewage Disposal Plant of that city produces an illuminating gas, derived directly from sewage, containing about 60 percent methane, the rest being CO_2 with only traces of N_2. After absorption of CO_2 by soda-lime a very pure methane remains. Particularly important is the fact that no ethane, propane or higher hydrocarbons can be detected in it by modern methods; thus it is an ideal gas for carbon isotope separation in thermal diffusion columns. (The one-half percent of hydrocarbon impurities in the purest petroleum methane (99.5 percent) concentrate in the thermal diffusion columns together with $C^{13}H_4$ and thus greatly pollute the concentrate.) Six hundred liters of this biomethane were used and concen-

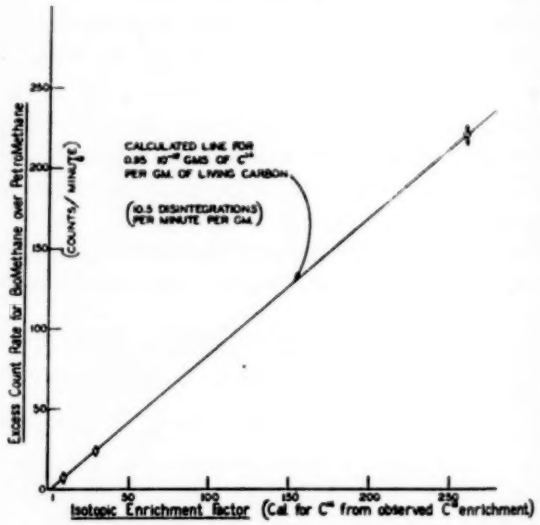

FIG. 1. Radioactivity of biomethane samples *vs.* isotopic enrichment. (6.5-mm Hg pressure in 1900-cc counter at room temperature.)

trated in the two thermal diffusion plants at Marcus Hook, Pennsylvania. The concentrates were purified from substantial percentages of nitrogen by appropriate condensations and distillations in a usual vacuum train at liquid to solid nitrogen temperatures. The purity of the final samples, submitted for radioactivity measurements, were determined by the Consolidated Engineering mass spectrometer and are given in column 4 of Table I.

The degree of enrichment of any C^{14} present was determined by measurement of the C^{13} enrichment and calculation of the corresponding enrichment factor for C^{14} as described in Section 5. The calculated factors were submitted together with the samples by the Houdry Process Corporation group before they were measured at Chicago. It would have been possible, of course, to calibrate the columns empirically with synthetic C^{14} but fear of contamination would preclude such a hazardous step. Such a procedure should, however, increase the accuracy of the determination in the future.

The measurement of the radioactivity was accomplished by utilizing the principles that living carbonaceous material will differ from chemically identical material which has been buried for times long with respect to the 5000-year half-life of radiocarbon by containing radiocarbon, and that isotopically enriching living material will increase its radiocarbon content. The material used in all cases was pure methane

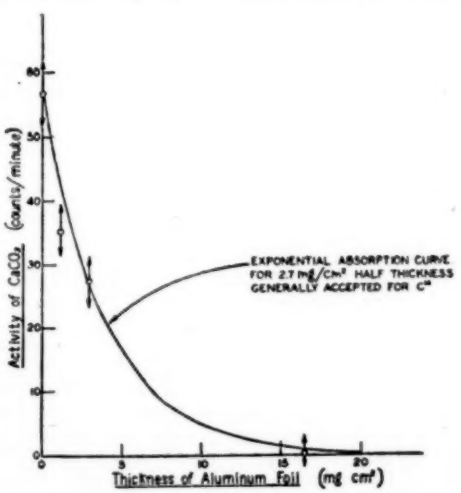
Activity of $CaCO_3$ (counts/minute)
EXPONENTIAL ABSORPTION CURVE FOR 2.7 mg/cm² HALF THICKNESS GENERALLY ACCEPTED FOR C^{14}
Thickness of Aluminum Foil (mg cm²)

FIG. 2. Absorption of $CaCO_3$ radiation in aluminum and aluminum-absorption curve for synthetic radiocarbon (C^{14}).

TABLE II. Bio VIII sample in standardized counter.

Sample (6.5-cm Hg press.)	Total count rate (counts/min.) including background
Petro II	312.5±1.4
Bio VIII	429.2±2.4
Difference	116.7±2.8
Difference, corrected for end loss	125±3
Moles CH_4 in counter	$3.82 \cdot 10^{-3}$
Unenriched specific activity of living carbon	2.1±0.3 counts/sec./mole
Unenriched specific activity of living carbon	10.5±1 counts/min./g
Abundance of C^{14} in living carbon (gms/gm)	$0.95 \cdot 10^{-12}$

gas. The counters of about two-liter volumes were filled alternately with "biomethane" from the Baltimore sewage and with the same pressure of "petromethane" from oil wells. Careful measurements were made of the count rates with the two fillings. The main part of the rate, in general, except for the richest biomethane sample, was due to cosmic radiation and general laboratory background. It was expected that this would be identical for both types of gas and that any difference in these rates would be due to inherent radioactivity of the gas itself. The proof that the activity was due to C^{14} was that burning of the methane to CO_2 and precipitating $CaCO_3$ carried the activity and that the absorption curve in aluminum of the $CaCO_3$ radiation was identical within the experimental error with that for synthetic C^{14}. In addition, the proportionality of the activity of the gaseous methane to the C^{14} enrichment factor proved further that the radioactivity was due to a carbon atom of mass 14.

3. MEASUREMENT OF RADIOACTIVITY

The gaseous methane was introduced into a brass cylinder counter with glass heads cemented in place with de Khotinsky cement. The volume between the heads was 1900 cc, the diameter being 3 inches, and the length 18 inches. Alternate readings were taken with 6.5-cm Hg pressure of petro- and biomethane samples in the counter. A standard external sample of U_3O_8 was used to check that the counter sensitivity was the same for all fillings. The counter was completely surrounded by a 1.5-inch thick lead shield to reduce the background.

For the accurate absolute assay a somewhat

TABLE III. Data on chemical and physical identity of the radioactivity.

A. *Activity of $CaCO_3$ obtained by combustion of the CH_4*

Weight of $CaCO_3$ counted	1.2 g
Average thickness of layer of $CaCO_3$	5 mg/cm²
Total activity in $CaCO_3$ if all in CH_4 was carbon	386 counts/min.
Expected[13] count from smooth solid $CaCO_3$ of this total activity and thickness	111 counts/min.
Observed count	56.6±5 counts/min.

B. *Aluminum absorption data*

Absorber thickness	Expected for C^{14}	Observed
0 mg/cm²	(56.6)	56.6±5
1.14	42.5	35.0±3.5
2.94	27.1	27.3±4
16.40	1.0	0 ±3

smaller counter was used with plane heads machined out of Lucite. This counter, 2×24 inches in dimensions, was calibrated for loss at the ends by counting a gas sample containing synthetic radiocarbon at comfortable intensity in two counters of the same diameter, but different lengths. Taking the difference in rates at a given pressure of gas then gave the true rate for a counter with no end losses and of length equal to the difference in lengths. The end loss correction for the counter used on the methane samples was 7 percent.

The most concentrated biomethane sample (Bio VIII) was burned and $CaCO_3$ precipitated to establish that the radioactivity was chemically carbon rather than hydrogen (possibility of tritium existed). This was measured in a screen wall counter[14a, b] with the chamber wall maintained at a negative potential of about 135 volts with respect to the screen so the maximum sensitivity to the $CaCO_3$ radiation was obtained. The expected radioactivity was found and the absorption curve in aluminum was obtained by mounting foils over the sample and remeasuring in the same counter.

4. DATA

Tables I and II give the enrichment data and the corresponding count rates for the large glass head counter.

Figure 1 presents the difference between bio- and petromethane count rates plotted against enrichment factor. The fact that the three points fall on a single straight line demonstrates the internal consistency both of the enrichment factors and the counting data.

Table II gives the counting data for the 260-fold enriched biomethane sample (Bio VIII) in the standardized Lucite head counter.

The data on the identity of the radiation are given in Table III.

The absorption data are given in Table III and plotted in Fig. 2, together with the generally accepted curve for synthetic radiocarbon radiation.

5. C^{14} ENRICHMENT CALCULATION

In a two-component gas, the general equation[15] giving the transport τ, of one species in a diffusion column is

$$\tau = H(1-c)c - K(dc/dz) \qquad (1)$$

where c is the mole fraction of the species, z is the coordinate along the column, and H and K are net transport coefficients. It is necessary to determine H and K experimentally because of ignorance of the force law involved and limitation in determining the functional effect of conditions in an operating column.

The extension of the treatment[16] to the separation of three isotopic species simultaneously can be made so that if the mole fraction of one can be experimentally determined, the concentration of the other two can be calculated. The general case is quite complicated and difficult of solution, but solutions can be made for cases with limiting conditions. Specifically, in the separation of $C^{12}H_4$, $C^{13}H_4$, and a very small concentration of $C^{14}H_4$, the fundamental transport equations become:

$$\tau_1 = H(1-c_1)c_1 - K\frac{dc_1}{dz}, \qquad (2)$$

$$\tau_2 = \frac{33(2-c_1)}{34+c_1}Hc_2 - K\frac{dc_2}{dz}, \qquad (3)$$

[13] W. F. Libby, Ind. Eng. Chem., Anal. Ed. 19, 2 (1947).

[14] (a) W. F. Libby, Phys. Rev. 46, 196 (1934). (b) D. D. Lee and W. F. Libby, *ibid.* 55, 245 (1939).

[15] R. C. Jones and W. H. Furry, Rev. Mod. Phys. 18, 151 (1946). This very excellent review, entitled "The separation of isotopes by thermal diffusion," gives a comprehensive picture of the fundamentals involved in general gaseous thermal diffusion. Because of the diverse origin and development of the concepts, this article is used for general reference.

[16] The development of the relationships used and their application is to be described separately by A. F. Reid and D. Tanguy.

where subscripts 1 and 2 refer to $C^{13}H_4$ and $C^{14}H_4$, respectively, and H and K are the $C^{13}H_4$ transport coefficients.

Upon application of the equations to the separation system used, calculation of the relative concentrations of $C^{14}H_4$ could be made for simultaneous enrichments of $C^{13}H_4$. The measured concentration change with time of the $C^{13}H_4$ followed the theoretical values faithfully, indicating a uniformity of column operation, which permitted some simplification. However, a small amount of nitrogen was present which concentrated in the same direction as the heavy methane; some uncertainty as to its distribution is reflected in the limit of the $C^{14}H_4$ enrichment calculations.

Figure 3 is a plot of the characteristic ratios of bottom to top isotope ratios for the system used when it is originally filled with an atmosphere of normal methane. Because of the nitrogen present and early withdrawals made to purge a large portion of it, calculation of the C^{14} enrichment required individual modifications for each case.

6. DISCUSSION AND CONCLUSIONS

In earlier brief reports[17a,b] the observations were given and certain deductions made in abbreviated form. A more complete discussion seems in order.

The enrichment factor count-rate correlation (Fig. 1) indicates that the activity is carried in a molecule with the thermal diffusion characteristics of methane of mass 18 present in low concentration in the original biomethane. The fact that the activity follows the chemistry of carbon rather than hydrogen indicates that the activity is due to a carbon isotope of mass 14. Finally, the agreement of the absorption data with those for synthetic C^{14} further confirms the identification of the activity with C^{14}.

One might worry about the disagreement in Table IIIA between the expected count from the solid $CaCO_3$ (111 c/m) and the observed (56.6 c/m). We believe this is not serious, however, since the precipitate certainly was not smooth, as had to be assumed to make the calculation of the expected figure of 111. The $CaCO_3$ was purposely allowed to crystallize in large crystals to reduce the chance of loss due to exchange with atmospheric CO_2 during the necessary exposure to air while the sample and the foils were being mounted. It was also true that the mounting, by moistening with ethanol and allowing to dry, resulted in a sample visibly rough with ridges and thick spots.

The possibility that the C^{14} found in Baltimore sewage had an origin other than the cosmic radiation is very remote. Our sample was taken on September 2, 1946, at which time no radiocarbon from the Atomic Energy Commission had been sent to anyone in Baltimore, according to Dr. P. C. Aebersold of the Isotopes Research Branch in Oak Ridge. The possibility that the atomic bombs or the piles may have been the origin seems very remote also when one realizes that our result corresponds to the existence of some 10^8 curies or about 20 metric tons of radiocarbon in nature—an amount far larger than any synthetic source could have produced to date. Of course, it will be desirable to examine other samples of living carbon to establish the uniformity of the distribution, and efforts in this direction are intended. In this connection it is hoped that all plants concentrating C^{13} will use "live" feed and arrange to measure their products for radioactivity to collect further data on the natural abundance.

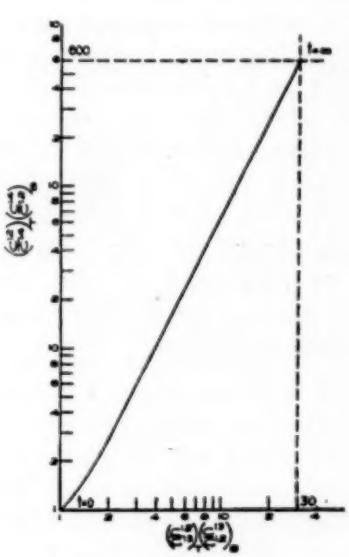

FIG. 3. Characteristic concentration curve of the Marcus Hook thermal diffusion unit.

[17] (a) E. C. Anderson, W. F. Libby, S. Weinhouse, A. F. Reid, A. D. Kirshenbaum, and A. V. Grosse, Science **105**, 576 (1947).
(b) A. V. Grosse and W. F. Libby, *ibid.* **106**, 88 (1947).

In a strict sense our data show only that our particular sample of Baltimore sewage methane contained radiocarbon to the extent of 10.5 disintegrations per minute per gram of carbon, and that our sample of petroleum methane contained considerably less than this. These results fit so well with the theory of cosmic-ray production of radiocarbon, and are so difficult to explain at present on any other basis, that we believe the theory to have been confirmed. We plan further tests, particularly on the assumption of uniformity of distribution, and have at hand at the moment samples of living matter from Antarctica, killed in Antarctica, through the kindness of the Navy Department and Operation Highjump. It is anticipated that improvements in our counting technique will make the assay less difficult. In fact, we anticipate that isotopic enrichment may not be necessary for material at the present living level.

Since the radiocarbon originates in the top layers of the atmosphere, thereby entering the life cycle and all living matter, and since the neutron intensity at sea level is negligible, we are led to the prediction that the intake of radiocarbon by living bodies will cease when they die, and that the period of time elapsed since death will be measurable by direct comparison of the specific activity of the specimen with that of living matter in general. In other words, if we can assume that the specific activity of living matter has remained constant over the time interval being measured, a specimen 5000 years buried will have 5.3 counts per minute per gram of carbon rather than the original 10.5. By invoking isotopic enrichment it should be possible to measure samples as old as 40,000 years. Of course, the limit could be extended by further enrichment, though the effort required would probably be prohibitive in most cases. It is planned to measure certain dated samples as a check on these conclusions.

It is clear from the nature of our postulates that the specific activity of living matter gives the ratio of the number of cosmic-ray neutrons per cm^2 and per unit time to the amount of living and exchangeable carbon per cm^2. It is hoped that the result will be useful to both the cosmic-ray physicists and geochemists in establishing these two quantities. The present result seems to indicate that either the number of neutrons is about three times as large as the data of Korff and Hammermesh[7] indicate, or that the amount of exchangeable carbon is about one-third the figures postulated in the references cited above. It is impossible at the moment to say which of these is more likely, or whether some intermediate situation obtains.

A search for other cosmic radio elements has been started.

7. ACKNOWLEDGMENTS

We are grateful to Messrs. George E. Finck and R. J. Trautman of the Department of Public Works of the city of Baltimore, to Dr. H. G. Swope, Secretary of the A.C.S. Committee on Water, Sewage and Sanitation and to Dr. Abel Wolman of Johns Hopkins University for their cooperation, to the Sun Oil Company for the use of their thermal diffusion columns, to Mr. W. H. Johnston for assistance in the counting measurements, to Mr. D. Tanguy for assistance in calculations, and to Mr. J. T. Dooley for technical assistance.

Note added in proof: Since submitting this article a second sample of Baltimore sewage methane obtained from a different disposal plant a few miles away has been isotopically enriched 60-fold for C^{14} (22.2 percent C^{13}) and counted. The result was 10 ± 1 counts per minute per gram, in agreement with the earlier measurements.

Ionization of High Energy Cosmic-Ray Electrons

EVANS HAYWARD
Department of Physics, University of California, Berkeley, California

(Received August 4, 1947)

The ionization produced by high energy cosmic-ray electrons has been measured in a cloud chamber in order to determine whether the probable ionization produced by a high velocity particle continues to rise logarithmically with the energy, or whether it takes on a constant value as has been predicted theoretically. A lateral clearing field was arranged so that the ionization could be measured in the upper half of the cloud chamber; lead plates were placed in the lower half so that the electron would produce a shower from which its energy could be estimated. The ionization produced by electrons was measured and compared to the minimum ionization as determined from the average ionization produced by mesotrons. According to the theoretical formula of Halpern and Hall, the maximum ionization should be 1.4 $I_{\min}$. In most of the pictures taken the ionization was consistent with this value. There were several pictures, however, where the ionization was extremely high. These may either indicate that the theoretical formula is invalid, or that they may result from the coincidence of two or more particles. Such an event does not seem unlikely when the production of pairs is considered. When a high energy gamma-ray produces an electron-positron pair, the probability that the two particles come off in practically the same direction is very high; in the cloud chamber they would produce one track with doubly dense ionization.

1. INTRODUCTION

FOR low energies the ionization by a charged particle increases as its energy decreases because the particle spends a longer time in the vicinity of each molecule of the gas being traversed. On the other hand, when the velocity of the particle approaches that of light, relativistic effects must be taken into account; the field of the particle becomes extended in the direction perpendicular to the direction of motion, and is thus felt by more molecules. This results in an ionization that rises logarithmically with the energy. The usual expression[1] for the energy loss by a particle traversing a medium is given by:

$$K_\eta(E)=(2C\mu_e/\beta^2)\times\{\log[2\mu_e\beta^2\eta/(1-\beta^2)I^2(Z)]-\beta^2\}. \quad (1)$$

$K_\eta(E)$ is the energy loss per g/cm² produced by collisions in which the energy transferred is smaller than η, $I(Z)$ is the average ionization potential of an atom of atomic number Z, and C is $0.15\,Z/A$. The specific ionization differs from the rate of energy loss by an essentially constant factor, and hence we need make no distinction in the present instance where only relative values of specific ionization will be considered. For low energies the $1/\beta^2$ factor outside the parenthesis is important, but as β approaches unity the logarithmic term predominates.

Fermi[2,3] has calculated that the field of the oncoming particle polarizes the medium in such a way that some of the molecules that would be ionized according to the ordinary formula are shielded from the exciting field. This results in a much lower ionization for high energy particles. The most recent calculation of this reduction in energy loss was made by Halpern and Hall.[4] For very high energies the quantity which they suggest should be subtracted from Eq. (1) is:

$$2C\mu_e\{\log[ne^2/\pi m\nu^2(1-\beta^2)]-1\}, \quad (2)$$

where ν is the geometric mean of the atomic frequencies or $13.5\,Z$ ev $=3.5\,Z\times10^{15}$ sec.$^{-1}$. The subtraction of this term results in the prediction that the collision loss will be constant above a certain energy, when only energy transfers up to $\eta<750$ ev are considered, and that the collision loss depends only on the electron density, n, of the medium being traversed. Figure 1 shows a plot of the ionization equation for electrons traversing helium. No collisions in which the energy transferred is greater than 750 ev are considered. The horizontal curve is the one predicted by Halpern and Hall. The density effect should set in at about 90 Mev and the maximum ionization should be 1.4 $I_{\min}$.

[1] B. Rossi and K. Greisen, Rev. Mod. Phys. **13**, 240 (1941).

[2] E. Fermi, Phys. Rev. **56**, 1242 (1939).
[3] E. Fermi, Phys. Rev. **57**, 485 (1940).
[4] O. Halpern and H. Hall, Phys. Rev. **57**, 4596 (1940).

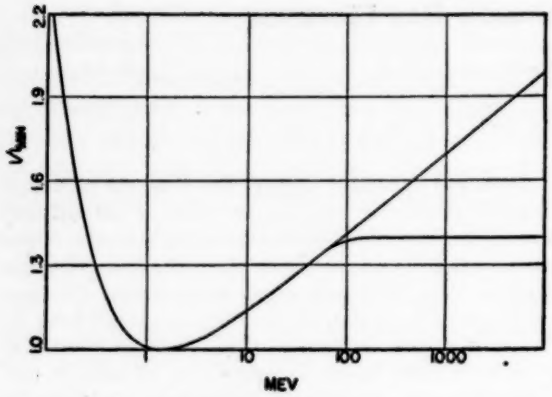

FIG. 1. The ionization curve for electrons traversing helium at normal temperature and pressure. Only energy transfers up to 750 ev are included. The horizontal curve, branching off near 100 Mev, is the one predicted by Halpern and Hall.

A rise in the ionization for energies just above that corresponding to the minimum ionization has been detected.[5,6] It seemed desirable to measure the ionization produced by the very high energy electrons contained in cosmic rays, because their energy can be estimated from the size and character of the showers they produce in passing through lead. The purpose of this experiment, then, was to measure the ionization by high energy electrons and to determine whether the ionization becomes constant or whether it increases with the energy.

2. APPARATUS AND EXPERIMENTAL PROCEDURE

A cylindrical cloud chamber having a diameter of 30 cm and a depth of 30 cm was arranged to observe both the ionization and the energy of the electrons. The ionization was measured in the upper half of the chamber and the energy in the lower. Five electrodes, extending from one end to the other, lined the upper half of the chamber and supplied a lateral clearing field (Fig. 2). Potentials of -200, -100, 0, 100, and 200 volts were applied to the electrodes. The cosmic-ray track was thus separated into a positive and a negative ion column, the separation being about 2 cm. Bagley[7] and Nielsen[8] have studied the condensation efficiency for the vapor mixture of three parts ethanol to one of water. Nielsen has shown that if the negative ion column is at least one-fifth as dense as the positive one, then drops are formed on all the ions in the positive column. This criterion for 100 percent condensation efficiency was used, and the ionization was measured by counting the drops in the positive column with a traveling microscope. Clusters corresponding to energy transfers greater than 750 ev, i.e., those containing more than 25 drops, were omitted. Those tracks that exhibited particularly high ionization were examined stereoscopically, and some of them proved to be due to two particles traveling through the cloud chamber. The remaining highly ionizing particles will be discussed in a later paragraph.

The lower half of the cloud chamber contained lead plates in which showers were produced by the incident electrons. In the first part of the experiment there were three one-quarter-inch lead plates; these were later replaced by two one-half-inch plates. The use of lead plates in this manner allows one to observe the shower at various stages in its development. A set of shower curves, in which the average number of particles is plotted as a function of the depth in shower units for various values of the energy of the initiating particle, was used to estimate the energy of the electron. These curves were plotted from Eq. (2.104) of Rossi and Greisen.[1]

The chamber was illuminated by two argon flash tubes. These were made from 12-mm Pyrex tubing with nickel electrodes sealed in the ends, the electrodes being separated by about 40 cm. The tubes were filled with 5 cm of argon and 0.1 cm of hydrogen. These were placed on either side of the chamber near the back in such a way that the light beams crossed in the center and passed out through the sides just behind the front glass. The resulting illumination was so intense that the cameras had to be stopped down to $f:12.5$ in order to make the drop images so small that their overlapping became unimportant.

Geiger counters in triple coincidence were arranged one above the chamber and two below. The two lower counters were placed in a vertical plane when the tracks of mesotrons were photographed and in the horizontal plane when those of electrons were selected, for a mesotron would

[5] D. R. Corson and R. B. Brode, Phys. Rev. **53**, 773 (1938).
[6] W. E. Hazen, Phys. Rev. **67**, 269 (1945).
[7] G. D. Bagley, Phys. Rev. **56**, 851(A) (1939).
[8] C. E. Nielsen, Ph.D. Thesis (University of California, Berkeley, 1941).

go straight through the chamber whereas the shower produced by the electron would spread laterally and trip the counters in the horizontal plane. The expansion was delayed for a few hundredths of a second to give the tracks time to diffuse before the vapor was condensed on the ions.

The energy distribution of mesotrons at sea level is such that the ionization distribution resulting therefrom is narrow, and a small number of observations suffice to establish a reasonably accurate value for the mean. The minimum ionization is the same for both electrons and mesotrons, and since the average mesotron ionization is 1.12 times the minimum ionization,[6] the minimum ionization can be determined from the study of a few mesotron tracks. The average mesotron ionization was determined from thirty-four tracks, and the minimum ionization calculated from the average. The ionization caused by each shower-producing particle was then compared to the minimum ionization.

Since the pictures were taken under various conditions, i.e., different pressures and temperatures, the vapor pressure of the ethanol and water mixture was not constant. The ionization in the vapor was then different for each set of circumstances. A correction for this effect was made assuming that the ionization in each component of the gas is proportional to its atomic number Z and to its partial pressure. The total or observed ionization multiplied by the total gas pressure may be written as a function of the partial pressures of the component atoms:

$$IP = P_{gas} I_{gas} + I_H(2P_1 + 6P_2) + I_O(P_1 + P_2) + 2I_C P_2,$$

P_1 is the partial pressure of the water vapor and P_2 that of the alcohol vapor. If helium is the gas, I_H becomes $\frac{1}{2}I_{He}$, I_O becomes $4I_{He}$, and I_C becomes $3I_{He}$. The equation then reduces to:

$$IP = I_{He}(P_{He} + 5P_1 + 13P_2).$$

The ionization in helium was found by this method, using the partial pressures of alcohol and water, as given by Gautier and Ruark.[9] The results were then reduced to normal temperature and pressure.

The experiment was begun with air as a gas in the chamber, but it soon became apparent that the ionization by high energy electrons in air at atmospheric pressure is too dense to be easily measured with the magnification of the present experiment. The chamber was then filled with about one and two-thirds atmospheres of helium; the remainder of the pictures were taken under these circumstances.

3. RESULTS

In helium the density effect should set in at an energy not greater than 100 Mev, and the maximum ionization should be $1.4\,I_{min}$. The effect should be apparent in the ionization caused by particles that later produce showers having more than four or five particles at the maximum. Only about ten percent of the electrons observed had an energy smaller than 100 Mev. Most of the electrons observed were well within the region where the density effect should be observed. In fact, many electrons had energies so great that there was still a solid core of particles in the shower as it passed through the bottom of the chamber after it had already traversed an inch of lead. This indicated that the particles of which the shower is composed are very energetic since they scattered very little in the lead. The particle initiating such a shower probably had an energy exceeding 1 Bev.

Figure 3 is a block diagram showing the ionization distribution for mesotrons. The weighted average mesotron ionization is 12.1 ± 0.3 drops/

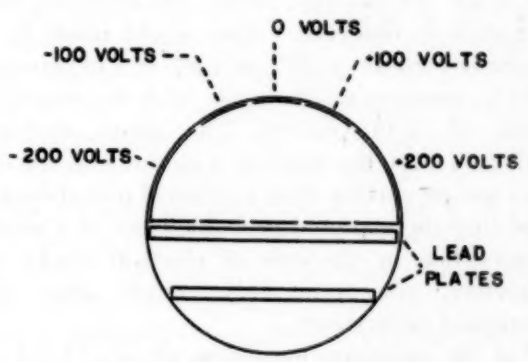

FIG. 2. Front view of the cloud chamber showing the lead plates and the electrodes that supply the clearing field.

[9] T. N. Gautier and A. E. Ruark, Phys. Rev. **57**, 1040 (1940).

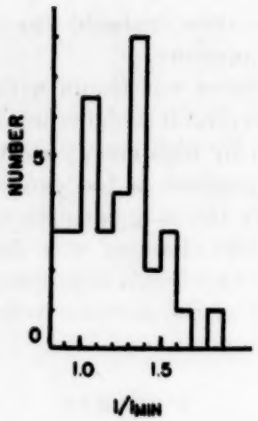

FIG. 3. Ionization distribution for mesotrons. The number of observed tracks is plotted as a function of the relative ionization.

cm. The observed probable deviation of a single observation is ± 14 percent. The spread in observed values of the ionization is due to the statistical variations in the ionization, the spread in energy of the mesotrons, and experimental uncertainties. The first two can be calculated and the last estimated. The statistical uncertainty is $\pm 0.67/N$, where N is the number of primary events or about half the observed number of drops.[10] An average track has about 100 drops so that its statistical uncertainty would be about ± 10 percent.

The energy distribution[11] of the mesotrons results in an ionization distribution. This distribution is asymmetric but can be approximated by a Gaussian curve with a probable deviation from the mean of about ± 6 percent of the central value. The experimental uncertainties that might result in random errors probably amount to about ± 5 percent. Hence the expected distribution in observed values would result in a probable error of $\pm(10^2+6^2+5^2)^{\frac{1}{2}} = \pm 13$ percent, which compares satisfactorily with the observed value of ± 14 percent. The above analysis indicates that the random experimental uncertainties are smaller than statistical uncertainties and that the expected probable error of a single observation in the case of electron tracks is, therefore, not appreciably greater than the statistical uncertainty.

For the minimum ionization we get 12.1/1.12 or 10.8 drops/cm. This is the value to which the ionization by electrons is compared.

Figure 4 is a block diagram showing the ionization distribution for electrons. If we omit for the present those points representing ionization above approximately $2.0\, I_{min}$, we see that the distribution appears to be symmetrical and the mean value is $1.45\, I_{min}$. The probable deviation of a single observation from the mean is ± 10 percent. Since it is believed that the probable error resulting from statistical and experimental uncertainties is ± 10 percent, the electron-ionization distribution seems to represent observations of a single-valued quantity. This is consistent with the prediction that all electrons with $E > 100$ Mev should have the same value for probable specific ionization.

The points corresponding to higher ionization cannot belong to the same group of observations of a single-valued quantity since they have no counterpart in the low ionization region. Nor can they be reasonably explained by assuming that the probable ionization loss continues to increase with increasing energy since the sea level electron spectrum is certainly a monotonically decreasing function of the energy. The most probable explanation is that heavily ionized tracks result from pairs produced in the upper wall of the counter above the cloud chamber. In order that the pair be unresolved in the cloud chamber, the initial angular separation of the two particles

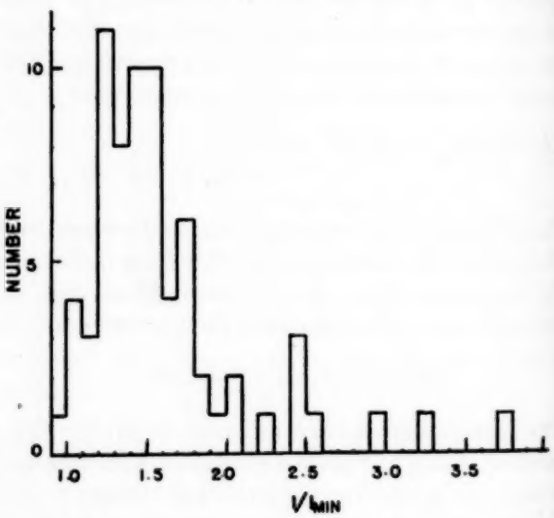

FIG. 4. Ionization distribution for electrons. The number of observed tracks is plotted as a function of the relative ionization.

[10] P. Kunze, Zeits. f. Physik **83**, 1 (1933).
[11] P. M. S. Blackett, Proc. Roy. Soc. **A164**, 257 (1938).

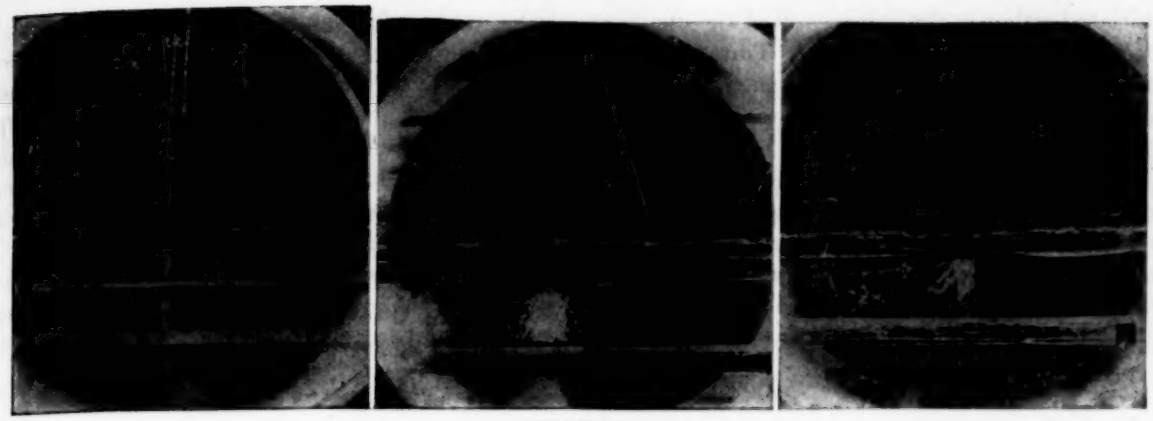

(a) (b) (c)

FIG. 5. Cloud-chamber photographs of unusual events, as described in the text.

must be small and the separation should not be appreciably increased by subsequent scattering in the material through which they pass. Both of these conditions will be fulfilled if the energy of the pair-producing gamma-ray is great enough. Since the average angle of emission of an electron of energy U is μ_e/U, the angular separation of the electron and positron depends on how the energy of the gamma-ray is divided between them. For gamma-ray energies above 10^8 ev all divisions of the energy of the pair-producing gamma-ray between the positron and electron are about equally probable except a division in which one particle takes off less than 10 percent of the energy. The latter case is much less probable. In this experiment we are concerned only with particles having an energy of at least 200–300 Mev, so that the average separation of the two particles would be of the order of 10^{-3} radians and the scattering in the upper glass wall of the chamber would not be enough on the average to resolve those of energy greater than 300 Mev. The showers associated with the "heavily ionizing" particles indicated that they had energies of at least this amount.

If we consider only gamma-rays in the energy range 3×10^8 to 10^{10} ev, we can calculate the probability that a pair will be produced in the material above the cloud chamber. There were effectively 0.105 radiation units of material above the chamber and the cross section for pair production is $\sim$0.6 for 3×10^8 ev and $\sim$0.8 for 10^{10} ev[1]. The number of gamma-rays that produce pairs, $1-\varepsilon^{-\sigma t}$, then, varies from 6 to 8 percent in this energy range. Shower theory predicts that the ratio of the number of quanta to electrons is 1.7,[12] so that we would expect 10–12 percent of the observed showers to result from unresolved pairs. Since 10 percent of the shower-producing particles displayed heavy ionization, this seems to be a reasonable explanation for the observed results. If so, we may conclude that the density effect as calculated by Halpern and Hall is real, and that the ionization by high energy particles takes on a constant value independent of the energy.

4. SINGULAR EVENTS

Several interesting pictures, not directly connected with the experiment, were taken. The first (Fig. 5a), one of those taken in air, is a photograph of the track of a particle that ionized above five times as much as an average mesotron and also seems to have produced a huge shower in the lead below. The delta-ray near the top of the track gives slight evidence that the particle is moving downward and is not the result of a nuclear explosion in the lead. Other possible explanations are that it is an extremely high energy electron if no dielectric absorption effect exists, or several coincident electrons, or that it is a negative proton giving up all of its energy in interacting with the lead plate.

The second (Fig. 5b) is a huge shower which is

[12] W. Heisenberg, *Cosmic Radiation* (Dover Publications, New York, 1946), p. 24.

initiated either in the upper wall of the chamber or in the counter just above. This picture is unusual, not only because of the size of the shower, but also because of the associated proton that stops in the first lead plate.

The third (Fig. 5c) is a picture of a mesotron shower. This shower differs in its nature from all the others because its particles do not spread out from a central core as the shower progresses, but each particle goes through the second lead plate without multiplying. Most of these particles are heavier than electrons and several may be specifically identified as mesotrons. It may be noted that there are about four particles in the top of the chamber which seem to converge toward the point where the shower begins. One of these may have been the initiating particle, though the shower may have been started by a non-ionizing particle such as a neutron.

The author wishes to express great appreciation to Dr. Wayne E. Hazen for suggesting the problem and for many very helpful discussions.

PHYSICAL REVIEW VOLUME 72, NUMBER 10 NOVEMBER 15, 1947

The Shape of X-Ray Diffraction Lines from Colloidal Magnesium Oxide

CHESTER RIDLON BERRY*
Cornell University, Ithaca, New York
(Received July 10, 1947)

The broadened diffraction lines from colloidal particles have shapes which depend on the particle size and shape and on the geometrical features of the experiment. An analytical method is developed for eliminating the effect of the geometry of the experiment, thereby giving the shape of the diffraction line. The method is applied to the 200, 220, and 222 lines from colloidal magnesium oxide. The shapes of these diffraction functions in the low intensity regions are not sufficiently accurate to permit the determination of particle shape. The relative half-intensity breadths of curves give best agreement with the values to be expected for cube-shaped particles. The particle size, determined from the Scherrer equation, is 140 angstrom units, and the average deviation from this value is 3.1 percent.

I. INTRODUCTION

MURDOCK[1] gives a theoretical treatment of the breadths and shapes of the x-ray diffraction lines from colloidal powders of the cubic symmetry class. The purpose of the present paper is to give a method for calculating ideal line shapes from experimentally measured line shapes and to apply this method to several diffraction lines. Many investigations have been made on the breadths of broadened diffraction lines, but the shapes of the lines have not been measured because of the difficulty of correcting the measured shape for the effect of experimental conditions.

II. METHOD OF SOLVING FOR THE IDEAL DIFFRACTION FUNCTION

The procedure used in these experiments has been suggested by Jones.[2] For a given diffraction line a correction curve, $f(y)$, is measured, using a powder containing particles larger than 1000 angstrom units. An uncorrected diffraction curve, $\phi(x)$, is measured, using a colloidal powder of the same material. Jones has shown that these measured functions are related to the ideal diffraction function, $F(y)$, by the integral equation:

$$\phi(x)=\int_{-\infty}^{\infty} f(y)F(x-y)dy=\int_{-\infty}^{\infty} f(x-y)F(y)dy.$$

Knowing the functions $\phi(x)$ and $f(y)$ from experiment, the solution of the equation for $F(y)$

* Present address: Eastman Kodak Company, Research Laboratories, Rochester 4, New York.

[1] C. C. Murdock, work not yet published in full but some of the results are given in Phys. Rev. **63**, 223 (1943).

[2] F. W. Jones, Proc. Roy. Soc. London **166**, 16 (1938).

may be accomplished in the following manner. If the Fourier transforms of $\phi(x)$, $f(y)$, and $F(y)$ are, respectively:

$$A(x)=\frac{1}{(2\pi)^{\frac{1}{2}}}\int_{-\infty}^{\infty}\phi(\beta)\exp(-i\beta x)d\beta,$$

$$B(y)=\frac{1}{(2\pi)^{\frac{1}{2}}}\int_{-\infty}^{\infty}f(\beta)\exp(-i\beta y)d\beta,$$

and

$$u(y)=\frac{1}{(2\pi)^{\frac{1}{2}}}\int_{-\infty}^{\infty}F(\beta)\exp(-i\beta y)d\beta,$$

then

$$u(z)=\frac{1}{(2\pi)^{\frac{1}{2}}}\frac{A(z)}{B(z)},$$

and

$$F(y)=\frac{1}{2\pi}\int_{-\infty}^{\infty}\frac{A(z)}{B(z)}\exp(iyz)dz. \qquad (1)$$

Since the experimental curves, $\phi(x)$ and $f(y)$, look somewhat like Gaussian distribution curves, they may be approximated rather well by a few terms of a series of Hermitian orthogonal functions,[2] the first term of which is the Gaussian distribution. Then let $\phi(x)$ and $f(y)$ be represented as:

$$\phi(x)=\sum_{K=0}^{n}\gamma_K H_K(x/a)\exp(-x^2/2a^2)$$

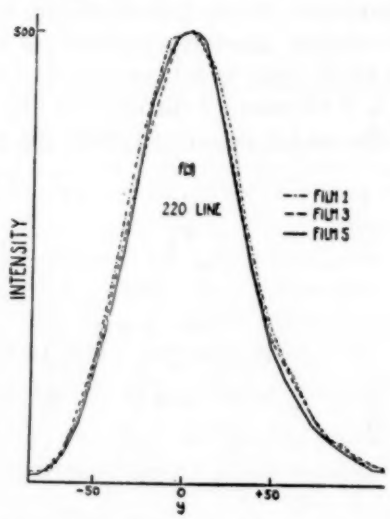

FIG. 1. Correction functions for the 220 reflection from relatively large particles of magnesium oxide.

[2] For definitions and some of the properties of Hermitian functions and Hermitian polynomials see: L. Pauling and E. B. Wilson, *Introduction to Quantum Mechanics* (McGraw-Hill Book Company, Inc., New York, 1935), pp. 73–82.

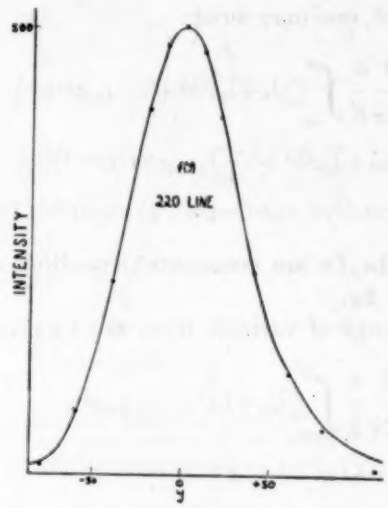

FIG. 2. Average correction function for the 220 magnesium oxide reflection. Crosses show the representation of the correction function by the sum of six terms of a Hermitian expansion.

and

$$f(y)=\sum_{K=0}^{n}p_K H(y/b)\exp(-y^2/2b^2),$$

where a, b, γ_K, and p_K are constants and $H_K(z)$ is the Kth order Hermitian polynomial.

The Fourier transforms of $\phi(x)$ and $f(y)$ may then be expressed in the following form:

$$A(z)=a\sum_{K=0}^{n}\gamma_K(-i)^K H_K(za)\exp(-z^2a^2/2)$$

and

$$B(z)=b\sum_{K=0}^{n}p_K(-i)^K H_K(zb)\exp(-z^2b^2/2).$$

Inserting these expressions in Eq. (1) a relation for $F(y)$ is obtained:

$$F(y)=\frac{1}{2\pi}\frac{a}{b}\int_{-\infty}^{\infty}\left[\frac{\sum_{K=0}^{n}\gamma_K(-i)^K H_K(za)}{\sum_{K=0}^{n}p_K(-i)^K H_K(zb)}\right]$$

$$\times\exp(iyz)\exp(-z^2a^2/2)\exp(z^2b^2/2)dz. \qquad (2)$$

Inserting the polynomials $H_K(za)$ and $H_K(zb)$ in Eq. (2), the expression in brackets can be simplified, and if higher power terms in z are

neglected, one may write:

$$F(y)=\frac{1}{2\pi}\frac{a}{b}\int_{-\infty}^{\infty}[(l_0+l_2z^2b^2+\cdots l_{2n}z^{2n}b^{2n}) +i(l_1zb+l_3z^3b^3+\cdots l_{2n-1}z^{2n-1}b^{2n-1})] \times\exp(iyz)\exp(-z^2a^2/2)\exp(z^2b^2/2)dz, \quad (3)$$

where the l's are constants depending on a, b, γ_K, and p_K.

A change of variable from zb to z gives:

$$F(y)=\frac{1}{2\pi}\frac{a}{b}\int_{-\infty}^{\infty}[(l_0+l_2z^2+\cdots l_{2n}z^{2n}) +i(l_1z+l_3z^3+l_{2n-1}z^{2n-1})] \times\exp(iyz/b)\exp(-z^2a^2/2b^2)\exp(z^2/2)dz. \quad (4)$$

If this change of variable is not made, the coefficients of z in the two sums of Eq. (3) become very large for large powers of z, zince b is of the order 30 in the units used for measuring x and y in these experiments. But in Eq. (4) the coefficients become very small for large powers of z.

Then Eq. (4) may be integrated term by term, giving for $F(y)$ an equation of the form:

$$F(y)=\text{constant}\times\exp(-y^2/2a^2-2b^2)\times\sum_{K=0}^{2n}C_K(y/b)^K.$$

The constants C_K will decrease rapidly as K increases only if the breadth of the function $f(y)$ at half-maximum intensity is at the most approximately half the breadth of the function $\phi(x)$.

III. EXPERIMENTAL PROCEDURE

To obtain a narrow, intense correction function, $f(y)$, an experimental arrangement was used which gave some focusing of the x-rays at the photographic film. A rocksalt crystal, bent to a radius of 20 cm and ground to a radius of 10 cm, was used as a focusing monochromator.[4] The $K\alpha$-radiation reflected from the monochromator was converged to the slit on the circumference of the camera. The x-rays diverged from the slit and fell on the flat powder sample which was mounted at the center of the camera. For each diffraction line the surface of the powder was set at the Bragg angle to the ray passing through the center of the camera. Better focusing was obtained by curving the surface of the powder, but the diffraction patterns from flat surfaces could be reproduced more accurately.

Relatively large particles of MgO were obtained by catching the smoke from burning magnesium ribbon. Small particles were obtained by decomposing $MgCO_3$ in an oven at a temperature of about 640 degrees centigrade.

Sensitometric exposures were made on Eastman Kodak, Type-K, industrial x-ray film for cobalt $K\alpha$-radiation reflected from a calcite crystal. While maintaining the characteristic $K\alpha$ x-ray intensity constant to within 2.7 percent, exposure times were varied. The densitometer readings were proportional to the time of exposure up to a density of at least 0.60 above chemical fog. In diffraction experiments densities were kept smaller than 0.60 and, assuming no reciprocity failure, were recorded as intensities.

IV. EXPERIMENTAL RESULTS

Figure 1 shows the three determinations of the correction function, $f(y)$, for the 220 line and indicates the accuracy to which measurements were reproduced. At the half-maximum of intensity the average absolute deviation of breadth from the mean value is 2.9 percent. The abscissa unit, y, is a measure of distance on the photographic film and is equal to 1/8000 the angle in

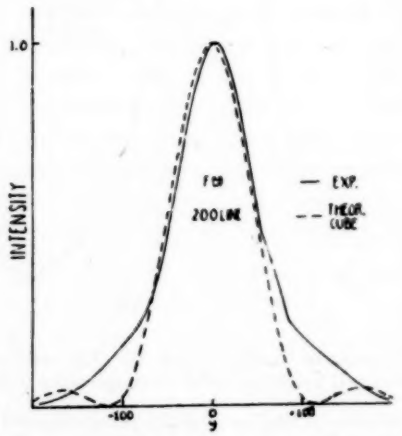

FIG. 3. Corrected diffraction function for the 200 reflection from magnesium oxide and the theoretical diffraction function for cube-shaped particles of uniform size.

[4] For description of bent rocksalt monochromators see: R. M. Bozorth and F. E. Haworth, Phys. Rev. 53, 538 (1938).

radians subtended at the center of the camera. One degree subtended at the center of the camera is very nearly equal to 140 units of y.

Figure 2 shows the curve obtained by taking the average ordinate of the three curves in Fig. 1. The crosses show the representation of $f(y)$ as the sum of the first six terms of a Hermitian expansion. Obviously, greater accuracy in determining line shapes may be obtained by using a larger number of terms in representing the experimental curves, but the computations outlined above become very lengthy. In Fig. 2 the average absolute deviation of the crosses from the experimental curve is 4.3-intensity units, 0.9 percent of the maximum intensity. This was the order of accuracy in representing the various experimental curves by Hermitian sums of six terms.

Figures 3–5, show the plots of the expressions

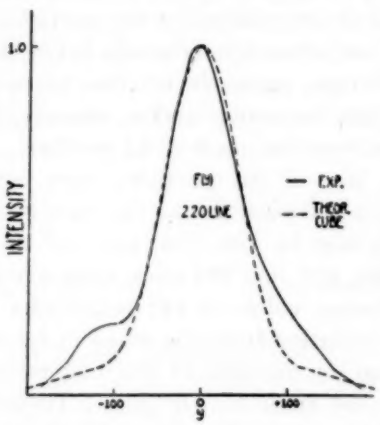

FIG. 4. Corrected diffraction function for the 220 reflection from magnesium oxide and the theoretical diffraction function for cube-shaped particles of uniform size.

for the corrected diffraction functions, $F(y)$, for the 200, 220, and 222 lines, respectively. Plotted in the same figures are the theoretical functions for cube-shaped particles of uniform size. According to Murdock,[1] these functions are

$$F(y)=\sin^2 y/y^2 \text{ for the 200 line,}$$
$$F(y)=6(y-\sin y)/y^3 \text{ for the 220 line,}$$

and

$$F(y)=3(y^2-\sin^2 y)/y^4 \text{ for the 222 line.}$$

Each theoretical function is matched to the corresponding experimental function with respect to breadth at half-maximum intensity. The experimental curves are considerably broader near

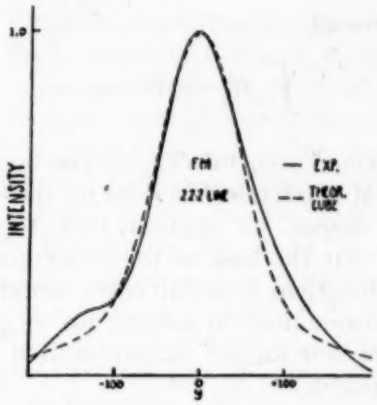

FIG. 5. Corrected diffraction function for the 222 reflection from magnesium oxide and the theoretical diffraction function for cube-shaped particles of uniform size.

the base than the theoretical functions. Moreover, the theoretical functions for particles having tetrahedral, octahedral, rhombic dodecahedral, and spherical shapes lie closer to the theoretical cube function than to the experimental curves.

The irregularities near the position $y=-120$ in the experimental determinations of $F(y)$ for the 220 and 222 lines indicate the inability of the method to produce accurate results in the region of low intensity. The higher order Hermitian coefficients, which are the least accurately known, determine the behavior of $F(y)$ in the region of low intensity. Since the theoretical functions for particles of various shapes differ widely only in the low intensity region, it is not possible to determine the shape of the particles from the shape of the curves shown here.

To check the accuracy of the approximations used in calculating $F(y)$, the second member of the equation

$$\phi(x)=\int_{-\infty}^{\infty} f(x-y)F(y)dy$$

can be evaluated by graphical integration for various values of x and may be compared to the experimentally measured values of $\phi(x)$. Such integrations were performed for each of the diffraction lines at nine values of x. The average absolute deviations of the calculated values of $\phi(x)$ from the measured values were 1.7, 1.4, and 1.3 percent for the 200, 220, and 222 lines, respectively. This error is smaller by a factor of at least two than that obtained when the graphical

integrations of

$$\int_{-\infty}^{\infty} f(x-y)F(y)dy$$

are performed using for $F(y)$ various breadths of theoretical diffraction functions for the different particle shapes. It appears that the excess breadth near the base of the experimental diffraction functions is not an effect introduced by the approximations in solving for $F(y)$. Later discussion will suggest an explanation for this excess breadth.

From the half-maximum intensity breadths of the diffraction functions and the Scherrer equation,[5] information concerning the size and shape of the particles may be obtained. A form of the Scherrer equation suggested by Murdock[6] is: $B=K\lambda/V^{\frac{1}{3}}\cos\theta$, where B is the half-maximum intensity breadth of the diffraction line, K is a coefficient depending on the shape of the particles and on the Miller indices of the reflection, θ is the Bragg angle, V is the volume of the particles, and λ is the wave-length of the x-rays. To determine particle size from this equation, the shape must first be known. If the relative breadth of two diffraction lines is calculated, the size of the particles is eliminated, and there remains

$$R=\frac{B_1}{B_2}=\frac{K_1\cos\theta_2}{K_2\cos\theta_1}.$$

B_1/B_2 can be evaluated from the experimental curves and may be compared with the values obtained from the right member of the equation when the values of K corresponding to the various particle shapes are inserted. The relative breadths of the experimentally measured diffraction functions are $B_{200}/B_{220}=0.993$, $B_{222}/B_{200}=1.244$, and $B_{222}/B_{220}=1.236$. The ratios of the observed relative breadths to the theoretical relative breadths for particles of various shapes are given in Table I.

TABLE I. Ratios of the observed relative breadths to the theoretical relative breadths of the diffraction lines for particles of various shapes.

Form—	Tetrahedron	Octahedron	Dodecahedron	Sphere	Cube
$\frac{R_{200/220}\text{ observed}}{R_{200/220}\text{ theoretical}}$	0.820	1.220	1.170	1.155	1.090
$\frac{R_{222/200}\text{ observed}}{R_{222/200}\text{ theoretical}}$	1.050	0.790	0.870	0.905	0.940
$\frac{R_{222/220}\text{ observed}}{R_{222/220}\text{ theoretical}}$	0.855	0.965	1.005	1.050	1.020

From Table I the shape which gives the best approximation to the value 1.000 is the cube. The average absolute deviation for the various shapes from the value 1.000 is 0.057 for the cube, 0.100 for the sphere, 0.102 for the dodecahedron, 0.125 for the tetrahedron, and 0.155 for the octahedron.

Assuming the particles are cubes, the mean size can be found from the Scherrer equation. The measured half-maximum intensity breadths of the three calculated diffraction functions are: $B_{200}=1.27\times10^{-2}$ radian, $B_{220}=1.28\times10^{-2}$ radian, and $B_{222}=1.59\times10^{-2}$ radian. Then the cube root of the volume of the particles as calculated from these line breadths is 134, 145, and 142 angstroms, respectively. This gives a mean value of 140 angstroms and an average absolute deviation from the mean of 3.1 percent.

If the size of the particles were calculated assuming a spherical shape, the cube root of the volume would be 134, 154, and 147 angstroms for the 200, 220, and 222 lines, respectively. This gives a mean value of 145 angstroms and an average deviation from the mean of 5.1 percent.

Electron micrographs of the magnesium oxide powder were made by Dr. James Hillier of the RCA Laboratory. The size of the particles appears two to three times larger in linear dimension than the above values. It seems likely that aggregates and not single crystals appear in the micrographs. The shape of the particles cannot readily be determined, but it does not appear that they are regular cubes in aggregates, except in a few instances.

A study was made of the effect on the diffraction function of a distribution of particle sizes. The theoretical calculations by Murdock[1] give the diffraction functions for the case o particles of uniform size. If $F(a_m y)$ is the theoretical diffraction function for particles of a given size, the resultant diffraction function for a discrete distribution of sizes will be

$$F(y)=\sum_m W_m F(a_m y)/\sum_m W_m,$$

[5] P. Scherrer, Göttinger Nachrichten **2**, 98 (1918).
[6] C. C. Murdock, Phys. Rev. **35**, 8 (1930).

where W_m is a weighting factor which depends on the particle size. W_m is proportional to the number of particles, N_m, of a given size, to the intensity, I_m, diffracted by a single particle of a given size, and inversely proportional to the area, A_m, of the diffraction function for particles of a given size. I_m is very nearly proportional to the volume of the crystal. It can be seen from the Scherrer equation and the theoretical diffraction functions that A_m is inversely proportional to the cube root of the volume of the crystals. Then the weighting factor is $W_m = CN_m V_m^{4/3}$. The resultant diffraction function due to a mixture of sizes will then be

$$F(y) = \sum_m N_m V_m^{4/3} F(a_m y) / \sum_m N_m V_m^{4/3}.$$

The half-maximum intensity breadth of this function will give the observed mean size of the particles. Since the diffraction function is weighted in favor of the larger particles, the measured mean size will be expected to be too large in practice. The effect on the diffraction function of various distributions of particle size was investigated using the above relation. A discrete distribution of particle sizes, approximating the continuous Gaussian distribution, does not seem to change the shape of the diffraction function appreciably. However, a distribution in which there are a large number of relatively small particles gives a diffraction function which is broad near the base. For example, the calculation was made for the 220 reflection from cube-shaped particles when there are four times as many particles of 75 angstrom edge length as of 150 angstrom edge length. The half-intensity breadth gave a mean edge length of 135 angstrom units, but the resultant line shape corresponded to the shape for cubes of uniform size only in the upper half. In the lower half the resultant function was much broader than the function for cubes of uniform size. It seems reasonable that some such distribution of particle sizes may account for the experimentally determined diffraction functions.

The author wishes to thank Professor Carleton C. Murdock, who suggested the problem, for his encouragement and assistance in carrying out the research.

PHYSICAL REVIEW VOLUME 72, NUMBER 10 NOVEMBER 15, 1947

On the Dissociation Energy of Carbon Monoxide and the Heat of Sublimation of Carbon

HOMER D. HAGSTRUM
Bell Telephone Laboratories, Murray Hill, New Jersey

(Received June 26, 1947)

None of the values of the dissociation energy of carbon monoxide, D(CO), proposed on the basis of interpretations of predissociations in the spectrum of CO is in satisfactory agreement with the results of electron-impact experiments. The only possible interpretation of these experiments gives D(CO) = 9.6 ev. Compelling reasons can be given for considering this result of sufficient accuracy to make it irreconcilable with any of the values from the band spectrum. A new interpretation of the effects in the spectrum which brings agreement with the electron impact value is possible, however. It involves a potential curve with maximum for $J=0$ for the state $a'\,^3\Sigma^+$ of CO which predissociates $B^1\Sigma^+$ and $b^3\Sigma^+$ at 11.11 ev. Various data favor this interpretation and its consequences. Satisfactory agreement among all data bearing on D(CO) and L_1(C), the heat of sublimation of carbon, can be attained in this way.

1. INTRODUCTION

THE dissociation energy of carbon monoxide, D(CO), is a particularly important quantity because of its relation to the heat of sublimation of carbon, L_1(C), and through it to the heats of formation and bond energies of every carbon-containing molecule. The relation between L_1(C) and D(CO) is obtained from the well-known

thermochemical cycle:

$$\begin{aligned} CO(X^1\Sigma^+)+D(CO)&=C(^3P)+O(^3P)\\ C(^3P)&=C_{solid}+L_1(C)\\ O(^3P)&=\tfrac{1}{2}O_2(X^3\Sigma_g^-)+\tfrac{1}{2}D(O_2)\\ C_{solid}+\tfrac{1}{2}O_2(X^3\Sigma_g^-)&=CO(X^1\Sigma^+)+Q(CO)\\ \hline D(CO)&=L_1(C)+\tfrac{1}{2}D(O_2)+Q(CO). \end{aligned}$$

With the well-established values:

$$D(O_2)=5.082 \text{ ev } (117.2 \text{ kcal})^{1,2}$$
$$Q(CO)=1.180 \text{ ev } (27.20 \text{ kcal})^{3}$$

there is obtained:

$$L_1(C)=D(CO)-3.721 \text{ ev } (85.78 \text{ kcal}).$$

General agreement concerning the value of $D(CO)$ has not yet been reached. The most widely accepted value is that proposed by Herzberg,[4] $D(CO)=9.14$ ev, based on an interpretation of the evidences of predissociation in the spectrum of CO. However, it is one of three divergent values, based on as many interpretations of intensity breakoffs in the band spectrum, currently supported in the literature. Furthermore, one cannot reconcile the electron-impact value, $D(CO)=9.6$ ev, with any of the values from the band spectrum without assuming an error of about 0.5 ev or more. The main purpose of this paper is to discuss critically the data from electron impact and the band spectrum and to propose a new interpretation of the evidences of predissociation in the spectrum which brings agreement with $D(CO)=9.6$ ev.[5] Other data bearing on $D(CO)$ and $L_1(C)$ are discussed and shown to be in harmony with the contention that $D(CO)=9.6$ ev.

2. ELECTRON-IMPACT EXPERIMENTS

Criticism of Method

A review of the literature on electron-impact experiments indicates a considerable lack of agreement among the results obtained by several different methods for a number of molecules. This is no doubt the reason for the evident lack of confidence in the results for CO and the feeling that, in general, the electron impact results give at most upper limits for the quantities measured. Such need not necessarily be true of all the electron impact results, however. A criticism of the methods used and a conclusion as to which may be expected to yield credible results is demanded.

The electron-impact apparatus which have been used in the study of ionization and dissociation processes in CO are these: (a) a Lenard-type apparatus with positive-ray analysis of the ions produced;[6] (b) an apparatus which detects the ions formed as well as the variation of the electron current passing through the gas as a function of electron energy;[7] (c) a mass spectrometer having a "transverse," magnetically-collimated electron beam;[8–10] and (d) a retarding potential apparatus used to study ions which receive appreciable initial kinetic energies in their formation.[11,12]

The first of these apparatus belongs to a general type used by several investigators with which was obtained no general agreement or convincing evidence concerning the ionization *and dissociation* of molecules at a single electron collision. The gas pressures employed were high enough to cause secondary processes to occur. For some molecules, in fact, it could not be decided whether the atomic ions observed resulted from a primary process involving ionization and dissociation of the molecule or a second-

[1] G. Herzberg, *Molecular Spectra and Molecular Structure, I. Diatomic Molecules* (Prentice Hall, New York, 1939), pp. 474ff.

[2] In this paper, the conversion factors: 1 ev = 8066.0 cm^{-1} = 23.053 kcal/mole are used. See Table II, G. Herzberg, reference 1. Values in the literature based on other conversion factors have been recalculated for quotation in this paper.

[3] D. D. Wagman, J. E. Kilpatrick, W. J. Taylor, K. S. Pitzer and F. D. Rossini, J. Research Nat. Bur. of Stand. Wash. **34**, 143 (1945).

[4] G. Herzberg, Chem. Rev. **20**, 145 (1937).

[5] The gist of this interpretation has been published as a preliminary report in a Letter to the Editor of this journal, H. D. Hagstrum, Phys. Rev. **71**, 376 (1947) and was discussed at the Washington meeting of the American Physical Society, May 1, 1947, H. D. Hagstrum, Phys. Rev. **72**, 158 (1947).

[6] T. R. Hogness and R. W. Harkness, Phys. Rev. **32**, 936 (1928).

[7] J. Savard, Rev. Fac. Sci. Univ. Istanbul **II**, 235 (1937); M. de Hemptinne, J. Savard, and P. Capron, Compt. Rend. Acad. Sci. Paris **204**, 1039 (1937); J. Savard and M. de Hemptinne, J. de phys. et rad. **10**, 30 (1939). See also the report of the work on N_2: M. de Hemptinne and J. Savard, J. de phys. et rad. **6**, 499 (1935).

[8] A. L. Vaughan, Phys. Rev. **38**, 1687 (1931).

[9] J. T. Tate, P. T. Smith, and A. L. Vaughan, Phys. Rev. **48**, 525 (1935).

[10] H. D. Hagstrum and J. T. Tate, Phys. Rev. **59**, 354 (1941).

[11] J. T. Tate and W. W. Lozier, Phys. Rev. **39**, 254 (1932).

[12] W. W. Lozier, Phys. Rev. **46**, 268 (1934).

ary process in which a molecular ion (the result of a primary electron-impact process) is dissociated on collision with another molecule. Furthermore, the sensitivity of the apparatus was generally considerably lower than that attained in later work. Thus Hogness and Harkness,[6] although they thought that the O^+ ion resulted from the primary process $CO+\epsilon^-\rightarrow C+O^++2\epsilon^-$, could not measure its appearance potential and had difficulty in distinguishing $CO+\epsilon^-\rightarrow C^++O+2\epsilon^-$ from $CO^++CO\rightarrow C^++CO_2$. For these reasons it is believed that appearance potentials obtained by this method as well as their interpretation, may be unreliable and should not be used to calculate dissociation energies.

About 1930 there were constructed apparatus in which the ions are formed in a magnetically-collimated electron beam of restricted cross section [methods (c) and (d)].[13] Greater sensitivity was attained and care taken to avoid the occurrence of secondary processes in the ionization chamber. This marked a definite turning point in the study of ionization and dissociation processes in molecules by electron impact.

The method employed by Savard and de Hemptinne,[7] listed as (b) above, is for several reasons considered to be unreliable and to yield questionable results. The ions produced in the apparatus were not identified by (m/e)-analysis nor distinguished on the basis of their initial kinetic energy. No positive means of attributing the breaks in the collector-current curve to the onset of particular ionization processes was available. Some processes were attributed to the collision of an electron with an ion formed in an earlier collision. The occurrence of these processes can only mean that the gas pressure used, although not specified, was sufficiently high to cause other secondary processes to occur and thus to make questionable any of the results claimed. On the basis of the appearance of what were thought to be C^+ ions at 20.0 ev, the authors maintain that $D(CO)=8.8$ ev.[7] However, similar measurements in N_2 yielded $D(N_2)=6.72$ ev[7] in disagreement with the value $D(N_2)=7.384$ ev now generally accepted.[14]

[13] W. Bleakney, Phys. Rev. **34**, 157 (1929); **35**, 139 and 1180 (1930); W. W. Lozier, Phys. Rev. **36**, 1285 (1930).

[14] G. Herzberg and H. Sponer, Zeits. f. physik. Chemie **B26**, 1 (1934); reference 1; W. W. Lozier, Phys. Rev. **44**, 575 (1933); **45**, 840 (1934); H. D. Hagstrum and J. T. Tate, Phys. Rev. **59**, 354 (1941).

Other aspects of the experiment of Savard and de Hemptinne confirm one's doubts as to its validity. Ion and electron currents were allowed to mix, leading, as the authors themselves admit, to spurious maxima in the collected current. The observation of some ionization processes was said to depend critically upon the attainment of what was considered to be a balance between the rates of gas inlet into the apparatus and gas removal in the form of ions produced. It was claimed that as many as 58 critical potentials had been found in CO in the electron-energy range 12.5 to 34.0 ev.[15] Some of these potentials depend upon the deviation of a single datum point from the general course of the current curve. This work has been refuted in such detail because it has been injected into the discussion of $D(CO)$ by Long and Norrish[16] alongside other electron-impact results as evidence of discord among such results.

In contrast to the methods (a) and (b) just discussed, methods (c) and (d) are believed now to yield trustworthy results. The reasons for this belief are to be discussed in detail presently. The deficiencies in the work of Vaughan,[8] Tate, Smith, and Vaughan,[9] and Tate and Lozier[11] in CO have been removed in the later work.[10,12] Reference is made to the original literature for discussions of the apparatus and the methods of their use.[17]

Criticism of Data and Interpretation

The value of $D(CO)$ from electron-impact experiments rests on the onset potentials of the following observed ionization and dissociation processes:

(A) $CO+\epsilon^-\rightarrow C^++O+2\epsilon^-$
(B) $CO+\epsilon^-\rightarrow C^++O^-+\epsilon^-$
(C) $CO+\epsilon^-\rightarrow C+O^++2\epsilon^-$
(D) $CO+\epsilon^-\rightarrow C+O^-$.

The measured onset potentials of these processes are given in Table I. Typical experimental data

[15] In this connection see E. Rudberg, Proc. Roy. Soc. London [A]130, 182 (1930) in which the energy losses of electrons in passing through CO are measured directly.

[16] L. H. Long and R. G. W. Norrish, Proc. Roy. Soc. London [A]187, 337 (1946).

[17] A general description of mass spectrometers is to be found in E. B. Jordan and L. B. Young, J. App. Phys. 13, 526 (1942). For a discussion of the extension of the mass-spectrometric method [method (c)] to include an analysis of ion-peak shapes see reference 10. The retarding-potential method [method (d)] is described in reference 12.

TABLE I. Onset potentials of ionization and dissociation processes in CO.

		Lozier[12] (ev)	Hagstrum and Tate[10] (ev)
Process (A)	$A(C^+)$	22.8±0.1	22.8±0.2
Process (B)	$A(C^+)$	20.9±0.1	20.9±0.2
	$A(O^-)$	20.9±0.1	20.9±0.2
Process (C)	$A(O^+)$	—	$23.1^{+0.0}_{-0.4}$
Process (D)	$A(O^-)$	9.5±0.1	9.5±0.2

from which they are obtained are reproduced in Figs. 1 and 2.

If these data are to be used to determine dissociation limits of the molecule, it is essential (1) that each process be identified correctly, (2) that its measured onset potential be the appearance potential of ions of zero initial kinetic energy, and (3) that the electron energy at the onset of ionization be correctly determined from the ionization-efficiency curve at its foot.

When a mass spectrometer is employed [method (c)], the nature of one of the dissociation products is evident from the (m/e)-analysis. The retarding-potential apparatus [method (d)], with which no (m/e)-analysis is made, can distinguish positive and negative ions and the ions which, because they result from a dissociation process, possess appreciable initial kinetic energies. At a given retarding potential, the appearance potential of the positive ion formed at the lowest electron energy is measured by this method. This ion may be identified by the mass spectrometer. Thus in CO, the C^+ ion is found in the mass spectrometer to occur at lower electron energies than the O^+ ion, identifying the positive ion studied in Lozier's work. The negative ion is identified as O^- in the mass spectrometer.

From the simultaneous appearance of positive and negative ions or from the magnitude of the onset potential, one can generally determine the state of ionization of the other dissociation product. Thus the appearance of C^+ and O^- at 20.9 ev in equal numbers up to 22.8 ev (see Fig. 1) identifies process (B). Since the value 22.8 ev for the second appearance potential of C^+ ions is less than the sum of the ionization energies of C and O one concludes with confidence that only C^+ ions are formed at 22.8 ev and that process (A) has been identified correctly. Similar arguments apply to processes (C) and (D). Because $A(O^+)>A(C^+)$, process (C) could not be studied by method (d). No evidence of the occurrence of secondary processes is to be found in these experiments.

The identification of the state of excitation of the products cannot be made directly in an electron-impact experiment. From the onset potential of a single process, a series of possible levels for a given dissociation limit may be calculated for various assumed states of excitation of the products. From such results for more than one process, a unique determination is possible in CO as is to be explained.

In the retarding potential method the kinetic energy of the ion as well as its appearance potential is measured. From these data the appearance potential of ions formed at rest may be calculated by the law of conservation of momentum at the collision.[12] This determination is valid even if ions of zero initial kinetic energy are not formed as is the case when the potential curve involved has a maximum. In addition, the analysis of the shapes of ion peaks has demonstrated

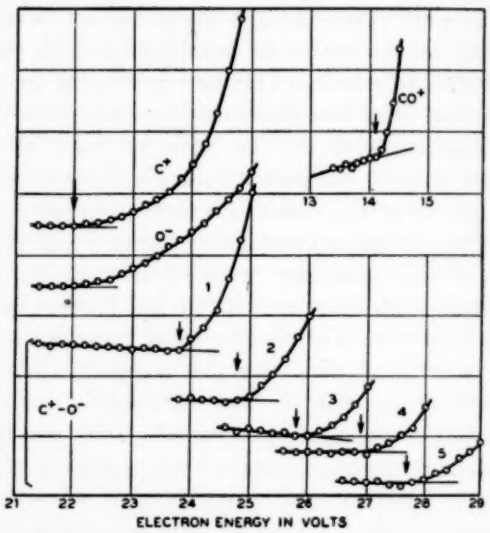

FIG. 1. Typical experimental data of Lozier (Figs. 8 and 9 of reference 12) from which appearance potentials are obtained in the study of CO by method (d). The appearance potential of CO^+ is used to calibrate the voltage scale. The total kinetic energy of the C^+ and O^- ion products is 1 ev. The curves 1 to 5 for the difference current C^+-O^- correspond to total kinetic energies of 1, 2, 3, 4, and 5 ev, respectively. Note the equality of the C^+ and O^- currents to 22.8 ev (for ions of zero initial kinetic energy), the onset potential of the process yielding C^++O. These curves show how difficult it would be to assume an experimental error of greater than ±0.1 ev in these results.

that considerable information concerning the distribution in initial kinetic energy of the ions formed and hence the nature and position of the potential curve involved can be obtained with the mass spectrometer.[10] Study of a single molecule by both methods gives more information than by either method alone. In CO, the appearance potentials of ions of zero initial kinetic energy in processes (A), (B), and (D) determined by the retarding-potential method agree with those for ions at the maximum of the peak observed with mass spectrometer. This, together with the observed peak shape, demonstrates that the ions are formed at rest and that the data may be used to fix dissociation limits of the molecule. The study of process (C) with the mass spectrometer, on the other hand, showed that O^+ ions of zero initial kinetic energy are not formed. This necessitated the use of a special method to obtain the energy level of the corresponding dissociation limit.[10]

In the electron impact experiments of interest here, the lowest electron energy at which an ion is detected is taken as the onset potential of the process of its formation. The voltage scale is calibrated against the ionization of a rare gas, due precautions being taken to adjust to comparable instrumental sensitivity. The appearance potential is the point at which the ionization-efficiency curve first breaks away from the base line in Figs. 1 and 2.

The justification of the whole procedure of these experiments, and of the choice of the onset potentials in particular, is to be found in the

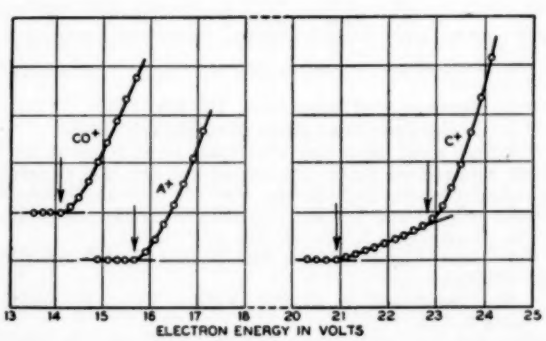

FIG. 2. Typical experimental data of Hagstrum and Tate (Fig. 12 of reference 10) from which appearance potentials are obtained in the study of CO by method (c). The appearance potential of A^+ ions is used to calibrate the voltage scale. The onset of the two processes forming C^+ ions [(*A*) and (*B*)], here of zero initial kinetic energy, are clearly seen. The maximum experimental error is given as ±0.2 ev.

TABLE II. Comparison of dissociation energies from electron impact and other data.

Molecule	Appearance potential (ev)	Dissociation energy (ev) Electron impact	Established value
H_2	$A(H_2^+)=18.0\pm0.2$[19] $=17.96\pm0.03$[20] $=18.0\pm0.2$[10]	4.5[20,10]	4.4776[22]
N_2	$A(N^+)=24.27\pm0.1$[20] $=24.3\pm0.2$[10]	7.4[20,10]	7.384[14,22]
NO	$A(N^+)=21.7\pm0.2$[21] $=21.8\pm0.2$[10]	5.3[21,10]	5.29[22]

results for molecules whose dissociation energies are well established by other means. Studies have been carried out in H_2, N_2, NO, and O_2 with apparatus and procedure identical to that used in CO. In Table II the relevant appearance potentials are listed and the dissociation energies obtained from them compared with the generally accepted values.[18] Further evidence of the reliability of the method is to be found in the values obtained for various ionization potentials known by other means (see Table III).

In the earlier work of Vaughan[8] with a mass spectrometer and of Tate and Lozier[11] with a retarding-potential apparatus, processes (A) and (B) were not satisfactorily distinguished. This has now been done, as has been discussed, with excellent agreement between the two methods (Table I). Tate, Smith, and Vaughan's value[9] of $A(O^+)$ was measured at the maximum of the O^+ peak which later work[10] showed not to correspond to ions of zero initial kinetic energy.

A consistent interpretation of the onset potentials in Table I is obtained only if $D(CO)=9.6\pm0.1$ ev. The 22.8 ev onset potential of process (A) makes the values $D(CO)=11.6$, 9.6, 7.4, 6.4 and 4.4 ev possible for various choices of excitation of the products. The onset potential of process (C), however, yields a series of values which contains only the value 9.6 ev of those

[18] In the case of O_2, Lozier did not study the process $O_2+\epsilon^-\rightarrow O^++O+2\epsilon^-$ (reference 12) and the analysis with the mass spectrometer indicates that the potential curve involved possesses a maximum.[10] No definite statement concerning $D(O_2)$ can be made on the basis of electron-collision experiments alone without the retarding-potential study.

[19] W. Bleakney, Phys. Rev. **35**, 1180 (1930); **40**, 496 (1932).

[20] W. W. Lozier, Phys. Rev. **44**, 575 (1933); **45**, 840 (1934).

[21] E. E. Hanson, Phys. Rev. **51**, 86 (1937).

[22] See reference 1, Tables 36 and 37, pp. 482 and 500.

TABLE III. Comparison of ionization potentials from electron impact and other data. Note: In these cases transitions between the lowest vibrational states of the ground electronic states of the ion and molecule can occur by the Franck-Condon principle.

Ionization potential	Electron impact (ev)	Spectroscopic (ev)
$I(H_2)$	15.4 ± 0.1[19,10]	15.427[22]
$I(N_2)$	15.7 ± 0.1[9,10]	15.581[22]
$I(O_2)$	12.3 ± 0.1[10]	12.2[22]
$I(Ne)-I(A)$	5.65 ± 0.15[23]	5.78

listed. The processes (B) and (D) can be interpreted satisfactorily with $D(CO)=9.6$ ev.[10,12] It should be emphasized that the value of $D(CO)$ rests upon $A(C^+)=22.8\pm0.1$ ev from both electron-impact methods. $A(O^+)$ is not as accurate as $A(C^+)$ and is used only to discriminate among the values of $D(CO)$ listed above.

A schematic diagram of the energy levels at which the various ionization and dissociation processes commence and the assignment of dissociation limits of CO, CO^+, and CO^- is shown in Fig. 3. Included in the figure are the assignments based on three values of $D(CO)$ proposed on the basis of band spectroscopic evidence. These are to be discussed in detail later. Note that only the dissociation limits based on $D(CO)=9.6$ ev can account for the observed processes. It is difficult to see the justification for the remark of Gaydon and Penney[24] that this result is obtained from a curve which "appears to be of complex structure and might be capable of an alternative explanation." $D(CO)=9.6\pm0.1$ ev gives $L_1(C)=5.9\pm0.1$ ev $=136\pm2$ kcal.

3. PRESENT INTERPRETATIONS OF THE SPECTROSCOPIC EVIDENCE

Inasmuch as no band convergence has been found in the spectrum of CO and little if any evidence is to be obtained from absorption continua, one must rely on predissociation data in attempting to fix dissociation limits of the molecule by spectroscopic means. The Birge-Sponer extrapolation of vibrational levels in the ground state yields the value $D(CO)=11.34$ ev,[25] but, as pointed out by Herzberg,[26] this may be as much as 20 to 40 percent too high. This conclusion is in agreement with Gaydon's summary of results of the use of the Birge-Sponer extrapolation for neutral molecules with nonionic binding.[27] Gaydon finds that the average ratio of the known dissociation energy to the value found by linear extrapolation of the vibrational levels for a number of such molecules is 0.79.

Evidences of Predissociation

A number of intensity weakenings or breakoffs in the rotational structure of CO bands have been found and are reported in the literature. Those which are now considered by any investigator to indicate predissociation are listed in Table IV. In Table V are listed the energy levels of the supposed predissociation limits for no

TABLE IV. Intensity breakoffs in the rotational structure of CO bands.[28]

State	v	J	$J(J+1)$	cm^{-1} above $X^1\Sigma^+$	Band system
$A^1\Pi$	4[29]	26	702	71526.8	Angström $[B^1\Sigma^+\rightarrow A^1\Pi]$
		27	756	71608.3	
	7[29]	47	2256	77636.0	*IV* Positive $[A^1\Pi\rightarrow X^1\Sigma^+]$
		48	2352	77774.1	
	8[29]	36	1332	77509.2	*IV* Positive $[A^1\Pi\rightarrow X^1\Sigma^+]$
		37	1406	77613.6	
	9[30]	21	462	77479.4	*IV* Positive $[A^1\Pi\rightarrow X^1\Sigma^+]$
		22	506	77540.5	
	13[30,31]	16	282	81620	*IV* Positive $[A^1\Pi\rightarrow X^1\Sigma^+]$
$B^1\Sigma^+$	0[32]	37	1406	89655.2	Angström $[B^1\Sigma^+\rightarrow A^1\Pi]$
		38	1482	89801.3	
	1[32]	17	306	89598.0	Angström $[B^1\Sigma^+\rightarrow A^1\Pi]$
		18	342	89666.8	
$b^3\Sigma^+$	0[34,35]	55	3080	89950.6	*III* Positive $[b^3\Sigma^+\rightarrow a^3\Pi]$
		56	3192	90181.1	
	1[34]	42	1806	89768.3	*III* Positive $[b^3\Sigma^+\rightarrow a^3\Pi]$
		43	1892	89946.5	
$C^1\Sigma^+$	0[37]	28	812	93495.8	Herzberg $[C^1\Sigma^+\rightarrow A^1\Pi]$
		29	870	93607.9	
$c^3\Sigma^+$	0[38,39]	~27	~756	~93500	"3*A*" $[c^3\Sigma^+\rightarrow a^3\Pi]$

[23] D. P. Stevenson and J. A. Hipple, Phys. Rev. **62**, 237 (1942).
[24] A. G. Gaydon and W. G. Penney, Proc. Roy. Soc. London [A]**183**, 374 (1945).
[25] R. T. Birge and H. Sponer, Phys. Rev. **28**, 259 (1926).
[26] G. Herzberg, J. Chem. Phys. **10**, 306 (1942).
[27] A. G. Gaydon, Proc. Phys. Soc. **58**, 525 (1946).
[28] Where more than one rotational level is listed for a given vibrational state, the levels are the last of undiminished intensity and the first after the intensity breakoff.
[29] R. Schmid and L. Gerö, Physik. Zeits. **39**, 460 (1938).
[30] L. Gerö, Zeits. f. Physik **100**, 374 (1936).
[31] R. Schmid and L. Gerö, Zeits. f. physik. Chemie **B36**, 105 (1937).
[32] D. Coster and F. Brons, Nature **133**, 140 (1934); Physica **1**, 155 (1934).
[33] R. Schmid and L. Gerö, Zeits. f. Physik **93**, 656 (1935).
[34] F. Brons, Nature **135**, 873 (1935).
[35] L. Gerö, Zeits. f. Physik **95**, 747 (1935).
[36] R. Schmid and L. Gerö, Zeits. f. Physik **96**, 198 (1935); L. Gerö, Zeits. f. Physik **101**, 311 (1936).
[37] R. Schmid and L. Gerö, Zeits. f. Physik **96**, 546 (1935).
[38] R. Schmid, Physik. Zeits. **37**, 55 (1936).
[39] L. Gerö, Zeits. f. Physik **109**, 210 (1938).

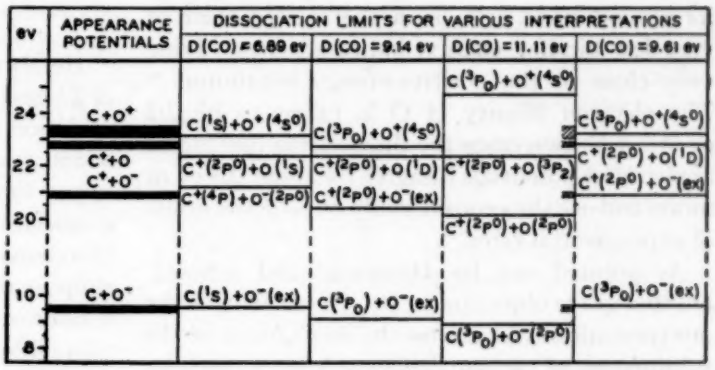

FIG. 3. An energy-level diagram showing the appearance potentials measured in electron-impact experiments and the closest dissociation limits for the appropriate ions predicted by four values of $D(CO)$. $D(CO)=6.89$, 9.14, and 11.11 ev are the values based on interpretations of the spectrum of CO currently supported in the literature (see Fig. 4). $D(CO)=9.61$ ev is the value obtained from the interpretation of the band spectrum proposed in this paper and from the electron-impact experiments. The line widths in the appearance potential column indicate the limits of experimental error.

rotation ($J=0$) obtained from the data of Table IV.

The predissociations in $B^1\Sigma^+$ and $b^3\Sigma^+$ are thought both to be caused by the state $a'^3\Sigma^+$ whose vibrational levels converge to the same limit at 89620 cm^{-1}.[34, 35, 40] The vibrational levels of $a'^3\Sigma^+$ have been followed by perturbations in $A^1\Pi$ and $b^3\Sigma^+$ to $v=41$, 900 cm^{-1} from the convergence limit.[40]

Intensity breakoffs observed in the vibrational structures of various CO band systems have also been attributed to predissociation. In Table VI are listed such breakoffs as have been considered by Schmid and Gerö to be evidences of predissociation.[38, 31]

The three conflicting interpretations of the evidences of predissociation listed in Table IV now supported in the literature give $D(CO)=6.89$, 9.14, and 11.11 ev. Several other values for $D(CO)$ proposed on the basis of the CO spectrum have been withdrawn, are no longer supported, or are based on such scanty evidence as not to warrant further consideration. Each of the present interpretations will now be discussed.

Criticism of $D(CO)=6.89$ ev

Schmid and Gerö[41, 31] consider all of the five effects listed in Table V to be true predissociations occurring at or just above dissociation limits of the molecule. The latest assignment of dissociation limits by Schmid and Gerö[29] is summarized in Table VII in which are also listed the vibrational breakoffs from Table VI. In Fig. 4 the assignment of dissociation limits is depicted graphically for comparison with other interpretations. The contention that $D(CO)=6.89$ ev has recently been defended by Valatin.[42]

The $X^1\Sigma^+$ ground state is thought to dissociate into $C(^1D)+O(^1D)$ at 81660 cm^{-1} in Schmid and Gerö's scheme. The lowest atomic term combination $C(^3P_0)+O(^3P_2)$, however, is 55600 cm^{-1} (6.89 ev) above the ground molecular state. This specifies $D(CO)$ as ordinarily defined.

Assignment of $C(^5S)+O(^3P_0)$ to the limit at 89620 cm^{-1} is used to calculate the excitation energy $[C(^5S)-C(^3P_0)]=33800$ cm^{-1}.[43] This was considered at the time the interpretation was proposed to be in passable agreement with the value 34994 cm^{-1} (4.34 ev) calculated by Bacher and Goudsmit[44] and the value 34000 cm^{-1} (4.2 ev) obtained by extrapolation by Edlén.[45] Shenstone has recently reported[46] the successful identification of intercombination lines with $C(^5S)$ from which the level is now definitely fixed at 33735.2 cm^{-1} (4.16 ev) above $C(^3P_0)$.

A first objection to $D(CO)=6.89$ ev is the fact that it cannot be reconciled with the results of electron-impact experiments. In Fig. 3 are plotted in the column headed $D(CO)=6.89$ ev the dissociation limits of the appropriate ions closest to the observed appearance potentials, both divalent and tetravalent states of C and C^+ being considered.[47, 31] The ion O^- is taken to exist either in

[40] R. Schmid and L. Gerö, Zeits. f. Physik **105**, 36 (1937); **106**, 205 (1937).
[41] R. Schmid and L. Gerö, Zeits. f. Physik **99**, 281 (1936).
[42] J. G. Valatin, J. Chem. Phys. **14**, 568 (1946); Nature **158**, 237 (1946).
[43] In Table VI, 89620 cm^{-1} is enclosed in parenthesis to emphasize that it is assumed and not related to the other levels by known excitation energies.
[44] R. F. Bacher and S. Goudsmit, Phys. Rev. **46**, 948 (1934).
[45] B. Edlén, Zeits. f. Physik **84**, 746 (1933).
[46] A. G. Shenstone, Phys. Rev. **72**, 411 (1947); see also B. Edlén, Nature **159**, 129 (1947).
[47] R. Schmid, Zeits. f. Physik **99**, 274 (1936).

its ground state, $^3P^0$, or in the excited state of very low binding energy, indicated O(ex), lying very close to the positive-energy continuum.[48] The electron affinity of O is taken to be 2.2 ev.[10,12,49] In two cases the dissociation limits and appearance potentials disagree by about 0.5 ev or more, and are thus considerably outside the limits of experimental error.

As pointed out by Herzberg[4] and others,[50] another grave objection to $D(CO)=6.89$ ev is the interpretation it places on the mechanism of the sublimation of carbon. $D(CO)=6.89$ ev gives for $L_1(C)$ the extremely low value 3.17 ev (73.1 kcal). To reach agreement with thermochemical measurements, it is necessary for Schmid and Gerö to assume[31] that carbon atoms come out of the solid in the tetravalent state, C(^5S), from which, even in equilibrium measurements, they cannot return to the ground state in the vapor outside the solid. This appears extremely unlikely in view of Shenstone's statement[46] that the existence of intercombination lines with C(^5S) "implies that ^5S can hardly be considered as a metastable state, and should not, therefore, enter in that role into thermochemical theory."

The results of Kenty *et al*, to be discussed later, in which the failure of Xe metastable atoms to dissociate CO in collisions of the second kind is taken to mean that $D(CO)>9.4$ ev, also provides evidence against Schmid and Gerö's interpretation of the band spectrum of CO.

TABLE V. Supposed predissociation limits ($J=0$) from intensity breakoffs in the rotational structure of CO bands.

State	v	cm^{-1} above $X^1\Sigma^+$
$A^1\Pi$	4	~71500[29]
$A^1\Pi$	7, 8, 9	77497±44[30]
$A^1\Pi$	13	>81620[30]
$B^1\Sigma^+$, $b^3\Sigma^+$	0, 1	89620±47[30]
$C^1\Sigma^+$, $c^3\Sigma^+$	0	<93550[37-39]

[48] Electron-collision experiments in both CO and NO appear to demonstrate the existence of this state. See references 10 and 12. It has been discussed theoretically by H. S. W. Massey, *Negative Ions* (Cambridge University Press, Teddington, England 1938) and by D. R. Bates and H. S. W. Massey, Phil. Trans. Roy. Soc. Lond. [A]239, 269 (1943).

[49] It should be noted that poorer agreement results from the choice of a larger value for the electron affinity such as that of D. T. Vier and J. E. Mayer, J. Chem. Phys. 12, 28 (1944). Vier and Mayer's value is considered by the present writer to be erroneous.

[50] A. G. Gaydon, Proc. Phys. Soc. 58, 704 (1946); L. H. Long and R. G. W. Norrish, Nature 158, 237 (1946).

Criticism of $D(CO)=9.14$ ev

Herzberg[4] considers only the predissociations in $B^1\Sigma^+$ and $b^3\Sigma^+$ at 89620 cm^{-1} to occur at a dissociation limit of the molecule. The effect at 93550 cm^{-1} in $C^1\Sigma^+$ is thought to represent an upper limit for a dissociation limit as the predissociation occurs in one vibrational level only. Herzberg considers the slightness of the intensity drop in the (9, 18) IV Positive band and its extension over only two or three successive rotational levels to indicate an accidental predissociation or a perturbation.[51] This is also applied to the effects in the $v'=7$ and 8 levels. Thus the effect at 77497 cm^{-1} in $A^1\Pi$ is thought to yield at most an upper limit for a dissociation limit. Although Herzberg has not commented upon the supposed predissociations at $v=4$ and 13 of $A^1\Pi$ (see Table V), he must of necessity reject them.

Of the several possible choices for the states of excitation of the products at the 89620 cm^{-1} limit, Herzberg prefers C($^3P_0$)+O(^1D) giving $D(CO)=9.14$ ev (73750 cm^{-1}). This interpretation is summarized in Fig. 4.

Against the value $D(CO)=9.14$ ev may also be brought the charge that it does not satisfactorily account for the electron-collision experiments as Fig. 3 shows. It also is below the lower limit for $D(CO)$ indicated by the experiment of Kenty *et al* (see below). Furthermore, the evidences on which Herzberg based his interpretation of the effect in the (9, 18) IV Positive band are no longer as convincing as they might once have been. It has since been shown[52] that the intensity rise at the lines $P(25)$, $P(26)$, and $P(27)$ followed by a second intensity drop, is the result of the superposition of lines of the (0, 1) band of the so-called "3A" system ($c^3\Sigma^+\rightarrow a^3\Pi$). Thus the intensity drop following $P(22)$ actually extends over several more rotational levels than was first supposed. Schmid and Gerö[31] report that on new plates the intensity breakoffs in $A^1\Pi$ at 77497 cm^{-1} show up as strongly as those in the Angström bands ($B^1\Sigma^+$). They present what appears to be a rather convincing argument that the effect can be neither an accidental predissociation nor an ordinary perturbation.

[51] This has since become subject to some revision as will be discussed below.

[52] R. Schmid and L. Gerö, Nature 139, 928 (1937); L. Gerö, Zeits. f. Physik 109, 210 (1938).

$D(CO) = 9.14$ ev is in satisfactory agreement with thermochemical experiments.[4] The present writer feels that the real choice for $D(CO)$ now is between this value of 9.14 ev and that of 9.6 ev from electron-collision experiments.

Criticism of $D(CO) = 11.11$ ev

The most recent contention that $D(CO) = 11.11$ ev has been made by Gaydon and Penney.[24] The interpretation of the evidences of predissociation in the spectrum is essentially the same as that of Herzberg[4] except that the effect at 77497 cm^{-1} must now definitely be considered a perturbation. The choice of $C(^3P_0)+O(^3P_2)$ as the atomic term combination at 89620 cm^{-1} above $X^1\Sigma^+$ is based on a rigorous application of the noncrossing rule.[53]

Certainly the noncrossing rule has not been neglected in previous work as Gaydon and Penney seem to imply. Herzberg[54] and Herzberg and Mundie[55] have discussed several cases of predissociation in which the interaction between the vibrational levels of two states (whose potential curves cross in zero approximation) varies from "slight" to "strong." In a "slight" interaction ($^2\Sigma$ and $^2\Sigma$ in NO[55]) the two potential curves "almost cross." In a "strong" interaction two states are in effect produced ($^3\Pi_0$ and 0^+ in ICl).[56] This appears to cast considerable doubt on the basic assumption of Gaydon and Penney's argument, namely, that either a "crossing" occurs which always results in a strong interaction, or the states and dissociation limits are so situated that a crossing cannot occur at all.

The assumption of $D(CO) = 11.11$ ev also fails to account for the electron-impact experiments (see Fig. 3). It is too large both to account for the bulk of the thermochemical results and the general conclusion that the Birge-Sponer extrapolation lies 20 to 40 percent too high for molecules like CO.[26,27]

4. PROPOSAL OF A NEW INTERPRETATION OF THE SPECTROSCOPIC EVIDENCE

Perhaps the most cogent argument against the present spectroscopic values for $D(CO)$ and in favor of $D(CO) = 9.6$ ev from electron-impact experiments is the fact that it is possible to reinterpret the spectroscopic evidence to bring agreement with the electron-impact value. This new interpretation will now be proposed and its consequences discussed.

TABLE VI. Intensity breakoffs in the vibrational structure of CO bands.[29,31,38]

State	cm^{-1} above $X^1\Sigma^+$	Band system
$a^3\Pi$ ($v'=4$)	55400	Cameron [$a^3\Pi \rightarrow X^1\Sigma^+$]
$a'^3\Sigma$ ($v'=11$)	66500	Asundi [$a'^3\Sigma^+ \rightarrow a^3\Pi$]
$d^3\Pi$	72000	Triplet [$d^3\Pi \rightarrow a^3\Pi$]
$C^1\Sigma^+$ ($v'=0$)	92000	Herzberg [$C^1\Sigma^+ \rightarrow A^1\Pi$]
$c^3\Sigma^+$ ($v'=0$)	92000	"3A" [$c^3\Sigma^+ \rightarrow a^3\Pi$]
$E^1\Sigma^+$ ($v'=0$)	93000	Hopfield-Birge [$E^1\Sigma^+ \leftrightarrow X^1\Sigma^+$]

Effects at 9.61 and 11.60 ev

If $D(CO)$ is in fact 9.6 ± 0.1 ev, the lowest atomic-term combination of carbon and oxygen atoms, $C(^3P_0)+O(^3P_2)$, must lie 9.6 ± 0.1 ev above $v=0$, $J=0$ of $X^1\Sigma^+$. Thus the evidences of predissociation in the levels $v=7$, 8, and 9 of $A^1\Pi$ (see Table V) could be genuine. The limiting curve of dissociation, shown at the bottom of Fig. 5, is of the form for case *Ib* of predissociation.[55,57] It places the limit for $J=0$ at 77500 cm^{-1} (9.61 ev) above $X^1\Sigma^+$. This assignment is in agreement with Schmid and Gerö's arguments as to the genuineness of this predissociation.[31] Acceptance of the assignment of $C(^3P_0)+O(^3P_2)$ to the level 77500 cm^{-1} (9.608 ev) places $C(^1D)+O(^3P_2)$ at 87692 cm^{-1} (10.87 ev), $C(^3P_0)+O(^1D)$ at 93368 cm^{-1} (11.58 ev), etc. These dissociation limits are plotted graphically in Fig. 4 in the column headed $D(CO) = 9.61$ ev.

The effect at approximately 93550 cm^{-1} in $C^1\Sigma^+$ on this basis could also be a true predissociation. The 180 cm^{-1} between the dissociation limit and the intensity weakening is attributable to kinetic energy of the dissociation products. At the top of Fig. 5 is shown a possible limiting curve of dissociation drawn through the intensity breakoff and the $J=0$ intercept at 93368 cm^{-1} determined by the dissociation limit $C(^3P_0)+O(^1D)$. The slope of this limiting curve at the intensity breakoff is approximately 0.25 cm^{-1} giving 3.1A as the internuclear distance of the potential maxi-

[53] J. v. Neumann and E. Wigner, Physik. Zeits. **30**, 467 (1929).
[54] See reference 1, pp. 324ff and 449ff.
[55] G. Herzberg and L. G. Mundie, J. Chem. Phys. **8**, 263 (1940).
[56] W. G. Brown and G. E. Gibson, Phys. Rev. **40**, 529 (1932).
[57] See reference 1, pp. 428–464.

mum of the effective potential curve for $J=28$.[55,57] Since r_e for $A^1\Pi$ is 1.23A,[58] this predissociation probably also belongs to case *Ib*. Although it appears likely on the basis of $D(CO)=9.6\pm0.1$ ev that this effect and that at $v=7$, 8, 9 of $A^1\Pi$ are genuine predissociations, the interpretation would not be affected should they later be shown to be accidental predissociations or perturbations.

Effects at 8.86 and 10.12 ev

The intensity drop observed at low pressure by Schmid and Gerö[29] in $v=4$ of $A^1\Pi$, 8.86 ev above $X^1\Sigma^+$ cannot be accepted as a predissociation if $D(CO)=9.61$ ev. The effect is observed only in the Q-branch and is the only one thought to be a predissociation in CO attributed to the *final* state of the emission bands in which it is found. No effect was found on the same plates at $v'=4$ in the IV Positive bands [$A^1\Pi\rightarrow X^1\Sigma^+$]. To explain this observation, Schmid and Gerö argue by analogy with a similar pressure effect in AlH that it should appear in the IV Positive bands only at appreciably lower pressures at which no plates were exposed. Schmid and Gerö feel that there is evidence of the effect at $v'=4$ of $A^1\Pi$ in some absorption spectrograms of Hopfield and Birge reproduced by Bonhoeffer and Harteck[59] which show an intensity minimum at 1400A ($v'=5$). All told, the effect does not appear to be so well established as a predissociation, however, that its rejection as such is critical. All the evidence pointing to $D(CO)>9$ ev is also evidence against the interpretation of this effect as a predissociation.

Similarly, the effect in $v=13$ of $A^1\Pi$, 10.12 ev above $X^1\Sigma^+$, cannot be a genuine predissociation if $D(CO)=9.61$ ev. The experimental evidence is Schmid and Gerö's failure to observe any rotational levels higher than $J=16$ even though some of the places where lines from such levels should appear were free of superpositions and were investigated carefully.[30,31] $A^1\Pi$ is admittedly perturbed here so one cannot predict where the lines should be. In fact, Schmid and Gerö think perturbation to be the reason why the breakoff itself was not observed. Although the effect could be an accidental predissociation, it is more likely entirely the result of a perturbation. It cannot possibly be a genuine predissociation if *any* of the values proposed for $D(CO)$ except that of Schmid and Gerö is correct.

Effect at 11.11 ev

The intensity weakenings which have been observed in $B^1\Sigma^+$ and $b^3\Sigma^+$ in the vicinity of 11.11 ev (see Table IV) have been accepted in every interpretation of the CO spectrum proposed to date as genuine evidences of predissociation. The limiting curve of dissociation, drawn by Gerö[30] and generally accepted, is shown in the middle section of Fig. 5, curve 1. The shape of the limiting curve and the fact that its slope at the ordinate axis is zero have been taken as evidence that the predissociation belongs to case *Ib*, putting a dissociation limit of the molecule 89620 ± 47 cm^{-1} above $X^1\Sigma^+$. This interpretation of the effect at 11.11 ev cannot represent the

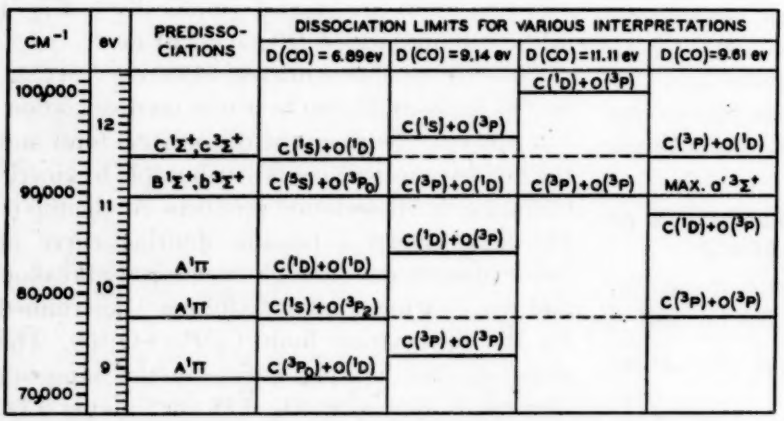

FIG. 4. An energy-level diagram showing the positions of five supposed evidences of predissociation in the spectrum of CO and their interpretation in terms of dissociation limits of the molecule. The interpretations giving $D(CO)=6.89$, 9.14, and 11.11 ev are currently supported in the literature. $D(CO)=9.61$ ev results from the interpretation proposed in this paper in agreement with the electron-impact experiments.

[58] H. Sponer, *Molekülspektren I. Tabellen* (Julius Springer, Berlin, 1935).
[59] K. K. Bonhoeffer and P. Harteck, *Grundlagen der Photochemie* (Dresden and Leipzig, 1933).

TABLE VII. Interpretation of predissociations in CO spectrum yielding $D(CO)=6.89$ ev (Schmid and Gerö).

Dissociation products		Predissociations			
		Rotational breakoffs		Vibrational breakoffs	
States	cm^{-1} above $X^1\Sigma^+$	States	cm^{-1} above $X^1\Sigma^+$	State	cm^{-1} above $X^1\Sigma^+$
$C(^1S)+O(^1D)$	93115	$C^1\Sigma^+$; $c^3\Sigma^+$	<93550	$C^1\Sigma^+$; $c^3\Sigma^+$; $E^1\Sigma^+$	~92500
$C(^3S)+O(^3P_0)$	(89620)[62]	$B^1\Sigma^+$; $b^3\Sigma^+$	89620±47		
$C(^3P_2)+O(^1D)$	89435				
$C(^1D)+O(^1D)$	81660	$A^1\Pi$	>81620		
$C(^1S)+O(^3P_0)$	77474	$A^1\Pi$	77497±44		
$C(^3P_0)+O(^1D)$.	71468	$A^1\Pi$	~71500	$d^3\Pi$	72000
$C(^1D)+O(^3P_2)$	65792			$a'^3\Sigma^+$	66500
$C(^3P_0)+O(^3P_2)$	55600			$a^3\Pi$	55400

facts if $D(CO)=9.61$ ev for the closest dissociation limit then is $C(^1D)+O(^3P)$ at 10.87 ev.

It is suggested that $B^1\Sigma^+$ and $b^3\Sigma^+$ are predissociated at 11.11 ev by $a'^3\Sigma^+$ as has been supposed, but that $a'^3\Sigma^+$ has a potential curve with a maximum for no rotation. The dissociation limit of $a'^3\Sigma^+$ is then in all probability $C(^1D)+O(^3P)$ at 10.87 ev, requiring the maximum to be about 0.2 ev high. The vibrational levels under these circumstances converge to the energy of the maximum of the potential curve for $J=0$.

It is well known that such maxima in the potential curves of electronic states of molecules like CO are possible,[60] and considerable evidence for their existence has been found.[55,56,57] In this case the potential curve for $a'^3\Sigma^+$ could be formed by the "avoidance" of potential curves which in zero approximation are curves for a stable state having its dissociation limit at $C(^3P)+O(^1D)$, 11.58 ev above $X^1\Sigma^+$, and an unstable state with its dissociation limit at $C(^1D)+O(^3P)$, 10.87 ev above $X^1\Sigma^+$. The atomic-term combinations at these dissociation limits can each give rise to a $^3\Sigma^+$ state by the Wigner-Witmer correlation rules.

In an entirely different connection, Gaydon and Penney[24] have suggested that $a'^3\Sigma^+$ may possibly have a potential curve with maximum. It was mentioned as a way of sidestepping violation of the noncrossing rule entailed in the intersection of $a'^3\Sigma^+$ with the $^3\Sigma^+$ states from $C(^3P)+O(^3P)$ if $D(CO)<11.11$ ev. However, Gaydon and Penney thought "the exact coincidence of this extrapolated limit at 11.11 ev with the energy of two known strong predissociations is too striking for this hypothesis to appear tenable," thus missing what is apparently the real significance of this coincidence.

[60] R. S. Mulliken, J. Phys. Chem. **41**, 5 (1937).

Type of Predissociation at 11.11 ev

In the type of predissociation proposed here, the intersection of the potential curve of the state being predissociated ($B^1\Sigma^+$ or $b^3\Sigma^+$) with the potential curve of the state causing the predissociation ($a'^3\Sigma^+$) in all probability lies below the dissociation limits of both curves. In this way, the predissociation resembles that of case *Ib* classified by Herzberg.[57] However, as the state $a'^3\Sigma^+$, to which the nonradiative transition takes place and which later dissociates, has a potential curve with maximum, the limiting curve of dissociation should be of the form appropriate to case $I(c)$ or case *III*. Thus the type of predissociation proposed here is properly not included in any of Herzberg's cases.

The limiting curve of dissociation for this type of predissociation is a straight line whose slope specifies the internuclear distance of the maximum of the potential curve causing the predissociation and not that of the intersection with the curve of the predissociated state. A strong interaction of the state causing the predissociation ($a'^3\Sigma^+$) with an unstable state is required to produce the potential curve with maximum whereas a weak interaction is required with the predissociated states ($B^1\Sigma^+$, $b^3\Sigma^+$). The radiationless transition from $B^1\Sigma^+$ into $a'^3\Sigma^+$ is an intercombination for which there seems to be evidence in the magnitude of the observed intensity weakening.[32]

Limiting Curve of Dissociation

A criterion for predissociation of the kind proposed here is that its limiting curve of dissociation must be a straight line having a slope which gives a reasonable value for the internuclear distance

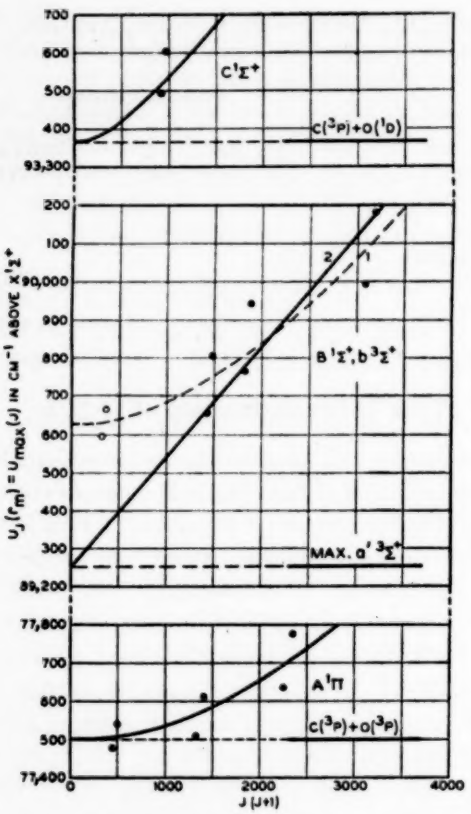

FIG. 5. Limiting curves of dissociation for predissociations observed in the spectrum of CO. The points plotted are the last rotational level of undiminished intensity and the first after the breakoff, between which the limiting curve must pass. In the bottom section of the figure the data for $v=9, 8, 7$ of $A^1\Pi$ are plotted (from left to right). In the middle section, similarly, the data for $v=1, 0$ of $B^1\Sigma^+$ and $v=1, 0$ of $b^3\Sigma^+$ are plotted. Curve 1 is that drawn by Gerö (reference 30). Curve 2 is that proposed in this paper. In the top section the data for the breakoff in $C^1\Sigma^+$ are plotted. The dissociation limits shown and the level marked *MAX.* $a'\,^3\Sigma^+$ are based on the interpretation proposed in this paper.

(r_m) at which the maximum occurs.[61] If all the intensity weakenings reported in $B^1\Sigma^+$ and $b^3\Sigma^+$ (Table IV) are accepted as predissociations by $a'\,^3\Sigma^+$, the straight line of maximum slope which can be drawn through the data gives $r_m=3.9$A. This value is impossibly high for states of a molecule like CO with covalent binding since the potential curves must lie very close to their asymptotes at such an internuclear distance. However, it is to be observed that the four evidences of predissociation at 11.11 ev are not equally credible as such. The breakoffs in $v'=0$ of $B^1\Sigma^+$ and $v'=1$ of $b^3\Sigma^+$ observed in the P, Q, and R-branches of the bands are good examples of predissociations and can hardly be questioned. Similarly, the predissociation in $v'=0$ of $b^3\Sigma^+$ appears well founded. The effect in $v'=1$ of $B^1\Sigma^+$, on the other hand, was observed by Schmid and Gerö[33] only in the P-branch of the (1, 0) and the Q-branch of the (1, 1) Angström bands despite considerable overlapping of lines from CO^+ and CO_2 bands. Coster and Brons,[32] although they looked for such an effect, could not find it because of the presences of crowded lines of CO_2. If this effect, indicated by open circles in Fig. 5, is considered to be an accidental predissociation, a perturbation, the result of superposition of other band lines, or predissociation by a state other than $a'\,^3\Sigma^+$, one can draw a straight line through the remaining data (curve 2 in Fig. 5) of maximum slope giving $r_m=2.9$A. Since the maximum of the potential curve is low and broad (see Fig. 6), one would not expect any observable leakage through it.

Although the effect in $v'=1$ of $B^1\Sigma^+$ may well be predissociation by a state other than $a'\,^3\Sigma^+$, interpretation of such an effect as something other than predissociation is not without precedent. Two other effects in the spectrum of CO, once thought to indicate predissociation, have been shown to be spurious. A second weakening in the rotational structure of $v=9$, $A^1\Pi$ at $P(28)$,[30] as mentioned earlier, is now known to result from a superposition of lines from the (0, 1) band of the "$3A$" system on the lines $P(25)$, $P(26)$, $P(27)$ preceding it.[52] The sudden ending of the rotational structure of $v=10$, $A^1\Pi$ at $P(16)$ and $Q(17)$ observed by Brons[62] was later shown by Gerö[63] to be the effect of insufficient exposure of the plates causing the perturbation of $A^1\Pi$ by a $^3\Sigma^+$ state to look like a predissociation. Gerö points out how easily one may be misled in considering a sudden intensity decrease as a predissociation if the initial state is perturbed. With insufficient exposure, the perturbed lines disappear as they are generally weaker than the unperturbed lines. If the plates are overexposed, on the other hand,

[61] The effective potential curve is represented by $U_J(r)=U_0(r)+(h/8\pi^2c\mu r^2)J(J+1)$. (See reference 55.) The limiting curve is $U_J(r_m)=U_0(r_m)+(h/8\pi^2c\mu r_m^2)J(J+1)$. Its slope is thus $h/8\pi^2c\mu r_m^2$ and its intercept at the ordinate axis is $U_0(r_m)$. This latter gives the energy level of the maximum in the rotationless potential curve above the ground molecular state.

[62] F. Brons, Physica **2**, 1108 (1935).

[63] L. Gerö, Zeits. f. Physik **99**, 52 (1936).

one is bothered by superpositions of band lines from other molecules. These comments are also pertinent to the interpretation of the effects in the spectrum 8.86 and 10.12 ev above $X^1\Sigma^+$ (see above).

Inasmuch as the $v=1$, $J=0$ level $B^1\Sigma^+$ lies at about 89100 cm^{-1}, which is below curve 2 of Fig. 5, one would expect predissociation to commence in one of the lower rotational levels. Failure to observe it may well be the result of the superposition of CO^+ and CO_2 lines known to be present. Furthermore, predissociation by $a'\,^3\Sigma^+$ requires an intercombination interaction which is not very intense in the first place.

Potential Curve of $a'\,^3\Sigma^+$

The question now arises as to whether a potential curve for $a'\,^3\Sigma^+$ which possesses a maximum approximately 0.2 ev above its asymptote and at a nuclear separation of 2.9A or greater is at all reasonable. Since the dissociation energy of CO in the $a'\,^3\Sigma^+$ state is certainly greater than 4 ev, a maximum only 0.2 ev high may be expected to lie at an internuclear distance quite large with respect to r_e. Enough is known about the molecular constants of $a'\,^3\Sigma^+$, however, to make a more detailed investigation possible.

Schmid and Gerö[40] have determined the rotational constant, B_e, of $a'\,^3\Sigma^+$ to be about 1.31 cm^{-1} from which $r_e=1.37$A. The frequency ω_e is given as 1180 cm^{-1} (see also Sponer[58]). Assuming $a'\,^3\Sigma^+$ in zero approximation (no interaction with an unstable state) to become asymptotic to the limit at $C(^3P)+O(^1D)$, one can calculate by the Morse function the potential curve plotted in Fig. 6. $v=0$, $J=0$ of $a'\,^3\Sigma^+$ is 55380 cm^{-1} above $X^1\Sigma^+$.[40] The avoidance of crossing of this potential curve with that of an unstable state from $C(^1D)+O(^3P)$ can produce a resulting potential curve having a maximum of the proper height and at an internuclear distance of greater than 3A as the construction in Fig. 6 shows.

The objection may immediately be raised that the Morse function could lie considerably below the true potential curve near its asymptote. This would mean that the maximum actually lay at a smaller value of r than shown in Fig. 6. However, there are two considerations which indicate that the state of affairs depicted in Fig. 6 is not seriously in error and may in fact predict too small a value of r_m. The first of these is the fact that the r_e calculated from Schmid and Gerö's B_e for $a'\,^3\Sigma^+$ may be low. Using the relation $\omega_e r_e^2=$ constant, known to hold approximately for the states of a given molecule,[64] with an average constant evaluated from the ω_e and r_e of well known states of CO, one calculates $r_e=1.52$ cm^{-1}. This is significant because ω_e for $a'\,^3\Sigma^+$ is undoubtedly much more accurate than B_e. The second consideration is the fact that the Morse function does in all probability provide a good approximation for this particular case. Lotmar[65] and Coolidge, James, and Vernon[66] agree that more accurate representations of potential curves such as those of Rosen-Morse and Pöschl-Teller

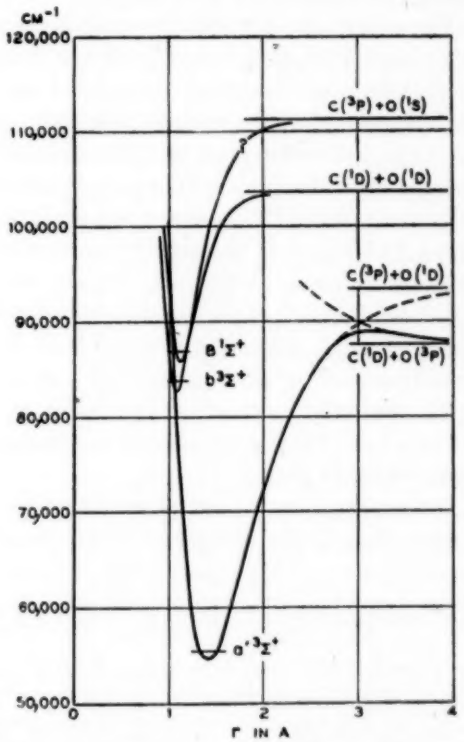

FIG. 6. Potential curves of the electronic states involved in the predissociation at 11.11 ev. The curve for $a'\,^3\Sigma^+$ is formed from the avoidance of curves for a stable and an unstable state. The curve for the stable state is plotted from a Morse function and the curve of the unstable state drawn so as to produce a maximum of the resulting curve 89250 cm^{-1} above $X^1\Sigma^+$. The curves for $B^1\Sigma^+$ and $b^3\Sigma^+$ are also plotted from Morse functions. The question mark indicates that the dissociation limit of $b^3\Sigma^+$ is uncertain (reference 68). The positions of the dissociation limits are those given by the interpretation proposed in this paper.

[64] See reference 1, p. 498.
[65] W. Lotmar, Zeits. f. Physik **93**, 528 (1934/35).
[66] A. S. Coolidge, H. M. James, and E. L. Vernon, Phys. Rev. **54**, 726 (1938).

reduce to the Morse function if $(D/\delta)^{\frac{1}{2}}=1$. D is the distance from minimum to asymptote and $\delta=3\omega_e(B_e)^{\frac{1}{2}}/(\alpha_e\omega_e+6B_e^2)$. Admittedly B and certainly α_e are not known very well for $a'\,^3\Sigma^+$. However, taking $D=38580$ cm, $\omega_e=1180$ cm^{-1}, $B_e=1.31$ cm^{-1}, and determining $\alpha_e=0.014$ cm^{-1} from the relation[67] $\alpha_e/B_e\approx1.4\omega_e x_e/\omega_e$ with $\omega_e x_e=9$ cm^{-1} from Sponer,[58] one calculates $(D/\delta)^{\frac{1}{2}}=0.99$.

The maximum in the potential curve of $a'\,^3\Sigma^+$ would on the above considerations lie at an internuclear distance approximately twice the equilibrium internuclear distance r_e. $r_m=2r_e$ has been suggested by Herzberg and Mundie[55] as an approximate upper limit for the r value of a maximum of a rotationless curve.

In Fig. 6 are also plotted the potential curves of $B^1\Sigma^+$ and $b^3\Sigma^+$ which are predissociated by $a'\,^3\Sigma^+$.[68] Within the limits of accuracy of the diagram, it is seen that the intersections demanded by the Franck-Condon principle can occur. There is perhaps some further evidence here also that the value of r_e for $a'\,^3\Sigma^+$ in Fig. 6 is a little low.

Curve 2 of Fig. 5 is the straight line of maximum slope which can be drawn between the two data points[28] for each of the three predissociations accepted as such. Should the maximum in the potential curve of $a'\,^3\Sigma^+$ lie somewhat higher than the 2.9A predicted by this line, the limiting curve would be a line of less slope passing easily through the experimental points.

In the preliminary report of this work[5] it was suggested that if the stopping of the rotational structure in $v=0$ of $b^3\Sigma^+$ (see Table IV) were the result of something other than predissociation by $a'\,^3\Sigma^+$ one could draw a straight line limiting curve through the two remaining sets of points having a slope which gives r_m as small as 2.1A. The interpretation can be carried out satisfactorily, it appears, without this assumption.

Consequences and Comparison with Other Interpretations

For $D(\mathrm{CO})=9.61$ ev the position with respect to the interpretation of effects in the spectrum as genuine or accidental predissociations, perturbations, or other effects is no less tenable than that required by $D(\mathrm{CO})=9.14$ ev, now widely accepted. The interpretation of the effects at 8.83 and 10.12 ev must be the same. As opposed to the interpretation of the breakoff in $v=0$ of $C^1\Sigma^+$ at 11.60 ev as an upper limit for a predissociation and those in $v'=7$, 8, and 9 of $A^1\Pi$ at 9.61 ev as accidental predissociations or perturbations if $D(\mathrm{CO})=9.14$ ev, only a single breakoff, namely that in $v'=1$ of $B^1\Sigma^+$ at 11.11 ev, need be reinterpreted if $D(\mathrm{CO})=9.61$ ev.

In Herzberg's energy level diagram of the CO molecule[69] the dissociation limits of a number of electronic states are drawn under the assumption $D(\mathrm{CO})=9.14$ ev. It would appear that no difficulty is encountered if all these limits are raised by the 0.47 ev demanded if $D(\mathrm{CO})=9.61$ ev. Schmid and Gerö's data[31, 40, 70] on the convergence of vibrational levels in $a^3\Pi$, $d^3\Pi$, and $e^3\Sigma^-$ are not in conflict with the new energy level scheme. However, the convergence of $I^1\Sigma^-$, known only through its perturbation of $A^1\Pi$,[40] cannot be fitted to the new scheme. There is no limit corresponding to two singlet atomic terms close enough to the supposed convergence. If the state were not a singlet as is now supposed,[71] there would be no such difficulty.

Some of the intensity breakoffs in the vibrational structure of CO bands listed in Table V cannot be attributed to predissociation if $D(\mathrm{CO})=9.61$ ev. Their explanation may equally well be found in the Franck-Condon principle.

Finally, $D(\mathrm{CO})=9.61$ ev is in satisfactory agreement with all data bearing on $D(\mathrm{CO})$ and $L_1(\mathrm{C})$ from sources other than electron impact and the band spectrum. These results will now be discussed.

5. PHOTO-DISSOCIATION OF CO

In 1938, Faltings, Groth, and Harteck[72] demonstrated that CO is dissociated by the Xe resonance line 1295A forming CO_2 with quantum yield unity. This was interpreted to mean that $D(\mathrm{CO})\leqq221$ kcal (9.57 ev), with which interpretation Herzberg has agreed.[26] The failure of

[67] See reference 1, p. 114.

[68] The data for the Morse functions in these cases were obtained from Sponer's tables (reference 58) except that $r_e=1.09$A was used for $b^3\Sigma^+$. This was calculated from a more recent value of the rotational constant, $B_e=2.075$ cm^{-1} reported in R. Schmid and L. Gerö, Zeits. f. Physik **96**, 198 (1935).

[69] See reference 1, Fig. 174, p. 481.

[70] L. Gerö and R. Schmid, Zeits. f. Physik **112**, 676 (1939).

[71] R. Schmid and L. Gerö, Zeits. f. Physik **94**, 386 (1935).

[72] K. Faltings, W. Groth, and P. Harteck, Zeits. f. physik. Chemie **B41**, 15 (1938).

the line 1470A to dissociate CO was taken to mean $D(CO) \geqq 194$ kcal (8.43 ev).

Gaydon and Penney,[73] however, object to the interpretation giving $D(CO) \leqq 9.57$ ev on the grounds that the only lines in the known absorption bands of CO (IV Positive) in the vicinity of 1295A correspond to transitions from rotational or vibrational levels very sparsely populated at room temperature. They propose a mechanism of the photo-dissociation involving absorption of the quantum (1295A) to form $CO(A^1\Pi)$, which, on collision with $CO(X^1\Sigma^+)$, forms CO_2 and C. On this basis no conclusion concerning $D(CO)$ may be drawn from the experiments.

To Gaydon and Penney's picture of the photochemical decomposition of CO Schmid and Gerö[74] raise the rather similar objections that, considering line half-widths, the accuracy of coincidence of the line 1295A with the closest line of the IV Positive system [$Q(38)$ of the (10, 0) band] is not sufficient; that the probability of exciting this line is only 0.0001 percent by the Boltzmann distribution law; and that a single absorption line, even if it coincided properly, could not absorb 70 percent of the strongly broadened Xe line, as observed in the photochemical experiments. Schmid and Gerö feel that absorption by a continuum must be assumed and link the process to the continuum they believe begins at the predissociation limit 77497 cm^{-1} above $X^1\Sigma^+$. It is shown that enough transitions can occur from higher, but sufficiently well populated, rotational states in $v=0$ of $X^1\Sigma^+$ to account for the experimental results. Failure to observe a continuous absorption in this region at rather low resolving power is attributed to the narrowness of the "effective region" in the continuum and the low transition probability into the continuum evidenced by the extent and magnitude of the predissociation in $A^1\Pi$. In rebuttal, Gaydon[75] refers again to the failure to observe continuous absorption near 1295A and expresses his opinion that line broadening may be sufficient to make absorption by a single band line possible.

$D(CO) = 9.6$ ev may be reconciled with either the interpretation of the photodissociation of CO proposed by Gaydon and Penney or that proposed by Schmid and Gerö. The latter argument is unaffected by a change in the assignment of dissociation products to the dissociation limit. Of the two, Schmid and Gerö's interpretation is perhaps preferable in the light of the interpretation of the band spectrum proposed in this paper. The objections to the conclusions of Faltings, Groth, and Harteck agreed to by Herzberg appear adequate.

6. DISSOCIATION OF CO BY METASTABLE ATOMS

Recently, Kenty, Aicher, Noel, Paritsky, and Paolino[76] have observed some new bands in the green, excited in a mixture of xenon and oxygen, which, if the source of the bands and mode of their excitation are correctly interpreted, provide independent evidence of a lower limit for $D(CO)$. That the bands are emitted by O_2 is evident from the fact that they are produced when O_2 itself or gases such as CO_2 and H_2O, from which O_2 may be produced by dissociation by metastable Xe atoms, are admitted to the Xe discharge. The bands are not produced in mixtures of Xe with N_2, H_2 or CH_4. The mode of excitation of the new band system is thought to be a resonant-energy exchange between the metastable Xe atom and the O_2 molecule. Failure of the bands to appear with a CO admixture is taken as evidence that $D(CO)$ is greater than the excitation energy of the higher metastable state of Xe, 9.4 ev. Taken at face value this result does provide additional evidence for discrimination among the several proposed values of $D(CO)$. Only $D(CO) = 9.61$ ev and 11.11 ev are allowed.

7. ELECTRON COLLISION EXPERIMENTS IN CH_4 AND CS_2

Ionization and dissociation processes have been observed in electron-impact studies of CH_4 and CS_2 in which, one can be quite certain, all the bonds are broken and the molecule completely fragmented. These processes are:

(1) $CH_4 + \epsilon^- \rightarrow H^+ + C + 3H + 2\epsilon^-$
$A(H^+) = 29.4 \pm 0.6$ ev

(2) $CH_4 + \epsilon^- \rightarrow C^+ + 4H + 2\epsilon^-$
$A(C^+) = 26.7 \pm 0.7$ ev

(3) $CH_4 + \epsilon^- \rightarrow C^- + C^+ + 3H + \epsilon^-$
$A(C^-) = 27.4 \pm 0.6$ ev

(4) $CS_2 + \epsilon^- \rightarrow C^+ + 2S$
$A(C^+) = 21.5 \pm 1.0$ ev

[73] A. G. Gaydon and W. G. Penney, Nature **150**, 406 (1942).
[74] R. F. Schmid and L. Gerö, Proc. Phys. Soc. **58**, 701 (1946).
[75] A. G. Gaydon, Proc. Phys. Soc. **58**, 704 (1946).
[76] C. Kenty, J. O. Aicher, E. B. Noel, A. Paritsky, and V. Paolino, Phys. Rev. **69**, 36 (1946).

(1), (2), and (3) were observed by Smith,[77] (4) by Smyth and Blewett.[78] Processes like these are not very probable, making measurement of their onset potentials difficult. This accounts for the rather wide limits of error. In each case the calculation of an upper limit for $L_1(C)$ from the onset potential has been possible as the appropriate heat of formation, ionization energy (electron affinity, if needed), and dissociation energy are known.

Smith has done this for (1), (2), and (3), Lozier[12] for (4). The results are:

(1) $L_1(C) \leqq 6.1 \pm 0.6$ ev or 141 ± 14 kcal,
(2) $L_1(C) \leqq 5.7 \pm 0.7$ ev or 131 ± 16 kcal,
(3) $L_1(C) \leqq 6.0 \pm 0.9$ ev or 139 ± 21 kcal,
(4) $L_1(C) \leqq 5.8 \pm 1.0$ ev or 134 ± 23 kcal.

The reason these values were considered upper limits only is that the kinetic energy of the fragments in the processes are not known. If $L_1(C)$ is actually less than these values, the activation energies of the processes inverse to each of the four processes must be very nearly the same. As this appears unlikely, it seems more reasonable to assume that ions can be formed at rest in each process. The results quoted above agree better with $L_1(C) = 5.9$ ev (136 kcal) corresponding to $D(CO) = 9.6$ ev than with any other value proposed for $L_1(C)$.

8. DISSOCIATION ENERGIES OF CO^+ AND CN

The dissociation energy of CO^+ can be determined from the cycle $I(CO) + D(CO^+) = D(CO) + I(C)$. $I(C)$ is known to be 11.27 ev. $I(CO)$ has been determined by electron-collision experiments as 14.1 ± 0.1 ev.[10,79] (See also Fig. 2.) This value in all probability represents the distance from $v=0$ of $CO(X^1\Sigma^+)$ to $v=0$ of $CO^+(X^2\Sigma)$ as the internuclear separations for these states are 1.13A and 1.114A,[58] respectively, and the width of the Franck-Condon region is about 0.1A. From these ionization potentials one obtains $D(CO^+) = D(CO) - 2.8$ ev. With $D(CO) = 9.6$ ev, $D(CO^+) = 6.8$ ev.

Gaydon and Penney[24] have discussed what is known of the electronic states and dissociation limits of CO^+. Their scheme of dissociation limits is in agreement with $D(CO^+) = 6.8$ ev if the limit of $B^2\Sigma$ is $C^+(^2P) + O(^1D)$ at 8.8 ev. This seems reasonable in view of the extrapolation by Biskamp[80] of vibrational levels of $B^2\Sigma$ to 9.3 ev above $X^2\Sigma$. $v=0$ of $B^2\Sigma$ lies at 5.66 ev and its vibrational levels are known to 7.46 ev above the ground state. Biskamp's linear extrapolation for the ground state, $X^2\Sigma$, puts its limit at 9.9 ev. Since the extrapolation is a long one from the highest known level at 3.2 ev, its relation to the actual limit $C^+(^2P) + O(^3P)$ at 6.8 ev is not surprising.

Herzberg[4] has calculated the relation $D(CN) = D(CO) - 3.18$ ev from a cycle involving thermochemical and spectroscopic quantities.[3] He has more recently given compelling reasons for preferring the value[81] of the dissociation energy of C_2N_2 into 2CN used in his original calculation to a newer value of White.[82] With $D(CO) = 9.61$ ev, $D(CN) = 6.43$ ev. The only independent evidence concerning $D(CN)$ comes from rather long extrapolations of vibrational levels. Gaydon[27] gives 9.9 ev as the result of a linear Birge-Sponer extrapolation. Schmid, Gerö and Zemplén[83] think the ground state $CN(X^2\Sigma)$ converges to 7.5 ev with the lowest atomic term combination lying considerably lower. Neither of these results is in disagreement with the conclusion $D(CN) = 6.43$ ev. On the other hand, Schmid, Gerö and Zemplén's contention that the $CN(A^2\Pi)$ converges to 7.50 ± 0.12 ev and $CN(B^2\Sigma)$ to 8.12 ± 0.12 ev cannot be reconciled with the present interpretation. There is no direct contradiction of experimental data involved, however.

The spectra of CO^+ and CN thus provide no direct evidence for or against $D(CO) = 9.61$ ev, nor in fact any basis for preferring it over $D(CO) = 9.14$ ev. Either value of $D(CO)$ provides an adequate basis for interpretation.

9. THERMOCHEMISTRY OF CARBON

The value $D(CO) = 9.61$ ev demands no change in the general interpretation of the thermochemistry of carbon supported by Herzberg.[4,26] The thermochemical evidence is not definite enough

[77] L. G. Smith, Phys. Rev. **51**, 263 (1937).
[78] H. D. Smyth and J. P. Blewett, Phys. Rev. **46**, 276 (1934).
[79] J. T. Tate and P. T. Smith, Phys. Rev. **39**, 270 (1932).
[80] H. Biskamp, Zeits. f. Physik **86**, 33 (1933).
[81] G. B. Kistiakowsky and H. Gershinowitz, J. Chem. Phys. **1**, 432 (1933).
[82] J. U. White, J. Chem. Phys. **8**, 459 (1940).
[83] R. Schmid, L. Gerö and J. Zemplén, Proc. Phys. Soc. **50**, 283 (1938).

to distinguish values of $L_1(C)$ as close as 125 and 136 kcal. However, what indications there are point to a value higher than that supported by Herzberg. Goldfinger and Jeunehomme,[84] in a paper which reviews the thermochemical evidence available at the time, calculated vapor-pressure curves for $L_1(C)=170.2$, 124.8, and 108.3 kcal, corresponding to $D(CO)=11.11$, 9.14, and 8.41 ev, respectively.[2] These were compared with the experimental results of direct measurements of the vapor pressure of carbon. Most of the data lay between the curves calculated for $L_1(C)=170.2$ and 124.8 kcal. However, the latter value was considered correct on the grounds of Herzberg's value for $D(CO)$. As has been pointed out before,[10] $D(CO)=9.6$ ev giving $L_1(C)=136$ kcal is in better agreement with the vapor pressure measurements. Duchesne, Goldfinger and Rosen[85] have stated that the more recent measurements of the vapor pressure of carbon by Ribaud and Bégue[86] similarly are too high for $L_1(C)=170$ kcal and too low for $L_1(C)=125$ kcal.

10. OTHER EVIDENCE

Arguments favoring $L_1(C)=170$ kcal have been presented by several investigators but appear to have been successfully refuted by others. Baughan's objections[87] to the low C—H bond energy calculated from $L_1(C)=125$ kcal have been answered by Herzberg[26] and Long and Norrish.[16] The agreement by Kynch and Penney's calculation[88] of the long wave length limits of absorption spectra in benzene, butadiene, and hexatriene on the basis of $L_1(C)=170$ kcal with the observed limits is considered fortuitous by Herzberg,[26] and to provide no basis for deciding on $L_1(C)$ by Mulliken and Rieke.[89] The calculation is also criticized by Long and Norrish[16] and by Duchesne, Goldfinger and Rosen.[85] Sidgwick and Springall's support[90] for $L_1(C)=170$ kcal, found in the calculation of Hg—C bond energies in several molecules, is questioned by Long and Norrish.[91] In none of this does there appear any convincing evidence against a value of 136 kcal for $L_1(C)$.

Long and Norrish in their general review of the thermochemistry of carbon[16] accept the value $L_1(C)=125$ kcal. They feel they have evidence, however, that $L_2(C)$, the heat of sublimation into tetravalent carbon $C(^5S)$, is approximately 190 kcal making $L_2(C)-L_1(C)\sim 65$ kcal. This is unacceptable to Shenstone and Edlén,[46] on the basis of the recent fixing of the $C(^5S)$ excitation energy at 96.4 kcal (33735.2 cm^{-1}). The argument of Long and Norrish thus seems to need fundamental revision. It certainly cannot be used against a somewhat higher value of $L_1(C)$. The use of Shenstone's excitation energy for $C(^5S)$ makes $L_2(C)=232.1$ kcal.

Finally, the calculation of Duchesne, Goldfinger and Rosen[85] should be mentioned. It yields the value $D(CO)=9.4$ ev [$L_1(C)=132$ kcal] which is independent of spectroscopic data on the CO molecule. This result is as good if not better evidence for $D(CO)=9.61$ ev as for $D(CO)=9.14$ ev.

11. CONCLUSION

It has been the purpose of this paper to show that a satisfactory interpretation of all the relevant data can be made only if the value of the dissociation energy of carbon monoxide is 9.61 ev. As consequences of this position we obtain the values

$$\begin{aligned} D(CO) &= 9.608 \text{ ev} = 77500 \text{ cm}^{-1}, \\ L_1(C) &= 5.887 \text{ ev} = 135.7 \text{ kcal}, \\ L_2(C) &= 10.07 \text{ ev} = 232.1 \text{ kcal}, \\ D(CO^+) &= 6.8 \text{ ev}, \\ D(CN) &= 6.43 \text{ ev}. \end{aligned}$$

[84] P. Goldfinger and W. Jeunehomme, Trans. Faraday Soc. **32**, 1591 (1936).
[85] J. Duchesne, P. Goldfinger, and B. Rosen, Nature **159**, 130 (1947).
[86] G. Ribaud and J. Bégue, Comptes Rendus **221**, 73 (1945).
[87] E. C. Baughan, Nature **147**, 542 (1941).
[88] G. J. Kynch and W. G. Penney, Proc. Roy. Soc. London [A]**179**, 214 (1941).
[89] R. S. Mulliken and C. A. Rieke, Rev. Mod. Phys. **14**, 259 (1942).
[90] N. V. Sidgwick and H. D. Springall, Nature **156**, 599 (1945).
[91] L. H. Long and R. G. W. Norrish, Nature **157**, 486 (1946).

Extensive Air Showers and the Cascade Theory

GIUSEPPE COCCONI*
Institute of Physics, University of Catania, Catania, Italy
(Received August 7, 1947)

The barometric effect, the density spectra at different barometric pressures and the variation of frequencies with height above sea level have been calculated for extensive air showers, on the basis of the cascade theory. Good agreement has been found between theoretical results and experimental data.

SECTION 1

THE aim of this work is to study, on the basis of the cascade theory, some phenomena related to the extensive cosmic-ray air showers. In the present state of our knowledge, it is reasonable to think that the extensive showers are due to primary electrons and photons of very high energy (10^{14}–10^{17} ev), which multiply rapidly in the upper atmosphere and give rise in the lower atmosphere to showers consisting of millions of electrons and photons spread over very large surfaces (thousands of square meters), always with the same spatial-distribution law. If the above assumptions are correct, the properties of the extensive showers should depend only on the thickness of air traversed, i.e., on the atmospheric pressure. A given variation Δp in the atmospheric pressure, caused either by barometric change or by a change of height of the recording apparatus above sea level, should cause the same variation in the frequency of the recorded showers.

In the following sections the results of our calculations are collected and compared with the experimental results available to date.

SECTION 2

The barometric effect of the extensive showers has been investigated experimentally by Cosyns[1] and by Auger and Daudin.[2] Their results are rather uncertain, because of the small frequencies of the showers. Nevertheless, all the measurements indicate a high negative barometric effect, i.e., a large increase in the frequencies when the barometric pressure decreases.

Let H be the frequency of the recorded showers, and ΔH be the variation related to a variation Δp of the atmospheric pressure. Then we have

$$\Delta H/H = -\alpha \Delta p. \quad (1)$$

If Δp is measured in cm Hg, the above experiments indicate $\alpha \approx 0.1$ to 0.2 (10 to 20 percent per cm Hg). The surfaces of the counters used in these experiments were about 200 cm^2 and the distances between them were some meters. Both Cosyns and Auger and Daudin found that α increases when the distance between the counters is increased. It seems that α does not depend on altitude.

SECTION 3

In order to evaluate theoretically the barometric effect of the extensive showers, the density spectrum at different barometric pressures was calculated, following the method described elsewhere.[3] We used again the Molière[4] distribution curve of the particles in the shower, but evaluated the number of particles following Rossi and Greisen,[5] whose formulas are more accurate than Heisenberg's[6] in the low pressure range.

For the primary spectrum we assumed

$$H(E) = 0.05(10^{10} \text{ ev}/E)^x \text{ cm}^{-2} \text{ sec.}^{-1},$$

where $H(E)$ is the number of primary electrons coming isotropically from free space with energies above E, and x is a constant for which we chose the values 1.6 and 1.8.

The calculated barometric effect is practically

* At the present, Research Associate at Cornell University, Ithaca, New York.
[1] M. G. E. Cosyns, Nature **145**, 668 (1940).
[2] P. Auger and J. Daudin, Phys. Rev. **61**, 91 (1942).
[3] G. Cocconi, A. Loverdo, and V. Tongiorgi, Phys. Rev. **70**, 846 (1946).
[4] G. Molière, *Vorträge über Kosmische Strahlung* (Berlin, 1943), p. 24.
[5] B. Rossi and K. Greisen, Rev. Mod. Phys. **13**, 240 (1941).
[6] W. Heisenberg, *Vorträge über Kosmische Strahlung* (Berlin, 1943), p. 10.

independent of the mean barometric pressure, at least in the lower half of the atmosphere, in agreement with the experimental results. The calculations also indicate that the barometric effect should vary noticeably with changes in the area S of the counters' surface. This is caused by the dependence of the mean density of the recorded showers on the counter area.

In Table I are collected the values of α calculated for a threefold coincidence system among three counters (or groups of counters) each of area S, arranged on a horizontal plane 10 or more meters apart in order to record only extensive showers. Nearly the same values should have been obtained for a fourfold coincidence system.

A comparison between our theoretical results and the experimental data cannot be precise, because the recording arrangements used by the above mentioned authors are rather unlike that to which we refer. Nevertheless there is fair agreement between theory and experiment as to the magnitude of the effect. As Table I shows, α does not depend strongly on x, so that it is impossible by this method to determine the shape of the primary spectrum. It appears that a systematic measurement of the barometer effect performed with counters of different areas would be very interesting in order to test the dependence of α on S.

The theory does not predict the dependence of α on the distance between the counters, at least for not too large distances. We shall discuss this point below.

TABLE I. Calculated values of the barometric coefficient α for a threefold coincidence system.

	$S=10$ cm²	$S=50$ cm²	$S=200$ cm²	$S=1000$ cm²	$S=5000$ cm²
$x=1.6$	0.075	0.085	0.095	0.11	0.12
$x=1.8$	0.08	0.10	0.11	0.125	0.14

SECTION 4

The theoretical density spectra at various atmospheric pressures, i.e., at various heights above sea level, always have the form

$$H(\Delta)=A(10^{-4}\ \text{cm}^{-2}/\Delta)\gamma\ \text{sec}^{-1}$$

where $H(\Delta)$ is the frequency of showers of density $\geqslant\Delta$. The calculated values of the constants A and γ, for particular values of the pressure p and of the constant x, are collected in Table II. (In reference 3 the same calculation was made for zero- and 2200-m elevation and $x=1.8$. The values of A and γ found in reference 3 differ a little from the present ones, owing to the use of Heisenberg's formulas instead of those of Rossi and Greisen.) In the last column of Table II are collected the experimental values of A and γ as they result from our experiments[2] at 120 and 2200 m above sea level.

TABLE II. Values of the constants A and γ in the theoretical shower frequency formula.

	$x=1.6$		$x=1.7$		$x=1.8$		Experim. values	
	A	γ	A	γ	A	γ	A	γ
$p=760$-mm Hg (0 m)	0.22	1.22	0.083	1.29	0.032	1.36	0.124	1.46
$p=565$-mm Hg (2300 m)	2.3	1.35	1.07	1.43	0.5	1.50	1.0	1.55
$p=452$-mm Hg (4100 m)	8.9	1.45	4.7	1.55	2.5	1.64		

As for γ, the agreement between theory and experiment is rather good ($x=1.8$), and the theoretical increase of γ with height is confirmed also. It must be observed that other experimenters,[7] on the contrary, have found a reduction of γ with increasing altitude, in disagreement with our experimental and theoretical results. We think that further experiments carried out in order to look into this point might be very interesting. One notes that the variation of γ with altitude is directly related to the variation of α with S in the barometric effect.

As for the constant A, the theoretical results are rather lower than the experimental ones. This may be ascribed, in addition to the uncertainties in the primary spectrum and the cascade theory, also to the fact that the distances between the counters in our experiments were too small (4 m) to eliminate local showers due to non-electronic particles (see the decoherence curve in Molière).[4]

As mentioned above, we think that 10- to 20-m distance between the counters is necessary in order to record only extensive showers. Possibly even the values of γ determined at larger counter distances may differ from those obtained in reference 3. This may also explain why the above

[7] P. Auger and J. Daudin, J. de phys. et rad. 6, 233 (1945).

mentioned experimenters found a barometric effect depending on the distances between the counters.

SECTION 5

From our calculations of the barometric effect one can deduce the manner in which the frequency of recorded showers varies with height above sea level, for the apparatus described in Section 3 (threefold coincidences among identical counters). It follows directly from Eq. (1) that

$$H_s(p) = H_s(p_0)e^{-\alpha\delta p}$$

where $\delta p = p - p_0$ and $H_s(p)$ is the frequency of showers recorded at atmospheric pressure p by counters of area S. If δp is measured in cm Hg, the values of α are those collected in Table I.

Experimental data may be deduced from Hilberry's measurements.[8] Hilberry recorded fourfold coincidences among counters of 200 cm² area arranged 2.5 m apart, at elevations between 0 and 4300 m above sea level. From Hilberry's measurements we deduce $\alpha = 0.10$, in agreement with the data of Cosyns and Auger on the barometer effect, and with the theoretical results in Table I. In our opinion this agreement is a good proof of the reliability of the assumptions on which the calculations are based.

SECTION 6

Elsewhere[9,10] the author and co-workers have shown that all extensive showers are associated with penetrating showers (i.e., showers recorded under layers of lead thick enough to eliminate the electronic component), and that the penetrating showers are generated locally in the materials screening the counters. If these results are correct, we can expect that both the barometric effect and the height effect of the penetrating showers associated with extensive ones follow the same laws found for the extensive showers alone.

No experiments have yet been performed in which the barometric effect and the height effect have been measured only for those penetrating showers which are associated with extensive showers. However, all kinds of penetrating showers (regardless of association with extensive showers) have been investigated by Janossy and Rochester,[11] who studied the barometer effect and deduced $\alpha = 0.12$ (with sevenfold coincidences among counters of ≈ 150 cm²), and by Wataghin,[12] who studied the height effect up to 8500 m and found $\alpha = 0.136$ (fourfold coincidences among counters of 400 cm²). These results agree with those reached for extensive showers, testifying probably to the local generation of the penetrating showers and their connection with extensive showers. This agreement, of course, might be only chance, since penetrating showers not depending on extensive showers were also recorded in the above mentioned experiments.

In conclusion, we remark that many phenomena pertaining to extensive air showers fit rather well the cascade theory. To the points discussed in this work we should add the agreement between theory and experiments concerning the decoherence curve.[13] Therefore we think that, up to date, many properties of extensive cosmic-ray showers may be described in terms of the cascade theory of electrons and photons.

[8] N. Hilberry, Phys. Rev. **60**, 1 (1941).
[9] G. Cocconi, A. Loverdo, and V. Tongiorgi, Phys. Rev. **70**, 852 (1946).
[10] G. Cocconi and C. Festa, Nuovo Cimento **3**, 293 (1946).
[11] L. Janossy and G. D. Rochester, Proc. Roy. Soc. **183**, 186 (1944).
[12] G. Wataghin, Phys. Rev. **71**, 453 (1947).
[13] G. Cocconi, Phys. Rev. **72**, 350 (1947).

The Isotopic Constitution of Lanthanum and Cerium*

MARK G. INGHRAM, RICHARD J. HAYDEN, AND DAVID C. HESS, JR.
Argonne National Laboratory, Chicago, Illinois

(Received August 8, 1947)

The isotopic abundances of lanthanum and cerium have been determined by means of a mass spectrometer. In addition to the known lanthanum isotope of mass 139, a new isotope of mass 138 and abundance 0.089 percent has been discovered. Since this isotope is isobaric with two neighboring stable isotopes it should be radioactive. No activity was observed. Upper limits for the non-existence of other lanthanum isotopes were determined. The abundances of cerium isotopes of masses 136, 138, 140, and 142 were shown to be 0.193, 0.250, 88.48, and 11.07 percent, respectively. Upper limits for the non-existence of other cerium isotopes were determined.

I. INTRODUCTION

IN view of the fact that all previous measurements of rare earth isotopic constitution have been made photometrically, it was decided to repeat these measurements, using electrometric methods. The determination of isotopic abundances by the measurement of positive-ion currents eliminates several of the difficulties inherent in obtaining these abundances from the relative blackening of a photographic plate. The usual photometric method is to relate isotopic abundances to optical densities of mass spectra lines by means of a density curve. The methods of printing standard intensities are liable to introduce errors if they are made by x-rays, light, different ions from those examined, or by ions of different velocity, because the slope of the exposure-density curve depends on the method of producing the densities and may be different for the standard and the ions being studied. This leads to discriminations dependent upon isotopic abundance. In addition, errors may arise because of the fact that different isotopes traverse different paths in a spectrograph.

In this paper electrometric measurements of the isotopic constitution of lanthanum and cerium, together with upper limits for the non-existence of possible neighboring isotopes of these elements, are given.

II. APPARATUS

The mass spectrometer used in this investigation was a Nier type, 60°, 6-inch radius of curvature, single-focusing mass spectrometer.[1] Ions of the elements studied were obtained by heating their oxides on a tungsten filament.[2] The samples were placed on the filament in nitric acid solution, and upon heating these reverted to the oxide. No organic binder was used. Ion emission began at approximately 1000°C. The ions formed were collimated into an ion beam of 2000-volts energy by the collimating plates of the source and directed normally into a wedge-shaped magnetic field. This magnetic field resolved the ion beam into its various mass components and refocused a beam of a single mass through the collector slit to a collector plate. The collector plate was surrounded by an electron-repelling field of 22.5 volts, so that secondary electrons formed at the collector plate by positive-ion bombardment could not leave that plate. Ion currents were measured by a vibrating reed electrometer.[3] The electrometer output was recorded on a Brown Electronik strip chart recorder so that permanent records of peak shapes and intensities were obtained. Succeeding isotopes were focused on the collector by an automatic, continuous variation of the analyzer magnetic field.

The pumping system consisted of a two stage, glass mercury diffusion pump backed by a Welch Duo-Seal fore pump. A liquid air trap was used between the diffusion pump and the mass spectrometer tube to trap out vapors. The operating

* This document is based on work performed under Contract No. W-31-109-eng-38 for the Atomic Energy Commission at the Argonne National Laboratory.

[1] A. O. C. Nier, Rev. Sci. Inst. 11, 212 (1940).
[2] J. P. Blewett and E. J. Jones, Phys. Rev. 15, 464 (1936).
[3] H. Palevsky, R. K. Swank, and E. Gvenchik, Rev. Sci. Inst. 18, 298 (1947).

TABLE I. Isotopic constitution of lanthanum.

Reference	Method	138 (percent)	139 (percent)
Aston[6]	Photometric	—	100
Present work	Electrometric	0.089 ±0.001	99.911 ±0.001

pressure in the tube was about 3×10^{-7} mm Hg as measured by an ionization gauge.

III. DISCUSSION OF OBSERVATIONS

In discussing corrections which must be applied to the observed abundances, possible preferential emission of the lighter mass ions, caused by their higher thermal velocities, must be considered. Theoretically, evaporation from the liquid phase gives a change in the abundance ratio of two isotopes proportional to the square root of the ratio of the masses. This separation is attained only if there is perfect mixing at the surface of the liquid. In the solid phase there is little mixing, and so there should be little separation. Since the material on the filament was not in the molten state, little mass discrimination was expected. To test this hypothesis, isotope ratios were taken from the time emission began until the sample was completely evaporated from the filament. If any such mass discrimination had taken place the last determinations would have given larger relative abundances of heavier masses than did the first. No such effect was noted and hence it was concluded that no vapor pressure discrimination took place.

Another error would have been introduced if the ratio of ions to atoms emitted from the filament were dependent on the mass of the isotope. However, since the efficiency of ionization in this type of source depends on the ionization potential and not on the mass, it is concluded that this effect is negligible.

Possible space-charge discriminations near the filament are negligible because the emission from the filament is temperature limited rather than space charge limited.

With this ion source the electron focusing magnet usually used on the source of Nier-type mass spectrometers was unnecessary and was omitted. Thus no magnetic isotope discriminations could have occurred in the source.[4]

[4] E. F. Cogshell and N. D. Jordan, J. App. Phys. 13, 539 (1942).

The condition for no discrimination between light and heavy ions in their passage through a mass spectrometer is that the ion paths for different ions be identical. This condition was fulfilled in these measurements by bringing different masses to focus at a fixed point by varying the analyzer magnetic field and keeping the ion energy constant.

Inaccuracy in the current measuring system could have been caused by non-linearity of the 2×10^{10}-ohm input resistor of the vibrating reed electrometer or by non-linearity of response through the electrometer and the recorder. However, measurement showed the input resistor to be constant to better than 1 percent in the range of 1 millivolt to 10 volts, the range used in these experiments. Measurements of the linearity of the amplifying and recording system showed its response to be linear to within 0.2 percent. Thus all systematic errors are less than 1 percent, and to this degree of accuracy the observed peak heights are proportional to isotopic abundances.

IV. EXPERIMENTAL RESULTS

Lanthanum Abundances

La_2O_3 heated on a tungsten filament gives rise to LaO^+ ions. A typical recorder curve of these ions is shown in Fig. 1. Peaks at masses 154,

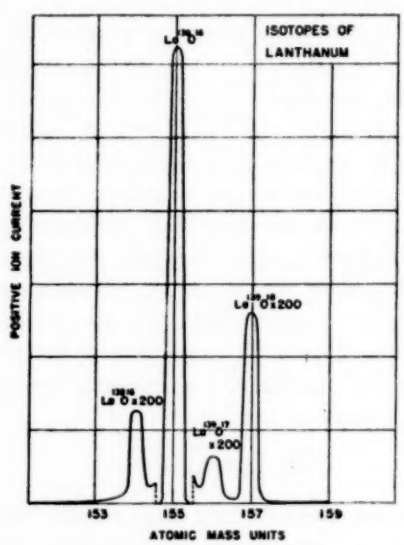

FIG. 1. Recorder tracing of isotopes of lanthanum as observed in the LaO^+ position. The peak at mass 155 is recorded at one two-hundredth of the sensitivity used for the rest of the tracing.

TABLE II. Isotopic constitution of cerium.

Reference	Method	136 (percent)	138 (percent)	140 (percent)	142 (percent)
Aston[6]	Photometric	—		89.0	11.0
Dempster[3]	Photometric	1	1	—	—
Cohen*	Electron multiplier	0.18	0.22	—	—
Present work	Electrometric	0.193±0.005	0.250±0.005	88.48±0.10	11.07±0.10

* Arnold A. Cohen, Phys. Rev. 63, 219 (1943).

155, 156, and 157 are present. The sensitivity of the recorder at mass 155 is less by a factor of 200 than the sensitivity over the rest of the curve. The peaks at 155, 156, and 157 are due to $La^{139}O^{16}$, $La^{139}O^{17}$, and $La^{139}O^{18}$ ions, respectively. Calculation of the isotopic constitution of oxygen from the heights of these peaks gives 99.752 percent O^{16}, 0.041 percent O^{17}, and 0.207 percent O^{18}. These results agree with those of Murphey[5] within 2 percent so that within this limit these peaks are ascribed entirely to $La^{139}O^{16}$, $La^{139}O^{17}$, and $La^{139}O^{18}$. Thus, if there are any La^{140} and La^{141} isotopes they must be less than 2 percent of the height of the last two peaks. The ion at mass 154 we ascribe to the oxide of a new isotope, La^{138}.

The possibility that this peak is due to another element has been ruled out by the following considerations: If the peak at mass 154 were due to an impurity of some other element in lanthanum, this impurity would probably not be of the same intensity in various samples. We observed the 154 peak in three specially purified samples; a sample of spectrographically pure La_2O_3 prepared by Professor Rolla and obtained from Adam Hilger, Inc. as Laboratory Number 6781, a second sample of $La(NO_3)_3 \cdot 6H_2O$ obtained from Kahlbaum, and a specially purified third sample. Within 1 percent no difference could be detected in the ratio of the 154 to 155 peaks in these three samples. Further evidence that the mass 154 is not due to an element other than lanthanum is provided by the characteristics of surface ionization. For example, if a mixture of lanthanum and cerium is placed on the filament, the ratio of the cerium to the lanthanum increases strongly with time, because the lanthanum ions are emitted at a lower temperature than the cerium ions. This effect is present in varying degrees between lanthanum and any other element which emits positive ions from a tungsten filament. No variation with time of the 154 to 155 ratio could be detected. This indicates that the 154 peak belongs to lanthanum. A final argument that the 154 peak is due to $La^{138}O^{16}$ is based on a consideration of the other elements which could conceivably give rise to this peak. These are barium, cerium, samarium, and gadolinium; since O^{15}, if it exists, exists to less than one part in one hundred thousand, this could not be the cause of this peak. A barium peak at mass 154 would have to be $Ba^{138}O^{16}$. Since barium does not emit as BaO^+, but rather as Ba^+ and because the $Ba^{137}O^{16}$ line was not observed at mass 153, this possibility is ruled out. Cerium is ruled out because if the 154 peak were due to $Ce^{138}O^{16}$ the 156 peak due to $Ce^{140}O^{16}$ would have to be 700 times larger than was actually observed. The possibility of CeN is ruled out by the fact that with the rare

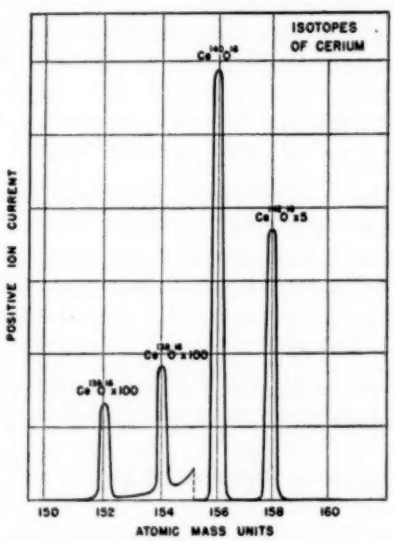

FIG. 2. Recorder tracing of isotopes of cerium as observed in the CeO^+ position. The peak at mass 156 is recorded at one-hundredth the sensitivity, and the peak at 158 at one-twentieth the sensitivity, used at masses 152 and 154.

[5] B. Murphey, Phys. Rev. 59, 320 (1941).

earths no charged nitrides are observed. Samarium and gadolinium are likewise ruled out because their other isotopes did not appear. The possibility of dissociation of LaOH between the accelerating electric field and the magnet is ruled out by the fact that LaOH was not present, and that no similar line appears with cerium. It must therefore be concluded that the isotope of mass 138 exists in lanthanum as it occurs in nature.

The results of this investigation, together with the previous results of Aston,[6] are summarized in Table I. The results are the average of forty separate determinations. The uncertainty tabulated is the mean deviation of these determinations. Any other isotope of lanthanum is present to less than 0.002 percent.

Calculation of the chemical atomic weight from these abundances, using Dempster's[7] value of -3.2×10^{-4} for the packing fraction of lanthanum and the factor 1.000275 in converting from physical to chemical atomic weight, gives 138.92, which is in complete agreement with the international chemical atomic weight of 138.92.

Lanthanum Activity

Lanthanum^{138} is an unusual isotope in that it occurs between two stable isobars, Ba^{138} and Ce^{138}. It should therefore be unstable. Three consecutive isobars occur at only two other places in the atomic table, namely, in the cases of K^{40} and Lu^{176}. It is similar to these isotopes also in that its nucleus contains an odd number of protons and an odd number of neutrons. No naturally occurring odd-odd isotopes heavier than N^{14} are stable. Both K^{40} and Lu^{176} are known to be radioactive, with half-lives of 4×10^{8} years and 7.3×10^{10} years, respectively. In view of the similarity between La^{138} and these two isotopes, it was thought that the La^{138} would probably have an observable activity, and a search for this activity was carried out. A 200-mg La_2O_3 sample, especially purified from all alpha-contaminations, spread over 5-cm^2 area and counted at 40 percent geometry with a 3 mg/cm^2-window counter, showed less than 1 count/min. activity.

CERIUM

Cerium was first studied by Aston[6] and shown to consist mainly of isotopes 140 and 142. Later Dempster[8] found two rare isotopes at masses 136 and 138. A typical recorder curve for cerium obtained with our apparatus is shown in Fig. 2. The mass 156 was recorded at sensitivity 100 times less, and mass 158 recorded at sensitivity 20 times less, than the sensitivity used over the rest of the curve. Only the masses 152, 154, 156, 157, 158, 159, and 160 were observed. These were due to the ions Ce^{136}O^{16}, Ce^{138}O^{16}, Ce^{140}O^{14}, Ce^{140}O^{17}, Ce^{142}O^{16}, Ce^{140}O^{18}, Ce^{142}O^{17}, and Ce^{142}O^{18}, respectively. The cerium isotopic abundances, corrected for the rare oxygen isotopes are given in Table II. These results are the averages of forty separate determinations. The uncertainty tabulated is the mean deviation of these determinations.

No peaks other than those caused by the oxides of these four cerium isotopes formed with O^{16}, O^{17}, and O^{18} could be detected. The following upper limits for possible cerium isotopes of neighboring masses were obtained: 134, 135, and 137, less than 0.004 percent; 139 and 141, less than 0.02 percent; 143, 144, 145, and 146, less than 0.004 percent.

Calculation of the chemical atomic weight from these abundances, assuming a packing fraction of -3.0×10^{-4}, and the factor 1.000275 in converting from physical to chemical atomic weight, gives 140.10, which is in agreement with the international chemically determined atomic weight of 140.13.

We wish to express our appreciation to Prof. A. J. Dempster for many helpful discussions.

[6] F. W. Aston, Phil. Mag. **49**, 1191 (1925).
[7] A. J. Dempster, Phys. Rev. **53**, 869 (1938).
[8] A. J. Dempster, Phys. Rev. **49**, 947 (1936).

Letters to the Editor

PUBLICATION of brief reports of important discoveries in physics may be secured by addressing them to this department. The closing date for this department is five weeks prior to the date of issue. No proof will be sent to the authors. The Board of Editors does not hold itself responsible for the opinions expressed by the correspondents. Communications should not exceed 600 words in length.

The Hyperfine Structure of Atomic Hydrogen and Deuterium*

DARRAGH E. NAGLE, RENNE S. JULIAN, AND JERROLD R. ZACHARIAS
Research Laboratory of Electronics, Massachusetts Institute of Technology, Cambridge, Massachusetts
September 29, 1947

IN a recent Letter to the Editor, Nafe, Nelson, and Rabi[1] reported on measurements of the hyperfine structure separations of the ground states of atomic hydrogen and of atomic deuterium. We have performed very similar atomic-beam magnetic-resonance experiments and have obtained similar values of these constants.

Figure 1 shows the variation with magnetic field of the energy levels for atoms with a $^2S_{\frac{1}{2}}$ electronic ground state and with nuclear spins $\frac{1}{2}$ and 1. These are appropriate to hydrogen and deuterium, respectively, and the transitions indicated by arrows are the ones being reported here. The molecular-beam apparatus used here is similar to that reported by one of us in a paper[2] on the spin of K^{40}. The major differences between the present apparatus and that one is that the source and detector are appropriate to atomic hydrogen and the frequencies are measured by direct comparison with the 5-megacycle standard signal of the Bureau of Standards radio station WWV. Unfortunately, the magnet used to produce the homogeneous field in which the transitions occur is unduly influenced by stray fields of the deflecting and refocusing magnets, with the result that the line widths are considerably larger than could theoretically be expected from the relation $\Delta\nu\Delta T\sim 1$. This effect is larger in the case of hydrogen than deuterium because in weak fields the transition frequencies ν_4 and ν_5 are almost independent of field, whereas the transition frequencies ν_1 and ν_2 are dependent on field for all values of the field.

The value of $\Delta\nu$ for hydrogen is obtained simply and rigorously by subtracting ν_1 from ν_3. Using frequencies obtained for several different values of magnetic field, we obtain $(\Delta\nu)_H = 1420.47 \pm 0.05$ Mc. The large error quoted is due to the magnetic field broadening of the two lines observed. For deuterium the value of $(\Delta\nu)_D$ is calculated by the Breit-Rabi formula from ν_4 and ν_5, unresolved, evaluating the magnetic field from the value of ν_3. ν_6 is used only as a consistency check on ν_3. The value of $(\Delta\nu)_D$ for deuterium is more precise and is 327.380 ± 0.003 Mc.

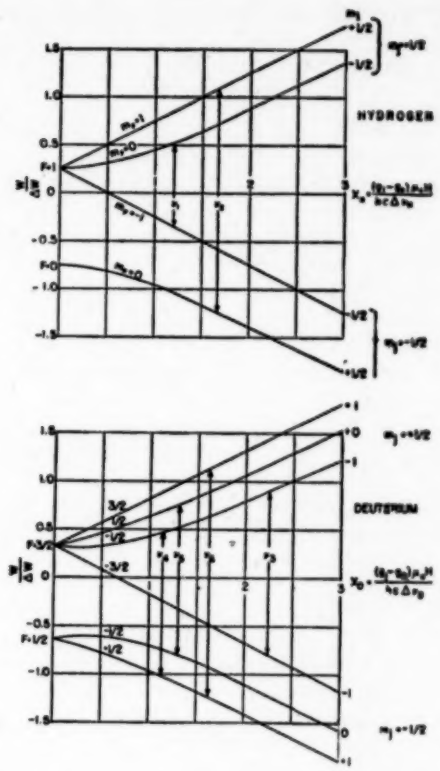

FIG. 1. Hyperfine structure of hydrogen and deuterium; energy levels in a magnetic field.

Like the results of Nafe, Nelson, and Rabi, the absolute values of the $\Delta\nu$'s are in violent disagreement with those calculated using the Fermi formula[3] and the proton and deuteron magnetic moments published by Millman and Kusch.[4] The modification of the Fermi formula, proposed by Halpern,[5] does not improve this situation. On the other hand, the ratio $(\Delta\nu)_H/(\Delta\nu)_D$ is 4.33890 ± 0.00016, and this is to be compared with the ratio as calculated by the Fermi formula, using the ratio of the nuclear moments given by Kellogg, Rabi, Ramsey, and Zacharias,[6] $\mu_P/\mu_D = 3.2570 \pm 0.001$. The calculated ratio $(\Delta\nu)_H/(\Delta\nu)_D$ is 4.3391 ± 0.0013. The agreement is better than one could expect from the uncertainty in the moment ratio.

It is our intention to improve our results both by improvements in the uniformity of the field and by measurements of transitions in hydrogen which are not sensitive to field. We are given to understand that Nafe, Nelson, and Rabi have obtained results considerably improved over their former values and that they are in agreement with ours.

* This work was supported in part by the Joint Service Contract No. W-36-039 sc 32037.
[1] J. E. Nafe, E. B. Nelson, and I. I. Rabi, Phys. Rev. 71, 914 (1947).
[2] J. R. Zacharias, Phys. Rev. 61, 270 (1942).
[3] E. Fermi, Zeits f. Physik 60, 320 (1930).
[4] S. Millman and P. Kusch, Phys. Rev. 60, 91 (1941).
[5] O. Halpern, Phys. Rev. 72, 245 (1947).
[6] J. Kellogg, I. I. Rabi, N. Ramsey, and J. R. Zacharias, Phys. Rev. 56, 728 (1939).

Newly Observed Structure in He II λ 4686

J. E. MACK AND N. AUSTERN
University of Wisconsin, Madison, Wisconsin
September 25, 1947

IN the λ 4686 (3 *s*, *p*, *d*, −4 *s*, *p*, *d*, *f*) line complex of ionized helium the fourth strongest component ($3_{\frac{1}{2}}-4_{\frac{1}{2}}$, in the notation n_j) has been observed to consist of two lines with a separation tentatively evaluated at 0.16±about 0.02 cm^{-1}. The red member appears the stronger, in a ratio of at least 2 to 1 and possibly as great as 5 to 1.

Upon the Dirac theory for one-electron spectra, the ($3_{\frac{1}{2}}-4_{\frac{1}{2}}$) component would be single, since the energy would depend only on n and j. However, the hydrogen alpha-anomaly, long emphasized by Houston[1] and confirmed by the microwave study of Lamb and Retherford,[2] has led to recent conjectures that the $ns_{\frac{1}{2}}$ level lies above the value predicted by the Dirac theory by the amount $r_n(Z^4)$, or r_n, where the dependence on n is approximately $r_n \doteq r_1 n^{-3}$. Thus in the line studied the third ($3_{\frac{1}{2}}-4_{\frac{1}{2}}$), fourth ($3_{\frac{1}{2}}-4_{\frac{1}{2}}$), and seventh ($3_{\frac{1}{2}}-4_{\frac{1}{2}}$) components are split, each into two members, making the line system 11-fold instead of eightfold.

Bethe's[3] approximate calculation of the interaction of the atom with the radiation field leads to a value of about 0.13 cm^{-1} for r_3(He^4); here we are assuming that the average excitation potential is so nearly independent of the principal quantum number that, for a two-digit approximate calculation, we may neglect its variation. If the level shift is treated as varying exactly as n^{-3}, our observation of the splitting yields a tentative value of 0.113±about 0.014 cm^{-1} for r_3(He^4). These two values appear to be in satisfactory agreement. Details are given in Fig. 1.

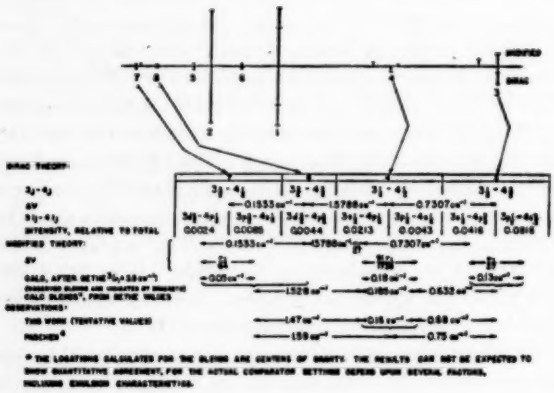

FIG. 1. Certain separations in the He II line complex λ 4686.

All the plates used up to the present were made in the second order of a grating with a nominal second-order resolution of 0.130 cm^{-1} for lines of equal intensity. Thus it could resolve the 0.16 cm^{-1} separation of the component described, but not the expected somewhat smaller separation of an adjacent component of this line complex with a calculated intensity ratio of almost 2:1.

Work is in progress upon this line complex and upon the lines 3–5 and 4–5 of the He II spectrum, and a more detailed account will be submitted. The project is being supported by the Office of Naval Research.

We are grateful to F. E. Geiger, Jr. for his collaboration in the early stages of this research.

[1] W. V. Houston and Y. M. Hsieh, Phys. Rev. **45**, 263 (1934).
[2] W. E. Lamb, Jr. and R. C. Retherford, Phys. Rev. **72**, 241 (1947).
[3] H. A. Bethe, Phys. Rev. **72**, 239 (1947).
[4] F. Paschen, Ann. d. Physik **82**, 689 (1927).

Half-Life of Tritium*

AARON NOVICK
Argonne National Laboratory, Chicago, Illinois
October 3, 1947

BY collecting and measuring the He^3 produced by the beta-decay of tritium, a value of 12.1±0.5 years has been obtained for the half-life of tritium. This value is based on results on two samples and is markedly different from the accepted value of 31±8 years obtained by counting "radioscale" quantities.[1]

Each sample of tritium was first analyzed for its tritium and protium content. Each sample's volume was measured and each was allowed to stand to permit the He^3 to accumulate. At the end of a given period of time the He^3 was separated from the gas by removing all the hydrogen (tritium and protium) through a palladium valve. The helium was further purified by passing it over copper oxide at 450°C (to burn any hydrogen to water) and then through an activated charcoal trap at liquid nitrogen temperature. The volume of He^3 collected was observed. This helium showed no trace of He^4 in an emission spectrum obtained by electrodeless discharge, and the He^3 lines exhibited the expected shift.

The isotopic analysis of the original hydrogen was accomplished in two ways. First, a sample of hydrogen of measured volume was quantitatively burned to water, and the water was weighed. Assuming atomic weights of 1 and 3, calculation was made of the tritium to protium ratio. The second method of analysis involved comparison of the intensities of the T_α and H_α lines from emission spectra obtained on calibrated plates. These spectroscopic observations and those on the He^3 plates were made by Dr. J. K. Brody and Dr. Frank Tomkins of this Laboratory.

These analyses agreed with each other to within 5 percent and were found to be consistent with readings obtained on the beta-activity of each sample by means of an ion chamber.

The $T_2/(H_2+T_2)$ ratio for the first sample was 0.71 and for the second 0.74. After an elapsed time of 51 days, the conversion of T to He^3 was 0.00815 in the first sample; after 197 days, the conversion was 0.03025 in the second sample. The tritium half-life was 11.85 years in the first case and 12.35 years in the second.

* This document is based on work performed under Contract No. W-31-109-eng-38 for the Atomic Energy Project, and the information contained therein will appear in Division IV of the *National Nuclear Energy Series* (Manhattan Project Technical Section) as part of the contribution of the Argonne National Laboratory.
[1] R. D. O'Neal and M. Goldhaber, Phys. Rev. **58**, 574 (1940).

The Half-Life of Tritium*

M. GOLDBLATT, E. S. ROBINSON, AND R. W. SPENCE
University of California, Los Alamos Scientific Laboratory, Los Alamos, New Mexico
September 19, 1947

WE are measuring the half-life of tritium by following with time the decrease in ion current from an ion chamber containing a mixture of hydrogen and tritium. The work is still in progress, but we feel that a preliminary report of our results is of interest, since we find that the tritium half-life is considerably lower than the previously reported value of 31 years.[1]

The ion chamber contained two concentric gold electrodes, spaced about 1 cm apart. The outer electrode was connected to the positive side and the inner electrode to the negative side of the voltage supply. The ion current was determined by measuring the IR drop across a 10,000-ohm standard resistance. Readings were made over a period of eighteen days. The logarithm of the IR drop when plotted against time gave a straight line whose slope corresponded to a half-life of 10.7 years.

The precision of the points on the decay curve was very good, corresponding to an error of about 1 percent in the half-life. However, we can make no correction at present for two possible sources of error: the first caused by absorption of tritium in the ion chamber, the second caused by the slight increase in pressure as tritium molecules are replaced by He^3 atoms. We do not feel justified in claiming an error less than about 20 percent; therefore our preliminary measurement of the tritium half-life gives a value of 10.7 ± 2.0 years.

* This document is based on work performed at Los Alamos Scientific Laboratory of the University of California under contract with the U. S. Atomic Energy Commission.

[1] R. D. O'Neal and M. Goldhaber, Phys. Rev. 58, 576 (1940).

Microwave Absorption Spectra of N_2O

D. K. COLES, E. S. ELYASH, AND J. G. GORMAN
Westinghouse Research Laboratories, East Pittsburgh, Pennsylvania
September 26, 1947

THE rotational transition $J=0$ to $J=1$ has been observed for the isotopic molecules $N^{14}N^{14}O^{16}$ and $N^{15}N^{14}O^{16}$. It was expected that these lines would exhibit hyperfine structure, because of electric quadrupole interaction between the N^{14} nuclei and the electric fields in the neighborhood of these nuclei.

Rotational levels of the $N^{15}N^{14}O$ molecule should possess a triplet structure, since the N^{14} nucleus has a spin of 1. Rotational levels of the $N^{14}N^{14}O$ molecule should be nonets in general. For the particular case $J=0$ no hyperfine structure is to be expected. This makes transitions involving the lowest rotational level particularly simple to observe and interpret, since any structure appearing in the absorption line must be just that of the upper rotational level.

The method of Stark-effect modulation, described by Hughes and Wilson,[1] was used to locate the two absorption lines. The electric field applied to the gas varied sinusoidally with time at 200 kilocycles per second, and the output of the crystal was picked up on a communications receiver tuned to 400 Kc. A high electric field strength of 2000 r.m.s. volts per centimeter was used, since N_2O is known to have a rather small dipole moment. Absorption lines caused by $N^{15}N^{14}O^{16}$ and $N^{14}N^{14}O^{16}$ were found at 24,274.60 and 25,123.24 megacycles per second, respectively. The latter frequency is a remarkably good confirmation of the infra-red value.[2]

In order to make precision frequency measurements and study the hyperfine structure of these lines, the gas was held at a temperature of 195°K and a pressure of 10 microns. Under these conditions it was possible to observe the lines while sweeping the Klystron at 30 cycles per second and amplifying the crystal output with a wide-band amplifier.

The $N^{15}N^{14}O$ line was found to be an extremely close triplet, as shown in Fig. 1a. The intensities and spacings are in agreement with a quadrupole coupling constant $[eQ(\partial^2 V/\partial z^2)]$ of -0.27 mc. For the $N^{14}N^{14}O$ line the structure observed is shown in Fig. 1b. Although it was not

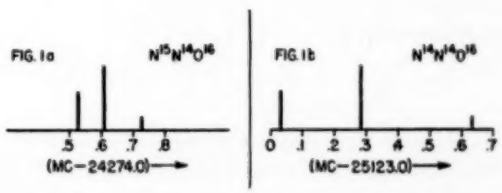

FIG. 1. Observed hyperfine structure for the $J=0$ to $J=1$ rotational transition of nitrous oxide.

possible to resolve the complete structure because of the two N^{14} nuclei, the comparatively wide triplet observed shows that the N^{14} nucleus in the end position of the molecule interacts much more strongly than the same nucleus in the central position. The observed triplet may be considered as essentially caused by the nucleus in the end position, except that the nucleus in the central position has the effect of slightly increasing the frequency for the two low frequency components. For the nucleus in the end position we estimate the coupling constant to be -0.84 mc. Both of these constants are much smaller than previous coupling constants obtained by microwave absorption.[3]

Molecular moments of inertia derived from the above line frequencies are

$$N^{15}N^{14}O^{16}\cdots I_0 = 69.12\times10^{-40}\ \text{g cm}^2,$$
$$N^{14}N^{14}O^{16}\cdots I_0 = 66.79\times10^{-40}\ \text{g cm}^2.$$

If the effect of zero-point vibrations on the internuclear distances is ignored, one may calculate a distance of 1.126A for N−N, and a distance of 1.191A for N−O. These distances are in excellent agreement with those proposed by Pauling.[4]

[1] R. H. Hughes and E. Bright Wilson, Jr., Phys. Rev. 71, 562 (1947).
[2] G. Herzberg, *Infrared and Raman Spectra of Polyatomic Molecules* (D. Van Nostrand Company, Inc., New York).
[3] C. H. Townes, A. N. Holden, J. Bardeen, and F. R. Merritt, Phys. Rev. 71, 644 (1947).
[4] L. Pauling, *The Nature of the Chemical Bond* (Cornell University Press, Ithaca, New York, 1940).

The Absolute Strength of Radioactive Sources

M. L. WIEDENBECK
Department of Physics, University of Michigan, Ann Arbor, Michigan
September 15, 1947

IT has been the custom to determine the strength of a radioactive material by comparing the counting rate of the material in question with a "standard" source. Usually the energies of the "standard" and test sources are not comparable and, as such, corrections for absorption are required. Thus absolute source strengths usually are not very reliable, thereby sometimes preventing the accurate comparison of work from different laboratories.

In the case of ThC'', Dunworth[1] has pointed out a method for obtaining the β- and γ-efficiencies of counters as well as the strength of a source. The calculations are set up for the modified-level scheme proposed by Oppenheimer.

We have found that the absolute number of disintegrations per second in a source can be found simply from the simultaneous β- and γ-counting rates and from the β–γ-coincidence rate, independently of the solid angle subtended by the counters and of the β- and γ-efficiencies of the counters.

The relationship is

$$\frac{N_\beta N_\gamma}{N_{\beta\gamma}} = N. \tag{1}$$

N_β and N_γ are the respective counting rates of the β- and γ-counters, $N_{\beta\gamma}$ is the β–γ-coincidence rate, and N is the number of disintegrations per second occurring in the source placed between the two counters.

For a nucleus which has a simple β-spectrum followed by γ-radiation, no assumptions need be made. The value obtained is independent of the absorption of the β-radiation in the window of the β-counter as well as the absorption of the γ-rays in the walls of the γ-counter.

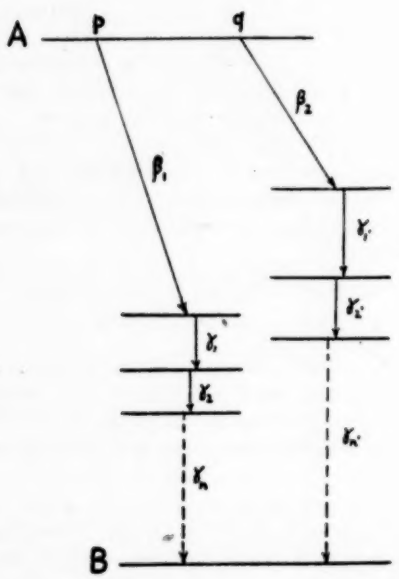

FIG. 1. Decay scheme for a complex β-spectrum.

For complex β-decay (Fig. 1)

$$\frac{N_{\beta\gamma}}{N_\beta} = \frac{[pF_1(\sum_1^n \epsilon_n e^{-K_n T}) + qF_2(\sum_{1'}^{n'} \epsilon_{n'} e^{-K_{n'} T})]\sigma_\gamma}{(pF_1 + qF_2)}, \tag{2}$$

$$N_\gamma = [p(\sum_1^n \epsilon_n e^{-K_n T}) + q(\sum_{1'}^{n'} \epsilon_{n'} e^{-K_{n'} T})]N\sigma_\gamma. \tag{3}$$

p = fraction of disintegrations in which a beta-ray of maximum energy β_1 is emitted ($p+q=1$). F_1 = fraction of β_1 transmitted through absorber. F_2 = fraction of β_2 transmitted through absorber. ϵ_n = efficiency of γ-counter for γ_n. K_n = absorption coefficient for γ_n. T = thickness of γ-absorber (counter wall, etc.).

At zero beta-absorber thickness F_1 and $F_2 = 1$. Then $N_\gamma N_\beta / N_{\beta\gamma} = N$ as in Eq. 1. That is, the absolute disintegration rate can be obtained for a complex β-decay if the value $N_{\beta\gamma}/N_\beta$ is taken at zero absorber thickness. In practice this would require that an extrapolation be made for the thickness of the counter window. This should introduce little error, however, since counter windows of only a few mg/cm^2 thickness are in common use.

It would seem that this method would offer a simple, accurate method of measuring long lifetimes, since no special care need be taken in reproducing counter efficiencies or geometries from one measurement to the next.

[1] J. V. Dunworth, Rev. Sci. Inst. **11**, 167 (1940).

Further Work on Satellites in the Microwave Spectrum of Ammonia*

DUDLEY WILLIAMS
The Ohio State University, Columbus 10, Ohio
September 26, 1947

SINCE the publication of our work[1] on hyperfine structure in the microwave spectrum of ammonia, we have observed additional satellites near lines involving J values as high as 10. The intensities of these satellites are apparently in agreement with theoretical predictions; i.e., intensity relative to the main line decreases rapidly as J value increases. In observing line positions, incident power was varied until the satellite intensity relative to the main line was a maximum; i.e., until saturation phenomena had set in. This technique was also used in our published work.[1] The separation of the satellites from the main line is also in apparent agreement with theory. Since as J values increase the satellites appear closer together and experimental measurements of $\Delta\nu/\Delta\nu'$ become less accurate, this type of check of the theory becomes less exact as J values increase. As the results already published are in agreement with and merely extend other published work[2] and give satisfactory values for quadrupole coupling, we shall not pursue the subject further.

* This work has been done in connection with the research contract W28-099-ac-179 between Watson Laboratories, Air Materiel Command, Army Air Forces and The Ohio State University Research Foundation.
[1] R. J. Watts and Dudley Williams, Phys. Rev. **72**, 263 (1947).
[2] Daily, Kyhl, Strandberg, Van Vleck, and Wilson, Phys. Rev. **70**, 984 (1946).

Magnetic Resonance Absorption of Chromic Ammonium Alum*

P. R. Weiss, C. A. Whitmer, H. C. Torrey, and Jen-Sen Hsiang
Department of Physics, Rutgers University, New Brunswick, New Jersey
October 6, 1947

MEASUREMENTS of the paramagnetic susceptibility of some hydrated salts such as those of the iron group have been explained by the supposition that the lowest energy states of the paramagnetic ion are split by the large electric field created by the surrounding water molecules. This large field "freezes" the angular-momentum vector of the ion, leaving only the spin free to contribute to the paramagnetic and other properties of the crystal. There is, in addition, a small splitting of the lowest level of the order of several tenths of a wave number which makes itself felt in low temperature measurements on susceptibility and specific heat.

This small splitting has the consequence that the energy levels in a magnetic field are not those of a free spin but are displaced from these by amounts which depend upon the splitting in zero magnetic field. Therefore, at a fixed microwave frequency there are several values of the magnetic field at which the condition for resonant absorption is fulfilled. These values of the magnetic field lead directly to the nature and numerical value of the small splitting produced by the electrical field.

The method used in the work reported here is similar to that employed by Zavoisky[1] and Cumerow and Halliday[2] in that the d.c. magnetic field is applied perpendicular to the a.c. magnetic field. The a.c. frequency was 9375 mc/sec. The resonance absorption was observed by employing a magic tee essentially as an impedance bridge. The sample is placed in a resonant cavity on one arm of the tee, the symmetrical arm of which is loaded with a matched termination. The cavity consists of a shorted piece of wave guide provided with a sliding micrometer tuning screw. The cavity containing the sample is tuned with the d.c. field off, so that no power is detected by a low level detector crystal placed in the fourth arm of the tee. About one milliwatt of r-f power is absorbed by the sample. As the d.c. field is varied the resonance absorptions produce changes in the impedance of the loaded cavity which are indicated by the rectified current of the detector crystal. It can be shown that in this arrangement the rectified current is proportional to the absolute value squared of the susceptibility of the salt. The rectified currents are of the order of several microamperes.

An example of measurements made on chromic ammonium alum ($NH_4Cr(SO_4)_2 \cdot 12H_2O$) is shown in Figs. 1 and 2. Figure 1 shows the detector current as a function of the d.c. field for a powdered sample of 3 g. Figure 2 shows a similar curve for a sample consisting of four small single crystals all oriented with the d.c. field along one of the body diagonals of the face-centered cubic lattice. The position of the principal maxima shows the Lande g-factor to be 1.97 rather than 2.00, but this difference is of the order of the experimental error. The number and positions of the

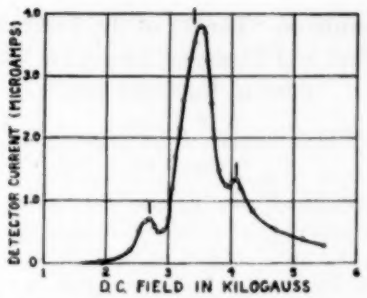

FIG. 1. Absorption curve for powdered chrome alum at a frequency of 9375 mc/sec. The vertical lines show the positions of the peaks computed with $g=1.97$ and a zero-field separation of 0.15 cm^{-1}.

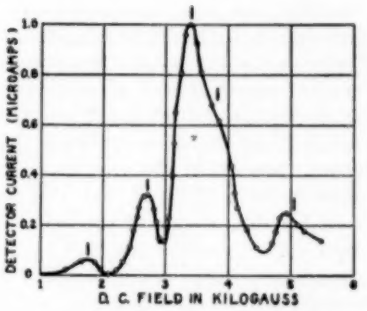

FIG. 2. Absorption curve for single crystals of chrome alum at a frequency of 9375 mc/sec. The vertical lines show the positions of the peaks computed with $g=1.97$ and a zero-field separation of 0.15 cm^{-1}.

maxima can be explained on the basis that the small splitting is 0.15 ± 0.01 cm^{-1} and is produced by an axially symmetric electric field. The computed positions are shown on the figures. The spin of the Cr^{+++} ion being $\frac{3}{2}$, there are three groups of transitions possible in the case of the powder. Averaging the absorption over the various orientations of the axis of the electric field yields three different peaks as shown. In the orientation of the single crystals stated above there are two types of ions in the lattice; in one type the magnetic field is along the axis of the electric field, in the other the magnetic field makes an angle of 70°33′ with the axis of the electric field. Consequently, six transitions are possible. Two of these, however, are superimposed, while a third is not completely resolved from these two. The result, 0.15 cm^{-1}, is somewhat different from the value 0.12 cm^{-1} deduced by Hebb and Purcell[3] for chromic potassium alum from measurements made on the specific heat in the neighborhood of 0.1°K.

The oscillator frequency has not been stabilized and consequently small frequency drifts occur which affect somewhat the reproducibility of the magnitude of the peaks. The positions of the peaks are reproducible within 50 gausses. The technique of the measurements is being improved to remove this difficulty.

* This work was supported by the Rutgers University Research Council, the Research Corporation, and the U. S. Navy under Contract N6ori-203.
[1] E. Zavoisky, J. Phys. U.S.S.R. **9**, 211 (1945).
[2] R. L. Cummerow and D. Halliday, Phys. Rev. **70**, 433 (1946).
[3] M. H. Hebb and E. M. Purcell, J. Chem. Phys. **5**, 338 (1937).

Comments on "Theory of the Ferroelectric Effect and Clamped Dielectric Constant of Rochelle Salt"

W. P. MASON
Bell Telephone Laboratories, Murray Hill, New Jersey
October 6, 1947

IN a paper of the above title appearing in the November 1, 1947 issue of this journal, the ferroelectric properties of rochelle salt are discussed on the basis of a hydrogen-bond dipole by the use of classical statistics. The non-appearance of a ferroelectric effect near absolute zero was ascribed to the disappearance of the dipole moment as the two potential wells coalesced into a single one at low temperatures. It has been pointed out by J. Bardeen that if quantum statistics are used, the zero-point energy of hydrogen does not allow the dipole moment to disappear.

This difficulty can be avoided by developing further the two dissymetrical potential well distributions shown by Fig. 2 of the above paper and discussed in note 6. Since the oxygen molecule 1 and the water molecule 10 are not exactly equivalent, one would not expect the symmetrical potential distribution of Fig. 2a, but the dissymetrical distribution of Fig. 2b for two of the four bonds. Since, however, the x axis of rochelle salt is a binary axis, the other two bonds will have potential distributions that point in the opposite direction, and the second set will have potential wells as shown by the right-hand side of Fig. 2b. By developing the polarization equations for the two sets, as discussed in the paper, one arrives at two equations for the two sets of bonds.

$$\begin{aligned}\frac{1}{\Gamma}\frac{dP_{d_1}}{dt}e^{\Delta v/kT} &= \frac{N\mu}{2}\sinh\left[\frac{\Delta}{kT}+A\left[\frac{E+\beta P_d}{\beta N\mu}\right]\right] \\ &\quad -P_{d_1}\cosh\left[\frac{\Delta}{kT}+A\left[\frac{E+\beta P_d}{\beta N\mu}\right]\right], \\ \frac{1}{\Gamma}\frac{dP_{d_2}}{dT}e^{\Delta v/kT} &= \frac{N\mu}{2}\sinh\left[-\frac{\Delta}{kT}+A\left[\frac{E+\beta P_d}{\beta N\mu}\right]\right] \\ &\quad -P_{d_2}\cosh\left[-\frac{\Delta}{kT}+A\left[\frac{E+\beta P_d}{\beta N\mu}\right]\right],\end{aligned} \tag{1}$$

where 2Δ is a measure of the dissymmetry, and the other quantities are as given in the paper. Using these two equations, one can show that the dielectric constant for low field strengths becomes very closely

$$\epsilon=\epsilon_0+\frac{\frac{4\pi A'}{\beta}\left[1-\left(\frac{P_s}{N\mu}\right)^2\right]}{1-A'\left[1-\left(\frac{P_s}{N\mu}\right)^2\right]+\frac{j\omega e^{\Delta v/kT}}{\Gamma\cosh\frac{AP_s}{N\mu}\cosh\frac{\Delta}{kT}}}, \tag{2}$$

where

$$A'=A\left[1-\tanh^2\frac{\Delta}{kT}\right]=\frac{e^2\delta^2\beta N\cos^2(25°)}{4kT[1-\beta\gamma]}\left[1-\tanh^2\frac{\Delta}{kT}\right]. \tag{3}$$

On this model the dipole moment does not have to vanish at low temperatures since $(1-\tanh^2(\Delta/kT))$ approaches zero very rapidly. Physically this means that the hydrogen molecules are frozen in the low potential wells of each bond at low temperatures and cannot be changed to the other potential well by an applied field. Since the form of (2) is the same as that derived for a symmetrical bond with A' replaced by A, all the conclusions regarding coercive force, the clamped dielectric constant, and the relaxation frequency are the same for the dissymmetrical set as for the symmetrical bond.

The value of Δ/kT cannot be larger than 0.66 at the upper Curie point without causing the separation δ to become too large. With this value a decrease in temperature from the upper to the lower Curie point need cause a decrease in δ^2 of only about 4.5 percent because $(1-\tanh^2\Delta/kT)$ is also decreasing. This probably indicates that the curve of δ *versus* oxygen separation is flatter than that given by Fig. 4 obtained from the simple calculations involving Morse potential functions. This is confirmed also by the measurements of Bancroft on the effect of hydrostatic pressure on the Curie points, which show that the lower Curie point can be made to come at 24°C with the application of 11,000 kilograms per sq. cm pressure. Hence A' has to have a value of 1 at zero pressure and at 11,000 Kg/sq. cm pressure. Under this pressure N and γ increase 5 percent and the factor by 20 percent. This has to be offset by a decrease in δ^2 due to pushing the oxygens closer together. Assuming that about $\frac{1}{4}$ the total cell contraction occurs across the oxygens, the value of δ^2 decreases by about 40 percent, indicating that the curve is flatter than Fig. 4 in agreement with the above data.

A Suggested Experiment to Detect the Shift of $1^2S_{\frac{1}{2}}$ Level of H and He^+

TA-YOU WU*
Randall Laboratory of Physics, University of Michigan, Ann Arbor, Michigan
October 1, 1947

RECENTLY Bethe[1] suggested a theory for the shift of the $2^2S_{\frac{1}{2}}$ level of hydrogen observed by Lamb and Retherford[2] by the microwave technique. The theory predicts a shift for all S states given by

$$W_{ns}'=\frac{8Z^4\alpha^3R}{3\pi n^3}\ln\frac{K}{\langle E_n-E_m\rangle}.$$

This is in agreement with the observed shift $\sim$0.033 cm^{-1} for $2S$ of H. For $2S$ of He^+ the predicted shift is $\sim 13\times 0.033$ cm^{-1}. If for the moment one disregards the small change caused by the logarithmic factor, this formula predicts a shift of 8×0.033 and $13\times 8\times 0.033$ cm^{-1} for the $1^2S_{\frac{1}{2}}$ of H and He^+, respectively. A detection of this shift in the $1^2S_{\frac{1}{2}}$ of H and He^+ by measuring the shift of the first line of their Lyman series immediately suggests itself, since it is of interest to verify the prediction of the theory and since the analysis of the experimental result would be comparatively simple in this case. This shift corresponds, however, to only 0.003,9A in the case of the Lyman α of H at $\sim$1210A, and 0.003,15A in the case of L_α of He^+ at $\sim$300A. To measure such small shifts in these spectral regions is very difficult indeed since it involves the question as to what is to be taken as the primary wave-length standards in these regions.

In discussions with Professor Uhlenbeck, the following method to avoid this difficulty was suggested. By means of a large vacuum-grating spectrograph one records, on the same plate, the Lyman α of H at ~1200A in the first order and the Lyman α of He^+ at ~300A in the fourth order. The former will be an unresolved doublet (separation ~0.005,4A), and the latter a doublet with separation 0.021,5A. On the Sommerfeld-Dirac theory the first-order line of $1^2S_{\frac{1}{2}}-2^2P_{\frac{1}{2}}$ of H and the fourth-order line of $1^2S_{\frac{1}{2}}-2^2P_{\frac{1}{2}}$ of He^+ would be separated by ~0.434A on account of the difference in the Rydberg constants in these atoms. On account of the shift predicted by Bethe's theory, this separation would become $0.434-(4\times0.003,15-0.003,9)\simeq0.425$A. By this method it is not necessary to have absolute wave-length measurements accurate to ~0.001A in these spectral regions; instead one has now only to detect and measure a shift of ~0.01A in the separation between two lines. With a spectrograph having a dispersion of about 1A/mm, this seems practicable. Of course, one employs, avoids, or minimizes the Doppler broadening by observing the radiation at right angles to the direction of an atomic beam.

* At present at Columbia University.
[1] H. A. Bethe, Phys. Rev. **72**, 339 (1947).
[2] W. E. Lamb, Jr. and R. C. Retherford, Phys. Rev. **72**, 241 (1947).

Behavior of Silver Chloride Crystal Counters

R. Hofstadter, J. C. D. Milton, and S. L. Ridgway
Palmer Physical Laboratory, Princeton University, Princeton, New Jersey
September 26, 1947

We have investigated several crystals of silver chloride in an attempt to study some of the properties of such crystals when used as detectors of ionizing radiations. We have concentrated on finding: (1) the mobility of electrons in the silver chloride lattice, and (2) the energy required to form a free electron (or ion pair).

Our technique has been similar to van Heerden's.[1] Opposite crystal faces were sputtered with platinum, and the crystal was then annealed at 400°C for several hours. After cooling to room temperature over a period of a day or so, the crystal was mounted in contact with a silver foil (at high voltage) on a crystalline quartz insulator in our crystal holder. A clip and foil made contact with the other face, and these in turn were brought to the grid of a Model 501 amplifier, designed by W. C. Elmore. This amplifier had a rise time of 0.15 microsecond. The crystal was then cooled, generally slowly, to liquid nitrogen temperature by thermal flow through the quartz.

We have employed γ-rays as the ionizing agent and have examined individual pulses on an oscilloscope screen. These pulses are presumably caused by high speed β-particles liberated in the crystal by the γ-rays. Both radium and thorium sources have been used. We have concentrated our interest on the pulses of maximum height and have measured both their rise time and height. In most cases we have also examined the strain pattern of the crystal by observing it through crossed Nicol prisms. Such observations were made before and after using the crystal as a counter.

Table I shows the results we have obtained with five

Table I.

Crystal	Strain pattern observed through crossed Nicol prisms	Rise time in microseconds at 5000 volts/cm	Mobility cm/sec. per volt/cm	Height of largest pulse in millivolts	k
A ½″×½″×0.2 cm	Not known	<0.15	>270	0.44 RaC γ	35
B 1″×1″×1.0 cm	Non-uniform; several large more or less uniform regions	0.5–2.5 Not unique	400–80	0.44 RaC γ	35
C 1½″ diameter ×1.0 cm	Non-uniform; several large more or less uniform regions	~0.5	?	~0.2 RaC γ	60–100
D 1½″ diameter ×1.0 cm	Not annealed; large number of small strained regions; crystal clear and transparent in unpolarized light	No pulses		<0.04 RaC γ	>500
E ½″×½″×0.40 cm	Fairly uniform except near edges	0.5–0.8	100–160	~1.3 Th (C+C″) γ	13–16

$$k=\frac{Ee}{CV}$$

"E" is the energy of the most energetic γ-ray, "e" the electronic charge, "C" (generally ~25 micromicrofarads) the capacitance of the crystal plus wiring plus input capacitance of amplifier, "V" the size of the voltage pulse.

$$\text{Mobility}=d^2/TV',$$

"d" is the distance between electrodes, "T" is the rise time, and "V'" is the voltage across the crystal.

crystals. In the last column of this table "k" is a quantity which would be the energy per ion pair if the secondary ionization electrons were able to drift completely across the crystal. The mobility has been calculated from the rise time, distance between electrodes, and the electric field.

In interpreting these data we believe that the largest pulses are to be ascribed to β-particles, having practically the whole of the γ-ray energies, which are released by γ-rays of the highest energy from either source, RaC, 2.4 Mev, Th(C+C″), 2.6 Mev. Furthermore, since we have used saturation voltages, the largest pulses are due to those β-particles which are released at points in the crystal where the ionization electrons may travel the greatest distance between electrodes. This distance, in an ideal crystal, is the entire thickness in the direction of the electric field. However, strained regions in the crystal probably act as electron traps and reduce the range of electrons in the conduction band.[2] We believe that such strains are at least partly responsible for the variation in mobility and energy per ion pair exhibited by the data of Table I. Since the exact strain pattern was not determined while the crystal was being used as a counter, we can only assume that the strains were similar to those observed before and after cooling. Furthermore, there is no satisfactory way of correcting for the strains at the present time. For these reasons we arbitrarily assume that the electrons corresponding to the maximum pulses have drifted completely through the crystal. If this is not the case, both the mobility and energy

per ion pair will be decreased. It is hoped that some of the high values of "k" will be understood in the light of these remarks.

The results shown in this table indicate that the mobility is at least a factor of 10 smaller than would be expected from the theory of Frohlich and Mott.[3] From this theory it can be calculated that the mobility is of the order of 2400 cm/sec. per volt/cm at 77°K. As indicated above, these results should not be considered as constants of the material since neither the strain pattern nor the purity of the crystals is known. The energy per ion pair in a favorable case (E) has been observed to be as low as 13 to 16 electron volts per ion pair. This value is about twice as large as that given by van Heerden. For the reasons given above, this result should be considered only as an approach to the true value.

All crystals have been obtained from the Harshaw Chemical Company and were made by H. C. Kremers.[4] Crystals A, B, E and crystals C, D were received in two separate groups from Harshaw. Another crystal not shown in the table, which was received in still another shipment, showed no pulses larger than noise, even though it was annealed.

Essentially all of the above information was given by one of the authors (R.H.) at the Symposium on Short Pulse Techniques and High Speed Counters held at the Brookhaven National Laboratory, August 14 and 15, 1947.

This work was supported in part by the U. S. Navy Contract N6ori-105 Task I. The interest of Drs. M. G. White and H. D. Smyth is gratefully acknowledged.

[1] P. J. van Heerden, *The Crystal Counter* (Dissertation, Utrecht, 1945).
[2] J. R. Haynes, to be published.
[3] H. Frohlich and N. F. Mott, Proc. Roy. Soc. **171A**, 496 (1939).
[4] H. C. Kremers, J. Opt. Soc. Am. **37**, 337 (1947).

The "Gigator"[1]—a Proposed New Circular Accelerator for Heavy Particles

ROLF WIDERÖE
Brown, Boveri and Company, Limited, Baden, Switzerland
September 15, 1947

THE synchrotron proposed by Veksler and McMillan[2] seems at present to be suitable only in the form of the synchrocyclotron for the acceleration of heavy particles to high voltages.

In order to reach extreme high voltages with heavy particles it would, however, be a great advantage to possess a circular accelerator constructed essentially like the electron synchrotron but with an increasing frequency of the accelerating voltage and with an approximately constant orbit, for accelerating ions. It seems possible that above a certain voltage such accelerators both as regards weight and cost will be much more favorable than the synchrocyclotron used today. A practical realization of this idea meets with considerable difficulties, however, because of the large change in velocity of the ions (for instance in the ratio 1:15) and because of the resulting large frequency variations in the accelerating voltages which consequently occur.

Already in the beginning of 1946 the undersigned[3] (quite independently and without knowledge of the proposals made by Veksler and McMillan) proposed new accelerating machines similar to the synchrotron. The proposals involved also a new method for overcoming the aforesaid difficulties. This is achieved by selecting the increasing frequency of the accelerating voltage to be M times higher than the circulating frequency of the particles, the multiple M being reduced in sudden steps as the particle velocity increases, that is, as the particle frequency increases. If, for instance, the accelerating frequency can be varied 25 percent by some mechanical means, then the multiple M may have the values 25, 20, 16, 13, 9, 8, 7, 6, 5, 4 in succession, and in this way a velocity range of 1:7, 8 (corresponding to a voltage increase for protons from 1 to 67 mv) can be dealt with.

The accelerating frequency must in this case be modulated according to a saw-tooth curve (i.e., a timely, relatively slow rise and a rapid fall).

This method can, of course, be used with any success only when it becomes possible to bring the ions from one synchronous condition to another synchronous condition (with smaller multiple M) without an excessive loss of ions.

This transition can be achieved very simply and with a minimum of phase disturbance to the ions if two separate accelerating systems accelerate the ions alternately. The two accelerating systems may then, for instance, work with the successive multiples $M=25$–16–9–7–5 for the first system and $M=20$–13–8–6–4 for the second system. To begin with, the particles shall be accelerated from the first system with $M=25$ and then (when the velocity and the frequency have increased to 125 percent) suddenly change over to the second system where they are now accelerated with $M=20$. Next the particles will shift back to the first system again, being now accelerated with a multiple $M=16$, and so on. During the transition period the first high frequency generator (with the large multiple) has to be de-excited, while the second generator (with the lower frequency and correspondingly smaller multiple) is energized to the full accelerating voltage. Since both accelerating voltages, even if they are "synchronous," may have a certain phase difference during the transition period, a small frequency change in the resulting accelerating voltage can occur during this time. This frequency variation can, however, be made considerably smaller than the limiting value dictated by the limit of stability of the phase oscillations, so that presumably a large part of the ions can be brought into the new synchronous condition.

The choice of a high multiple M for the accelerating frequency has the additional advantage (which may also be of interest as regards the electron synchrotron) that the phase oscillations become correspondingly smaller and also the radial oscillations $\Delta R/Ro$ are reduced in the ratio $1:(M)^{\frac{1}{2}}$. The result of this is that a narrow magnetic guide field can be used, and the magnetic wattless power required for exciting the accelerator will be correspondingly smaller.

[1] 1 Gigavolt (GV) = 10^9 volt.
[2] V. Veksler, J. Phys. U.S.S.R. **9**, 153 (1945); E. M. McMillan, Phys. Rev. **68**, 143 (1945).
[3] R. Widerõe, Norwegian Patent Application No. 84507 (filed Jan. 31, 1946).

The Magnetic Moment of the Deuteron

ARTHUR ROBERTS*
Columbia Radiation Laboratory, Columbia University, New York, New York
September 26, 1947

RECENTLY Nafe, Nelson, and Rabi[1] have made very precise measurements of the hfs separations of the $^3S_1$ ground state of the hydrogen and deuterium atoms. The ratio of the hfs separations depends theoretically only on the ratio of the nuclear magnetic moments and the ratio of the reduced masses of the hydrogen and deuterium atoms:

$$\frac{\nu_H}{\nu_D}=\frac{4}{3}\frac{\mu_H}{\mu_D}\left(\frac{m_H}{m_D}\right)^3. \quad (1)$$

The initial experimental value of ν_H/ν_D reported[1] did not agree with the computed value. Halpern[2] has given reasons why the reduced masses might enter to the $\frac{3}{4}$ power rather than the cube. Since the precision of the computed value depends upon the precision of measurement of μ_H/μ_D, we have undertaken to improve the precision of this value. Previous measurements gave the value 3.2571 ± 0.001.[3,4]

The measurements were carried out by means of the nuclear r-f absorption techniques of Purcell, Torrey, and Pound[5] and the author.[6] Two series of measurements were made in fields near 8000 gausses. In one series separate samples of D_2O and H_2O were placed in a magnetic field made as homogeneous as possible, and resonance absorption was detected simultaneously, using two detectors. The frequencies at which resonance occurred for both samples at the same value of the magnetic field were measured. The samples were then interchanged and the measurements repeated.

In the second series, a single sample of 85 percent D_2O was used, and two coils were wound about it; resonance was detected as before.

The results of the measurements are

$$\mu_H/\mu_D=3.25731\pm0.00015.$$

The precision of these results was limited by a phenomenon we have not been able to explain. The deuteron resonance, displayed on a cathode-ray tube sweep, did not appear at two points on the sweep corresponding to the same value of the magnetic field, as does the proton resonance when sine-wave magnetic-field modulation is used. Instead, two rather indefinite series of wiggles appeared on the trace at values of the magnetic field which were not equal, but corresponded to times slightly later than those at which resonance was expected to occur. The displacement was roughly constant in magnetic field, at about 3 gausses above and below the resonant field, respectively. The type of signal observed was not affected by the addition of $FeCl_3$ to the D_2O, by switching from the bridge type of detection to the super-regenerative detector, or by changing the amplitude of the magnetic-field modulation.

Because of this effect the measurements could not be made by superposing the deuteron and proton resonances, as had originally been intended. Instead, the proton resonances had to be located on the trace at points corresponding to a field midway between the values at which the deuteron signals appeared.

The computed value of the hfs separation rate ν_H/ν_D, using Eq. (1) and the new value for μ_H/μ_D, is 4.33954 ± 0.0002. A $\frac{3}{4}$ power dependence of the reduced mass gives a computed value of 4.34131 ± 0.0002.

This work was supported by Signal Corps Contract W-36-039 SC-32003.

* Physics Department, State University of Iowa, Iowa City, Iowa.
[1] J. E. Nafe, E. B. Nelson, and I. I. Rabi, Phys. Rev. 71, 914 (1947).
[2] O. Halpern, Phys. Rev. 72, 245 (1947).
[3] J. M. B. Kellogg, I. I. Rabi, N. F. Ramsey, and J. R. Zacharias, Phys. Rev. 56, 728 (1939).
[4] W. R. Arnold and A. Roberts, Phys. Rev. 70, 320 (1946).
[5] E. M. Purcell, H. C. Torrey, and R. V. Pound, Phys. Rev. 69, 37 (1946).
[6] A. Roberts, Phys. Rev. 72, 182(A) (1947); Rev. Sci. Inst. 18, (1947)

Disintegration Scheme of 1.7-Year Cs^{134}

L. G. ELLIOTT AND R. E. BELL
Division of Atomic Energy, National Research Council of Canada, Chalk River, Ontario
October 6, 1947

THE disintegration of the long-lived isomer of Cs^{134} has been studied with a short magnetic lens β-ray spectrometer together with coincidence techniques.

The shape of the β-ray spectrum was studied down to the low energy cut-off of the counter window ($\sim$0.015 Mev) by use of a source of thickness $\sim$0.1 mg/cm^2 mounted on a mica backing ($\sim$1.0 mg/cm^2). A Fermi plot of this spectrum, using the exact Fermi function of (Z, η) for $Z=55$, is shown in Fig. 1. The spectrum has a maximum energy

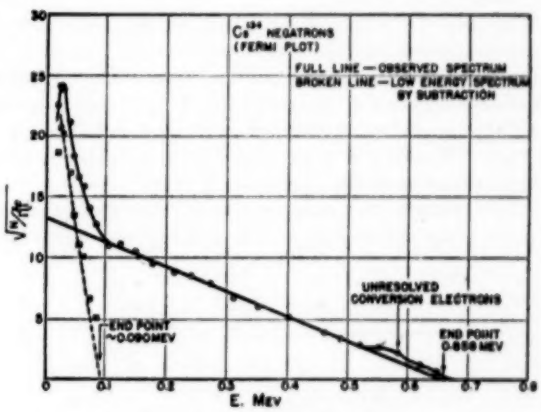
Cs^{134} NEGATRONS (FERMI PLOT)
FULL LINE — OBSERVED SPECTRUM
BROKEN LINE — LOW ENERGY SPECTRUM BY SUBTRACTION
UNRESOLVED CONVERSION ELECTRONS
END POINT ~0.090MEV
END POINT 0.658 MEV
E, MEV

FIG. 1. Fermi plot of β-ray spectrum of Cs^{134}.

of 0.658 ± 0.030 Mev, and the Fermi plot is very closely represented by a straight line down to an energy of $\sim$0.09 Mev. To determine whether the rise at low energies is due to the β-spectrum being complex, a calibrated γ-counter was placed behind the source in the β-ray spectrometer, and coincidences were observed between γ-rays and β-rays above and below the break in the Fermi plot. The two β-ray energies selected were 0.250 Mev and 0.035 Mev, respectively. An observation of the number of coincidences per recorded β-ray showed that, on the average, each β-ray at the 0.035-Mev point is accompanied by 1.20 ± 0.03 times as much γ-ray energy as each high energy β-ray. This indi-

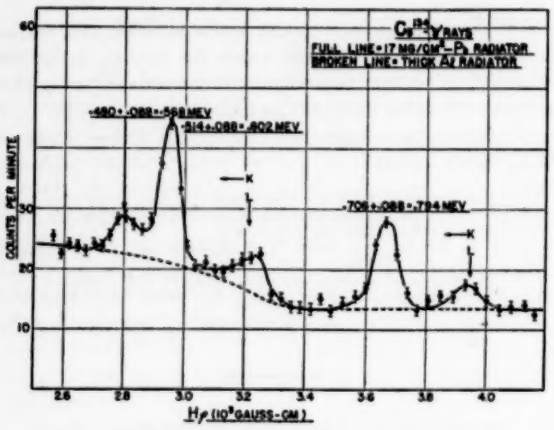
Cs134 γ-RAYS
FULL LINE = 17 MG/CM² - Pb RADIATOR
BROKEN LINE = THICK Al RADIATOR
.480 ± .008 = .568 MEV
.514 ± .008 = .602 MEV
.708 ± .008 = .794 MEV
K
L
COUNTS PER MINUTE
Hρ (10³ GAUSS-CM)

FIG. 2. Secondary-electron spectrum of photoelectric conversion of Cs^{134} γ-rays.

cates that there is a separate low energy β-spectrum superposed on the main β-spectrum. The above ratio remained unchanged when 3-mm Pb was placed in front of the γ-counter, thus demonstrating that the γ-ray quanta accompanying electrons of the low energy spectrum have energies of the same order as those accompanying the high energy spectrum. When the spectra are extrapolated to zero energy and subtracted under the assumption that each spectrum is represented by a straight line on a Fermi plot, the integrated number of electrons in the low energy spectrum represents about 28 percent of all the disintegration electrons.

The secondary-electron spectrum obtained by photoelectric conversion of the γ-rays in a thin (17 mg/cm²) Pb radiator is shown in Fig. 2. Three γ-rays are observed, whose energies are, respectively, 0.568±0.015, 0.602 ±0.015, and 0.794±0.015 Mev, with relative intensities of 0.26, 1.0, and 1.0, respectively, after allowing for the energy variation of the photoelectric cross section.

These results are consistent with the disintegration scheme proposed in Fig. 3. The order of the 0.602- and

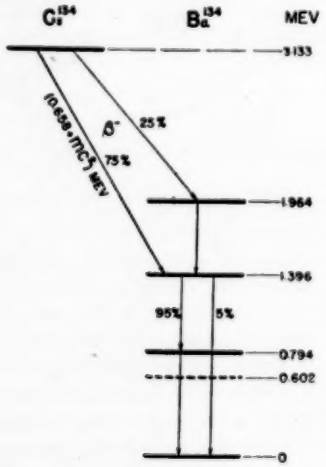

FIG. 3. The disintegration scheme of Cs^{134} (1.7 years).

0.794-Mev γ-rays is unknown. The portion of this scheme associated with the 0.658-Mev β-spectrum is in agreement with the results given by Siegbahn and Deutsch,[1] within the combined experimental errors. The activity available for the present work was not sufficient to observe the 5 percent crossover transition which was observed by Siegbahn and Deutsch. It should be pointed out that if the alternative level arrangement shown as a broken line in Fig. 3 is adopted, the crossover transition may occur from the 1.964-Mev level to the 0.602-Mev level. The accuracy of the energy measurements of the crossover γ-ray reported by Siegbahn and Deutsch is insufficient to decide between the two alternatives.

It is interesting to note that the fractional occurrence of the 0.09-Mev β-disintegrations obtained by extrapolation of the Fermi plot (~28 percent) agrees closely with that obtained from the γ-ray intensities (~25 percent). This suggests that the true shapes of these β-spectra may continue as a straight line on a Fermi plot to zero energies.

A more detailed report of this work will be submitted for publication in the Canadian Journal of Research.

[1] K. Siegbahn and M. Deutsch, Phys. Rev. **71**, 483(A) (1947).

A Modified Stark-Effect Modulation Spectrograph for Microwaves*

RICHARD J. WATTS AND DUDLEY WILLIAMS
The Ohio State University, Columbus 10, Ohio
September 26, 1947

HUGHES and Wilson[1] have described a novel form of microwave spectrograph which utilized a Stark-effect modulation at radiofrequency. In this instrument the usual type of absorption wave-guide section was fitted with a central electrode in the form of a flat brass strip inserted parallel to the broad sides of the wave guide and insulated from the walls.[2] An oscillator (80 Kc) supplied a radiofrequency to this electrode, which could also be given a d.c. bias if desired. The Klystron reflector was modulated with a saw-tooth voltage at 20 cycles per second; this saw-tooth voltage was also applied to the horizontal plates of an oscilloscope. When the frequency of the Klystron passed through an absorption frequency of the gas in the cell, a part of the microwave energy was modulated because of the varying absorption of the gas as the Stark components were varied in frequency by the alternating 80-Kc field. A narrow-band radio receiver was tuned to 80 Kc or a multiple of this frequency and used to amplify the appropriate radiofrequency components of the single-crystal detector output. Hughes and Wilson reported that this type of spectrograph was more sensitive than the types previously described. The shape of the curve (corresponding to an absorption line) displayed on the oscilloscope screen is a complicated function of the nature of the Stark effect for the molecule being studied and of the modulating voltage. Since the publication of their first note, Wilson and his colleagues have improved their spectrograph by using a square-wave modulation voltage on the central

electrode, and in other ways.[3] By proper biasing, a square-wave modulated spectrograph can be used to detect spectral lines and their Stark patterns with little distortion.

A second method of reducing distortion occurred to the writers shortly after the publication of Wilson's first note. This was to replace the flat central electrode in the absorption section by a small wire. In the case of a flat central electrode all the molecules in the wave guide are in a constant electric field at a given time, and hence the Stark pattern is well defined. When the fine wire is used as a central electrode the field is so highly divergent that at any given time very few of the molecules are subjected to the same field intensity, and hence there is no definite Stark pattern. This is indeed apparently the case when an ammonia line is examined by a simple method involving a single crystal; when a d.c. potential is applied to the central wire, the peak intensity of the ammonia decreases noticeably, but no Stark pattern is readily observable. We have done a number of experiments with absorption sections, using guide and central wires of different size with different modulating voltages. Preliminary results have been encouraging. This method of detection is extremely sensitive. In tests on methanol, as many lines have been observed as were reported by Dailey.[4] For high modulating voltage, lines begin to appear at pressures of the order of 1 mm of mercury and continue to increase in size as the pressure is decreased until electrical breakdown occurs at approximately 10^{-3} mm, thereby necessitating a decrease in modulating voltage. Receiver saturation occurs for many of the lines before breakdown. At still lower pressures the modulating voltage may be increased again. However, we have found the arrangement most useful as a tool for preliminary search and have achieved maximum sensitivity for relatively high pressures. Modulation frequencies of approximately 300 Kc have been used.

The lines observed are usually broader than those obtained when simpler methods of observation are used. This can be attributed in part to the fact that higher pressures are usually employed and in part to the fact that the residual Stark pattern, although much weaker than the main line, is still present and produces observable signals. The marked variation of line shape and intensity with pressure and modulating voltage is also disturbing. Observed intensities depend upon the nature of Stark effect for the transition involved as well as upon the true line intensity. One other source of difficulty encountered in the device is introduced by mechanical vibrations in the central wire which can produce a varying reflection pattern in the absorption section.

It is a pleasure to express our appreciation of helpful discussions with Professor E. Bright Wilson, who has done preliminary work on the development of a similar spectrograph.

* This work has been done in connection with the research contract W28-099-ac-179 between Watson Laboratories, Air Materiel Command, Army Air Forces and The Ohio State University Research Foundation.

[1] R. H. Hughes and E. B. Wilson, Jr., Phys. Rev. **71**, 562 (1947).
[2] T. W. Dakin, W. E. Good, and D. K. Coles, Phys. Rev. **70**, 560 (1946).
[3] E. B. Wilson, Jr., paper presented at Symposium on Molecular Structure, The Ohio State University, June 1947.
[4] B. P. Dailey, S. Golden, and E. Bright Wilson, Jr., Phys. Rev. **72** (1947).

Piezoelectric Effect in Polycrystalline Barium Titanate

W. L. Cherry, Jr. and Robert Adler
Research Department, Zenith Radio Corporation, Chicago, Illinois
September 29, 1947

WHILE investigating the rather large electrostrictive effect of a polycrystalline barium-titanate ceramic ($BaTiO_3$ sintered with a few parts per thousand of glass-forming oxides), we found that upon removal of the polarizing field there was a residual electromechanical effect of the linear (piezoelectric) kind.[1] The electromechanical coupling coefficient (a figure of merit for piezoelectric materials)[2] was found to exceed that of quartz by a factor of 4 or 5.

It was found that such polycrystalline aggregates of barium titanate may be rendered piezoelectric to a degree depending upon time of exposure to the electric field and on field intensity. After removal of the field the effect decreases with time, first rapidly for a few days, then more gradually, and appears to stabilize at a level which may be as high as 85 percent of the initial effect. Both magnitude and stability of the effect depend on field intensity and time of exposure. Highly piezoelectric pieces of good stability may be produced in a matter of minutes with field strengths of the order of 20,000 volts per centimeter, whereas several hours are required for similar results at lower field strengths. Measured while the field is applied, the effect increases rapidly (60 percent of final magnitude after two seconds at 20,000 volts per centimeter), but stability upon removal of field after such short exposure is very poor.

Excellent stability, on the other hand, is obtained by applying 20,000 volts per centimeter for one hour. Material thus treated, after showing an initial drop of about 15 percent, has remained piezoelectric for months without substantial change (see Fig. 1).

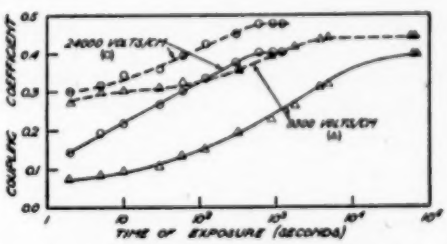

FIG. 1. Solid curves show magnitude of piezoelectric effect, measured one minute after exposure to field. Dotted curves show corresponding effect before removal of field.

Properly formed samples, held at 65 degrees C, drop more rapidly toward a stable value than they would at room temperature, but this stable value itself does not appear to be substantially lowered. Immersion in water does not seem to affect stability.

The piezoelectric axis coincides with the direction of the electric field used to polarize the material. Subsequent application of an alternating field in this direction produces alternate elongation and contraction of the material

in the direction of the field. Application of an alternating field in a direction perpendicular to that in which the polarizing field was applied sets up shear vibrations, the plane of shear embracing the directions of the polarizing and alternating fields. The converse phenomena are also observed.

The electromechanical coupling coefficient for shear is about 0.40; for the longitudinal effect it is near 0.35. These coefficients were obtained in two ways. First, the electrical output was observed with an alternating force of known magnitude at 800 cycles per second. Later, the electrical reactances of mechanically resonant slabs were measured in the radiofrequency range (about 500 kc per second).

Preliminary x-ray examination has shown no evidence of preferred orientation in the polarized material.

It is interesting to note that the material makes possible piezoelectric oscillators and transducers which cannot be formed from natural crystals. For example, a thin-walled cylinder is easily made in which the piezo axis is everywhere radial.

[1] Shepard Roberts, Phys. Rev. 71, 890 (1947).
[2] W. P. Mason, *Electromechanical Transducers and Wave Filters* (D. Van Nostrand Company, Inc., New York, 1942), p. 204.

The Specific Primary Ionization of 1-Mev Electrons Relative to Sea Level Cosmic Radiation*

FRANK L. HEREFORD
Bartol Research Foundation of the Franklin Institute, Swarthmore, Pennsylvania
October 6, 1947

THE average specific primary ionization of sea level cosmic radiation has been determined by Danforth and Ramsey,[1] Cosyns,[2] and Hazen.[3] Cosyns[2] has also determined the value of 1-Mev electrons and has pointed out that, considered relative to the cosmic-radiation results, it is incompatible with the theory of collision loss given by Bethe.[4]

In the course of the development of low efficiency self-quenching counters to be used in selective counter telescopes, an opportunity was afforded to repeat these measurements by a coincidence method. A quadruple coincidence train was employed as indicated in Fig. 1. An electron beam was provided by a specially prepared source consisting of a deposit of radium on a silver surface covered by a thin coating of palladium.

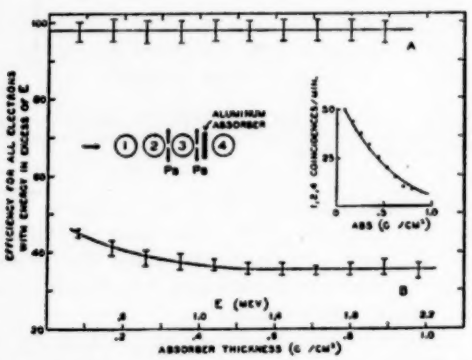

FIG. 1. The efficiency of the third counter *versus* absorber thickness. A schematic sketch of the apparatus and the electron-absorption curve is shown in inserts.

The ratio of coincidences 1, 2, 3, 4 to coincidences 1, 2, 4 was determined for various thicknesses of the aluminum absorber between the third and fourth counters, this ratio being a measure of the efficiency of the third counter. The path length through the counter was determined by a collimator as shown.

In order to insure the negligibility of parasitic effects such as accidental coincidences and scattering, the experiment was first carried through with four high efficiency (12-cm Hg argon-butane) counters in the system. Curve *A* indicates the results. The gamma-ray background was eliminated by a 3-in. lead shield between the source and the counter tray, the electron beam emerging through a $\frac{3}{16}$-in. hole. The insert in Fig. 1 shows the electron-absorption curve that was obtained.

The procedure was then carried through with a low pressure (3.5-cm Hg) helium-butane mixture in the third counter. This was the result of a search for a counter mixture which would operate at low pressures and retain adequate self-quenching properties. Curve *B* shows the results for the helium-butane mixture. The specific primary ionization, s, was computed from the efficiency by means of the relation,

$$\text{efficiency} = 1 - e^{-LsP/76},$$

In order to achieve a value corresponding to about 1 Mev and make possible comparison with Cosyns' results, the computation was made for electron energies equal to and in excess of 0.9 Mev.

The telescope was then mounted vertically, the collimator and absorber removed, and the efficiency determined for the ionizing component of cosmic radiation. A value of 44.3±3 percent was obtained. Exact calculation of the path length for this case, without the collimator, is extremely difficult. However, a rough computation indicates definite upper and lower limits. This makes possible the specification of an upper and lower limit for the specific ionization (see Table I).

TABLE I. Summary of results.

	Absorber	Specific primary ionization (N.T.P.) 1-Mev electrons s_e	Specific primary ionization (N.T.P.) cosmic rad. s_c	Ratio s_e/s_e
Danforth and Ramsey	Hydrogen		6.2	
Cosyns	Hydrogen	8.2±0.2	6.0±0.1	0.73±0.02
Hazen	Helium-alcohol	7.3±0.12	7.2±0.12	0.99±0.04
Author	Helium-butane	10.0±0.4	17.0±0.4 13.2±0.4	1.70±0.08* 1.32±0.07**
Bethe theory	Hydrogen			1.3

* Upper limit.
** Lower limit.

The theoretical value of s_c/s_a was determined from Bethe's theory, s_c being an average value computed from,

$$s_c=\frac{\int s(E)I(E)dE}{\int I(E)dE}.$$

The integration was performed graphically from Blackett's energy-distribution curve (I *vs.* E) for the ionizing component at sea level,[5] using Bethe's theory for the values of $s(E)$. Since the form of Bethe's curve is not dependent on the substance of the absorber, there is real meaning to the comparison of the theoretical value of s_c/s_a for hydrogen with the experimental value for the helium-butane mixture.

It is clear that the results given here are essentially in agreement with theory. Cosyns' method, which employs only one counter, seems to be subject to scattering effects to a greater extent than he indicates.

Hazen's value of s_r was obtained from the cloud-chamber tracks of twenty-one beta-particles in the 0.4–7.0-Mev range, which may account somewhat for the discrepancy in this case, since the primary ionization rises quite sharply for energies less than 1 Mev.

The construction of a beta-ray spectrometer is now in process, which should make possible an accurate determination of $s(E)$ for various gases. This measurement for hydrogen is being made at the present time by the method herein described.

The author wishes to express his sincere appreciation of the frequent advice and suggestions of Mr. W. E. Ramsey.

* Supported by the Office of Naval Research.

[1] W. E. Danforth and W. E. Ramsey, Phys. Rev. **49**, 854 (1936).
[2] M. G. E. Cosyns, Nature **139**, 802 (1937); Bull. Acad. Belg. **5**, 498 (1937).
[3] W. E. Hazen, Phys. Rev. **63**, 107 (1943).
[4] H. A. Bethe, *Handbuch der Physik* **24**, 522 (1933).
[5] P. M. S. Blackett, Proc. Roy. Soc. **159**, 1 (1937).

Divergent Beam X-Ray Photography of Metallic Single Crystals

A. H. Geisler, J. K. Hill, and J. B. Newkirk
General Electric Research Laboratory, Schenectady, New York
October 1, 1947

WE have observed a new type of x-ray diffraction phenomenon in Laue patterns of certain alloys. The phenomenon is similar to the Kikuchi lines which are found in electron-diffraction patterns of thick crystals; it is the same as that observed by Dr. Kathleen Lonsdale on using a very special x-ray tube as described in a recent report.[1] On using this tube which provided a widely divergent beam of x-rays, she found that a pattern of fine white absorption lines and black diffraction lines on a grey background could be produced, under suitable conditions, from single crystals of diamond and organic substances. Such patterns could be used for determinations of crystal orientation and precise lattice constants and for an evaluation of the perfection of the crystal.

On using a somewhat different technique we have observed similar patterns when single crystals of solid solution alloys, which contained iron or cobalt, were irradiated with copper radiation. Patterns for the alloy Cunico and for an Alnico alloy are shown by Figs. 1 and 2. Instead of a widely divergent primary beam, we used a collimated beam of radiation from a tube with a copper target and the usual transmission Laue camera. The normal Laue spots are evident in the patterns. Apparently the required widely

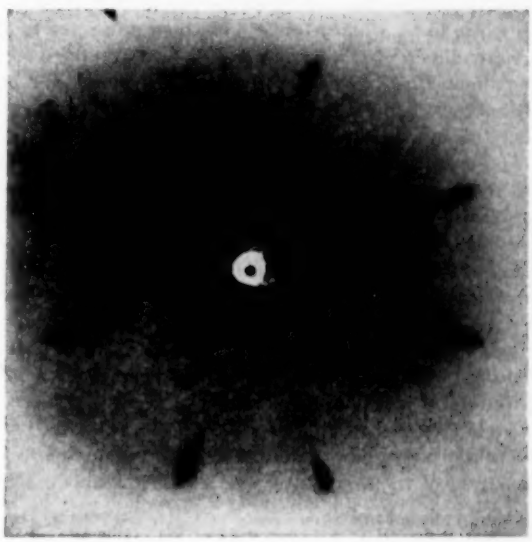

FIG. 1. Laue pattern of Cunico (50 percent Cu, 29 percent Co, 21 percent Ni). Face-centered cubic crystal oriented with [010] parallel to incident beam of Cu radiation. White arcs originated in diffraction from background Co secondary radiation.

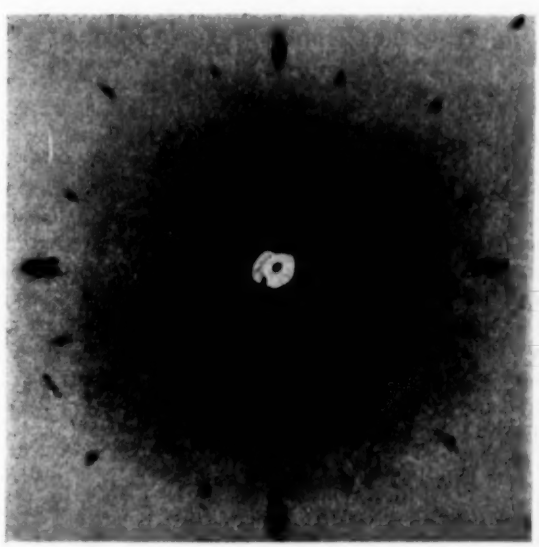

FIG. 2. Laue pattern of Alnico 4 (55 percent Fe, 28 percent Ni, 12 percent Al, 5 percent Co). Body-centered cubic crystal oriented with [010] parallel to incident beam of Cu radiation. White arcs originate in diffraction from background Fe secondary radiation.

divergent beam of x-rays originated at the specimen as secondary Co or Fe radiation which had been excited by the incident beam. The white arcs are quite prominent, while the dark lines are somewhat difficult to distinguish from the background. Fewer dark lines are expected since all reciprocal lattice points within the volume of reflection diffract corresponding rays from the scattered beam to leave the white lines, whereas only those rays diffracted in the forward direction reach the flat film and are detected as black lines. Black diffraction lines have been observed best where they fall in a region of the film remote from the center where background scattering is slight.

The technique which we used offers the advantage that the line pattern is supplemented by the normal Laue pattern on the same film and that the exposures are made with the sealed-off x-ray tubes which are so widely used today. The obvious disadvantages are the relatively long exposure times (8 to 16 hours) and possibly the limitation of materials which can be investigated directly; however, a technique probably could be developed for the examination of single crystals of other materials in which a piece of iron foil is placed in front of the sample as the source of divergent Fe radiation. Work is in progress to determine the utility of this new kind of x-ray diffraction analysis in the study of the solid-state reactions in the above alloys.

[1] Annual Meeting, American Society for X-Ray and Electron Diffraction, June 23–26, 1947, Ste. Marguerite Sta., P. Q. Philosophical Transactions of the Royal Society of London **240**, 219 (A) (1947).

Does the Electron Have an Intrinsic Magnetic Moment?

G. BREIT
Yale University, New Haven, Connecticut
September 29, 1947

THE hyperfine structure of the ground term of H^1 and H^2 is greater[1] than expected from nuclear magnetic moments by, respectively, 0.26 and 0.31 percent. The difference between these values is less certain than the approximate value 0.28 percent and will be assumed to be insignificant.[2] If the electron had a small, Pauli-type, intrinsic magnetic moment[3] μ_e the observed and calculated values would differ.

The effect of $\mu_e\rho_3(\mathbf{H}\sigma)$ in the Hamiltonian (Dirac's notation) is to change the hfs interval factor to

$$A=\frac{2e\mu_N}{ij(j+1)}\,Im\int_0^\infty\left[-k+\frac{\mu_e p_0}{e\hbar}\right]F^*G\,dr, \qquad (1)$$

where $k=l$, $-l-1$, respectively, for $j=l-\frac{1}{2}$, $l+\frac{1}{2}$. The functions F, G are, respectively, $-iF$, G of Roess.[4] Azimuthal, inner, and nuclear-spin quantum numbers are l, j, i. The magnetic field of nucleus at the electron is H, the nuclear magnetic moment is μ_N. The molecular-beam experiment gives $\mu_N/(\mu_0-\mu_e)$, where $\mu_0>0$ is the Bohr magneton. The atomic-beam experiment determines,[5] according to Eq. (1), the quantity $\mu_N(\mu_0+\mu_e/2)$. The theoretical ratio of the hfs to the molecular-beam value of μ_N contains, therefore, $1-\mu_e/2\mu_0$ as a factor. To explain the observed discrepancy one needs $\mu_e/\mu_0=-0.0056$, a small value which could have escaped detection. According to Eq. (1) the interval factors of s, $p_{1/2}$, $p_{3/2}$ terms contain μ_e in the factors $1+\mu_e/2\mu_0$, $1-\mu_e/2\mu_0$, $1+\mu_e/4\mu_0$ apart from factor $1-\mu_e/\mu_0$ which is needed in (1) if the apparent μ_N is substituted for the true value. In principle, ratios of interval factors for these terms could determine μ_e/μ_0.

One expects the following additional effects of μ_e: (a) A modification of the Landé g factor through factor $1-2\mu_e/\mu_0$ in $g-1$. (b) The term $(-\mu_e)\rho_2(\mathbf{E}\sigma)$ caused by nuclear electric field contributes to the energy

$$\Delta E=-2\mu_e Im\int_0^\infty F^*G\,dr\cong\frac{2\mu_e(1+k)Z^4Rch\alpha^2}{\mu_0(l+1)l(2l+1)n^3}, \qquad (2)$$

where n is the principal quantum number of a hydrogenic term, R is the Rydberg, and α is the fine structure constant. For $n=2$, $Z=1$ Eq. (2) gives

$$\Delta E=(-4,\,4/3)(\mu_e/\mu_0)(Rch\alpha^2/16)$$

for $2s$, $2p_{1/2}$, respectively. The displacement of $2s$ with respect to $2p_{1/2}$ of hydrogen is $(-16/3)(\mu_e/\mu_0)(Rch\alpha^2/16)$, which is about 1/33 of the $2p_{3/2}$, $2s$ doublet separation for $\mu_e/\mu_0=-0.0056$. The Lamb-Retherford $-2s+2p_{1/2}$ separation is roughly 3 times the above value. It is doubtful that Bethe's[6] electrodynamic shift theory of the Lamb-Retherford effect[7] is as yet quantitative enough to exclude the possibility of about $\frac{1}{3}$ of the effect arising from another cause.

The presence of the Coulomb energy in p_0 in Eq. (1) makes the integral diverge for s terms. The integral converges, however, if the Coulomb energy is made finite at small distances. A cut-off of the integral at $r\sim e^2/mc^2$ makes the contribution of the Coulomb energy to the integral of the negligible order $\alpha^2\log\alpha^{-2}$ of the term containing p_0. The quantity p_0 has accordingly been replaced by mc in the estimates.

It is not claimed that the electron has an intrinsic magnetic moment. Aesthetic objections could be raised against such a view. The only object of this note is to point out that the evidence considered above does not disprove a small μ_e of the order $\alpha\mu_0$.

If the discrepancy is due to an interaction between the electron and the nucleus of a local type, it is hard to see why it should have the same fractional value for the proton and the deuteron. In this case the effect would be practically confined to s terms, and one could, in principle, distinguish between it and the hypothesis of the intrinsic magnetic moment by comparing hfs interval factors for different spectroscopic terms.

[1] J. E. Nafe, E. B. Nelson, and I. I. Rabi, Phys. Rev. **71**, 914 (1947).
[2] Verbal communication from Professor I. I. Rabi. The writer is very grateful to Professors Rabi and Ramsey for this and other discussions of the subject.
[3] W. Pauli, *Handbuch der Physik* (Verlag Julius Springer, Berlin, 1933), Vol. 24/1, p. 211.
[4] C. G. Darwin, Proc. Roy. Soc. **A118**, 654 (1928); L. C. Roess, Phys. Rev. **37**, 532 (1931).
[5] G. Breit and F. W. Doermann, Phys. Rev. **36**, 1732 (1930), see p. 1737.
[6] H. A. Bethe, Phys. Rev. **72**, 339 (1947).
[7] Willis E. Lamb and Robert C. Retherford, Phys. Rev. **72**, 241 (1947).

The Absorption of 17-Mev Gamma-Rays in Lead and Aluminum*

BOYCE D. MCDANIEL, GUY VON DARDEL,** AND ROBERT L. WALKER
Cornell University, Ithaca, New York
October 8, 1947

A GAMMA-RAY spectrometer has been constructed and used to measure the energy distribution and absorption of gamma-rays which are emitted in the $Li^7(p, \gamma)Be^8$ reaction. The method utilizes the measurement of the momentum of the electrons emitted in pair production. The schematic arrangement is shown in Fig. 1.

A thin lead radiator is placed in a homogeneous magnetic field with the surface of the radiator parallel to the direction of the field. Gamma-rays striking the radiator normal to its surface produce positron and electron pairs which are deflected in opposite directions by the magnetic field to follow circular paths. Two counters, c_1 and c_2, are placed in the plane of the radiator with a separation distance $2r$. Coincidences between the counters are recorded. Except for a very low background of accidental coincidences, coincidences will be recorded only when the electron and positron of a pair have momenta such that the sum of their radii of curvature is equal to r.

It is readily seen that in the case in which both the electron and positron are emitted with an energy greater than 2 Mev, the sum of their momenta, and hence the sum of their radii of curvature, is nearly proportional to the energy of the incident gamma-ray. If the radii are calculated exactly for the case of a 17-Mev gamma-ray, one finds that the sum of the radii of curvature of the two particles varies only 3 percent over all possible distributions of energy between the two. If the energies of the electrons are restricted to be greater than 0.5 Mev, then the variation in the sum is one percent. Under the latter condition it is seen that for a given value of field strength and counter separation the spectrometer is sensitive to gamma-rays in a very narrow energy band.

While the above discussion is based on the assumption that the electrons are emitted in a direction perpendicular to the surface of the radiator, it is readily seen that the normal spread in the angle of emission does not seriously decrease the obtainable resolution. Since the average spread in angle of emission is of the order of m_0c^2/E, for E equal to 17 Mev the average angle is only 1/34 radian. Another factor contributing to the spread in angle of emission is the scattering of electrons in the radiator. This is dependent on the radiator thickness. A factor which minimizes the effect is that the spectrometer utilizes 180-degree focusing.

The experimental arrangement which was used is described below. A magnetic field of about 5000 gausses was supplied by a magnet having a pole face of 32-cm diameter and air gap 2.5 cm high. The lead radiator was 0.20 g/cm² thick with an area of 2 cm×15 cm. It was placed near a diameter of the magnet. The counters were symmetrically located at either end of the radiator, with a separation between centers of 24.6 cm. The counter diameters were 1.8 cm. The cyclotron target from which the gamma-rays originated was at a distance of 50 cm from the radiator. The incident gamma-ray beam was collimated in the vertical direction to have a spread of 1 cm. The counters were shielded from the direct beam by several centimeters of lead.

TABLE I.

Absorber	Thickness	Absorption coefficient Theoretical	Absorption coefficient Observed	Standard statistical error
Lead	21.8 g/cm²	0.066 cm²/g	0.062 cm²/g	0.003 cm²/g
Lead	11.4	0.066	0.067	0.004
Aluminum	20.6	0.022	0.024	0.003

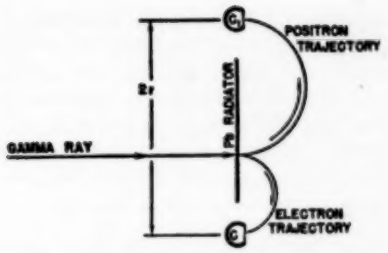

FIG. 1. Schematic diagram of geometrical arrangement. Magnetic field is perpendicular to the paper.

A distribution curve was obtained which gives the relative intensity of pairs observed as a function of Hr for the magnetic field. A third Geiger counter was used to monitor the primary beam intensity. The results of these measurements are given in Fig. 2. It is seen that there is a strong maximum indicated at about 17.5 Mev. The tail on the low energy side may indicate the presence of some further line structure, as has been suggested by previous investigators.[1] However, this tail may be due to the lack of resolution, electron scattering in the foil, or scattering of gamma-rays in the collimator.

The absorption coefficients of the gamma-rays in lead and aluminum were determined by measuring the transmission of absorbers when the spectrometer was adjusted for an Hr corresponding to the maximum of the distribution curve. It is believed that in this manner one measures the absorption coefficient without the confusing effects of degraded radiation. The results are given in Table I. The values predicted by the theory are also given.

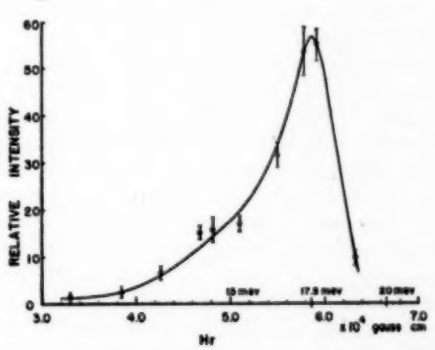

FIG. 2. Relative intensity of observed pair coincidences as a function of Hr. Ordinate scale is arbitrary. Standard statistical errors are indicated.

A new spectrometer is now under construction which is expected to yield improved resolution with much higher counting rates. It is hoped that the new apparatus will permit one to make measurements of absolute gamma-ray intensities in addition to measurements of the sort described here. Such absolute measurements will require determinations of the constants of the apparatus and the efficiency of the radiator for pair production.

* This work was supported in part by the Office of Naval Research.
** Tekniska Hogskolan, Stockholm, Sweden.
[1] L. A. Delsasso, W. A. Fowler, and C. C. Lauritsen, Phys. Rev. 51, 391 (1937).

Microwave Spectra and Zeeman Effect in a Resonant Cavity Absorption Cell*

C. K. JEN
Cruft Laboratory, Harvard University, Cambridge, Massachusetts
September 24, 1947

A MICROWAVE spectroscope has been constructed with a gas-filled resonant cavity instead of the wave guide currently used. The particular cavity tested here is of a type ordinarily used as an X-band wave meter. Such a large cavity gives a sufficiently high Q-value (i.e., long equivalent path length) and decreased effects of intensity saturation, when operated at K-band frequencies. When it is placed in an arrangement containing a Klystron source and a linear frequency sweep, there results an oscilloscopic display of a sharp cavity resonance curve. By tuning the cavity resonance to a spectral line at a sufficiently low pressure, a picture such as that shown in Fig. 1 is obtained.

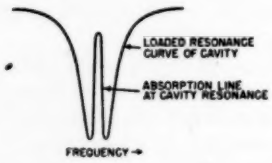

FIG. 1. Absorption line in cavity resonance.

The sensitivity of this method is enough to detect the nuclear hyperfine structure of ordinary ammonia lines of quantum numbers $JK = 11$, 22, 33, 44, 55, 66, and 77.

In attempting to increase the sensitivity of the apparatus the author has tried the method originated by Dr. W. D. Hershberger,[1] in which the reflector grid of the Klystron tube is frequency modulated by a 100-kc source, in addition to the low frequency sweep, and the detected output is amplified by a narrow-band receiver at the modulating frequency or its second harmonic. The resulting sensitivity is increased to such an extent that even the nuclear hyperfine lines seem to be almost as strong as the main lines without modulation.[2] By this method we have also confirmed many of the weaker lines of SO_2 found by Professor E. B. Wilson's group (to be published).

With the aid of the frequency-modulation scheme, the Zeeman effect for microwave spectral lines has been observed with a cavity, specially constructed out of a nonmagnetic cylinder and magnetic end plates acting as pole pieces, by applying an axial magnetic field up to 3000 gausses. In agreement with the results of Coles and Good[3] each absorption line of ammonia is split into a doublet. In the case of a cavity, a doublet is observed for a mode which has the microwave electric field perpendicular to the external magnetic field (TE modes), and a triplet for a cavity mode which has components both perpendicular and parallel to the magnetic field (TM modes).

Still more interesting is the fact that all the nuclear hyperfine lines of ammonia have been split by the magnetic field into doublet or triplet components in essentially the same way as the main lines themselves. A typical spectral diagram for a TE mode is shown in Fig. 2.

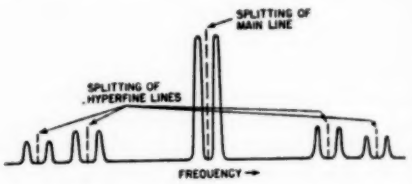

FIG. 2. Zeeman splitting of an NH_3 line and its hyperfine structure.

Measurements of the Zeeman separation as functions of the magnetic field strength and the quantum numbers of the spectral lines for ammonia and other gases are in progress.

My thanks are due Mr. S. P. Cooke and other members of the Microwave Group in this Laboratory for valuable discussions and technical help, and to Professor E. B. Wilson, Jr., for much advice.

* The research reported in this document was made possible through support extended Cruft Laboratory, Harvard University, jointly by the Navy Department (Office of Naval Research) and the Signal Corps, U. S. Army, under ONR Contract N5ori-76, Task Order I.
[1] Kindly communicated by Professor E. B. Wilson, Jr., from discussions at the Symposium on Molecular Structure and Microscopy, Ohio State University, Columbus, Ohio, June 9–14, 1947.
[2] Progress Report No. 4, for Contract N5ori-76, Cruft Laboratory, Harvard University, July 1, 1947.
[3] D. K. Coles and W. E. Good, Phys. Rev. 70, 979 (1946).

The Neutron-Scattering Cross Section at the Cadmium Resonance

W. W. BEEMAN*
Argonne National Laboratory, Chicago, Illinois
October 1, 1947

THE existence of slow neutron-scattering resonances was shown experimentally in 1944 by A. Langsdorf.[1,2] They have since been studied with neutron-filter methods by Wollan *et al.*,[3] Dancoff and Lichtenberger,[4] and Fermi and Marshall.[5] Independently, Goldhaber *et al.*[6,7] found a strong scattering resonance in manganese.

The scattering cross section at the cadmium resonance has recently been measured using a beam of neutrons from a single crystal monochromator.[8] The energy spread of the neutrons was about one quarter of the width of the reso-

nance ($\Gamma=0.115$ ev).[9] A sheet of cadmium 0.056 cm thick, whose surface made an angle of 24° with the beam, scattered neutrons into a boron-lined counter. The counter subtended about 15 percent of the 4π solid angle. Scattered neutrons making angles between 35° and 160° with the forward direction could be detected. The geometry was calibrated using an iron scatterer for which $\sigma_{scat}{}^{10}=10.3\times10^{-24}$ cm².

Counting rates were very low. Despite bulky shielding of the counter and scatterer the scattering was small compared to the fast neutron background in the pile room. It seems probably that a complete scattering resonance could not be measured in a reasonable time without extensive redesign of the shields and counters.

A total of 5372 counts from the cadmium and 5040 background counts were recorded during equal counting times. Corrections were made for the scattering of higher energy neutrons in the beam, for air scattering, and for absorption of scattered neutrons by the scatterer itself. The scattering chamber was lined with cadmium to eliminate double scattering from the beam to the chamber walls and into the counter. The cross section was found to be $40\pm15\times10^{-24}$ cm² referring to the normal isotopic mixture. Approximately half the indicated error is the probable error from the counting statistics. The other half represents an uncertainty in the corrections. Only the correction for absorption by the scatterer was large. It was not calculated more accurately because of the large and somewhat poorly defined solid angle subtended by the counter.

Recent work[9] has shown that the cadmium total resonance is accurately fitted by a one-level Breit-Wigner formula with $E_R=0.176$ ev and $\sigma_T=7200\times10^{-24}$ cm². Cd^{113} (abundance 12.3 percent, spin $\frac{1}{2}$) is known[11] to be the active isotope. If the spin of the compound nucleus is known, these data permit a calculation of the resonance-scattering cross section. Conversely, if the scattering cross section is measured, the spin may be determined.

The following equation,[12] valid when the scattering is small compared to the absorption, relates the quantities in question.

$$\sigma_S=\frac{\sigma_T{}^2}{f_A}\frac{E_R}{1.3\times10^{-18}\left(1\pm\frac{1}{2i+1}\right)}.$$

σ_T is the maximum total cross section at a resonance, and σ_S the maximum elastic scattering cross section at the same resonance. Both cross sections are measured in cm² and refer to the normal isotopic mixture. E_R is the energy of the resonance in electron volts, f_A is the fractional abundance of the active isotope, and i is its spin. The plus or minus sign in the denominator is to be used accordingly as J, the spin of the compound nucleus, is i plus or minus one-half. One calculates from this equation $\sigma_S=114\times10^{-24}$ cm² if $J=0$, and $\sigma_S=38\times10^{-24}$ cm² if $J=1$. To each of these must be added a potential scattering cross section[9] of 5.3×10^{-24} cm².

The comparison of the measured and calculated cross sections is not seriously complicated by crystal effects. Because of the spin and low isotopic concentration of Cd^{113}, more than 90 percent of the predicted Breit-Wigner resonance scattering will be isotropic. The potential scattering depends on the properties of all the isotopes, and a larger fraction might be expected in the Bragg reflected component. These considerations introduce smaller uncertainties than arise from the measurement of the cross section. They do not affect the conclusion that the scattering is in satisfactory agreement with the assignment $J=1$ to the compound nucleus and in definite disagreement with $J=0$.

I wish to thank Mr. W. Sturm and Mr. G. Arnold for their assistance with the spectrometer and Mr. R. Sternheimer for several helpful discussions on coherence and incoherence in neutron scattering. The following formula, relating the isotropic part of the resonance-scattering cross section to that calculated from the Breit-Wigner relations, is from an unpublished investigation of Mr. Sternheimer's.

$$\sigma_{\text{isotropic}}=\left[1-\frac{2J+1}{2(2i+1)}f_A\right]\sigma_S.$$

This document is based on work performed under contract No. W-31-109-eng-38 for the Manhattan Project at the Argonne National Laboratory.

* On leave from the University of Wisconsin.

[1] A. Langsdorf, CF-2161, Metallurgical Laboratory, University of Chicago, Sept. 1944, pp. 3–4.
[2] A. Langsdorf, CP-2301, Metallurgical Laboratory, University of Chicago, Oct. 1944, pp. 7–8.
[3] E. O. Wollan, R. B. Sawyer, and J. Blair, CP-G-3498, Clinton Laboratories, June 30, 1945.
[4] H. V. Lichtenberger, R. G. Nobles, G. D. Monk, H. Kubitschek, and S. M. Dancoff, Phys. Rev. **72**, 164(A) (1947).
[5] E. Fermi and L. Marshall, CP-3750, Oct.–Dec. 1945, pp. 56–63.
[6] M. Goldhaber and A. A. Yalow, Phys. Rev. **69**, 47 (1946).
[7] N. H. Barbre and M. Goldhaber, Phys. Rev. **71**, 141 (1947).
[8] W. H. Zinn, Phys. Rev. **71**, 752 (1947).
[9] L. J. Rainwater, W. W. Havens, Jr., C. S. Wu, and J. R. Dunning, Phys. Rev. **71**, 65 (1947).
[10] M. Goldhaber and G. H. Briggs, Proc. Roy. Soc. **A162**, 127 (1937).
[11] B. J. Moyer, B. Peters, and F. H. Schmidt, Phys. Rev. **69**, 666 (1946).
[12] H. A. Bethe, Rev. Mod. Phys. **9**, 116 (1937).

Rotors Driven by Light Pressure*

J. W. Beams
Rouss Physical Laboratory, University of Virginia, Charlottesville, Virginia
October 1, 1947

In a series of experiments[1] on the production of very intense centrifugal fields it was found that the frictional drag on a magnetically suspended spinning spherical rotor could be accounted for almost entirely by gaseous friction even when the pressure surrounding the rotor was as low as 10^{-6} mm Hg. For example, when a magnetically supported 1.59-mm rotor spinning at about 100,000 r.p.s., in air at a pressure of 2×10^{-6} mm Hg, was allowed to "coast" (without the driving torque applied) it required about an hour for it to lose 0.1 percent of its rotational speed. The existence of this exceedingly low frictional torque suggested that it might be possible to drive magnetically suspended rotors in a good vacuum by light pressure directed tangentially on the periphery of the rotor. It is well known that the pressure of sunlight is roughly 4.5×10^{-5} dyne per cm² at the surface of the earth. Consequently, if a few cm² of sunlight directed tangentially on

the periphery of, say, a 1.59-mm spherical rotor could be completely absorbed, it should be possible to drive the rotor to its explosion speed if the air pressure surrounding the rotor is less than 5×10^{-7} mm of Hg.

In order to determine whether or not rotor acceleration could be obtained by light pressure, light from a 100-watt concentrated arc-type lamp was focused by a large short focus lens and auxiliary mirror on the periphery of a magnetically suspended 1.59-mm rotor surrounded by air at a pressure of about 10^{-6} mm Hg. One-half of the spherical rotor was blackened and the other half left polished so that the speed of the rotor could be measured. The light was directed tangentially on the periphery of the rotor near the two ends of a diameter in such a manner as to exert a couple. If the rotor was spinning a few revolutions per sec., it was observed to accelerate when the light was applied. Experiments also were carried out with small cylindrical rotors both with and without small Duraluminum vanes, and acceleration, although sometimes small, was observable. Also the rotors could be started from rest or could be decelerated and their direction of rotation reversed. In order to start the rotors from rest by this method, it was found desirable to use "soft" iron rotors so that the magnetic axis of the material could be made to align itself automatically with the mechanical axis of rotation. However, the soft iron is not necessary when the rotor is once spinning.

It is believed that the acceleration of the rotors definitely was due to light or radiation pressure since, in the case of the symmetrical rotors, the radiometer effect should be practically eliminated. Also, at the pressures of 10^{-6} mm Hg used in these experiments Tear[2] found that the radiometer effect was very small. The fact that the radiometer effect should be either practically eliminated or reduced to a small value for a symmetrical spinning rotor suggests that it might be possible to obtain a precise measure of the pressure of light as well as of the angular momentum of light by this method. It is planned to investigate these possibilities further.

* This work has been supported by the Bureau of Ordnance, U. S. Navy under Contract NOrd-7873.

[1] J. W. Beams, J. L. Young, and J. W. Moore, J. App. Phys. 17, 886 (1946); Beams and Young, Phys. Rev. 71, 131 (1947); Beams, J. Wash. Acad. Sci. 37, 221 (1947).

[2] Tear, Phys. Rev. 23, 641 (1924); Rev. Sci. Inst. and J. Opt. Soc. Am. 11, 81 (1924).